DEVELOPMENT OF AN $\alpha_V\beta_6$-BINDING PEPTIDE FOR IN VIVO APPLICATIONS:

MODULATION OF SERUM STABILITY AND BIODISTRIBUTION

APPROVED BY SUPERVISORY COMMITTEE

Kathlynn Brown, Ph.D.

Joseph Albanesi, Ph.D.

John Minna, M.D.

Jennifer Kohler, Ph.D.

# DEVELOPMENT OF AN $\alpha_v\beta_6$-BINDING PEPTIDE FOR IN VIVO APPLICATIONS: MODULATION OF SERUM STABILITY AND BIODISTRIBUTION

by

DOROTHY LYNN CUPKA

DISSERTATION / THESIS

Presented to the Faculty of the Graduate School of Biomedical Sciences

The University of Texas Southwestern Medical Center at Dallas

In Partial Fulfillment of the Requirements

For the Degree of

DOCTOR OF PHILOSOPHY / MASTER OF SCIENCE / MASTER OF ARTS

The University of Texas Southwestern Medical Center at Dallas

Dallas, Texas

August, 2015

DEVELOPMENT OF AN $\alpha_v\beta_6$-BINDING PEPTIDE FOR IN VIVO APPLICATIONS: MODULATION OF SERUM STABILITY AND BIODISTRIBUTION

Publication No. _____

Dorothy Lynn Cupka, Ph.D.

The University of Texas Southwestern Medical Center at Dallas, 2015

Kathlynn Corinne Brown, Ph.D.

Targeted delivery of imaging and therapeutic agents to tumors improves detection, characterization, and treatment of many types of cancers. Peptides are capable of efficient and selective delivery of a variety of cargoes to their target cells and have been in development as targeting ligands for a variety of pathologies for several years. The H2009.1 peptide binds to $\alpha_v\beta_6$, an integrin expressed in 54% of non-small cell lung cancers (NSCLC), 80-100% of head and neck carcinomas, and 37% of colorectal cancers. This peptide binds and is internalized into $\alpha_v\beta_6$ positive cell lines, and successfully delivers cargo to xenograft tumors. This dissertation presents the optimization of this peptide for *in vivo* applications (i.e.

improvement of serum stability and reduction of renal accumulation). The N-termini of tetrameric H2009.1 peptide were capped by acetylation or by unnatural amino acids. This capping significantly increased the half-life of H2009.1 tetramer in human serum. *In vivo* near-infrared fluorescence (NIRF) imaging shows that N-terminal capping also decreases kidney accumulation of this peptide at short time periods while maintaining targeting to the tumor for up to 72 hrs. To further decrease off-target accumulation, the valency of the targeting ligands was reduced from a tetramer to a dimer. The dimeric H2009.1 peptide produces similar targeting capabilities compared to the tetrameric peptide, with decreased accumulation in the liver, lung, and kidney. The optimal peptide for long-term targeting of therapeutics to $\alpha_v\beta_6$ –positive NSCLCs is the AcH2009.1 dimer as it gives the highest accumulation and retention in target tumors while avoiding kidney and lung tissue. The best peptide for short-term applications is the AcD-Leu H2009.1 dimer, which differentiates well between $\alpha_v\beta_6$–positive and negative tumors and clears rapidly from the animal. While further work is necessary to bring the H2009.1 peptide into clinical use, the results and experiences of this thesis project have provided critical insights into the *in vivo* optimization of this and many other peptide targeting ligands.

TABLE OF CONTENTS

PRIOR PUBLICATIONS

MJ McGuire, BP Gray, S Li, **D Cupka**, LA Byers, L Wu, S Rezaie, YH Liu, N Pattisapu, J Issac, T Oyama, L Diao, JV Heymach, XJ Xie, JD Minna, and KC Brown. Identification and Characterization of a Suite of Tumor Targeting Peptides for Non-Small Cell Lung Cancer. Scientific Reports. 2014 Mar 27;4:4480. doi: 10.1038/srep04480.

LIST OF FIGURES

LIST OF TABLES

LIST OF APPENDICES

# LIST OF DEFINITIONS

ETS, environmental tobacco smoke
PAH, polycyclic aromatic hydrocarbons
SCLC, small cell lung cancer
NSCLC, non small cell lung cancer
SCC, squamous cell carcinoma
LCC, large cell carcinoma
EGFR, epidermal growth factor receptor
RTK, receptor tyrosine kinase
K-Ras, V-Ki-Ras2 Kirsten rat sarcoma viral oncogene homolog
EML4, echinoderm microtubule-associated protein-like 4
ALK, anaplastic lymphoma kinase
TKI, tyrosine-kinase inhibitor
PFS, progression free survival
FDG, Fluorodeoxyglucose
ADCC, antibody dependent cell-mediated cytotoxicity
VEGF, vascular epithelial growth factor
FRα, Folate receptor α
SPECT, single-photon emission computed tomography
CAIX, carbonic anhydrase IX
GnRH, gonadotropin-releasing hormone
DTPA, diethylene-triaminepentaacetic acid
PRRT, peptide receptor radionuclide therapy
PET, positron emission tomography
GRP, gastrin-releasing peptide
GRPR, gastrin-releasing peptide receptor
RME, receptor-mediated endocytosis
%ID/g, percent-injected dose per gram
NIRF, near infrared fluorescence
PEG, polyethylene glycol
ECM, extra-cellular matrix
FAK, focal adhesion kinase
PI3K, phosphoinositide-3 kinase
GRB2/SOS, growth factor receptor bound protein 2/son of sevenless
EMT, epithelial-mesenchymal transition
MET, mesenchymal-epithelial transition
MMP, matrix metalloproteinases
HAX1, HS-1 associated protein X-1
LAP, TGF-β latency associated peptide
SPPS, solid phase peptide synthesis
Fmoc, fluorenylmethyloxycarbonyl

HOBt, hydroxybenzotriazole
HBTU, O- (Benzotriazol-1-yl)-N,N,N′,N′-tetramethyluronium hexafluorophosphate
NMM, N-methylmorpholine
TFA, trifluoroacetic acid
EDT, ethanedithiol
TIPS, triisopropylsilane
HPLC, high performance liquid chromatography
MALDI, matrix-assisted laser desorption/ionization spectrometry
Acm, Acetamidomethyl
DMF, Dimethylformamide
EDTA, ethylenediaminetetraacetic acid
TMB, 3,3′,5,5′-Tetramethylbenzidine
BSA, bovine serum albumin
AF488, AlexaFluor 488
EC50, (1/2 Effective Concentration
NIRF, Near Infrared Fluorescence

# CHAPTER ONE

## MOLECULAR TARGETING OF NON-SMALL CELL LUNG CANCER

### Current State of Lung Cancer Diagnosis and Treatment

Lung cancer is a major health problem worldwide with an estimated 1.8 million new cases and 1.6 million deaths in 2012 [1]. For decades, lung cancer has been the second most common cancer among men and women as well as the most common cause of cancer-related deaths (See Figure 1.1) [2]. In 2014, roughly 224,210 patients were diagnosed with lung cancer in the United States. It is estimated that 17% of these patients will survive for five years beyond their diagnosis. While many malignancies such as breast and prostate cancer have seen significant improvement in survival rates in recent years, the mortality rates of lung cancer have remained stagnant for over 30 years [3].

The most common symptoms of lung cancer are persistent coughing, shortness of breath, and chronic bronchitis or pneumonia. Patients often dismiss these symptoms as insignificant, and fail to see a doctor for long periods of time. When a patient does present with these symptoms, a chest x-ray or CT scan is usually performed. If an abnormality is detected, sputum cytology or a biopsy is done to confirm the presence of malignant cells. In the case of a positive diagnosis, further imaging is performed, often an ultrasound or PET scan, to assess the extent to which the cancer has metastasized. All of this information is then used to assign the stage of the cancer, characterize the type of tumor, and prepare a treatment plan.

**Estimated New Cases**

| | Males | | | Females | |
|---|---|---|---|---|---|
| Prostate | 220,800 | 26% | | Breast | 231,840 | 29% |
| Lung & bronchus | 115,610 | 14% | | Lung & bronchus | 105,590 | 13% |
| Colon & rectum | 69,090 | 8% | | Colon & rectum | 63,610 | 8% |
| Urinary bladder | 56,320 | 7% | | Uterine corpus | 54,870 | 7% |
| Melanoma of the skin | 42,670 | 5% | | Thyroid | 47,230 | 6% |
| Non-Hodgkin lymphoma | 39,850 | 5% | | Non-Hodgkin lymphoma | 32,000 | 4% |
| Kidney & renal pelvis | 38,270 | 5% | | Melanoma of the skin | 31,200 | 4% |
| Oral cavity & pharynx | 32,670 | 4% | | Pancreas | 24,120 | 3% |
| Leukemia | 30,900 | 4% | | Leukemia | 23,370 | 3% |
| Liver & intrahepatic bile duct | 25,510 | 3% | | Kidney & renal pelvis | 23,290 | 3% |
| **All Sites** | **848,200** | **100%** | | **All Sites** | **810,170** | **100%** |

**Estimated Deaths**

| | Males | | | Females | |
|---|---|---|---|---|---|
| Lung & bronchus | 86,380 | 28% | | Lung & bronchus | 71,660 | 26% |
| Prostate | 27,540 | 9% | | Breast | 40,290 | 15% |
| Colon & rectum | 26,100 | 8% | | Colon & rectum | 23,600 | 9% |
| Pancreas | 20,710 | 7% | | Pancreas | 19,850 | 7% |
| Liver & intrahepatic bile duct | 17,030 | 5% | | Ovary | 14,180 | 5% |
| Leukemia | 14,210 | 5% | | Leukemia | 10,240 | 4% |
| Esophagus | 12,600 | 4% | | Uterine corpus | 10,170 | 4% |
| Urinary bladder | 11,510 | 4% | | Non-Hodgkin lymphoma | 8,310 | 3% |
| Non-Hodgkin lymphoma | 11,480 | 4% | | Liver & intrahepatic bile duct | 7,520 | 3% |
| Kidney & renal pelvis | 9,070 | 3% | | Brain & other nervous system | 6,380 | 2% |
| **All Sites** | **312,150** | **100%** | | **All Sites** | **277,280** | **100%** |

**Figure 1.1 Estimated cases and deaths of the top ten cancers observed in men and women in the United States in 2013**. Lung cancer is the second most common malignancy and the most common cause of cancer-related death in both sexes. Published with permissions from [4].

As with most cancers, lung tumors are classified by stage upon diagnosis. About 15% of lung cancers are diagnosed at stage I, before the tumor has metastasized [2]. These tumors can be removed surgically by specific tumor resection or lobectomy, the removal of a lobe of one lung [5]. These patients are usually treated with doublet chemotherapy (cisplatin-gemcitabine, carboplatin-paclitaxel, or carboplatin-docetaxel) and external radiation as well

[5]. A common measure of treatment success is the percentage of patients that survive for five years upon diagnosis. Lung cancer patients diagnosed at stage I have a 54% five year survival rate [2].

An estimated 22% of lung tumors are detected at stage II or III. These tumors have spread locally within the lung or to both lungs at the time of diagnosis. Depending on the degree of metastasis, patients in this category may or may not be candidates for surgical resection by lobectomy or pneumonectomy (removal of an entire lung). Patients diagnosed at this stage usually receive radiation and doublet therapy as well [5, 6]. Unfortunately, these patients often progress to late stage lung cancer, and only about 27% of these patients survive to five years [2].

The symptoms of lung cancer often do not develop until the cancer has metastasized. Therefore, over half of lung cancers go undiagnosed until the tumors have reached stage IV, defined as metastasis to distant organs. The most common sites of metastasis are the brain, liver, or bone [1, 3]. These cancers cannot be removed by surgical means, and patients diagnosed at stage IV are generally given palliative treatment. The goal of treatment in this case is to improve quality of life for the patient and slow tumor progression. Chemo/radiation combination therapy or targeted therapies are most often used in these situations [5]. Many patients enroll in clinical trials for new drugs at this point, particularly if chemotherapy and radiation have failed [6]. Patients diagnosed at this advanced stage of disease demonstrate a 4% five year survival rate [2].

## Lung Cancer Patient Demographics

### *Smoking Status*

Lung cancer is most often thought of as a smoker's disease. Indeed, nearly 90% of cases are attributed to tobacco use. Smoking increases the risk of lung cancer by 23-fold in men and 13-fold in women [7]. Rates of lung cancer related deaths closely mirror smoking prevalence with a roughly 25 year delay [8]. Smoking rates peaked in the early 1970s in the United States, and a subsequent plateau of lung cancer related deaths was observed in the early to mid 1990s [9]. Lung cancer patients are often divided into never-smokers and ever-smokers. Never-smokers are defined as patients who have smoked fewer than 100 cigarettes in their lifetime, and ever-smokers are those who have exceeded that threshold [10]. Ever-smokers are often further subdivided into former and current smokers. Significant variation is seen among these patients. Smoking behavior is often quantified in pack-years. These are calculated by multiplying the number of packs smoked in a day with the number of years a patient smoked. However, there are no official definitions for "light" and "heavy" smokers. There is no known threshold beneath which tobacco use is considered safe [2].

While smoking status is the most established risk factor for the development of lung cancer, the World Health Organization estimates that 25% of patients diagnosed with lung cancer are never-smokers [10]. The demographics of non-smokers with lung cancer vary significantly by gender and geographical location. Worldwide, about 15% of male and 53% of female lung cancer patients are never-smokers. In the United States, 10% of men and 20% of women diagnosed with lung cancer have never smoked. In contrast, over 50% of female lung cancer patients in Southeast Asia are never-smokers. These differences are often

attributed to the low rates of smoking among women, particularly in Asian countries. Some studies have also shown that the rate of lung cancer diagnoses among nonsmokers is increasing in Asia [9]. However, a large-scale meta-analysis of 23 studies performed between 1960 and 2004 showed no change within this time period in lung cancer incidence or mortality among never-smokers in the United States [11].

For never-smokers, exposure to environmental tobacco smoke (ETS) is a major risk factor for lung cancer development. Elevated levels of tobacco related carcinogens are found in the blood and urine of spouses and children of smokers [12]. These levels correlate to the degree of ETS experienced. ETS exposure is estimated to result in 3000-5000 lung cancer deaths each year in the United States [7, 9, 10, 13]. Other major risk factors include radon exposure, air pollution levels, and genetic pre-disposition [7, 9]. Several studies have concluded that tuberculosis infection increases the risk of lung cancer independently of smoking status [14, 15]. Hormone replacement therapies in post-menopausal women and infections of certain human papillomaviruses in both men and women have also been reported to increase the risk of lung cancer [13, 16, 17]. However, studies provide conflicting conclusions as to the significance of these factors [17-19]. Exposure to polycyclic aromatic hydrocarbons (PAHs) also increases the risk of lung cancer [7, 10]. PAHs are produced by cooking techniques that heat oils to very high temperatures like stir-frying and deep-frying, or by burning fossil fuels. High environmental PAH levels are often cited as a major risk factor for women in Asia where coal is often used as fuel for cooking in poorly ventilated kitchens. One study found that women in China who prepare meals every day are 3-8 times more likely to be diagnosed with lung cancer than women who never cook [20].

*Histology*

In addition to patient demographics, lung cancers can also be classified by tumor characteristics. Lung cancer is divided into two main categories, small cell lung cancer (SCLC) and non-small cell lung cancer (NSCLC). Small cell lung cancers originate from neuroendocrine cells in the bronchi and account for about 15% of all lung cancer diagnoses [2]. SCLCs occur almost exclusively in smokers [9]. The remaining 85% of lung cancers are designated as NSCLC and originate from many different progenitor cell types. NSCLC is further subdivided by histological features into adenocarcinoma, squamous cell carcinoma (SCC), and large cell carcinoma (LCC). These categories account for roughly 40%, 25%, and 15% of lung cancers respectively [2]. SCCs are usually seen at the proximal airways while adenocarcinomas originate at more distal locations, leading to speculation that tumors of different histologies arise from different progenitor cell types. However, researchers have been unable to conclusively identify a specific cell of origin for any of the NSCLC sub-classifications [21]. Unfortunately, these histological categories have done little to aid in treatment of NSCLC. Recently, histological analysis has often been used to triage tumor samples for further testing for molecular biomarkers.

*Mutation Status/Molecular Biomarkers*

In the last decade, several molecular biomarkers have been discovered that allow for personalized treatment of lung tumors. These biomarkers include mutations in epidermal growth factor receptor (EGFR), a receptor tyrosine kinase (RTK), and the small GTPase V-Ki-Ras2 Kirsten rat sarcoma viral oncogene homolog (K-Ras). Another common tumor

driving mutation is a chromosomal rearrangement that produces a fusion protein of echinoderm microtubule-associated protein-like 4 (EML4) and anaplastic lymphoma kinase (ALK). Small molecule inhibitors that specifically treat EGFR and EML4-ALK mutated tumors are already in the clinic, and several inhibitors for mutant K-Ras are in pre-clinical development. Several other mutations have been identified as putative biomarkers and are under investigation as drug targets. However, our current knowledge of biomarkers that contribute to tumorigenesis covers just over half of NSCLC patients. Efforts are being made on a large scale to expand our knowledge of tumor biomarkers by identification of changes in protein expression and genetic mutations that drive tumorigenesis.

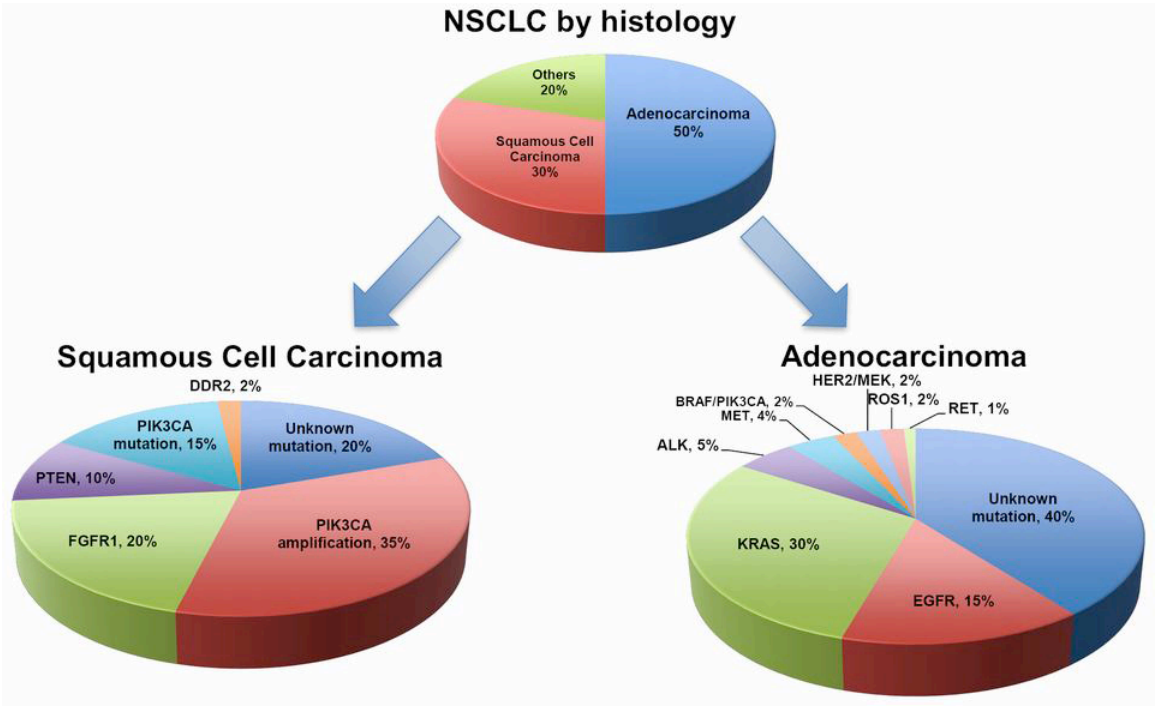


**Figure 1.2 Summary of major NSCLC classifications by histology and molecular biomarkers**. Simple classification by histological features does not sufficiently characterize a tumor for effective treatment. Many driver mutations have been identified, and chemotherapeutics are under development for each of these. However, a large fraction of tumors do not harbor any of the known mutations. Published with permissions from [22].

Mutations in the tyrosine-kinase domain of EGFR are among the most common "driver" mutations found in lung cancer patients. A variety of abnormalities including deletions and single nucleotide substitutions can occur in the tyrosine kinase domain of EGFR. These mutations lead to constitutively active EGFR signaling [23]. EGFR is mutated in 50% of Asian patients and 15% of American patients [24]. Mutant EGFR is almost always seen in adenocarcinomas. Amplifications of the EGFR gene leading to over-expression are detected in 7% of SCCs [24]. These mutations are more commonly These mutations are more commonly found in female patients and never-smokers [25].

Several small molecule tyrosine-kinase inhibitors (TKIs) have been approved for use in NSCLC cases including erlotinib, gefitinib, and afatinib. These drugs produce a response rate of approximately 70% in EGFR mutant tumors, with significant improvement in progression free survival (PFS) compared to traditional chemotherapy. Unfortunately, these drugs do not improve the overall survival. EGFR inhibitors do not increase median survival times due to resistance that usually develops within one year of treatment [25]. About half of tumors that become resistant do so through a single base substitution to produce the T790M mutation [26]. The T790M mutation is often referred to as a "gatekeeper" mutation. This residue substitution sterically prevents binding of the inhibitor to EGFR while increasing its affinity for ATP [27]. This precludes efficacy of ATP-competitive TKIs. Amplification of other RTKs such as HER2 [28] and Met [29] has also been observed to overcome EGFR inhibition, as well as constitutive activation of B-Raf, a kinase that functions downstream of many RTKs to promote growth and survival [30].

The EML4-ALK fusion protein is produced by an inversion in chromosome 2p [31]. The EML4 fusion partner facilitates dimerization of the fusion protein, leading to constitutive activation of ALK. This mutation is seen in 3 to 6% of NSCLC patients in the United States, and is more common in younger patients, never smokers, and in adenocarcinomas [32, 33]. Rare variations of this inversion producing fusions of ALK with other dimerizing partners have also been observed [34, 35].

The TKI crizotinib inhibits both ALK and Met, and has been clinically approved for the treatment of NSCLC. In phase III trials in patients positive for ALK re-arrangement, crizotinib demonstrated significant increases in median PFS (7.7 months) compared to chemotherapy plus pemetrexed or docetaxel (3.0 months) [36]. Crizotinib also showed improvement in overall survival with a hazard ratio for progression or death of 0.49.

Unfortunately, many tumors acquire resistance to crizotinib, often within one year [25]. About half of patients that develop resistance to crizotinib have activating mutation in EGFR or other RTKs, bypassing the ALK pathway [37]. Another 25% of patients had secondary activating mutations in ALK or amplifications of the fusion gene. A mutation at L1196M has been found to be a gatekeeper mutation against crizotinib in a similar manner to the T790M mutation in EGFR against erlotinib and gefitinib [38]. Several second and third generation ALK TKIs that overcome various resistance mechanisms are under development [25].

Activating mutations of amino acid 12 of the small GTPase KRas are seen in roughly 30% of NSCLC patients in the United States [24]. These mutations are more common in smokers and former smokers than in never-smokers [10]. However, KRas mutations are seen

in 10-15% of never smoking patients. The mutational profile of KRas differs depending on smoking status with G12T substitutions most commonly seen in ever-smokers and G12A mutations observed in never-smokers [39]. It has also been observed that tumors with KRas mutations almost never harbor activating mutations in EGFR and vice versa [40]. For decades, KRas was regarded as an undruggable target due to close sequence and structural similarity to other GTPases. In recent years, efforts have been made to indirectly target mutant KRas. Strategies include blocking interactions of KRas with guanine nucleotide exchange factors, inhibition of signaling factors downstream of KRas, and inhibition of post-translational processing of Ras family members [40]. As a result of these efforts, several small molecule inhibitors are in pre-clinical studies for the treatment of tumors harboring KRas mutations. As of yet, none of these drugs have reached clinical trials.

Many other mutations have been identified as driver mutations of NSCLC. These abnormalities are rare in comparison to previously discussed mutations, and our knowledge of the role of each of these mutations is limited. Met is amplified in 1-11% of NSCLCs, most often in SCC, and is a marker of poor prognosis [41]. The small molecule crizotinib, used in EML4-ALK re-arranged patients, also inhibits Met activity [42]. ROS1 and RET are proto-oncogenes that form active fusion proteins in the same manner as ALK when involved in chromosomal re-arrangements [43, 44]. Both of these mutations are seen in about 2% of patients, mostly young non-smokers with adenocarcinomas. FGFR1 has been seen to be amplified in 21% of SCCs and 3% of adenocarcinomas [45]. The broad-target TKI ponatinib inhibits FGFR1, but significant side effects limit the use of the drug [46].

Several abnormalities common to all cancers are also seen in NSCLC. The small GTPase BRaf is mutated in 2% of NSCLC patients [47]. Roughly half of these mutations are the well-studied V600E substitution [48]. HER2 mutations have been observed in 1-2% of patients, most often female non-smokers [49]. Loss-of-function mutations in the phosphatase PTEN have been observed in 2% of adenocarcinomas and 10% of SCCs [41]. PIK3CA, a member of the PI3K family, is mutated in about 10% of SCCs [41, 50]. The discoidin domain receptor 2 is mutated in nearly 4% of SCCs [51]. Targeted therapies for the treatment of tumors harboring these mutations are available or under development. Unfortunately, outside of the KRas/EGFR mutual exclusivity, many of these mutations co-exist within tumors. As of yet, roughly half of NSCLC patients in the United States do not have any of the known driver mutations [52].

**Targeting Ligands for the Characterization and Treatment of NSCLC**

The standard of care for the majority of NSCLC patients has been doublet therapy consisting of a platinum-based DNA damaging agent and a taxane microtubule stabilizer [5]. These are cell cycle specific cytotoxins, meaning that they are only toxic to dividing cells. Doublet therapy kills tumor cells efficiently because they divide so rapidly. However, many cell types divide at nearly the same rate including immune cells, epithelia of the digestive tract, and hepatocytes. This results in a very narrow “therapeutic window,” or the difference between a therapeutically effective dose and the dose that produces adverse side effects. Toxicity in these healthy cells results in severe side effects, limiting the administration of doublet therapy drugs and reducing quality of life for patients. Doublet chemotherapy is

therefore administered at the maximum tolerated dose for each individual patient. Unfortunately, this dosage is often insufficient to produce complete remission of tumors [24]. Surviving cancer cells are then able to metastasize and are frequently resistant to further chemotherapy treatments [25].

Targeting tumor cells more specifically decreases toxicity in healthy tissues, expanding the therapeutic window. This reduces side effects and allows oncologists to increase dosage to improve efficacy of treatment. Two major strategies have been employed to produce tumor specific cancer treatments. These are referred to as "targeted" therapies and "targeting" therapies. Targeted therapies inhibit pathways that are highly upregulated in malignant cells compared to normal cells. Sometimes targeted therapies specifically inhibit common mutants of proteins involved in tumor development. Several targeted therapies against known NSCLC molecular biomarkers were discussed in the previous section. These agents are already used clinically in cases of advanced stage NSCLC and have produced improvement in patient quality of life. However, tumors regularly develop resistance to targeted therapies. On average, targeted cancer therapies have had little effect on overall survival rates when compared to traditional chemotherapy [3, 25].

In contrast, targeting therapies utilize compounds that are much more generally toxic to all cell types. These potently cytotoxic agents are directed to the tumor by conjugation to a targeting ligand or delivery vehicle that produces accumulation of the drug in the tumors. Research into targeting therapies also allows for improvement of diagnostic and characterization of NSCLCs. The same targeting moieties used to direct drugs might also be conjugated to imaging agents. As will be discussed later, the identification of targeting

ligands can lead to a better understanding of the biology of NSCLC and other cancers. Targeting therapies are a newer field in cancer research and have not made as much progress into the clinic as targeted therapies. However, several are in clinical and pre-clinical development.

The nature of targeted and targeting therapies does require at least some level of personalization for each patient [25]. Each tumor relies on a unique set of mutations and signaling pathways to grow and invade normal tissue. Because of this, no one agent will be effective in treating all tumors, even within tumor types. In addition, the genetic instability of cancer cells produces heterogeneity within each tumor. A large repertoire of targeted and targeting therapies will be necessary to cover the treatment of all patients. These therapies can then be used in combinations to optimally treat each case. Both targeted and targeting therapies show great potential for improvement upon current treatment of NSCLC, particularly when used in concert. This dissertation focuses on the development of a peptide targeting ligand for purposes in imaging and treating NSCLC.

Most targeting therapies currently in development produce tumor-specific activity by interacting with receptors within the tumor. Receptors can be expressed on the cancer cells themselves or in the tumor microenvironment. Different types of receptors can be used to deliver different types of payloads. For example, CD-30 is expressed on the surface of malignant cells in large cell anaplastic lymphoma and Hodgkin's lymphoma [53]. The monoclonal antibody Brentuximab against CD-30 has been used to deliver drugs that act directly on tumor cells [54]. By contrast, the integrin $\alpha_v\beta_3$ is expressed by endothelial cells in the tumor vasculature [55]. Small peptides that contain the sequence RGD, such as

cilengitide, bind to $\alpha_v\beta_3$ and specifically deliver imaging agents or radiotherapeutics to tumors [56, 57].

Antibodies, peptides, and small molecules are all used as targeting moieties for therapeutics and imaging agents. These homing ligands are developed through a variety of methodologies. Tumor receptors may be known before development or identified later depending on the methods used to select the targeting ligand. Each of the categories of targeting ligands presents advantages and disadvantages (See Table 1.1). These will be discussed in the following sections.

| Monoclonal Antibodies | Peptides | Small Molecules |
|---|---|---|
| High Affinity | High Affinity | Moderate affinity |
| High Specifity | High Specificity | Low Specificity |
| Long circulation time | Short circulation time | Short circulation time |
| High MW (160 kDa) – low tumor penetration | Low MW (0.5-15 kDa) – penetrates tumors well | Low MW – penetrates tumors well |
| Produced in biological systems | Chemically synthesized | Chemically synthesized |
| Difficult to modify | Straightforward modification and optimization | Require significant investment in medicinal chemistry optimization |
| Most Expensive | Moderate Costs | Low Cost |
| Bevacizumab, Trastuzumab, Cetuximab, many others | Somatostatin, Bombesin, AgRP, RGD peptides | Folate, Fluorodeoxyglucose (FDG) |

**Table 1.1 Advantages and disadvantages of various targeting ligands.**

*Antibody Targeting Ligands*

At this point, monoclonal antibodies are the gold standard in the targeting field [54]. They bind their target receptors with affinities in the mid to high picomolar range. This high affinity produces efficient accumulation of the cargo within target tissue. Because of the manner in which they are produced, antibodies are highly specific for their target receptors,

lowering the risk of accumulation in off target tissues. Antibodies also bind to serum albumin when in circulation [58]. This interaction protects antibodies from degradation and delays clearance from the body through excretion, resulting in long circulation times. A typical monoclonal antibody demonstrates an *in vivo* half-life of 3 weeks. The stability of monoclonal antibodies ensures that targeting will be maintained of highly stable payload molecules.

Monoclonal antibodies are produced by immunization of animals using the target receptor as an antigen [54]. After several weeks, the animals are sacrificed, and their splenocytes are isolated. The splenocytes are then fused to myeloma cells to produce thousands of individual hybridomas, each producing a unique antibody. The conditioned media from each hybridoma is then assayed for the presence of an antibody that binds to the target receptor. This entire process often takes months or even years.

In addition, the animal source of these antibodies prevents the direct use of the selected antibody in the clinic [59]. A patient's immune system would recognize the foreign antibody and mount a response against it before any therapeutic benefits are produced. Monoclonal antibodies must therefore be "humanized" to replace regions unique to the host organism with those a human immune system will recognize as "self". Manufacturing and quality control are also difficult as the hybridoma models used to produce monoclonal antibodies can be unpredictable, and complex post-translational modification patterns must be maintained. This complex development and manufacturing process results in very high costs in the production of monoclonal antibodies as drugs. A single course of treatment with the monoclonal antibodies currently in the clinic costs an average of $100,000 [60].

Because the target tumor receptor is used as an antigen in the initial steps of monoclonal antibody development, the receptor must be known ahead of time. Expression of these receptors must be highly specific to tumors to avoid toxicity to other off target tissues. Generally, tumor receptors selected as antigens for therapeutic antigens must be well characterized, such as HER2, and RTK expressed in about 20% of breast cancers. HER2 had been studied as a target for breast cancer treatment for decades before trastuzumab was developed against it [28, 49].

Most of the monoclonal antibodies currently used in the clinic are not conjugated to cargo [54, 58]. They produce their therapeutic effects by antibody dependent cell-mediated cytotoxicity (ADCC) or by inhibition of signaling by their target receptors. Indeed, the two monoclonal antibodies currently approved for use in NSCLC patients are unconjugated [61]. Bevacizumab binds to vascular epithelial growth factor (VEGF) and prevents interaction with its receptor [62]. Cetuximab functions by blocking EGFR signaling and inducing ADCC [63]. However, ADCC requires interaction between the therapeutic antibody and Fc receptors on the surface of natural killer cells, macrophages, or other immune effector cells. The effector cells then release cytokines and other toxic agents to kill the pathogenic cell. These events are dependent on the glycosylation pattern of the Fc region of the therapeutic antibody and polymorphisms in the Fc receptors, leading to variable response rates among patients.

In order to deliver cargo to a tumor, antibodies must be conjugated to payload molecules to function as delivery ligands. Regioselective chemistry is necessary to attach payload molecules without interfering with the binding regions of the antibody. This can be difficult as antibodies are such large, complex molecules with many reactive functional

groups. In spite of these problems, the high affinity and specificity of monoclonal antibodies, as well as their favorable pharmacokinetic properties, has led several groups to invest significant efforts into their development as targeting ligands.

To date, four monoclonal antibodies have been developed as targeting delivery agents of cancer therapeutics. Gemtuzumab delivers calicheamicin, an immunotoxin, to CD-33 positive acute myeloid leukemias. Ibritumomab and tositumomab are both used to target radiotherapies ($^{90}$Y and $^{131}$I, respectively) to CD-20 positive non-Hodgkin's lymphomas. Brentuximab is used to deliver auristatin, a potent cytotoxin, to CD-30 expressing lymphoma cells. It is notable that none of these antibodies are indicated for use in solid tumors. This is likely due to low penetration of the targeted drugs into the tumor. Monoclonal antibodies have a total molecular weight of around 150 kDa. Large molecules and nanoparticles are becoming notorious for becoming trapped near the vasculature, preventing distribution of the payload therapeutic throughout the tumor [64].

Current efforts to utilize monoclonal antibodies as delivery ligands have shifted to the use of antibody fragments. Many groups are looking to optimize the size of the antibody fragment used to maximize penetration into solid tumors while maintaining affinity and *in vivo* half-life [65, 66]. These fragments, if they are single-chain polypeptides, may also be produced using recombinant gene expression rather than isolation from hybridomas. Reducing the size and complexity of the targeting moiety may also simplify conjugation of the payload drug. This would have the added benefit of increasing production efficiency while significantly reducing costs.

*Small Molecule Targeting Ligands*

Small molecules have not been used extensively as targeting ligands for therapeutic applications, but they are among the most common targeting moieties for imaging purposes. Small molecules are inexpensive to manufacture, penetrate tissue efficiently, and usually are cleared quickly through the kidneys or by metabolic processes. These are ideal qualities for imaging agents. Most small molecule drugs have binding affinities well below what is necessary for a specific targeting moiety. However, there are a few notable exceptions.

By far, the most common small molecule used as a targeting agent is folate. Folate receptor α (FRα) is expressed on the luminal surface of polarized epithelia and in many different cancers [67]. Of particular interest, FRα is expressed at significant levels in 82% of ovarian cancers [68], 74% of renal cancers [67, 69], 64% of endometrial cancers [70], 56% of colorectal cancers [69, 71], 56% of breast cancers [69, 72], and 81% of NSCLCs [73, 74]. In most normal tissue, the sub-cellular localization of the receptor prevents interaction with injected folate conjugates [71]. There are three other folate receptors with much broader tissue expression profiles [75]. However, these bind the reduced tetrahydrofolate with a high degree of specificity. These qualities allow for specific targeting to tumors. Folate targeting has generated quite a bit of excitement in recent years. Folate has been used in clinical trials to specifically deliver fluorescent dyes to tumors during surgical resection [76]. Specialized cameras are then used to detect fluorescent cells and improve cytoreduction. Folate has also been used in pre-clinical experiments to deliver toxins, radiotherapies, and single-photon emission computed tomography (SPECT) imaging agents [77-79].

While many of these studies are promising, no long-term biodistribution studies have been performed with folate-targeted molecules. SPECT imaging shows that a significant amount of accumulation in the kidneys at 1 hour post-injection [79]. This is usually dismissed as clearance through the kidney. It has also been suggested that folate-conjugated payloads would be recycled back into circulation following established folate reabsorption pathways in the proximal tubules [77]. However, as will be discussed in detail in the next section, many targeting ligands that accumulate in the kidneys are retained there for days [80]. It is also possible that the folate conjugate may degrade in the lysosome upon internalization in the proximal tubules. This would allow for re-circulation of the folate but leave its cargo trapped in the epithelial cells and lead to renal toxicity. Because this effect would be the result of the specific interaction of folate with its receptor, FRα, it seems unlikely that these obstacles could be avoided while maintaining targeting capacity of folate conjugates and complicates the use of folate to deliver toxic cargoes [67]. It may not, however, be an issue for imaging applications.

A few other small molecule ligands are under development including DUPA, an inhibitor of prostate specific membrane antigen, and ligands of carbonic anhydrase IX (CAIX) [81, 82]. These are in the very early stages of pre-clinical development and are, in fact, peptidomimetic analogs of naturally occurring peptides. Both DUPA and the presented CAIX ligands have affinities for their receptors of about 10 nM. However, Whether these analogs will demonstrate the same *in vivo* targeting abilities as their peptide counterparts or monoclonal antibodies remains to be seen.

*Peptide Targeting Ligands*

Peptides were first approved for use in cancer patients in the late 1980s. Leuprolide and goserelin, peptide agonists of gonadotropin releasing hormone (GnRH) receptors were found to decrease secretion of luteinizing hormone and follicle stimulating hormone from the pituitary [83]. This resulted in lower levels of androgen production, and was therefore used as androgen deprivation therapy for prostate cancer [84]. Shortly thereafter, antagonists of LHRH were developed which provide dose-dependent control of androgen levels, and cetrorelix was soon approved [85]. Since then, two peptide analog drugs have been approved for oncological purposes; bortezomib for treatment of multiple myeloma and the somatostatin analog octreotide for growth hormone producing tumors [86, 87]. Another peptide analog, mifamurtide, has been approved in Europe for the treatment of osteosarcomas [88]. However, mifamurtide was denied approval by the FDA. These peptides perform their therapeutic functions by directly acting as agonists or antagonists of their receptors.

One peptide-targeted imaging agent has been approved for clinical use. Growth hormone producing tumors are characterized by SPECT imaging with pentetreotide [89]. Pentetreotide consists of octreotide conjugated to the chelating agent diethylene-triaminepentaacetic acid (DTPA) loaded with an $^{111}$In atom. Recently octreotide has been modified for improved affinity and *in vivo* stability [90]. The most recent iteration, dubbed octreotate, is in clinical or pre-clinical trials for delivery $^{111}$In for SPECT imaging, as well as $^{90}$Y and $^{177}$Lu for peptide receptor radionuclide therapy (PRRT). Efforts to utilize octreotide, octreotate, and several other analogs of somatostatin as positron emission tomography (PET) imaging agents using $^{68}$Ga or $^{64}$Cu are also underway [91].

Several peptides have been developed as imaging agents for neuroendocrine tumors. Bombesin, an analog of gastrin-releasing peptide (GRP), has also reached clinical use in the imaging of tumors expressing the GRP receptor (GRPR) [92, 93]. GRPR is expressed in several neuroendocrine cancers including 53% of SCLCs [94]. Interestingly, GRPR is also found in 62% of NSCLC, much higher than one would expect from tumors of epithelial origin. Derivatives of neurotensin and neuropeptide Y have also been proposed as potential targeting ligands for imaging tumors with neuroendocrine-like characteristics [95]. Expression of neurotensin receptors has been observed in 59.7% of stage I pulmonary adenocarcinomas and is strongly correlated to lower 5-year survival rates [96].

It is important to note that none of the peptides discussed so far are internalized into their target cells. These peptides generally interact with G-protein coupled receptors that do not participate in receptor-mediated endocytosis (RME). These peptide hormone analogs function well as targeting ligands for radiotherapy. However, most cytotoxic drugs must interact with intracellular targets. Thus, new peptide ligands that induce RME are needed for effective delivery of therapeutics. This dissertation covers the development of one such peptide ligand.

## Development of Peptidic Targeting Ligands for Applications Against NSCLC

### *Selection of Peptides by Phage Display Biopanning*

Most novel peptides currently under development were identified using some form of phage display biopanning. Gray and Brown provide a thorough discussion of the various types of phage display used to select peptide ligands in their review [97]. The major

variations seen in different forms of phage display biopanning lie in the choice of the target. Briefly, phage display selection is achieved by applying a large library of bacteriophage, each displaying a unique peptide sequence fused to one of the viral coat proteins, to any of

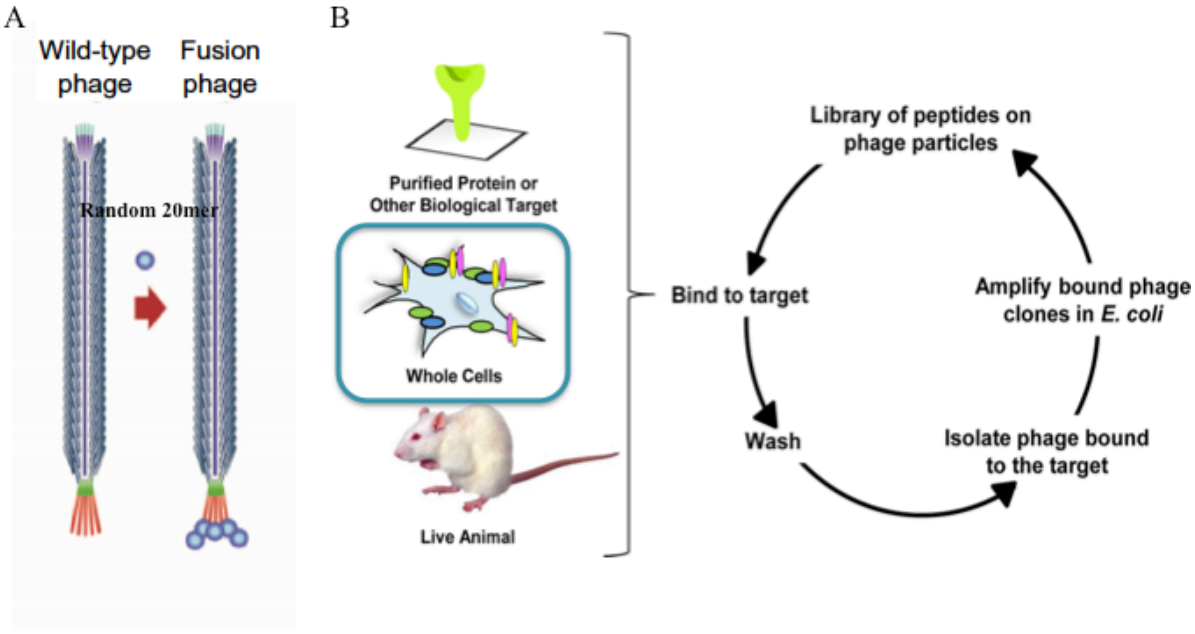


**Figure 1.3 Phage Display Biopanning for Peptidic Targeting Ligands. A)** A schematic of M13 bacteriophage commonly used in phage display indicating placement of random peptide sequences on PIII**.** Modified with permissions from [98]. **B)** A simplified protocol illustrating the basic steps of phage display biopanning. Modified with permissions from [99].

various targets. These libraries are genetically engineered so that each phage particle carries multiple copies of the same peptide sequence, usually between 10 and 30 amino acids in length [98]. The bacteriophages used do not exhibit tropism toward human cells, and thus, any binding interactions observed must be a result of peptide behavior. Phages that bind to the target are collected and amplified in the phage's host bacteria. Because the phenotype of binding the target corresponds directly to the phage genotype, peptide sequences that lead to target binding can be easily identified through DNA sequencing. After 3-7 iterations of the

selection/ amplification process, the recovered bacteriophages generally converge on one or a few different peptide sequences.

These peptide sequences are then validated by determination of their selectivity values. That is, the comparison of the affinity of an isolated bacteriophage for its target with a control phage. Of course, to function as targeting agents, the peptides must bind their targets outside the context of the bacteriophage. Thus, further validation is achieved by chemical synthesis of the peptide and assessment of binding affinity. Control peptides, comprised of the same amino acids in a scrambled sequence are used to determine if the binding interaction is sequence dependent or merely the result of nonspecific charge or hydrophobic interactions.

For most *in vitro* panning, well-studied cancer targets are used [97]. The phage library is applied to plates coated with purified target protein. After incubation and washing, bound phages are eluted and amplified in their host bacteria. This technique has been used extensively to produce potential targeting peptides for cancer and other diseases. However, it does have several problems. Expression of integral membrane proteins with their complex post-translational modifications, as well as purification of these proteins in their native state is notoriously challenging. It is also technically difficult to control the orientation of the target protein when adsorbed to a surface. As a result, selected peptides may interact with a region of the target protein that would not be available in a physiological setting. Also, the cell-free conditions give no selective pressure for peptides that induce internalization into a target cell. Target receptors known to participate in RME are often chosen for this biopanning method. However, there is no guarantee that the peptide-receptor interaction

selection would trigger RME. Few of the peptides identified in this manner have sufficiently high affinity to be clinically useful.

In response to these difficulties, many groups have developed methods for selection of ligands against unknown cellular receptors. Large peptide libraries containing tens of millions of unique random peptide sequences are new commercially available. *In vivo* panning has also become popular in the field of solid tumors. Since the ultimate goal is to target tumor tissue in a patient, it is logical to design selections to identify peptides that function *in vivo* [100]. These biopanning procedures involve intravenous injection of phage libraries into mice bearing xenograft tumors. The whole tumor is then collected and homogenized. The lysates are used to infect the bacteriophage host for amplification. Many groups also perform a negative selection against an off-target control before performing positive selection against target cells or proteins. The goal of this negative selection is to ensure the identification of a tumor specific ligand. This type of panning is excellent for selecting peptides for imaging applications and potentially radiotherapy, producing peptides that accumulate rapidly in tumor tissue have high affinity. Importantly, *in vivo* panning does not require prior knowledge of a target receptor. However, peptides identified through *in vivo* phage display may not be appropriate for delivery of chemotherapeutics. Peptides in the bloodstream often bind to targets in the tumor vasculature rather than on the tumor cells themselves. This may preclude distribution of peptide-targeted cargo throughout the tumor. This generally would not affect the quality of imaging, but peptides that do not distribute through tumor tissue and internalize into cells are ineffectual at expanding the therapeutic window of a cytotoxic drug. *In vivo* biopanning also does little to reduce the amount of post-

selection optimization that must be performed after the selection of peptide sequences. Due to factors that will be discussed in later sections, the biodistribution and pharmacokinetics of peptides displayed on a viral particle are very different from those that are chemically synthesized.

Our research group has taken a middle-ground approach to phage display. We perform our selections on human cancer cell lines. This approach allows for selection of ligands for tumor cell specific receptors while maintaining those receptors in a physiologically relevant context. The protocol by which most our lab's cancer-targeting peptides were identified is described in detail [101]. The phage library is incubated with the target cells before washing with saline solution to remove unbound phage. The cells were then washed with low pH solution to remove phage particles that are bound to the cell surface without internalizing into the cell. This biases the selection towards peptides that trigger RME. The cells are then lysed, and the lysates are used to infect host E. coli for amplification of the selected phages. Using this technique, our group has identified several peptides capable of delivering cargo to the inside of NSCLC cells. Similar to *in vivo* biopanning, this method also does not require previous knowledge of cellular receptors. This has allowed us to develop peptides that function as tools for biological study, as well as delivery agents for imaging and therapy of NSCLC.

*In Vitro Development of Selected Peptide Targeting Ligands*

The peptides identified through phage display are essentially lead compounds in the same manner of small molecules identified through high throughput screens. They must be

optimized for affinity, stability, pharmacokinetics, biodistribution, and ease of synthesis. This is the phase of development where peptides outshine monoclonal antibodies due to their relative chemical simplicity. Libraries of peptide analogs, such as the one presented in the next chapters, are straightforward to synthesize. Each research group in the peptide targeting field has their own process by which they optimize peptides for their intended purpose. However, many groups are discovering that exhaustive optimization *in vitro* often does not lead to optimal *in vivo* characteristics [102, 103]. *In vitro* and *in vivo* assays must be used in conjunction to arrive at a clinically useful targeting agent as quickly as possible.

The first steps of optimization are generally the identification of the minimum binding sequence. Commercially available phage libraries display peptides ranging from 7-35 residues in length. Like proteins, peptide interactions often rely on short regions within the whole sequence to interact with binding partners. Simplifying and shortening the sequence decreases manufacturing costs and time. Deletion of unnecessary residues may also improve binding affinity of the peptide by removing steric hindrance. Minimum binding sequences are usually determined by systematic alanine- and deletion scanning until all remaining residues are known to contribute to binding.

Peptides are then optimized for affinity. Most peptides selected by phage display have initial binding affinities in the mid-nanomolar to low micromolar range. Affinity can occasionally be improved by substitution scanning, as in the case of octreotide [104]. Recently, groups have also been developing ways to improve avidity of their peptide ligands by multimerizing peptides on various scaffolds [105-107]. Multimeric peptides could potentially bind to multiple receptors on the cell membrane or bind to repeated motifs on the

same receptor molecule. This approach can produce peptides with affinities in the mid to high picomolar range, as high as a monoclonal antibody. The use of multi-valency has allowed many peptides to become clinically feasible agents.

When optimizing for valency, several aspects must be kept in consideration, such as the overall size of the construct and the length of the linkers between each peptide in the multimer. Increasing the valency of peptide ligands can also impact solubility, although this may be controlled by the choice of linker. For example, hydrophobic peptides may become insoluble in aqueous solution when dimerized or tetramerized. This can be resolved by the addition of polyethylene glycol linkers between the monomeric branches. However, each addition increases the molecular weight of the full construct, which may impact penetration into tumor tissue.

It is important to note that improving affinity does not always improve targeting. Target receptors should be significantly over-expressed in tumor tissue relative to healthy cells. Nevertheless, the receptor will be expressed on off-target cells, ideally in very low copy numbers. An extremely high binding affinity of the peptide for its receptor could lead to off-target accumulation in these healthy cells. Under certain conditions, such as a rapidly recycling receptor, affinity that is too high could also reduce penetration into tumor tissue [108]. In this situation, cells near the vasculature may internalize large amounts of peptide-targeted constructs, preventing the drug or imaging agent from reaching more distal cells. For these reasons, the binding affinity of peptide ligands should be kept to the minimum necessary for effective *in vivo* targeting.

Another concern during peptide sequence optimization is specificity. Lead peptide sequences should be assessed for specificity before substantial resources are invested into optimization. None of the peptides our lab has selected against NSCLC cell lines accumulate in "normal" lung cells in significant amounts. However, as peptide sequences are reduced and modified, specificity must be routinely monitored. Increasing the valency of peptide ligands may also affect specificity as it amplifies weak interactions as well as strong ones. A peptide specific for one member of a protein family as a monomer may start to show binding to other family members as valency increases.

*In Vivo Optimization of Peptide Targeting Ligands*

The *in vivo* characteristics of a potential peptide targeting ligand should be assessed as early as possible in pre-clinical development. Does the peptide accumulate in tumor tissue? For how long is this accumulation observable? Is there significant accumulation in other organs? There are several aspects of targeting that can only be assessed by *in vivo* experimentation including delivery, biodistribution, clearance, metabolism, serum stability, and toxicity. Peptides that function well *in vitro* may be degraded or clear too quickly to be viable candidates for targeting. Off-target accumulation may arise from specific interactions with proteins related to the intended receptor. Metabolic processing may lead to accumulation of peptide conjugates, or some degraded form of them, in the liver. This may ultimately lead to toxicity, especially when a cytotoxic cargo molecule is involved. All of these characteristics are critical when developing targeting agents for clinical use and must be optimized. Modifications to lead targeting peptides may be designed or selected from

combinatorial libraries [109, 110]. During each round of modifications, the potential targeting peptides are usually assessed for binding and specificity using *in vitro* methods. Only those modifications that maintain high affinity and specificity are carried forward into *in vivo* experiments.

The gold standard technique for evaluation of a peptide's behavior in an organism is through radiolabeling. Peptides labeled with tritium or sometimes $^{131}$I are injected into mice intravenously [109]. At some timepoint, usually less than 24 hours, the animals are sacrificed and the radioactivity from the blood and various organs is quantified using a scintillation counter and expressed as percent-injected dose per gram (%ID/g). Peptides intended as PET or SPECT imaging agents are conjugated to bi-functional chelators that are then loaded with the appropriate radioisotopes [103]. Small animal versions of PET (microPET) and SPECT imaging allow for multiple scans of the same animal over several timepoints. Cold peptide can also be administered in competition with radiolabeled constructs. These experiments differentiate between accumulation produced by saturable, sequence specific interactions and more general non-specific uptake. While radiolabelling methods do provide reliable, quantitative data, they are time consuming, technically difficult, and expensive. These experiments are best reserved for later stages of development with peptides that have passed evaluation criteria by other methods.

Near infrared fluorescence (NIRF) imaging is becoming more common as a method of evaluating *in vivo* characteristics of peptide targeted agents [111, 112]. Here, peptide ligands are conjugated to fluorophores emitting in the near infrared region of 700-1000 nm. Photons of energy levels within this region are capable of penetrating tissue, allowing for

whole animal and *ex vivo* organ imaging. Additionally, very little auto-fluorescence has been observed in this range, providing a much higher signal-to-background ratio compared to dyes that fluoresce at low wavelengths. In addition to reduced safety concerns, fluorescent dyes are generally stable when protected from light. This drastically reduces production and usage costs of NIRF imaging in comparison to radiolabeling techniques. Radioactive materials are generally obtainable only on a strict schedule and in small amounts that must be used quickly. This is particularly true of $^{64}$Cu and $^{18}$F with half-lives of 12.7 hours and 109.8 minutes, respectively. Fluorescently labeled peptides can be produced at milligram scales and stored for months without significant degradation. This simplifies workflow and greatly expands the scale of experiments that can be performed. Due to these advantages, I would recommend that *in vivo* optimization of peptide targeting ligands begin with NIRF imaging, and that radiolabeling experiments be performed only with peptides that show the most potential for clinical use.

This dissertation will focus on the optimization of serum stability and biodistribution of a peptide-targeting agent selected for use in NSCLC patients. These features of *in vivo* behavior have proved to be major obstacles for the peptide targeting field overall. The work presented here demonstrates a simple and elegant modification strategy to improve serum stability and biodistribution simultaneously.

## Transitioning Peptidic Ligands Developed *In Vitro* to *In Vivo* Applications

### *Serum Stability of Peptides*

Peptides are notorious for their short half lives in the bloodstream. The earliest peptide drugs, developed in the 1970s, failed to reach the clinic due to inefficacy caused by short *in vivo* half-life [107]. Peptides and proteins are degraded within the bloodstream by serum peptidases and proteases. Because peptides are so short, they rarely contain cleavage sites for serum proteases within their sequences. The major sources of peptide degradation arise from amino- and carboxy-peptidases, which break down peptides from the termini, one residue at a time [103, 110]. These peptidases degrade most peptides so quickly that *in vitro* serum stability assays must be performed in 10% or 25% serum in order for intact peptide to be observed and quantified. Several strategies have been employed to increase the *in vivo* stability of peptide constructs.

Because peptides are generally degraded from the termini, several groups have sought to increase stability by protecting terminal residues from serum peptidases. Several naturally occurring peptides are post-translationally modified to prevent their degradation in this manner as well. In these cases, the N-terminus may be acetylated, the C-terminus may be amidated, or both [113, 114]. These additions preclude binding of peptidases to the terminal residues, shielding the entire peptide from degradation. The addition of unnatural residues, such as D-amino acids, at either or both termini often significantly extends the *in vitro* half-life of peptides in a similar manner [114-116]. Other modifications such as the addition of polyethylene glycol (PEG) polymers or the incorporation of serum albumin binding motifs have been published as well [92, 114, 117-119]. Each of these methods must be tested

empirically as any or all of these modifications may negatively impact binding affinity or specificity of the peptide ligand for its target if the free termini are involved in the binding interaction. Modifications that involve large mass additions, such as PEGylation or the addition of an albumin binding sequence may also restrict penetration of the peptide into tumor tissue [114].

An alternative to protection of the termini is to eliminate them altogether. Cyclic peptides have become increasingly popular over the last decade [107, 114, 120]. Initially, efforts to develop cyclic peptide ligands involved cyclization of peptides that had been originally selected as a linear molecule. This was originally intended to reduce entropy of linear peptides and improve affinity. These attempts met with limited success. Recently, several phage display libraries for selection of cyclic peptides have become commercially available. New peptide synthesis methods have also been introduced to simplify the manufacture of these selected peptides [121]. Many cyclic peptides are finding success in clinical and pre-clinical studies, but they do still carry some drawbacks. Cyclization restricts the conformations a peptide ligand may take, especially for peptides with only a few residues. This restriction may limit the binding affinity achievable against a certain target receptor. Elimination of the termini also removes two functional groups that may otherwise be used to conjugate the peptide to its cargo or to a multivalent core.

*Overview of Factors that Affect Biodistribution*

Several factors impact the overall biodistribution of a given peptide upon systemic administration into an animal. Most obvious of these is the affinity of the peptide for its

receptor. The targeting ligand must bind its receptor with sufficient affinity to produce accumulation of the conjugated payload in the target tissue. This is generally in the mid to low nanomolar range, depending on expression levels of the receptor in tumor cells. However, binding affinity that is too high may be detrimental to targeting. It is virtually guaranteed that the target receptor will be expressed to some degree in non-target tissue. Even if expression in healthy cells is low, peptides that bind with extremely high affinity may exhibit significant binding to these cells. Additionally, increasing affinity of a peptide for its receptor will likely increase its affinity to any closely related proteins with potentially very different expression profiles.

| Attribute | Effects |
|---|---|
| Size | Filtration in kidney and clearance, dispersion into tumor tissue |
| Charge | Non-specific interactions, clearance/retention in the kidney |
| Affinity | Targeting to tumor, accumulation in tissues with low expression of receptors, potential loss of specificity |
| Hydrophobicity | Non-specific interactions, metabolism in the liver |
| Serum Stability | Targeting ligand must outlast cargo in the bloodstream to avoid off target accumulation |

**Table 1.2 Factors that affect biodistribution of peptide-targeted molecules.**

As mentioned previously, stability of a peptide plays a major role in determining biodistribution. Peptide targeting ligands should be optimized to have roughly the same half-life in serum as their corresponding payloads. Degradation of the peptide ligand too early releases the cargo drug or imaging agent to distribute throughout the body. Peptides that survive in the bloodstream for much longer than their payloads would directly compete for

binding of whole peptide-drug conjugates, thus decreasing signal during imaging or efficacy of targeted therapeutics.

Size plays an interesting role in determining biodistribution of a targeted agent. In general, solid tumors are poorly vascularized, meaning that therapeutics must diffuse over longer distances to reach their target cells. Interstitial pressure is also high within tumors, hampering the diffusion of high molecular weight agents. As discussed previously, monoclonal antibodies are often too large to penetrate deeply into tumor tissue, and remain trapped near the vasculature. The small size of peptides avoids this obstacle, but creates another. Peptide conjugates are below the molecular weight threshold of the renal filtration system and are freely filtered in the glomerulus of the kidneys. This leads to rapid clearance of peptide-conjugated agents through the kidneys and contributes to off-target accumulation in the kidneys themselves. As of yet, no optimal size that efficiently infiltrates tumor tissue while avoiding renal filtration has been determined.

Overall charge and hydrophobicity regulate non-specific interactions that could lead to off-target accumulation of peptide-targeted constructs. Specific examples of this are often seen in the liver and kidneys. Highly hydrophobic molecules off accumulate in the liver as a result of nonspecific uptake by hepatocytes. Upon internalization, various cytochrome P450 enzymes and glutathione transferases metabolize lipophilic agents to increase their hydrophilicity [122]. This allows these compounds to be more readily excreted in bile or returned to the bloodstream for clearance in urine. In contrast, highly charged peptides are thought to bind more strongly to scavenger-receptors expressed by epithelial cells in the proximal tubules of the kidney [65, 123]. This binding interaction triggers RME in a clathrin-

dependent mechanism. Internalized peptide conjugates are then degraded in the lysosomes, and it is thought that the free amino acids are effluxed back into circulation. Autoradiography experiments where radiolabeled peptides are perfused into rat or mouse kidneys have shown that radioactivity is retained in the proximal tubule epithelium. Whether this signal indicates retention of the entire peptide-chelator conjugate, some degradation product, or the free radioisotope is unknown.

*Processing of Peptides in the Kidneys*

Even the most serum stable peptide conjugate will fail to reach clinical use if it is cleared from the system before it has a chance to deliver its cargo. Most peptide-drug conjugates under development are below 30 kD. When blood is filtered in the glomerulus of the kidney, molecules below the mass threshold, estimated at 30-50 kD, are filtered from the blood and enter the proximal tubules [123]. Naturally occurring peptides are re-absorbed at the brush border of the convoluted proximal tubules [124, 125]. However, high doses of exogenous peptides are thought the saturate the scavenger-receptors involved in this process, resulting in excretion of the peptide construct in urine. When a peptide conjugate is injected intravenously into a mouse, the vast majority of the construct is cleared from the animal in a matter of minutes [80, 123].

Hundreds of studies have been published examining biodistribution of peptide constructs upon systemic injection into mice. As can be seen in these examples [104, 107, 126-130], little has changed over the past decades. Most of these studies have been performed using microPET or SPECT imaging of mice. Because of the short timeframe of

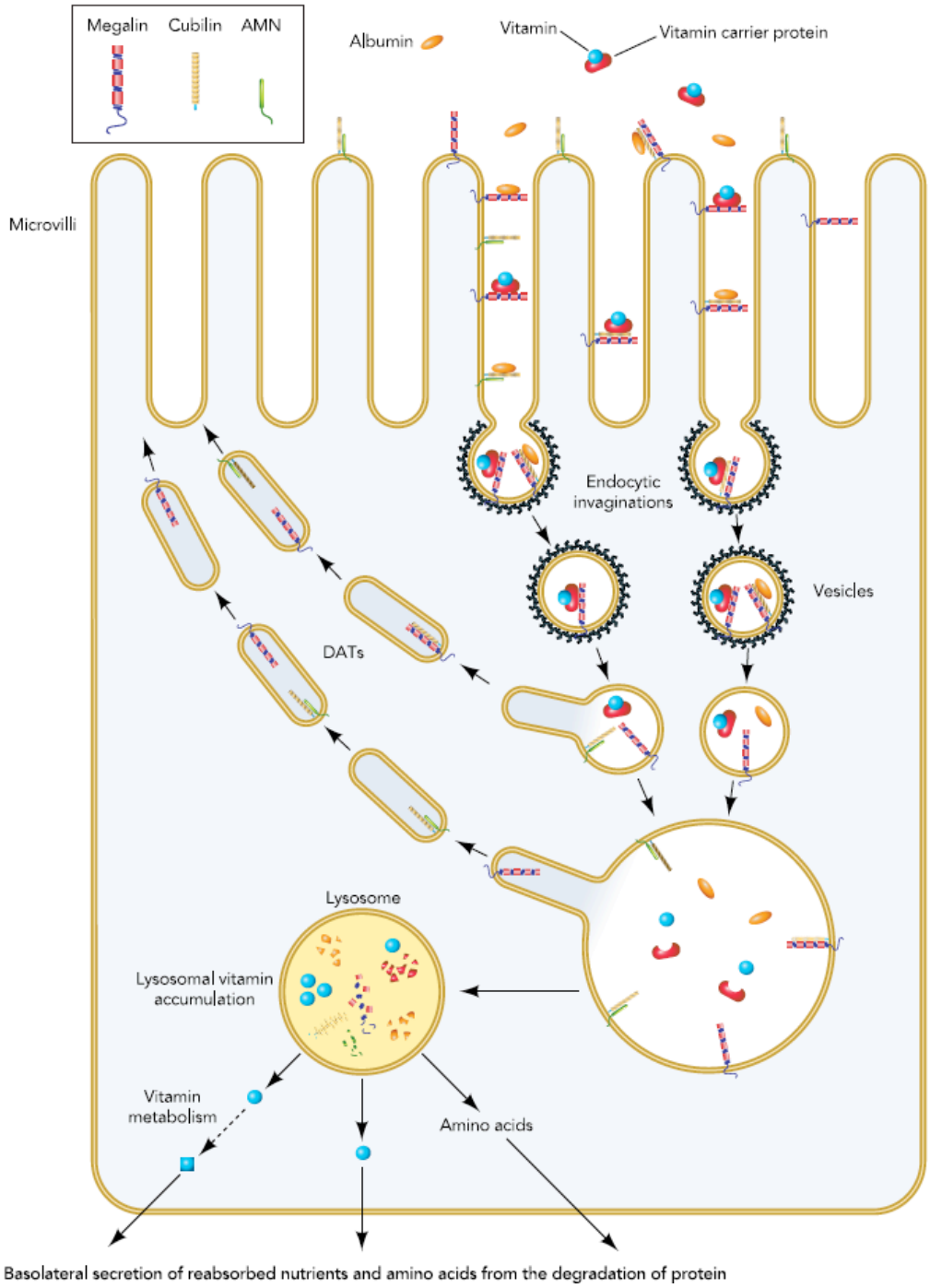


**Figure 1.4 Current model of protein and peptide recycling in the renal proximal tubules.** Small proteins and peptides are bind to megalin or the cubilin/AMN complex and are internalized via clathrin-mediated endocytosis. Receptors are recycled back to the brush-border from endosomes and peptide bonds are degraded in the lysosome. Amino acids and surviving peptides are secreted back into the bloodstream. Modified from [124].

imaging, most of these experiments quantify biodistribution at 1, 4, 12, and perhaps 24 hours post-injection. Virtually all of the studies show the majority of peptide signal present in the kidneys. Historically, this renal signal has been dismissed as simple clearance through the kidneys [131]. However, studies in our group, as well as others, have revealed a two-phase clearance process by which peptide signal decreases in target tissues. The first phase, during the first few hours post-injection, consists of rapid clearance of peptide conjugates in the urine. In contrast, the second phase is a much slower decline of peptide signal in the kidney, starting from a pool of peptide conjugates retained in the kidney during initial clearance. Whether or not this is a general pattern for all exogenous peptides remains unknown. Standard biodistribution studies still do not look at timepoints beyond 24 hours. I would hypothesize that many tumor-targeting peptides are retained in the kidney at least as efficiently as they accumulate in tumor tissue when analyzed one or more days post-injection.

Small endogenous proteins and peptides are freely filtered in the glomeruli of the kidneys and efficiently re-absorbed in the proximal tubules, with little to no protein observed in the urine of healthy individuals [124, 132]. Re-absorption is mediated through interactions with the megalin/cubilin scavenger-receptor complex, leading to clathrin-mediated endocytosis of these peptides and proteins. Upon dissociation from the megalin/cubilin complex in the lysosome, peptides are partially degraded and small peptides and individual amino acids are released back into circulation. Meanwhile, the receptors are recycled back to the apical membrane of the proximal tubule.

Drug targeting peptides follow a similar route through the kidneys [123]. However, when animals are treated with therapeutic doses of peptide-drug conjugates, the majority of the peptide escapes re-absorption in the proximal tubules, presumably by saturation of the megalin receptors. This excess peptide-drug conjugate is then excreted in the urine. The remainder is internalized in the proximal tubules. There, the peptide targeting ligand is often degraded, leaving the drug cargo to accumulate in the epithelial cells of the renal cortex, leading to nephrotoxicity [131, 133]. This nephrotoxicity is often a limiting factor in the dosing of untargeted chemotherapeutics, and therefore must be avoided in order for their peptide-targeted counterparts to be of clinical use.

Multiple strategies have been utilized to prevent this accumulation in the kidneys by avoiding interactions between peptide ligands and the megalin/cubilin complex. Megalin is 660 kDa protein with a large, negatively charged transmembrane protein that binds a wide variety of ligands including enzymes, hormones, drugs and toxins [124]. Due to its negative charge, megalin binds preferentially to positively charged molecules. Therefore, a common strategy to avoid re-uptake in the proximal tubules is the co-administration of lysine or arginine [123]. This tactic is effective in reducing retention in the kidney by up to 60% in certain cases, such as the peptide drug Octreotide. However, many peptides do not benefit fit co-injection of positive amino acids, suggesting that the presence of positively charged side chains does not completely dictate the re-absorption of peptides into the proximal tubules.

In fact, some groups have found that while peptides including bombesin, D-Glu-minigastrin, and exendin do not benefit at all from co-injection with lysine, their retention in kidney is significantly decreased by co-administration of poly-glutamic acid [123, 134].

These peptides may interact specifically with cubilin, a 460 kDa peripheral membrane protein that co-localizes with megalin [124], or with another as yet unknown scavenger-receptor. It has been suggested that the total number of charged side chains regulates retention in the kidney on given peptide. However the mechanism of this regulation is unclear. Co-injection of all of these peptides, including Octreotide, with plasma volume expanders such as Gelofusine decreases kidney retention, albeit to a much lesser degree [123, 135].

Many groups have chosen instead to modify the targeting peptide ligands themselves by incorporating them into nanoparticles such as dendrimers or liposomes or by PEGylation [64, 106, 118, 136]. This sufficiently increases the molecular weight so as to prevent filtration in the glomerulus and avoid the proximal tubules altogether. While this approach decreases accumulation in the kidneys, it creates another set of problems for the treatment of solid tumors. Nanoparticles often do not penetrate well into tumors and become stuck near the vasculature of tumors, and the targeting ability of peptide ligands is often unable to alter the biodistribution of nanoparticles due to enhanced permeability and retention effects [64].

Other groups have sought to reduce interactions between their peptides and the scavenger-receptors of the proximal tubules by decreasing the number of charged residues or by cyclization to remove the charged termini [137]. This strategy has proved fruitful in some situations. However, these alterations often result in significant loss of affinity for their target receptor making them unsuitable ligands for drug delivery.

New approaches are required to decrease accumulation of peptide targeting ligands in the renal cortex. These modifications must maintain the affinity and targeting capacity of the

peptide ligands while reducing re-absorption in the proximal tubules of the kidneys. The development of targeting ligands that meet these qualifications would substantially expand the therapeutic window available for the treatment of solid tumors by increasing concentrations of drug in the tumor while decreasing side effects such as nephrotoxicity.

# CHAPTER TWO
# The Integrin $\alpha_v\beta_6$ as a Target for the Treatment of NSCLC

## The Integrin Family of Adhesion Proteins

One potentially rich source of receptors for tumor targeting lies in the integrin family of cell adhesion proteins. Several members of the integrin protein family have been under investigation for their role in tumor development and progression for decades. Integrins are the best-studied group of cell adhesion receptors. These transmembrane proteins consist of heterodimers of α and β subunits. To date, 18 α and 8 β subunits have been identified, and these combine to form 24 different heterodimers [138]. They bind extra-cellular matrix (ECM) components or cell surface proteins on neighboring cells. In conjunction with other cell adhesion molecules, such as the cadherins, integrins mediate cell-cell and cell-ECM interactions.

However, integrin function is not limited to simple adhesion. Each of the integrins has a unique tissue expression profile, indicating that they have non-redundant functions [139]. This is supported by studies in mice demonstrating that knockout of each integrin subunit produces a different phenotype ranging from pre-implantation lethality to defects in angiogenesis and inflammation in viable mice [138]. Indeed, integrins have been shown to play a role in many cellular functions including shape, motility, polarization, differentiation, proliferation, and survival/apoptosis [138, 140]. The signaling pathways for integrin-mediated regulation of these functions often intersects with those of major growth factor signaling such as the MAP kinase pathway. These interactions have raised hopes of exploiting integrin signaling to target signaling mechanisms that commonly contribute to tumor progression [141].

The canonical signaling pathway of integrins is common between most members of the protein family. Binding of the integrin to extracellular ligands initiates signaling by causing aggregation of heterodimers at focal adhesion sites. This allows for binding of the adaptor protein talin to the intracellular C-terminal tail of the β subunit, which facilitates oligomerization and activation of focal adhesion kinase (FAK) [142]. FAK then autophosphorylates and recruits the kinases Src and Fyn to the focal adhesion site. FAK, Src, and Fyn then activate downstream effectors. These include phosphoinositide-3 kinase (PI3K), the growth factor receptor bound protein 2/son of sevenless (GRB2/SOS) complex, and the small GTPase RhoA along with a variety of other cell-type specific substrates. Activation of these proteins initiates several signaling cascades resulting in regulation of cell proliferation, adhesion, spreading, and migration [143].

The canonical signaling pathway described above is an example of traditional outside-in signaling associated with most plasma membrane receptors. Integrins are unique in that they also participate in inside-out signaling. Integrins exist in two major structural forms, and bent-knee configuration with low affinity for extracellular ligands and an upright, high affinity state [144]. Binding to extracellular ligands triggers a conformational change from the bent-knee state to the upright state (outside-in signaling) [145]. However, intracellular signaling events may also induce changes in the conformational state of an integrin heterodimer, exerting influence on its affinity for extracellular binding partners (inside-out signaling). The ability of integrin heterodimers to participate in both outside-in and inside-out signaling facilitates the dynamic role of the integrin family in many different cellular processes.

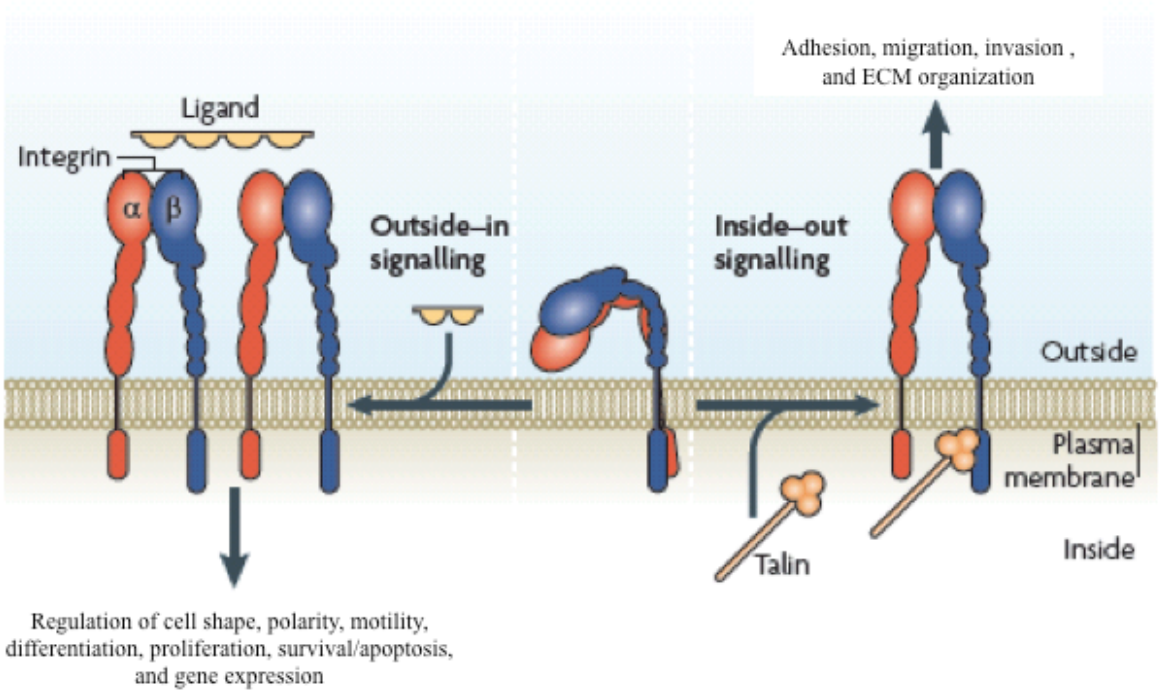


**Figure 2.1 Active and Inactive Structures of Integrins**. Binding of intracellular and extracellular ligands to the integrin heterodimer triggers a large conformational shift and initiates regulation of many cellular processes. Modified with permissions from [145].

Most of what is known about the large conformational shift associated with activation of integrins comes from studies done on $\alpha_v\beta_3$ and $\alpha_{IIb}\beta_3$ [140]. However, much of that information is thought to be general to the protein family as a whole. Each subunit of the integrin heterodimer consists of a large N-terminal extracellular domain, a single α-helical transmembrane domain, and a short C-terminal intracellular tail. In the inactive state, the extracellular domains are bent close to the plasma membrane, and the transmembrane and intracellular domains are closely associated with each other, sterically blocking the binding motifs from ligand interactions [142] (See Figure 2.1). Upon activation of the integrin, either through extracellular or intracellular events, a drastic conformational change occurs. Via a

switchblade motion, the extracellular domains extend away from the plasma membrane and form a binding pocket between the two subunits [138, 140]. The transmembrane helices and C-terminal tail regions dissociate, allowing for binding of intracellular adaptor and signaling molecules.

Until recently, the majority of the research on integrins has focused on $\alpha_v\beta_3$, $\alpha_5\beta_1$, and $\alpha_{IIb}\beta_3$. The $\alpha_{IIb}\beta_3$ heterodimer is expressed in platelets and megakaryocytes (i.e. platelet progenitor cells), and has been of great interest in the study of blood clot formation [146]. The $\alpha_v\beta_3$ and $\alpha_5\beta_1$ integrins are widely expressed in endothelial cells, particularly during angiogenesis [139, 147]. Integrin $\alpha_v\beta_3$ is also seen in osteoclasts, and fibroblasts while $\alpha_5\beta_1$ is also expressed in platelets, hepatocytes, and lymphocytes [148]. Because of their participation in angiogenesis, $\alpha_v\beta_3$ and $\alpha_5\beta_1$ have been intensively studied as targets in cancer [139, 147]. However, these integrins are both expressed in healthy cells as well, potentially limiting their use as therapeutic targets.

**The Integrin $\alpha_v\beta_6$**

The integrin $\alpha_v\beta_6$ is expressed at low levels in normal adult epithelial cells, and is upregulated during development, wound healing, and inflammation [149-151]. Integrin $\alpha_v\beta_6$ was recently discovered to be over-expressed in 54% of NSCLCs regardless of histological subcategory [152]. Increased expression has also been seen in several other types of epithelial derived tumors including breast [153], colon [154], head and neck [155], pancreatic, and ovarian cancers [156] (See Table 2.1). In NSCLC, this upregulation has been observed as early as the dysplastic stage and increases as masses develop into invasive

tumors [157]. Expression of the β6 subunit correlates to poor patient prognosis in several cancers including NSCLC (Figure 2.2) [152], pancreatic [158], and breast cancer [153]. The specific upregulation of $\alpha_v\beta_6$ in tumors compared to normal tissue may provide a window that can be leveraged by development of targeting ligands against $\alpha_v\beta_6$.

| Tumor Site | % Tumors Positive for $\alpha_v\beta_6$ Expression |
|---|---|
| NSCLC | 54 [157] |
| Pancreatic | 100 [159] |
| Ovarian | 100 [156] |
| Head and Neck | 80-100 [160-162] |
| Cervical | 85 [163] |
| Liver | 71 [164] |
| Endometrial | 42 [165] |
| Colorectal | 36 [154] |
| Breast | 18 [166] |

**Table 2.1 Prevalence of $\alpha_v\beta_6$ expression in patient tumor tissue samples**

Surprisingly, while $\alpha_v\beta_6$ is expressed at high levels during development, knockout of $\beta_6$ expression in mice does not lead to developmental problems. In fact, β6 knockout mice develop, grow, and reproduce normally. Wound healing also occurs normally in these mice. The major phenotypes observed in knockout mice are increased inflammation in the skin upon low level injury and decreased pulmonary fibrosis in response to bleomycin treatments [167]. An increase in the population of monocytes and macrophages in both the injured dermis and airway walls was observed.

This phenotype is consistent with defects in TGF-β activity [168]. Subsequent studies in over-expression models have shown that $\alpha_v\beta_6$ plays a direct role in activation of TGF-β

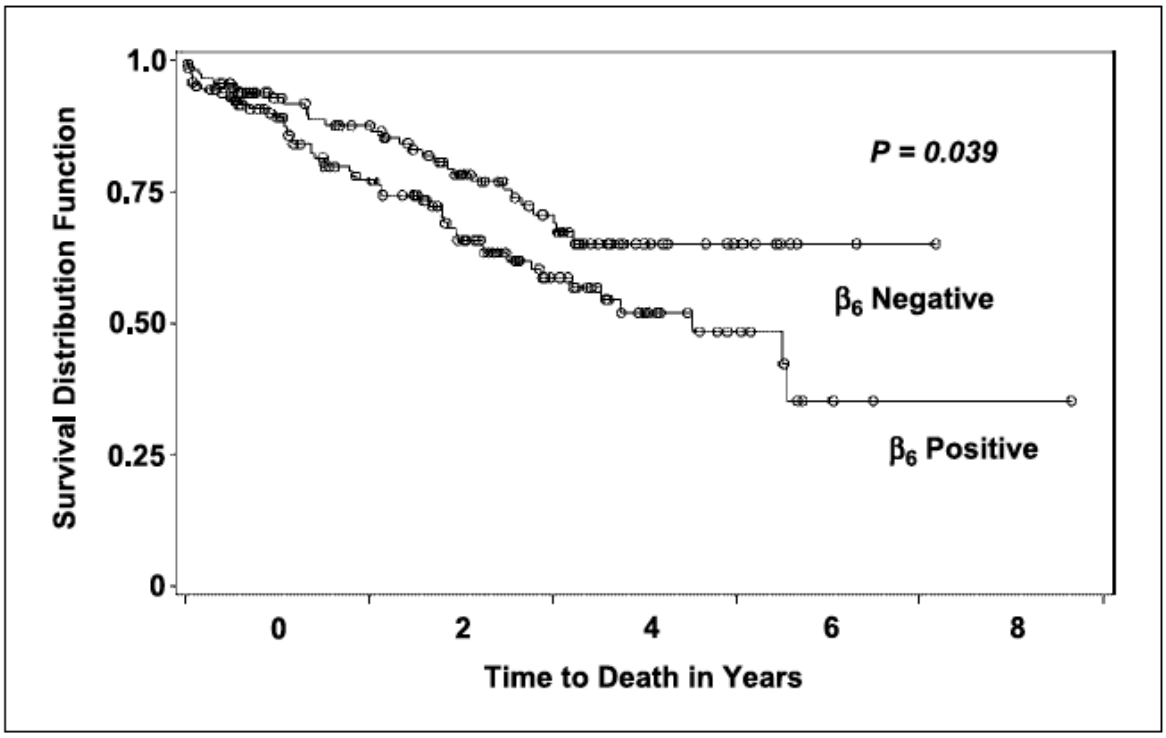


**Figure 2.2 Kaplan-Meier Curves displaying patient survival categorized by expression of the $\beta_6$ subunit.** Expression significantly correlates with poor prognosis with a hazard ratio of 1.9. Published with permissions from [157]

through binding to LAP [169]. This activation is protein kinase C and Rho kinase dependent and is thought to occur via mechanical perturbation of the latent TGF-β complex [169-172]. TGF-β signaling has also been shown to induce $\alpha_v\beta_6$ expression [173], creating a potential positive feedback loop. Interestingly, the activated TGF-β does not appear to be released into the media under *in vitro* conditions, in spite of initiation of TGF-β dependent signaling in co-cultured reporter cells [174]. The biology of TGF-β signaling is extremely complex and has filled hundreds of doctoral dissertations. It is likely that the role of $\alpha_v\beta_6$ in both normal tissue and in malignancies is similarly intricate.

### *Integrin $\alpha_v\beta_6$ in Epithelial-Mesenchymal Transition*

TGF-β signaling has been well established as a major contributor to epithelial-mesenchymal transition (EMT) [174-176]. EMT can be assessed in several ways. It has been defined as a morphological change of cells in culture. Epithelial cells form extensive contacts with surrounding cells to give a "cobblestone" appearance. Mesenchymal cells dissociate from neighboring cells and re-structure their cytoskeletons. EMT is often quantified by expression of molecular markers including E-Cadherin, N-Cadherin, and vimentin. *In vivo*, EMT is usually characterized by loss of cell-cell or cell-ECM adhesion and loss of cell polarity.

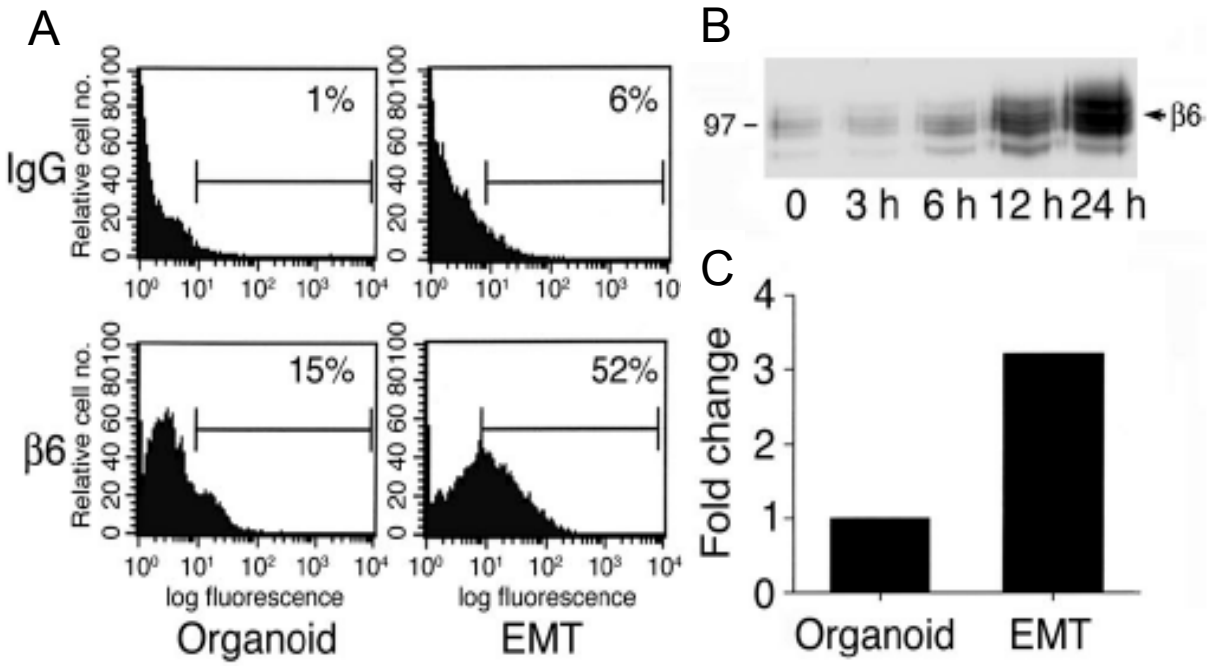


**Figure 2.3 Induction of EMT in colorectal cancer cells increases expression of β6.** Epithelial-like LIM1863 cells grown as organoids in 3D culture were treated with TGF-β for 24 hours to induce EMT. A) Organoids treated with TGF-β show significantly more $\beta_6$ expressing cells. B) Changes in $\beta_6$ expression over time were analyzed by Western blot. C) $\beta_6$ mRNA levels were also quantified by qRT-PCR. Published with permissions from [173].

As an activator of TGF-β1, $\alpha_v\beta_6$ expression is likely to have an impact on the process. There are several reports linking $\alpha_v\beta_6$ to EMT in both healthy and malignant tissue. During the process of wound healing after punch biopsy in healthy volunteers, $\alpha_v\beta_6$ expression was significantly increased at the leading edge of the healing skin [177]. In this process, known as re-epithelialization, dermal cells undergo EMT and migrate to close the wound. This expression was then down-regulated when cells went through the reverse mesenchymal-epithelial transition (MET). The integrin has also been associated with EMT in NSCLC [178], colorectal [179], oral [180], and breast cancer [181].

In both breast and colorectal cancer cell lines, treatment with TGF-β has been shown to induce EMT and significantly up-regulate $\alpha_v\beta_6$ expression (Figure 2.3). This is associated with increased migration and invasion, and can be abrogated by treatment with function

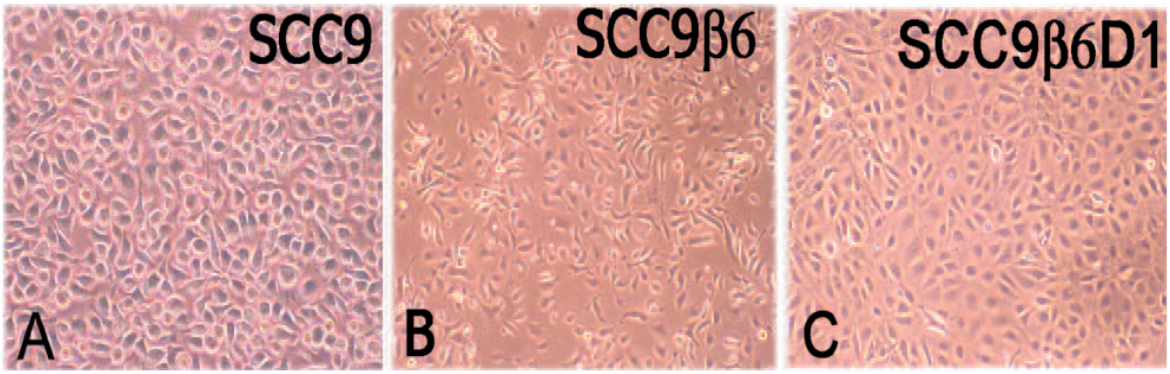


**Figure 2.4 Expression of $\beta_6$ is associated with EMT in oral cancer.** A-C) Ectopic expression of $\beta_6$ in SCC produces morphological changes from wild-type epithelial (A) to a more mesenchymal phenotype (B). Expression of truncated $\beta_6$ without the C-terminal 11 residues (β6D1) does not trigger this change. Published with permissions from [180].

blocking antibodies against $\alpha_v\beta_6$ [173, 181]. Interestingly, treating cells with tenascin-C, an ECM ligand of $\alpha_v\beta_6$ intensified this phenotype in breast cancer cells. These results are

supported by immunohistochemistry of patient samples illustrating increased $\alpha_v\beta_6$ expression at the leading edge of invading tissue.

Ectopic expression of $\alpha_v\beta_6$ in oral cancer cell lines also induces EMT as assessed by cell morphology, increased vimentin, and decreased E-cadherin expression (Figure 2.4) [180, 182]. The unique C-terminal 11 amino acids of the β6 subunit are required for this induction, suggesting that non-canonical integrin signaling is involved. However, these studies exclusively involve over-expression models, which may not re-capitulate physiologically relevant conditions.

The role of $\alpha_v\beta_6$ in EMT in NSCLC is less clear. A large study of patient tissue samples indicates that $\alpha_v\beta_6$ expression increases as tumor develop and become more invasive [178]. At the same time, E-cadherin levels decrease while N-cadherin expression increases, indicating that EMT has occurred (Figure 2.5). Brain metastases from NSCLC express lower levels of $\alpha_v\beta_6$ than their primary tumors, perhaps as a result of MET upon establishment in the brain [178, 183, 184]. Brain metastases that maintain their invasiveness, express lower levels of $\alpha_v\beta_6$ than isolated, well-demarcated tumors [185]. Additionally, an EMT gene signature in NSCLC significantly correlated $\alpha_v\beta_6$ expression with a more epithelial phenotype [186]. This gene signature was developed by proteomic analysis of 54 NSCLC cell lines and validated in an additional 39 lines as well as *in vivo.* Expression of $\alpha_v\beta_6$ as measured by binding of the H2009.1 peptide has also been correlated with increased E-cadherin and decreased N-cadherin expression, consistent with an epithelial phenotype (Figure 2.6) [187]. Un-published data from our lab shows that knockdown of $\beta_6$ expression in H2009 cells decreases N-cadherin, and vimentin expression, but does not affect E-cadherin levels. Taken

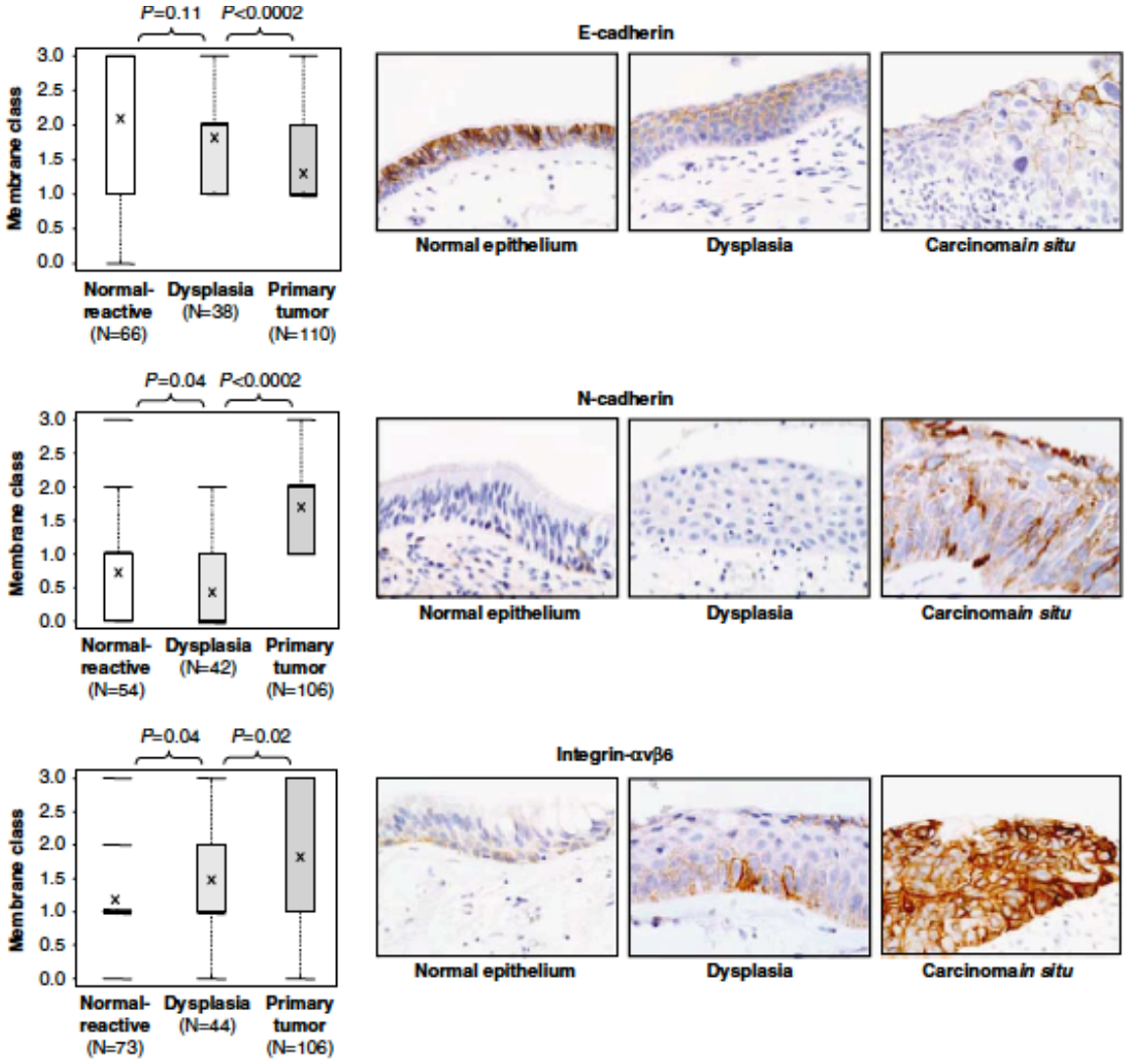


Fig**ure 2.5 Expression levels of E-cadherin, N-cadherin, and integrin $\alpha_v\beta_6$ in normal lung epithelium, dysplastic tissue, and carcinoma in situ.** E-cadherin levels drop while N-cadherin expression increases, indicating an EMT-like process. At the same time, $\alpha_v\beta_6$ levels increase significantly. Published with permissions [178].

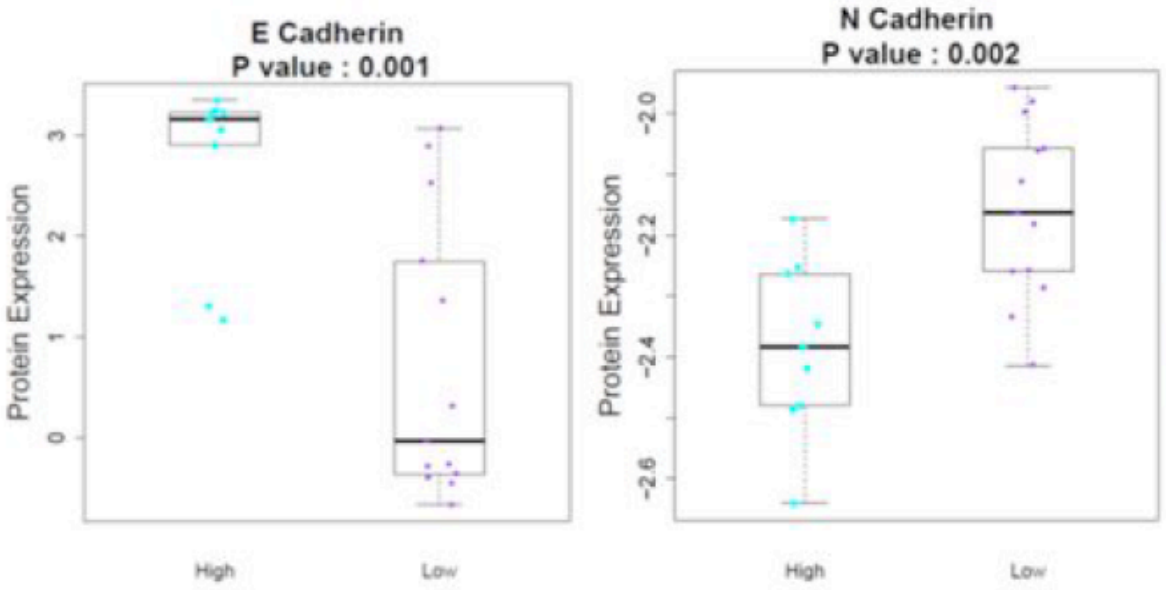


**Figure 2.6 Correlation of H2009.1 peptide binding with EMT Markers in NSCLC cell lines.** Binding and internalization of the H2009.1 peptide in NSCLC cell lines correlates with high expression of E-cadherin and low expression of N-cadherin, indicating that H2009.1 peptide internalizes into epithelial-like NSCLC cells. Published with permissions [187].

together, these results suggest that the impact of $\alpha_v\beta_6$ on EMT in NSCLC is dependent on expression of other factors or perhaps on tumor microenvironment.

### *Other Potential Roles of $\alpha_v\beta_6$ in Cancer*

Previous studies in oral and colon cancer cell lines have shown the cytoplasmic C-terminal tail of the $\beta_6$ chain contains a unique 11 amino acid sequence (EKQKVDLSTDC) that appears to confer functions beyond the canonical integrin signaling pathways [188]. These functions are illustrated in Figure 2.7. Knockdown of $\beta_6$ in colon cancer cells using antisense DNA significantly decreased the rate of ECM degradation, levels of phosphorylated ERK1/2, and subcutaneous tumor growth [189]. In colon and oral cancers,

$\alpha_v\beta_6$ over-expression is associated with increased secretion of matrix metalloproteinases 2 and 9 (MMP-2 and MMP-9), which are involved in degradation of surrounding ECM, allowing for invasion into surrounding tissue [190-192]. However, the mechanism by which $\alpha_v\beta_6$ participates in these processes is currently unclear. One must also remember that integrin signaling has been shown to be ligand and cell type specific. Thus the function of $\beta_6$ in NSCLC could differ significantly from other cancers.

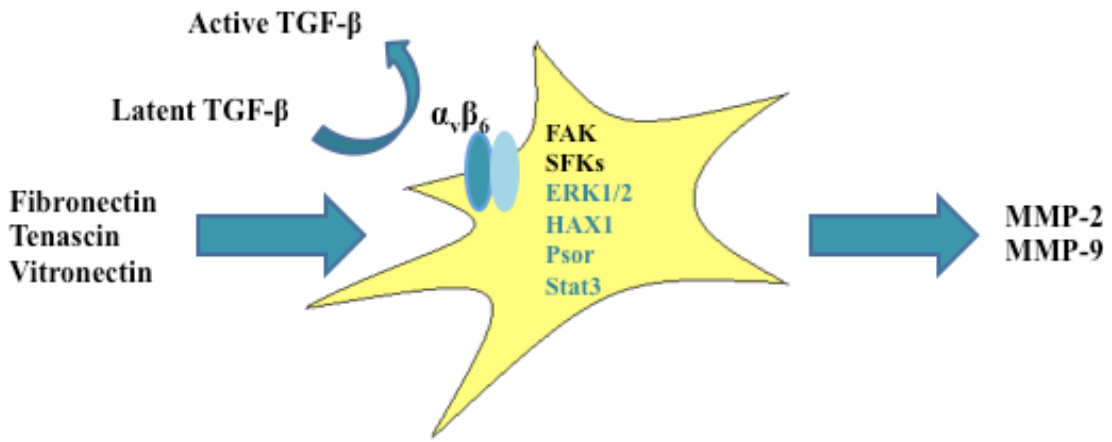


**Figure 2.7 Established and potential functions of $\alpha_v\beta_6$.** Integrin $\alpha_v\beta_6$ is known to bind to the ECM components shown above. Binding to the latent TGF-β complex results in activation of TGF-β in a kinase dependent manner. Expression of $\alpha_v\beta_6$ leads to increased MMP-2 and MMP-9 activity in several cancer cell lines. In addition to the canonical kinases involved in integrin signaling, proposed binding partners of the $\beta_6$ subunit are shown in blue.

Studies have also shown recycling of $\alpha_v\beta_6$ to be essential for motility of certain cancer cells [193]. However, the mechanism by which $\alpha_v\beta_6$ is internalized and returned to the plasma membrane is unknown. Some studies propose that $\alpha_v\beta_6$ internalization follows the clathrin-mediated endocytosis pathway in a manner similar to $\alpha_5\beta_1$ [194, 195]. However, data from our lab suggests that under some conditions $\alpha_v\beta_6$ uptake follows a clathrin-independent

endocytic route during which the integrin never co-localizes with endosomal or lysosomal markers [196]. This may suggest that the uptake mechanism for $\alpha_v\beta_6$ is cell-type or ligand specific. If this proves to be the case, it will have major effects on the delivery of drugs or imaging agents targeted to $\alpha_v\beta_6$.

Many reports have suggested roles for $\alpha_v\beta_6$ beyond canonical integrin signaling, though few have proposed mechanisms for how it performs these functions. Previous studies in other cancer types have suggested several intracellular binding partners for the unique sequence at the cytoplasmic C-terminus of $\beta_6$ that may be involved in $\alpha_v\beta_6$ specific signaling. ERK1/2 [189] and psoriasin [197] were identified using immunoprecipitation experiments from over-expression models in colon cancer while HS-1 associated protein X-1 (HAX-1) was identified from a yeast two hybrid screen, also in colon cancer cells [194]. Of these reported binding partners, the only one currently known to be expressed in NSCLC is ERK1/2. Surprisingly, expression of $\alpha_v\beta_6$ in NSCLC cell lines correlates to sensitivity to EGFR inhibition and levels of EGFR phosphorylation at Tyr1173 [187]. Phosphorylation of EGFR at this residue is associated with activation of STAT3 and STAT5 [198]. Phosphorylation of both of the signaling mediators at Y705 and Y694 (respectively) also correlates positively with $\alpha_v\beta_6$ expression. Thus $\alpha_v\beta_6$ expression levels may be useful as a surrogate for assessment of EGFR activity in NSCLCs. Efforts to illuminate the relationship between $\alpha_v\beta_6$ and EGFR are currently underway in our lab.

Research into the role of $\alpha_v\beta_6$ in cancer is just starting to gain momentum. In fact, it is currently unclear whether upregulation of $\alpha_v\beta_6$ is a driver of oncogenesis or merely a byproduct of other processes. In either case, the specific expression of $\alpha_v\beta_6$ in over half of

NSCLCs provides an opportunity to improve diagnosis, characterization, and treatment of these tumors. Our group, as well as others, has begun the development of ligands that bind $\alpha_v\beta_6$ for applications in NSCLC and other cancers.

## Binding partners of $\alpha_v\beta_6$

### *Naturally Occurring $\alpha_v\beta_6$ Ligands*

While the $\alpha_v$ subunit is capable of dimerization with several β subunits, $\beta_6$ has only been observed to dimerize with $\alpha_v$ (See Figure 2.8) [199]. As a member of the RGD-binding family of integrins, $\alpha_v\beta_6$ binds to components of the ECM including fibronectin, vitronectin, and tenascin-C. However, $\alpha_v\beta_6$ does not behave like a typical RGD-binding integrin. The binding motif for $\alpha_v\beta_6$ ligands is extended and includes the full sequence RGDLXXL. In addition to these, $\alpha_v\beta_6$ binds to the TGF-β latency associated peptide (LAP). The integrin is also the receptor for foot and mouth disease virus [200] and CagL, a component of the Helicobacter pylori type IV secretion system [201].

It has long been speculated that the LXXL region of this motif forms a helical structure that may interact specifically with the $\beta_6$ subunit. A recent study by Dong et al. confirmed this speculation [202]. Using crystals comprising the headpiece of the $\alpha_v\beta_6$ heterodimer bound to short peptides from LAP, they found that the LXXL sequence forms an amphipathic helix that binds in a hydrophobic pocket formed by three separate loops of the $\beta_6$ subunit. This additional interaction allows $\alpha_v\beta_6$ to bind to LAP with an affinity of 10.3 nM, more than 1000-fold better than $\alpha_v\beta_3$. Interestingly, the LAP peptides bound as a loop with

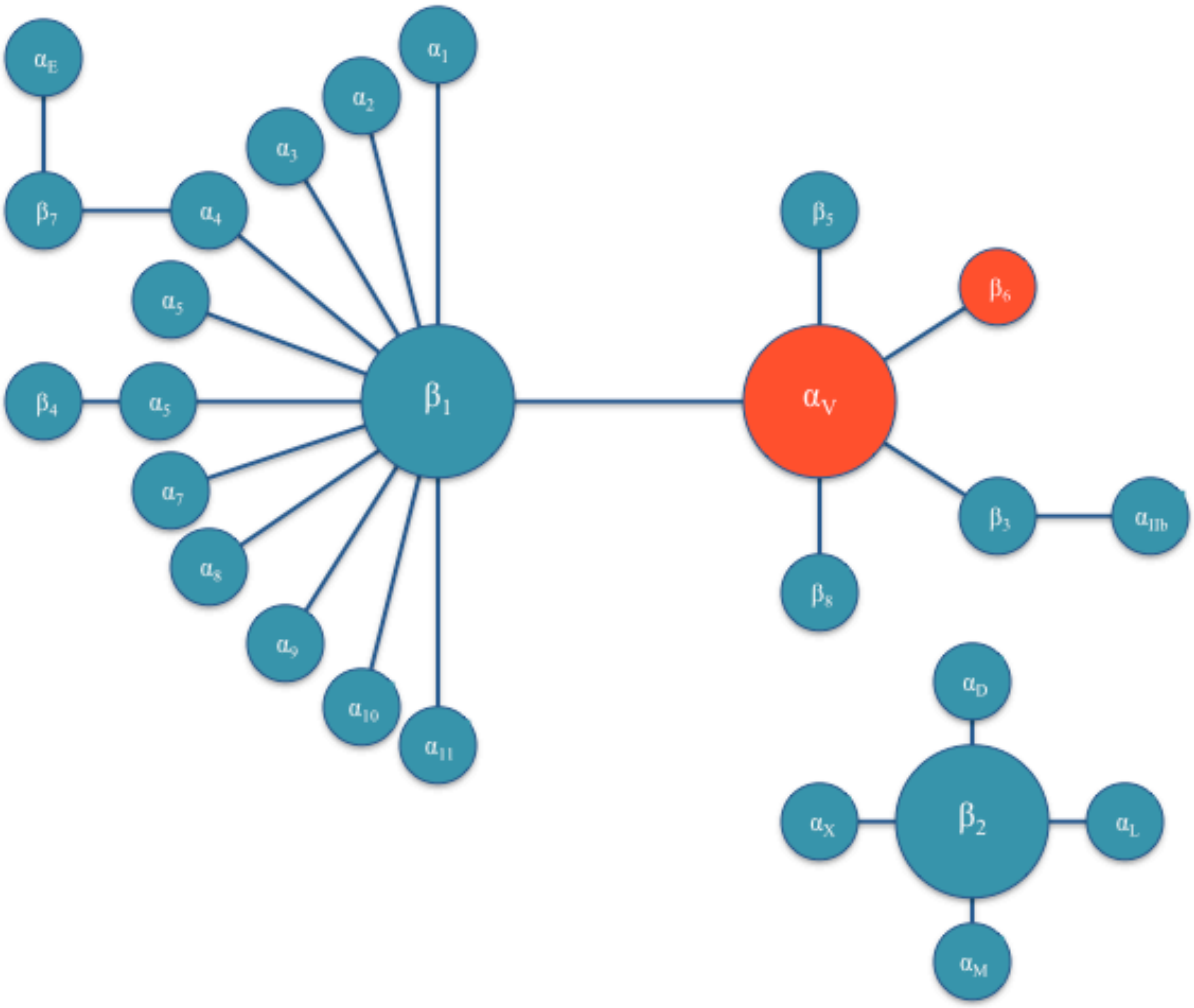


**Figure 2.8 Integrin subunits and they're heterodimer binding partners.** Note that $\alpha_V$ binds to several β subunits. However $\beta_6$ interacts exclusively with $\alpha_V$.

both ends extending away from the binding interface as shown in Figure 2.9. This may leave considerable space for modification of the ligand termini without loss of binding affinity.

### *Synthetic $\alpha_v\beta_6$ Ligands*

Due to its prevalence among a wide variety of cancers, $\alpha_v\beta_6$ is garnering attention as a target for the treatment of cancer. Ligands that bind to $\alpha_v\beta_6$ may be useful for targeted

delivery of imaging agents and therapeutics to tumors. This is particularly exciting for NSCLC as $\alpha_v\beta_6$ over-expression is observed in over half of patients. Because natural peptidic ligands already exist for $\alpha_v\beta_6$, synthetic peptides are the obvious choice in the development of targeting agents. The focus of this dissertation is the development of one such peptide ligand.

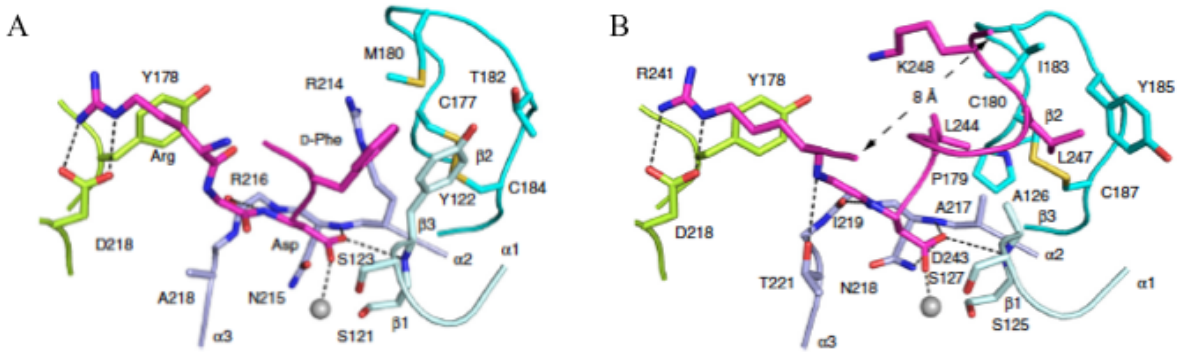


**Figure 2.9 Structures of RGD-binding integrin headpieces with bound ligand. A)** Cilengtide binds to $\alpha_v\beta_3$ solely through the tri-peptide RGD sequence. **B)** A peptide from TGF-β3 binds to $\alpha_v\beta_6$ through the extended RGDLXXL motif. Note that both termini of the TGF-β3 peptide extend away from the integrin, suggesting that other ligands with the RGDLXXL sequence may bind the same site. Published with permissions from [202].

A few other groups are also developing peptidic ligands for imaging $\alpha_v\beta_6$–expressing tumors [203, 204]. These are summarized in Table 2.2. John Marshall's group at the University of London identified a peptide derived from foot and mouth virus and dubbed it FMDV20A (sequence: NAVPNL**RGDLQVL**AQKVARTY) [205]. This peptide has a relatively high *in vitro* half-life estimated at 4-24 hours. Since then, Julie Sutcliffe's group at UC Davis has conjugated this peptide to bi-functional chelators for $^{64}$Cu and $^{18}$F PET imaging and $^{90}$Y for optical Cerenkov imaging in mice [129, 206, 207]. Tumor-to-blood ratios are acceptable for these constructs, though overall signal is low. These constructs use a

$PEG_{28}$ linker, which improves solubility and serum stability. As of yet, attempts at improving *in vivo* targeting of this peptide have all increased the already high kidney accumulation.

| $\alpha_v\beta_6$-Binding Peptide | Sequence |
|---|---|
| H2009.1 | **RGDLATL**QRL (AQEDGVVGVR) |
| FMDV20A | NAVPNL**RGDLQVL**AQKVARTY |
| HBP-1 | SP**RGDLAVL**GHKY |
| $R_0$1 | GCILNM**RTDLGTL**LFRCRRDSDCPGACICRGNGYCG |

**Table 2.2 Peptide targeting ligands under development for the diagnosis and treatment of $\alpha_v\beta_6$-positive tumors.** H2009.1 residues in parentheses are included in some studies but are not involved in integrin binding. Bolded residues indicate RGDLXXL motifs required for specific binding to $\alpha_v\beta_6$.

Uwe Haberkorn's group at the University of Heidelberg selected a $\alpha_v\beta_6$–binding peptide from phage display panning on head and neck cancer cell lines [208]. HBP-1 (sequence: SP**RGDLAVL**GHKY) is in the early stages of development. *In vitro* studies show that this peptide internalizes into cells with an $EC_{50}$ of 38.9 nM and has a serum half-life of 55 minutes. Biodistribution experiments demonstrate much lower than usual kidney uptake (4.48% ID/g at 6 HPI compared to 3.66% ID/g in tumors), but with low tumor-to-blood contrast (5.19% ID/g at 6HPI producing a tumor-to-blood ratio of 0.71). These assays were all performed using peptide labeled with $^{131}I$, which is chelated directly by Tyr residues within the peptide sequence. It will be interesting to see the effects of conjugation of a payload to this peptide.

Sanjiv Gambhir's group at Stanford has been working with a cystine knot peptide known as $R_0$1 for uses in PET and SPECT imaging [209, 210]. This is a longer peptide with a slightly altered $\alpha_v\beta_6$–binding motif (Sequence: GCILNM**RTDLGTL**LFRCRRDSDCPGAC-

ICRGNGYCG). The multiple Cys residues form disulfide bridges. These constrain the conformation lf the peptide and protect from serum peptidases. An *in vitro* serum stability assay showed that 87% of this peptide was intact after 2 hours incubation in human serum. Small animal PET imaging demonstrates $\alpha_v\beta_6$ –specific uptake of this peptide in tumors. However, this peptide still suffers from very high kidney uptake at short timepoints (19 ± 5% ID/g compared to 1.9 ± 0.4% ID/g in $\alpha_v\beta_6$ –expressing tumors). This study only goes out to 2 hours post-injection. Therefore, it is unknown whether this peptide is retained in the kidneys.

### *H2009.1: A High Affinity Peptide Ligand for $\alpha_v\beta_6$*

Our lab first identified the H2009.1 peptide utilizing phage display biopanning on whole H2009 adenocarcinoma cells [211]. The H2009.1 peptide was originally selected as a 20 amino acid peptide with the sequence **RGDLATL**RQLAQEDGVVGVR. By fluorescence microscopy, it was shown that M13 bacteriophages bearing this peptide on the PIII coat protein bind and internalize specifically into NSCLC cell lines and not into control normal lung cell lines. The chemically synthesized peptide blocked uptake of the H2009.1-bearing phage in a concentration dependent manner, and did so 300-fold better than a control phage bearing a non-binding sequence.

Through alanine- and deletion-scanning, Shunzi Li was able to reduce the peptide to the 10 N-terminal residues without loss of binding affinity [212]. This reduction in size has multiple benefits. As discussed previously, smaller peptides penetrate into dense tumor tissue more efficiently than larger constructs. Shorter sequences can be synthesized more rapidly and at lower costs as well. In fact, the minimized sequence binds to $\alpha_v\beta_6$ –positive cells with

higher affinity than the full-length sequence. This is most likely due to reduced entropic cost of binding or perhaps removal of steric hindrance.

Additionally, the reduction to the minimal binding sequence allowed for more reliable database searching to determine potential binding partners for H2009.1. The RGD sequence of H2009.1 initially suggested $\alpha_v$ integrins as the binding partners for the peptide. However, it was not until the sequence was shortened to 10 residues that statistically significant homology was observed specifically for ligands of $\alpha_v\beta_6$. The specific interaction between H2009.1 and $\alpha_v\beta_6$ was then confirmed by blocking of phage infection of H2009 cells with 10D5, a function-blocking monoclonal antibody against $\alpha_v\beta_6$ [152]. Since then, we have shown that H2009.1 binds and internalizes into many NSCLC cell lines, all of which express $\alpha_v\beta_6$ [187]. This peptide also binds and internalizes into cell lines of every cancer type known to express $\alpha_v\beta_6$ so far.

The binding affinity was also significantly improved by multimerization of the peptide. Increasing the valency of the peptide ligand to a tetramer increased binding affinity exponentially. The monomeric H2009.1 peptide binds to target cells with a $K_D$ of 10 nM as measured by competition with H2009.1-bearing bacteriophage. By the same assay, the tetramer binds with an affinity of 400 pM [212]. This was the state of H2009.1 development when I joined the lab. Thus, the 10-residue, tetrameric H2009.1 peptide was the lead compound for my project.

The H2009.1 dimer is a promising targeting ligand for PET imaging of $\alpha_v\beta_6$–positive tumors [105]. Our group, in collaboration with Xiankai Sun's lab, has been working toward the optimization of this peptide for imaging applications for quite some time. The

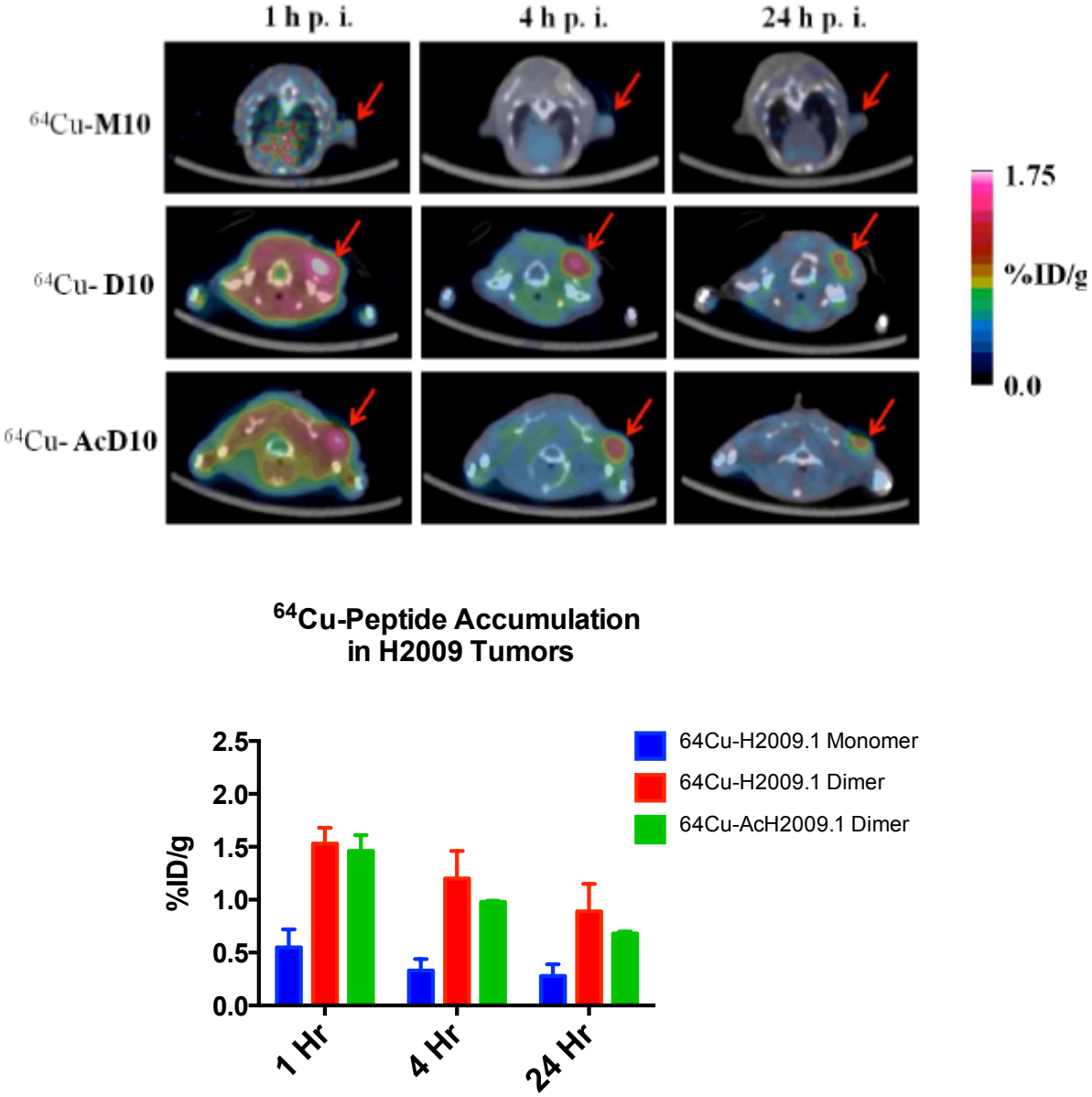


**Figure 2.10 Trans-axial PET Images of mice bearing H2009 xenograft tumors 1, 4, and 24 Hrs post-injection with H2009.1-targeted, $^{64}$Cu-loaded, bi-functional chelators.** Monomeric H2009.1 (M10) does not sufficiently accumulate in αvβ6-positive tumors for reliable imaging. Dimerization of H2009.1 (D10) significantly increases tumor signal. However, signal from other organs is also much higher. N-terminal acetylation reduces off-target accumulation of the dimeric H2009.1 (AcD10) without impacting tumor signal. Modified and published with permissions from [105].

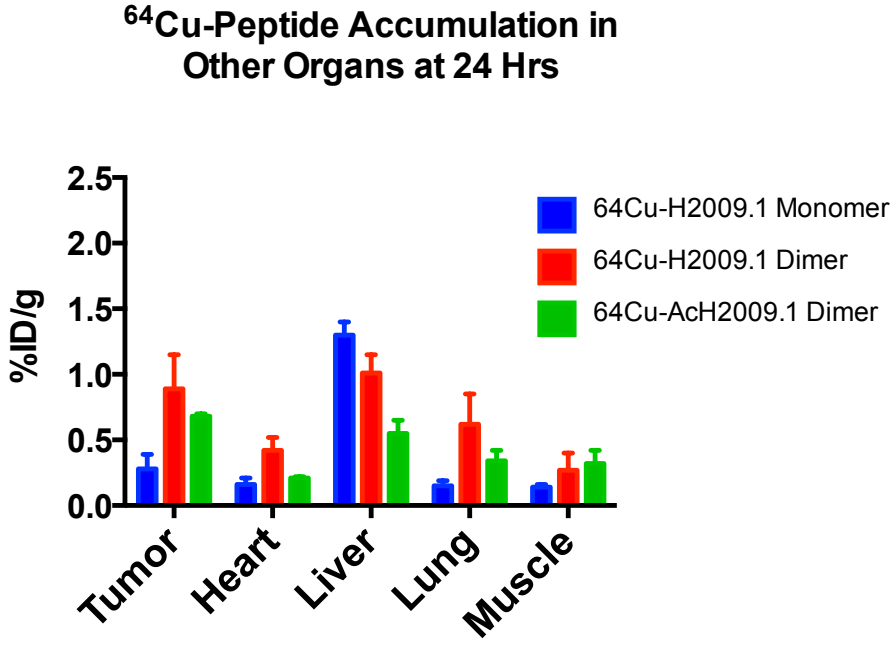


**Figure 2.11 Quantification of H2009.1 Peptide Accumulation in Organs 24 HPI.** Dimerization of H2009.1 significantly increases tumor signal. However, signal from other organs is also much higher. N-terminal acetylation reduces off-target accumulation of the dimeric H2009.1 without impacting tumor signal. Modified and published with permissions from [105].

dimerization of H2009.1 significantly improved tumor signal, but it also increased off-target signal, particularly in the kidneys (See Figure 2.10). In efforts to increase tumor signal, the N-terminus of H2009.1 was acetylated to stabilize the peptide in serum. The modification did not significantly impact PET signal in $\alpha_v\beta_6$ –expressing tumors. Surprisingly, it did decrease accumulation in off target organs (Figure 2.11). Importantly, acetylated of the H2009.1 dimer significantly decreased both initial accumulation in the kidneys and long-term retention (Figure 2.12). At the time that I joined the project, the N-acetylated H2009.1 dimer was the most promising *in vivo* targeting ligand the group had developed. I used this imaging data as a guide for much of my doctoral work.

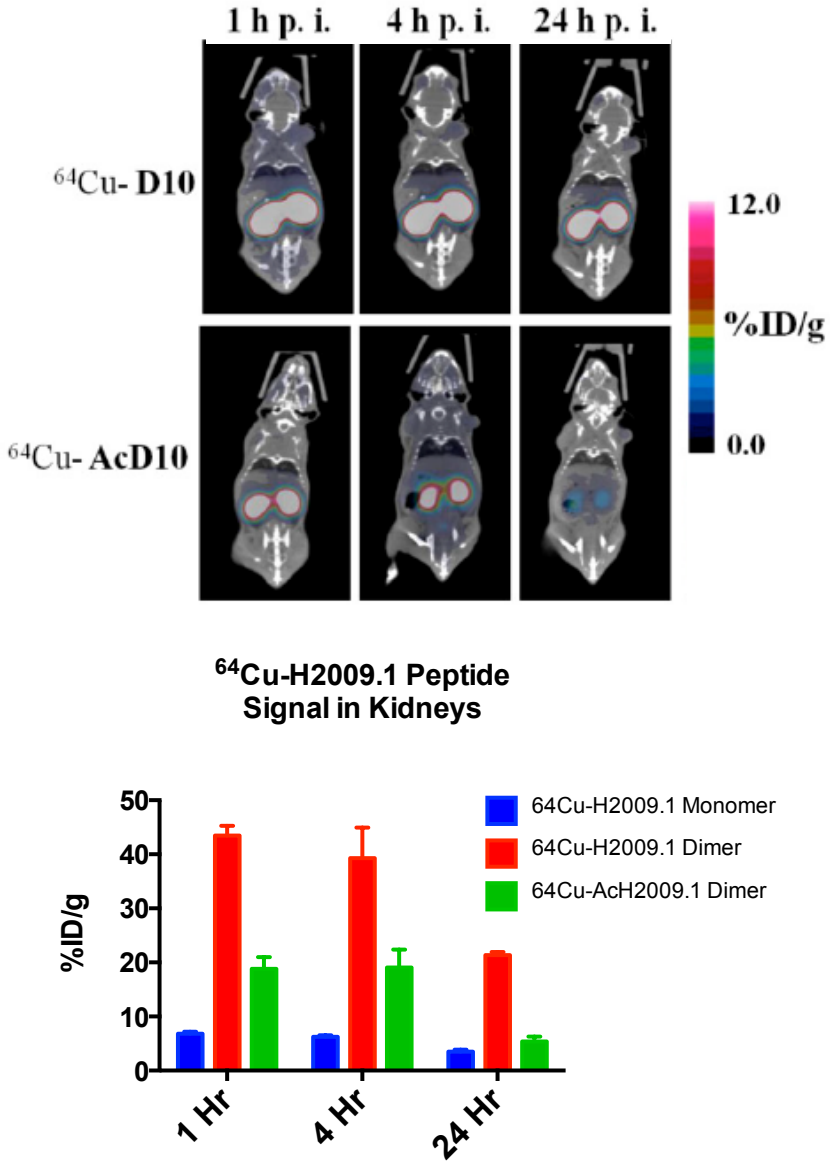


**Figure 2.12 Coronal PET Images of mice bearing H2009 xenograft tumors 1, 4, and 24 Hrs post-injection with H2009.1-targeted, $^{64}$Cu-loaded, bi-functional chelators.** N-terminal acetylation of the dimeric H2009.1 targeting ligand significantly decreases kidney signal 1 hr post-injection and also decreases retention in the kidneys at 4 and 24 hrs post-injection. Modified and published with permissions from [105].

# CHAPTER THREE
# SYNTHESIS OF H2009.1 ANALOGS AND OTHER PEPTIDES

## Introduction

Bruce Merrifield developed solid phase peptide synthesis (SPPS) in the early 1960s [213]. This approach uses an insoluble support upon which the peptide chains are built, moving from the C-terminus out to the N-terminus. Before the advent of SPPS, peptides were synthesized in solution, with each intermediate requiring isolation and purification. SPPS allows for the excess reagents to be filtered and washed away while retaining the growing peptide chain on polymeric beads. This facilitates rapid synthesis with significantly improved yields. The development of fluorenylmethyloxycarbonyl (Fmoc) protecting chemistry for amines in the 1970s allowed for much milder deprotection and cleavage conditions to be used [214]. Since then, SPPS has become the standard technique used for the synthesis of thousands of peptides and peptide analogs.

The basic flow of SPPS involves iterative deprotection and addition reactions punctuated by washing steps to remove excess reactants. The most common solvent for all of these steps is dimethylformamide. A wide variety of polymer support resins are commercially available for the synthesis of peptides of diverse lengths and C-terminal functional groups. The C- to N-terminal workflow of SPPS makes N-terminal modifications of peptides fairly straightforward. At the point of differentiation, the resin can be divided, and synthesis of each variation can continue.

**The workflow of SPPS**

Amino acids used in peptide synthesis are protected at the N-terminus with Fmoc groups. Therefore, the first step in each addition of an amino acid is the deprotection of the N-terminus. A solution of piperidine, an organic base of moderate strength, in DMF is added to the resin and mediates deprotection as shown in Figure 3.1. The advent of Fmoc chemistry in SPPS allows for acid labile protecting chemistry to be used on the reactive side chains of residues incorporated into the peptide. The peptide is maintained under neutral or basic conditions until it is cleaved from the resin.

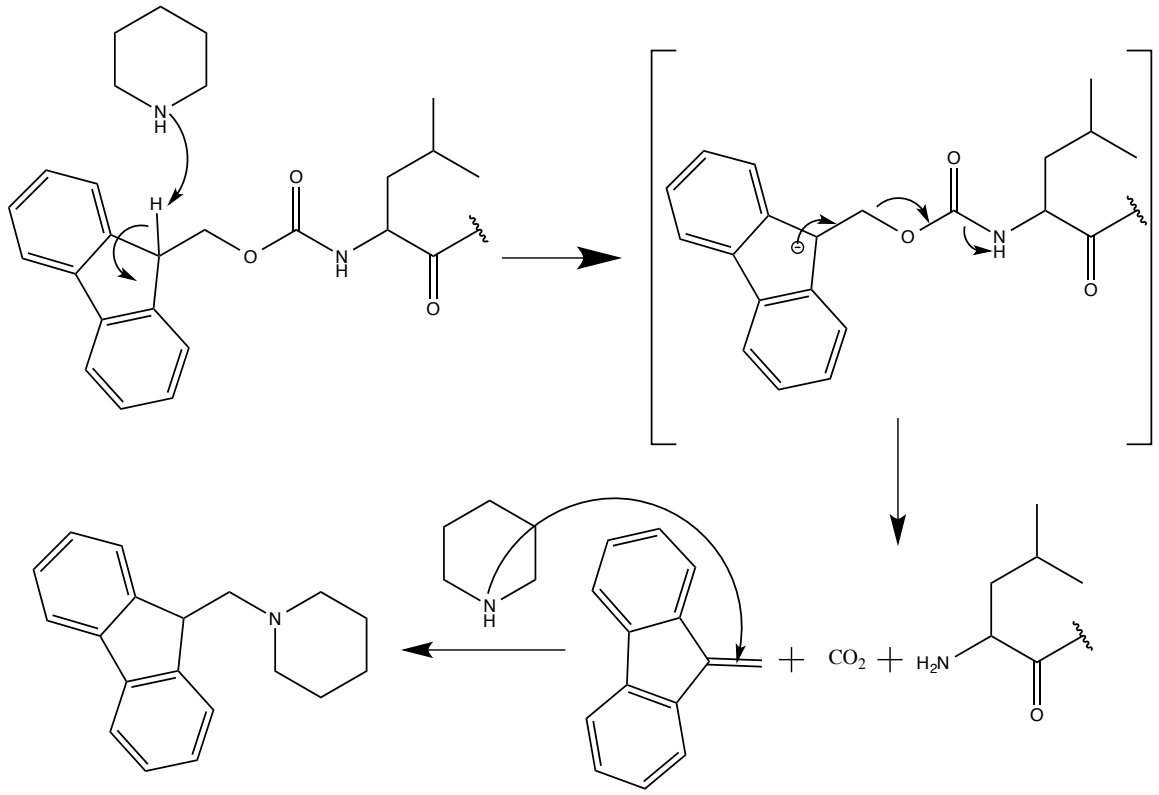


**Figure 3.1 Mechanism of deprotection of the Fmoc group with piperidine to produce a free N-terminus during peptide synthesis.** Piperidine deprotonates the tertiary carbon of the fluorenyl ring system, inducing β-elimination and the formation of carbon dioxide and dibenzofulvine. Excess piperidine scavenges dibenzofulvine, preventing reaction with the newly released primary amine.

The coupling of the newly deprotected amine to the carboxyl group of an incoming residue is not an efficient process. To achieve fast coupling without significant side reactions, the carboxyl group of the incoming residue must be activated. The conversion of the carboxyl to an ester provides a much more stable leaving group for the formation of the peptide bond. This significantly increases the rate of reaction and reduces unwanted side products. A myriad of reagents are available for the activation of Fmoc protected amino acids, each with their own advantages and disadvantages.

Reagents that produce the highest efficiency and specificity are more expensive. Synthesis is therefore performed using the most cost effective coupling reagents for the specific peptide bond being formed. In the case of this project, a combination of hydroxybenzotriazole (HOBt) and O- (Benzotriazol-1-yl)-N,N,N′,N′-tetramethyluronium hexafluorophosphate (HBTU) was used. N-methylmorpholine (NMM), a weak organic base, is also included to promote activation of the carboxyl group. This combination produces good yields in reasonable reaction times (45 minutes) with few side products. A major advantage of SPPS is that activation and addition of the N-terminal amino acid can be achieved in one step. The mechanism for this step is seen in Figure 3.2.

As discussed in the previous chapter, the N-terminus of a peptide can be modified in a variety of ways. For this project, several peptides bearing unnatural N-terminal residues were synthesized. Additionally, some peptides were N-acetylated. N-acetylation is performed by incubation of the resin-bound peptide with a basic solution of acetic anhydride. Acetic anhydride is a strong electrophile and does not require activation to promote addition to the

primary amine of the N-terminus. The mechanism for the N-acetylation of peptides is shown in Figure 3.3.

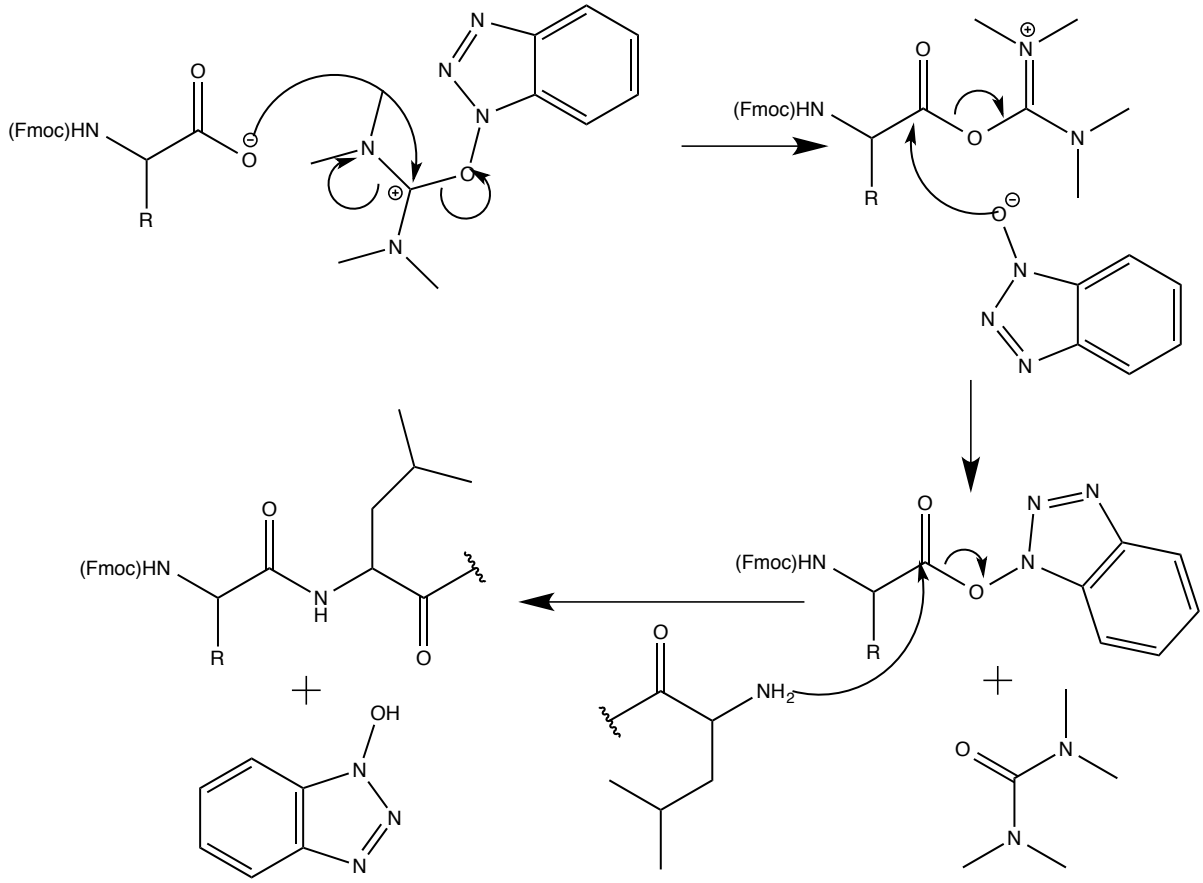


**Figure 3.2 Mechanism of amino acid activation and addition at N-terminus of nascent peptide chain.** In the presence of NMM, the carboxyl group of the new amino acid is deprotonated, allowing for attack on the tertiary cation of HBTU. HOBt than attacks the newly formed ester with tetramethylurea as the leaving group, forming a highly electrophilic carbonyl which is attacked by the free amine previously N-terminal amino acid. HOBt is then reformed as a leaving group.

After the addition of the final residue and deprotection of the N-terminal Fmoc group, the complete peptide is then cleaved from the resin using a strong acid, in our case trifluoroacetic acid (TFA). Protecting groups on any reactive side chains should be acid-labile so that they are also removed from the peptide during cleavage. When cysteine-

containing peptides undergo acid hydrolysis from the resin, a reducing agent such as ethanedithiol (EDT) should be present to prevent disulfide formation or other side reactions. A scavenger is also used to prevent unwanted reactions under the strongly acidic conditions. By far the most popular scavenger in peptide synthesis is triisopropylsilane (TIPS).

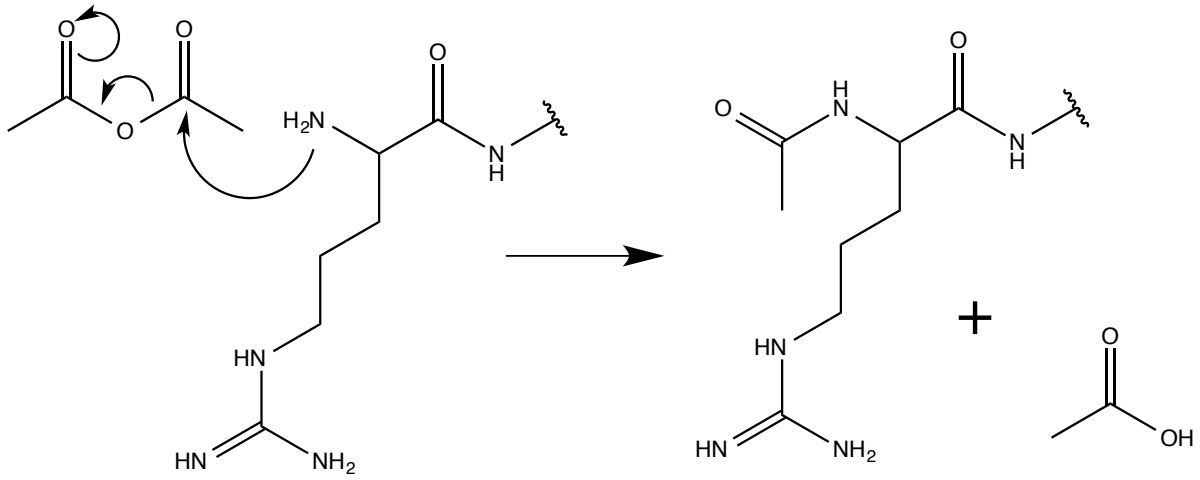


**Figure 3.3. Mechanism for acetylation of the N-terminus of a Peptide.** Acetic anhydride is a strong electrophile promoting addition to the free amino terminus and formation of acetic acid as a byproduct.

In order to stabilize the C-termini of our targeting peptides, we chose to cap them with primary amides rather than leaving the free carboxylate. The branched lysine core peptides, with their C-terminal β-alanine residues are sufficiently stable on their own, and do not require amidation. These and other C-terminal modifications are generally controlled by the choice of resin used in the synthesis. For the synthesis of targeting peptides, NovaPEG Rink Amide resin to produce C-terminal amide and promote solubilization of the relative hydrophobic peptide. Wang resin, already pre-loaded with β-alanine was used to produce the free C-terminus of the core peptides. The mechanisms for hydrolytic cleavage in both cases are shown in Figure 3.4.

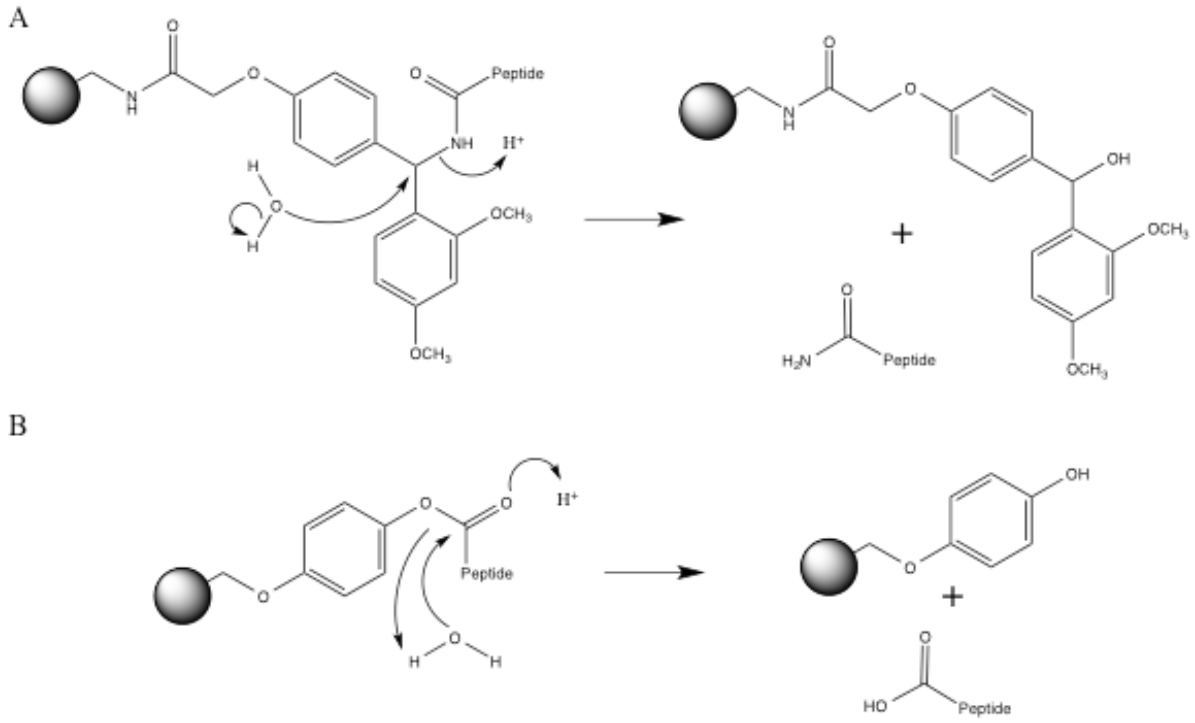


**Figure 3.4 Mechanisms for cleavage of peptides from resin to produce an amidated (A) or free (B) carboxy terminus.** Both reactions follow a simple acid hydrolysis mechanism. Protonation of the secondary amine or carboxyl oxygen activates the adjacent electrophilic carbon for attack by a water molecule. The peptide is released as a leaving group**.**

The targeting peptides and lysine cores are synthesized, cleaved, and purified by high performance liquid chromatography (HPLC) separately. At this point, and at each subsequent step of the synthetic process, the success of each reaction is verified by matrix-assisted laser desorption/ionization spectrometry (MALDI). For many groups, these are the final steps before conjugation of the peptide to a drug, imaging agent, or other cargo. However, upon observation of a significant loss of binding affinity when the H2009.1 peptide is removed from the context of the bacteriophage, our group determined further steps were necessary.

When the H2009.1 peptide is incorporated into the PIII protein of the M13 bacteriophage, it is displayed in 3-5 copies in a cluster on one end of the phage particle

(Figure 1.2A). We hypothesized that this clustering allowed for increased binding affinity by increasing the avidity of the peptides. A variety of common drug carrier systems effectively multimerize targeting ligands. These include dendrimers, liposomes, micelles, and other nanoparticles. These constructs are capable of incorporating hundreds or thousands of targeting peptides into one multimeric construct. However, these large carriers often fail to distribute throughout tumors, and spacing between targeting peptides is more difficult to control. Our group chose to closely mimic phage presentation by incorporation of small lysine based core peptides as shown in Figure 3.5. The simple design branches at each free amine of the lysine N-termini and side chains. PEG linkers were incorporated between the targeting H2009.1 peptides and the multimeric cores to act as spacers and to improve solubility.

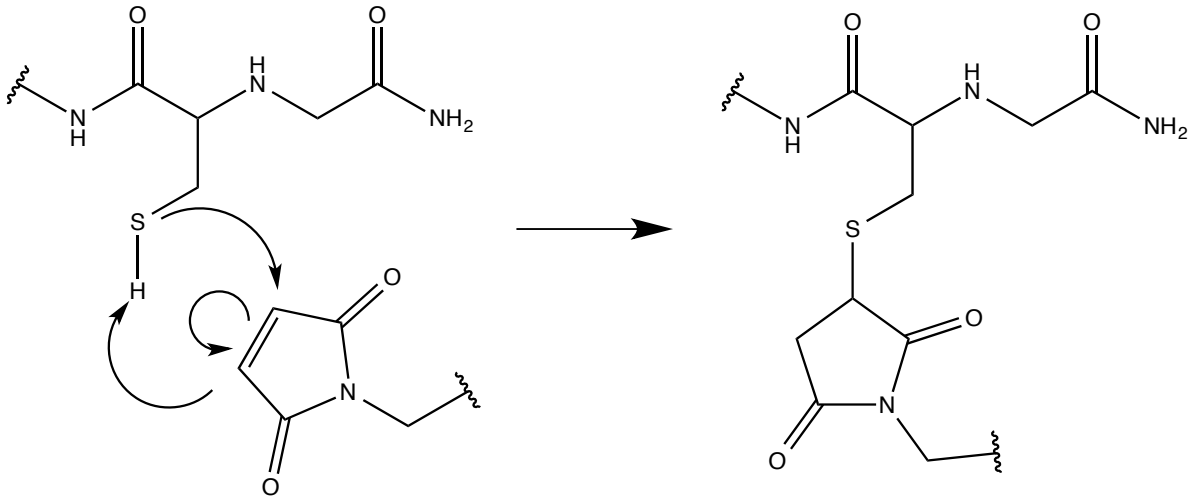


**Figure 3.5 Mechanism of multimerization by Michael addition of monomeric targeting peptides to lysine cores.** In PBS (pH 7.4), the alkene of the maleimide acts as a Michael acceptor, adding the free thiol of the C-terminal cysteine residue to form a stable thioether.

Initially, the multimeric H2009.1 peptides were manufactured in a single linear synthesis, building the H2009.1 peptide branches directly on the resin-bound lysine core. This method produced low yields with many byproducts, particularly for the tetrameric peptide. Incomplete addition of any amino acid on any single branch of the multimer produced contamination. The convergent synthesis, developed in our lab by Shunzi Li, involves separate synthesis of the lysine cores and targeting sequences with simple coupling of the two peptides in solution. This method produces much higher yields in comparison to synthesis of the full multimeric ligand on the resin [212]. The free thiols of the C-terminal cysteines of the targeting peptides add across the alkene of the maleimide group of the lysine cores following the mechanism of a Michael addition as shown in Figure 3.5. This reaction was used to produce multimers of all valencies used to core peptides bearing biotin or protected cysteine residues for downstream labeling.

The convergent synthesis also allows for modular design of peptides. Stocks of targeting sequences and cores can be produced in large scale. Our group predominantly uses lysine cores with C-termini cysteines or biotinylated glutamine residues. The appropriate targeting peptide and multimeric core can then be matched to specific experiments to maximize flexibility and use of resources. For example, this dissertation focuses on the H2009.1 peptide at two different valencies and several different labels depending on the nature of a given assay. The structures of these core peptides are shown in Figure 3.6. For *in vivo* NIRF imaging, the H2009.1 monomer is conjugated to a dimeric or tetrameric lysine core bearing a C-terminal cysteine. This cysteine is then utilized to covalently label the peptide with Cy5 dye. For ELISAs, the H2009.1 peptide is multimerized on a biotinylated

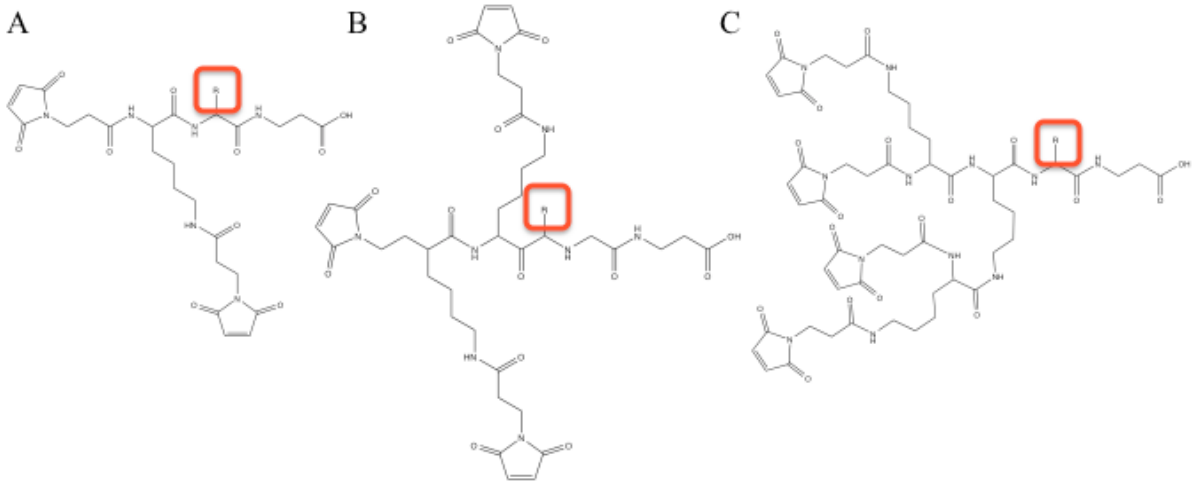


**Figure 3.6 Structures of multimeric cores.** Lysine-based branching peptides constitute the core of each multimeric targeting peptide. These are used to produce A) dimeric, B) trimeric, and C) tetrameric peptide ligands. Boxes indicate location of tag conjugation. This method of convergent synthesis allows for modular design of ligands with variable targeting sequence, avidity, and cargo [212].

core. This allows for the use of an avidin-HRP conjugate as a "secondary" in the standard ELISA protocol.

Peptides conjugated to cysteine bearing lysine cores require additional steps. The C-terminal cysteines of lysine cores used for covalent loading are orthogonally protected with acetamidomethyl (Acm) groups to prevent polymerization during the multimerization reaction. After purification of the multimer, these cysteine residues must be deprotected to allow for conjugation of the desired payload. There are several methods for deprotection of Cys(Acm) using heavy metals or iodine. Silver salts provide cost effective deprotection in reasonable reaction times. In our lab, deprotection is achieved using silver (I) acetate in TFA to produce a silver sulfide. The proposed mechanism for this step is shown in Figure 3.7. This is then stirred with dithiothreitol in acetic acid to chelate away the silver and protonate

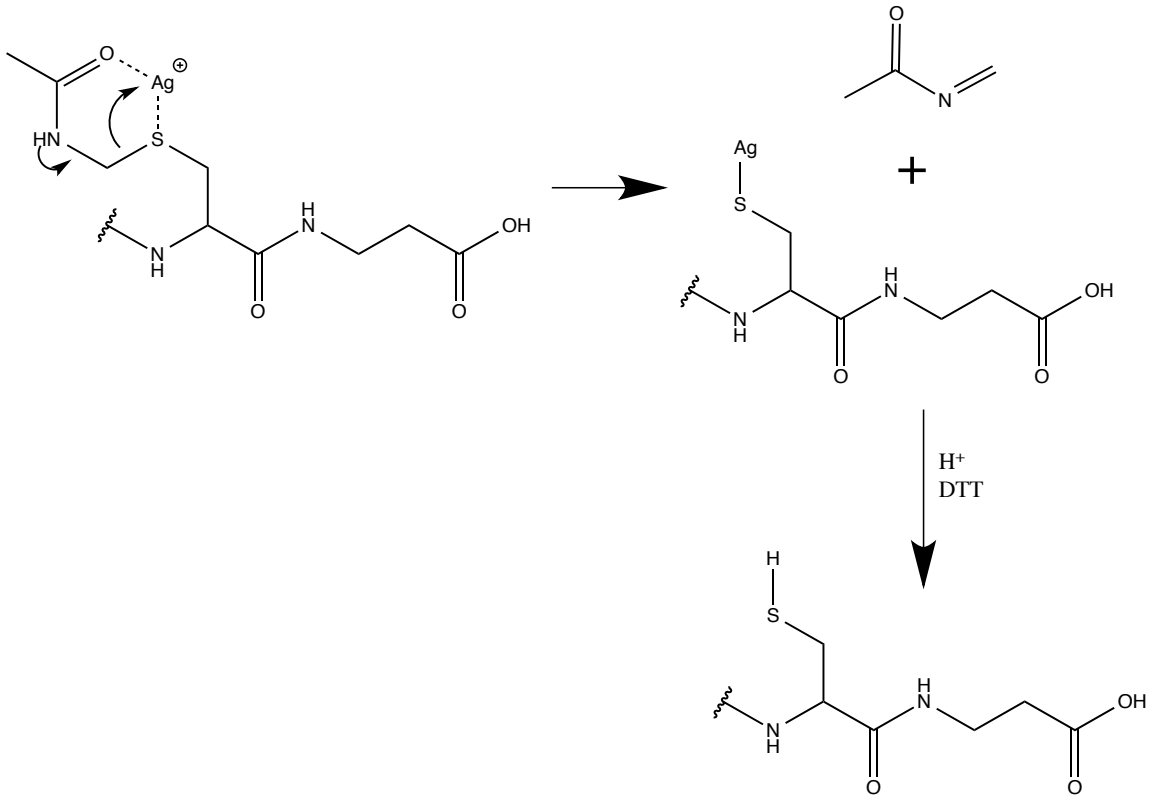


**Figure 3.7 Mechanism of Acm Deprotection to produce free thiol for conjugation of peptide to cargo.** The sulfur and carbonyl oxygen of the Acm group co-ordinate silver (I) leading to formation of the silver sulfide. The protecting group leaves as N-methylene-acetamide. After precipitation of the peptide-silver complex in ether, DTT and acetic acid reduce the silver sulfide to a free sulfhydryl group.

the cysteine to give the final product. After de-salting and purification by HPLC, the deprotected peptide can be loaded with maleimide-conjugated cargo by the same mechanism followed in multimerization as shown in Figure 3.5.

## Methods

*Synthesis of Monomeric Peptides*

Starting monomeric peptides were synthesized using standard Fmoc solid-phase peptide synthesis techniques on a Symphony Synthesizer. Amino acid reagents were purchased from EMD Millipore and Sigma-Aldrich (Table 3.1). Fmoc-$PEG_{11}$-OH was purchased from PolyPure. All reactions were performed at room temperature.

NovaPEG Rink amide resin was placed in disposable reaction vessels to 50-100 μmol (based on loading information provided by EMD Millipore). Dimethylformamide (DMF) was added to the reaction vessel (2.5 mL, 30 min, 2 times) and incubated to swell the resin and allow for maximal reactivity. Synthesis was performed in an iterative manner, starting at the C-terminus and working toward the N-terminus. Residues were added to the peptide chain by repeating cycles of N-terminal deprotection and formation of new peptide bonds. Deprotection of the Fmoc protected N-terminus was accomplished by incubation of the resin in 2.5 mL 30% piperidine in DMF, 3 times, 10 minutes each. Following deprotection, the resin was washed with 2.5 mL DMF 6 times, 30 seconds each wash. To conjugate the next amino acid, 2.5 mL activating solution consisting of HOBt, HBTU, and NMM in DMF was added to the deprotected resin-bound peptide along with 2.5 mL 200 mM amino acid solution (to reach 5 molar equivalents relative to deprotected N-terminus) and incubated for 40 minutes. Before the next deprotection step, the resin-bound peptide was again washed with 2.5 mL DMF 6 times, 30 seconds each wash.

| Amino Acid | Protecting Chemistry |
|---|---|
| Alanine | NA |
| Cysteine | Trityl (Trt) or Acetamidomethyl (Acm) |
| Aspartate | O-tertbutyl (OtBu) |
| Glutamate | O-tertbutyl (OtBu) |
| Phenylalanine | NA |
| Glycine | NA |
| Histidine | Trityl (Trt) |
| Isoleucine | NA |
| Lysine | Methyltrityl (Mtt) or Fluorenylmethoxycarbonyl (Fmoc) |
| Leucine | NA |
| Methionine | NA |
| Asparagine | Trityl (Trt) |
| Proline | NA |
| Glutamine | Trityl (Trt) |
| Arginine | Pentamethyldyhydrobenzofuran-5-sulfonyl (Pbf) |
| Serine | Tertbutyl (tBu) |
| Threonine | NA |
| Valine | NA |
| Trpytophan | NA |
| Tyrosine | Tertbutyl (tBu) |

**Table 3.1 Summary of Amino Acids Used in Peptide Synthesis.** Fmoc-protected amino acids with side chain protecting groups indicated where appropriate. When two protecting groups are listed, the second corresponds to protecting chemistry used in synthesis of the multimeric core peptides.

This process of deprotection and conjugation was repeated to produce the full peptide sequence, ending with a deprotection step to give a free N-terminus. The $PEG_{11}$ linker was added in a similar manner to the amino acids, with the exception of using 2.5 molar equivalents and increasing the reaction time to 3 hours. If appropriate, N-acetylation of

peptides was accomplished by mixing the resin-bound monomeric peptide in 90% DMF/5% N-methylmorpholine/5% acetic anhydride (30 min, 2 times, at room temperature). Upon completion of the peptide sequence, the resin beads are washed with DMF (30 sec, 6 times) followed by dichloromethane (30 sec, 9 times). The beads are then dried under nitrogen for 10 min and stored under vacuum for 48 hours before cleavage of the peptides from the resin.

The peptides were then cleaved from the resin support via hydrolysis in acidic solution. 5 mL of 94% trifluoroacetic acid (TFA)/2.5% water/2.5% ethanedithiol (EDT)/1% triisopropylsilane (referred to as cleavage solution) was added to the dried resin and the mixture was mixed on a rocker for 2 hours at room temperature. The resin was then filtered from the mixture, rinsing with an additional 5 mL cleavage solution, through the fritted reaction vessels used in synthesis of the peptide. The solution was then concentrated to 0.5-1 mL under nitrogen, and the peptide was precipitated by addition of 45 mL diethyl ether and placed in a – 80° freezer for 1 hr. The precipitated peptide was then pelleted by centrifugation at 3500 rpm for 5 min, and the pellet was washed twice with additional ether. The pellet was then allowed to air dry in the chemical hood for ~15 minutes before being placed under vacuum, in a desiccator, for a minimum of 3 hours.

*Synthesis of Multimeric Cores*

Synthesis of branched multimeric cores was performed using techniques similar to monomeric peptide synthesis, with several exceptions. A β-Alanine Wang resin was used as solid support, and each residue was mixed with the resin and HOBt/HBTU/NMM solution for 3 hours. C-terminal Cys residues were often included for later conjugation to drugs and

imaging reagents. Residues were added using 5 molar equivalents for each reactive amine. Deprotection of Fmoc-Lys(Fmoc)-OH was used to produce the branched peptide structure. Because the N-termini of the branches are maleimide groups, no final deprotection step is necessary. Also, the absence of free thiols in the peptide cores abolishes the need for EDT in the cleavage solution.

*Purification and Analysis of Synthesized Peptides*

The cleaved peptide products were purified by semi-prep HPLC on a C18 column. A gradient of 90% water/10% acetonitrile to 60% water/40% acetonitrile over 80 minutes was used as the mobile phase. Fractions were collected and analyzed by MALDI to ensure the identity of synthesized peptides by mass. Verified HPLC fractions were frozen at -80°C for 1 hr and dried on a lyophilizer for 48 hours. Purity of the synthesized peptides was then assessed using analytical HPLC on a 5 mm C18 column. A similar gradient was used for the mobile phase, shortening the total time to 40 minutes. These purification and analysis techniques were used upon synthesis of monomeric, multimeric, and labeled peptides.

*Synthesis of Multimeric Peptides*

Multimeric peptides were produced using convergent synthesis from the purified monomeric and core peptide. Multimeric core was dissolved in 1mL phosphate buffered saline (PBS) with 10 mM ethylenediaminetetraacetic acid (EDTA). Monomeric peptide was then added to the solution at appropriate equivalents for the multimer being synthesized (3

eq. for dimer, 6 eq. for tetramer). The reaction was mixed at room temperature for 2 hours and injected onto a semi-prep C18 HPLC column for purification as described above.

*Deprotection of Multimers with C-terminal Cysteines*

C-terminal cysteine residues were often used in the multimeric cores for later conjugation to various dyes. These residues were protected with Acm groups to provide regiospecific conjugation of the monomeric peptides to the cores. After purification and lyophilization, the multimeric peptides bearing these cysteines were deprotected to give the free thiol. Peptide was dissolved in TFA with 0.1% (v/v) anisole and 0.28% (w/v) silver acetate and incubated at 4°C for 2 hours. The reaction was concentrated to ~ 50 µL under nitrogen, and the peptide was precipitated by addition of 1.2 mL diethyl ether and incubated at -80°C for 1 hr. The precipitated peptide was pelleted by centrifugation at 16,000-x g for 5 minutes and re-suspended in 1 mL 1 M acetic acid with 0.3% dithiothreitol. This suspension was stirred at room temperature overnight. The mixture was then centrifuged at 16,000 x g form 5 minutes, and the supernatant was injected onto a semi-prep C18 HPLC column for purification as described above.

**Results**

These techniques were employed to synthesize roughly 75 unique peptide constructs as summarized in Table 3.2 and Figure 3.8. These include the peptides for my project including the H2009.1 peptide and modified versions of it, as well as other peptides used in several other projects in the lab. Additional H2009.1 peptides were produced at each valency

| Peptide | Sequence | Monomer | Dimer | Trimer | Tetramer |
|---|---|---|---|---|---|
| H2009.1 | RGDLATLRQL-$PEG_{11}$-YC | X | X | X | X |
| AcH2009.1 | (ac)RGDLATLRQL-$PEG_{11}$-YC | X | X | X | X |
| L-Leu H2009.1 | LRGDLATLRQL-$PEG_{11}$-YC | X | | | X |
| D-Leu H2009.1 | (d)LRGDLATLRQL-$PEG_{11}$-YC | X | X | | X |
| N-Leu H2009.1 | (n)LRGDLATLRQL-$PEG_{11}$-YC | X | | | X |
| L-Val H2009.1 | VRGDLATLRQL-$PEG_{11}$-YC | X | | | X |
| D-Val H2009.1 | (d)VRGDLATLRQL-$PEG_{11}$-YC | X | | | X |
| N-Val H2009.1 | (n)VRGDLATLRQL-$PEG_{11}$-YC | X | | | X |
| H2009.1 GGG | RGDLATLGGG-$PEG_{11}$-YC | X | X | | |
| ScrH2009.1 | DALRLQGTLR-$PEG_{11}$-YC | X | X | X | X |
| AcScrH2009.1 | (ac)DALRLQGTLR-$PEG_{11}$-YC | X | X | | X |
| HCC15.1 | ATEPRKQYATPRVFWTDAPG-$PEG_{11}$-C | X | | | X |
| ScrHCC15.1 | | X | | | X |
| HCC15.2 | FHAVPQSFYTAP-$PEG_{11}$-C | X | | | X |
| ScrHCC15.2 | QFSFHYPVAPTA-$PEG_{11}$-C | X | | | X |
| HCC1299.2 | YAAWPASGAWTGTAP-$PEG_{11}$-C | X | | | X |
| ScrH1299.2 | | X | | | X |
| H460.1 | EAMNSAEQSAAVVQWEKRRI-$PEG_{11}$-C | X | | | X |
| ScrH460.1 | | X | | | X |

**Table 3.2 Summary of Peptides Synthesized Over the Course of this Project.** Monomeric targeting peptides were synthesized for all of these peptides, with multimerization performed where indicated. Uncapped, multimeric peptides were generally labeled with biotin for use in other projects within our lab. H2009.1 and indicated analogs were labeled with biotin, AF488, Cy5, or 800CW dyes.

for use in a collaborative PET imaging project with Xiankai Sun's group in the UT Southwestern Advanced Imaging Research Center.

The targeting sequences of each of these peptides were identified through phage display biopanning against whole NSCLC cells in culture as described in the previous chapter [101, 187]. Each of these peptides binds to a subset of NSCLC cell lines in a

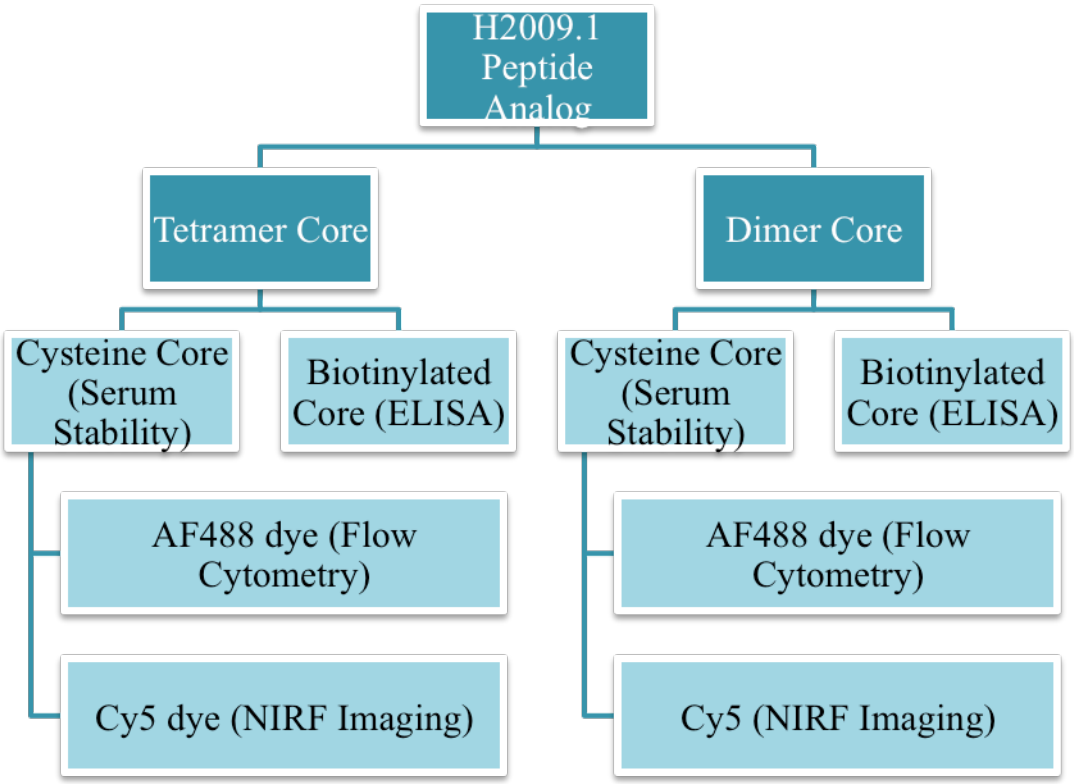


**Figure 3.8 Peptides Synthesized for Each H2009.1 Analog in the Optimization Library.** For each analog of the H2009.1 peptide examined in this dissertation, up to 8 separate constructs were synthesized as shown above. The assays in which specific peptide-label constructs were utilized are shown in parentheses.

saturable and sequence-specific manner. All of these peptides, with the exception of H460.1, induce RME to deliver cargo into cells as shown by a variety of methods. Importantly, binding and internalization of these peptides is not restricted to any histological subtype of NSCLC, and in fact is not restricted to NSCLC itself. Cell lines derived from breast, prostate, ovarian, pancreatic, liver, and colorectal cancer all bind and internalize at least one of member of this suite of peptides. Importantly, none of the selected peptides, either within the phage or as free synthetic peptide demonstrates binding and internalization into control cell

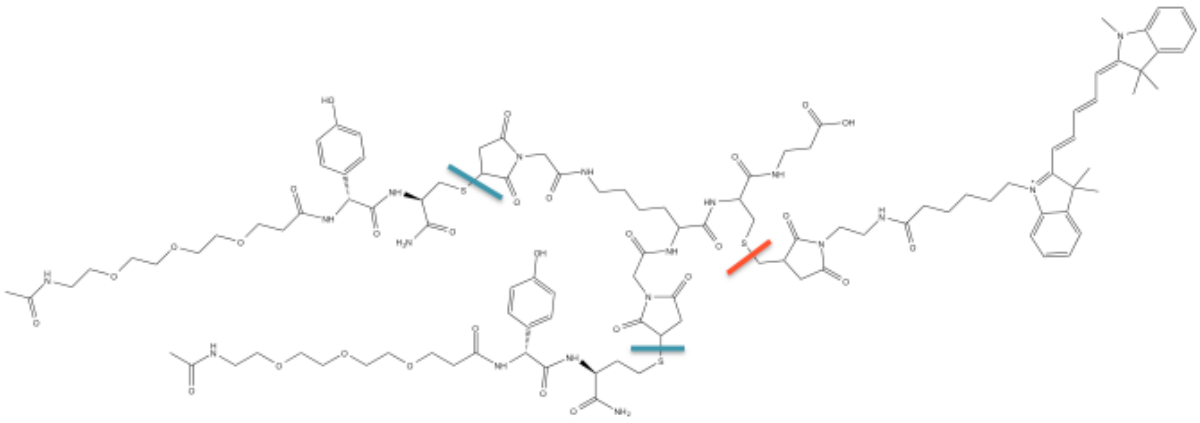

**Figure 3.9 Example Structure of a Labeled Peptide Conjugate.** H2009.1 Dimer labeled with Cy5 dye. Note the 11-mer PEG linker between the H2009.1 binding sequence and the branched lysine core. H2009.1 peptides also include a Tyr residue outside of the binding sequence to allow for concentration determinations by absorbance. All other peptides contain absorbing residues within their binding sequences, and this extra Tyr is not included. The Cy5 dye is conjugated via a cysteine-maleimide linkage. Peptides are also conjugated to dye through a biotin-streptavidin interaction in appropriate contexts. Lines indicate linkages between monomeric H2009.1 and lysine core (blue) as well as between the lysine core and cargo molecule (red).

lines. This work was recently published, and several projects to develop these peptides as NSCLC-targeting ligands are underway in our laboratory [187].

My project utilizes dimeric and tetrameric H2009.1 peptides, and required multiple syntheses of many analogs labeled with biotin or a maleimide-conjugated fluorophore as appropriate for each assay described in later chapters. Success of each synthesis was verified by MALDI and each of these peptides was purified to >95% purity as determined by analytical HPLC (see Appendix A). Yields were not calculated so long as sufficient peptide was produced to perform the necessary experiments. Example structures of the multimeric cores and a dimerized H2009.1 peptide are included in Figures 3.7 and 3.8 to illustrate the

final tumor targeting peptide ligand. The H2009.1 dimer is shown labeled with Cy5, the dye used in animal imaging experiments.

**Discussion**

Careful synthesis and purification of each peptide was absolutely critical to the success of the project presented in this dissertation as well as others performed in our lab. Without the development of SPPS and Fmoc protecting chemistry, this project, as well as the entire field of peptide targeting ligands, would be virtually impossible. Using these techniques, I was able to synthesize milligram quantities of many unique peptides quickly and at very high quality. Analysis of peptide quality and purity by MALDI and analytical HPLC are standard practice in the peptide field. These are fast, relatively inexpensive methods that provide information on total molecular weight and relative purity of a peptide in a given sample. However, they are not foolproof techniques, and must be used in conjunction with careful recordkeeping and good lab practices.

For example, MALDI gives the total molecular weight and, in some circumstances, molecular weights of ionization fragments in a peptide sample. However, this does not provide sequence or isomer information. If a peptide sample has the predicted molecular mass, but does not behave in the expected manner, analysis by Edman sequencing or LC/MS/MS may be required to confirm the correct sequence was manufactured. This can also be an issue when using proprietary dyes and other labels where specific mass and structural data is not available.

Additionally, the precision of MALDI varies significantly by method. For peptides under 3 kD, reflector methods are used where the path of the laser light is more precisely focused using mirrors. This produces more accurate mass-to-charge ratios and results in the detection of mono-isotopic masses. When using reflector methods on a recently calibrated MALDI, one can generally assume that the actual mass of the peptide is within a Dalton of the detected mass. For larger peptides, particularly hydrophobic peptides that do not ionize well, linear methods must be used. These are much more sensitive than reflector methods, but inexact. Peaks in a MALDI spectrum taken using linear methods are wide and give more of a range of masses. Depending on the reliability of the machine and how recently it was calibrated, the actual mass of the peptide may fall up to 5 Daltons away from the detected mass.

The methods used for MALDI also impact the detection of impurities in the sample. While MALDI is by no means a quantitative method of assessing purity, it does give some idea of what byproducts are present in a sample. Because reflector methods are less sensitive, only the major products are detected in these samples. It is possible that minor products may go completely undetected. In contrast, linear methods are so sensitive, that they may detect impurities that are present in trace amounts, particularly if those impurities ionize more efficiently than the major products. It can also become difficult to differentiate between ionization products of the target peptide and actual contaminants in a sample. These caveats emphasize the importance of careful purification during semi-prep HPLC and final analysis of peptides by analytical HPLC before use in experiments. If there is any question as to the quality of peptide, it is best not to use it in an experiment as it may confound the results.

While determination of purity by analytical HPLC is critical to the successful use of peptides, it should not stand on its own. The contaminating byproducts in a peptide synthesis are often very similar in hydrophobicity to the peptide being synthesized. It is possible that standard solvent gradients may not completely separate all species in a reaction. For this reason, MALDI should always be performed in conjunction with analytical HPLC. If impurities are detected by MALDI, the gradient must be optimized to separate the major and minor species so that accurate purity quantification can be performed.

# CHAPTER FOUR
# OPTIMIZATION OF THE H2009.1 TETRAMERIC PEPTIDE FOR IN VIVO APPLICATIONS

## Introduction

The goal of this project was to improve long-term targeting and biodistribution of the H2009.1 peptide upon systemic administration in mice. I reasoned that capping the N-terminus of the H2009.1 peptide to protect it from serum aminopeptidases would significantly extend serum stability and improve *in vivo* targeting to $\alpha_v\beta_6$-expressing cells. Our initial studies using the H2009.1 peptide as a targeting ligand for PET imaging showed that N-terminal acetylation significantly reduced accumulation of the PET signal in the kidneys. I hypothesized that further stabilization of the H2009.1 peptide against peptidase-dependent degradation might further reduce the non-specific accumulation of the peptide ligand in non-target tissue.

As discussed in Chapter 1, common strategies for improving serum stability of small synthetic peptides include cyclization and PEGylation. Cyclization would likely change the secondary structure of the H2009.1. In order to maintain affinity and specificity for $\alpha_v\beta_6$ over other RGD-binding integrins, an α-helix must form in the amino acids directly C-terminal to the RGD motif (LXXL) [202]. As cyclization would likely disrupt this structure, it was eliminated as a potential stabilization strategy. N-terminal PEGylation is a potentially viable option for protecting the N-terminus. However, the polydispersive nature of the PEG polymer complicates characterization of peptide ligands, and isolated PEG polymers are expensive.

It has been demonstrated that terminal capping with D-amino acids can provide nearly complete protection of peptides against serum and lysosomal peptidases [115, 215]. This simple, elegant modification was promising because it should not significantly impair binding affinity of the peptide for $\alpha_v\beta_6$. While the H2009.1 peptide has free N-terminus, many $\alpha_v\beta_6$ –binding partners, including LAP and fibronectin, do not. I hypothesized that the addition of an unnatural amino acid at the N-terminus of the H2009.1 would produce a serum stable $\alpha_v\beta_6$-targeting ligand with decreased kidney accumulation.

To determine which amino acids should be used to cap the N-terminus, we looked to previous phage display panning results from our lab. The H2009.1 peptide was selected from a library designed and produced by William Dower's group at the Affymax Research Institute [216]. Panning experiments were also performed with a commercially available library (Lei Wu, unpublished results). This panning produced peptides with similar sequences to H2009.1 as seen in Table 4.1. The RGDLXXL motif in these peptides was located in the middle of these peptides rather than the N-terminus. We noted that the amino acid at the -1 position to the binding sequence was always a large aliphatic residue. A review of the known natural ligands of $\alpha_v\beta_6$ shows that this is not the case for all ligands of this integrin, indicating that the side chain of this residue may not have significant impact on binding [169, 200]. However, our lab's panning data suggests that a hydrophobic residue is the least likely to decrease binding and internalization of the peptide into $\alpha_v\beta_6$–positive NSCLC cells.

Because the addition of leucine and isoleucine residues N-terminal to the RGDLXXL binding sequence did not affect binding or specificity in the context of phage display, I chose

to cap the H2009.1 peptide with unnatural isomers of hydrophobic amino acids. To avoid the potential complications of multiple stereocenters, valine and leucine were selected as the capping residues. I then synthesized H2009.1 analogs capped with D-Leu, D-Val, norleucine, or norvaline as well as the natural isomers of these amino acids as controls. Because the N-acetylated H2009.1 dimer performed well in PET experiments, this modification was included in the library of tetrameric analogs. Some studies have also demonstrated additive effects of combining these two capping strategies [114]. I therefore included an N-acetylated D-Leu capped H2009.1 analog (AcD-Leu H2009.1) in the peptide library. Standard solid phase synthesis using F-moc protection chemistry was used to create this library as discussed in detail in Chapter 3.

## Methods

### *Cell Lines and Reagents*

Cell lines were obtained from the Hamon Center for Therapeutic Oncology Research at UT Southwestern Medical Center and were maintained using standard protocols. Fetal bovine serum was purchased from Gemini Bio-products, and RPMI was purchased from Hy-Clone. The Ph.D. -12 Phage Display Peptide Library was purchased from New England Biolabs. AlexaFluor 488-maleimide and Cy5-maleimide dyes were purchased from Molecular Probes and Lumiprobe, respectively. NOD/SCID mice were purchased from the UT Southwestern Mouse Breeding Core. Avidin-HRP was purchased from Pierce Biologicals, and 3,3′,5,5′-Tetramethylbenzidine (TMB) was purchased from Millipore.

*Internalization into H2009 Cells*

H2009 cells were seeded at 100,000 cells/well in 12-well culture plates in 1 mL RPMI + 5% FBS and allowed to adhere overnight. Cells were incubated for 2 hours at 37°C in tetrameric H2009.1 + AF488 at concentrations ranging from 250 pM to 200 nM. Wells were then washed 3 times with PBS and twice with an acid wash (0.1 M HCl with 0.9% NaCl, pH 2.2 with glycine). All washes were incubated for 5 minutes at room temperature, protected from light. After a final rinse with PBS, 1 mL 10 mM EDTA in PBS was added to each well, cells were scraped and peptide-dye uptake was quantified for 10,000 cells per treatment group on a CellQuanta™ flow cytometer. Mean fluorescence intensity of each sample was determined using WinMDI software. Concentration curves were plotted and $EC_{50}$ values calculated using GraphPad Prism. Experiments were repeated at least 3 times and reported values are the average calculated $K_D$s ± standard deviation.

*Serum Stability Assays*

1.5 mg of tetrameric peptide were dissolved in 180 µL human serum and incubated 20 µL aliquots at 37°C for 0, 1, 4, 12, 24, and 48 hrs. 100µL ethanol was added to precipitate serum proteins and the supernatants were collected by centrifugation at 1000 x g for 5 min. at 4°C. The pellets were then washed twice with 80% ethanol, combining the supernatant from each wash, and the solvent was evaporated on a SpeedVac. Remaining material was dissolved in 10% acetonitrile in water and subjected to analytical HPLC on a 60-minute gradient from 10-90% acetonitrile in water using a Waters Breeze HPLC system.

Chromatograms were integrated to assess the amount of intact peptide by total area under the curve. Degradation products were characterized on a Voyager MALDI/TOF.

*Near IR Fluorescence Imaging for Peptide Biodistribution In Vivo*

Dual tumor models were established as previously described [217]. All animal protocols were approved by the Institutional Animal Care and Use Committee at UT Southwestern Medical Center (Animal Welfare Assurance Number A3472-01, protocol number 2010-0280). H2009 xenograft tumors were implanted into the right flank of NOD/SCID mice by subcutaneous injection of 1e6 H2009 cells on day 0. On day 10, H460 xenograft tumors were implanted into the left flank of these mice by the same method. When both tumors reached a palpable size, 30 μg tetrameric H2009.1 + Cy5 peptide-dye conjugate in PBS was injected via tail vein with 6 animals per group. At 24 or 72 hours, animals were sacrificed by $CO_2$ inhalation and their organs were imaged using an IVIS® Lumina (Caliper Life Sciences) imager. Peptide-dye signal was normalized by organ mass, and the signal from organs of untreated mice was subtracted to remove background. Graphs were made and statistical analysis performed using GraphPad Prism.

*ELISA for Binding of Peptides to Recombinant Integrins*

Recombinant integrins $\alpha_v\beta_6$ and $\alpha_v\beta_3$ were resuspended at a concentration of 0.5 μg/mL in sterile PBS. 96-well NuncMaxiSorp ELISA plates were coated with integrin at 100 μL/well in columns 2-12. 100 μL/well sterile PBS was placed in column 1. Plates were wrapped in plastic wrap and stored at 4°C overnight or up to 1 week. The next day, PBS and

integrin solutions were flicked from the plates, and all wells were filled to capacity with blocking solution (PBS with 500 μM $CaCl_2$/10 mM $MgCl_2$/0.01% Bovine Serum Albumin (BSA)). Plates were covered and incubated at room temperature for 1-2 hours. Serial dilutions of biotinylated peptides were made in blocking solution. Blocking buffer was flicked from the plates and 100 μL appropriate dilutions of peptide were added to each well. Control wells received blocking buffer only, and other concentrations were applied in quadruplicate. Plates were covered and incubated at room temperature for 30 minutes. Plates were then washed 9 times by submersion in wash buffer (PBS with 500 μM $CaCl_2$ and 10 mM $MgCl_2$) and the plates were inverted on paper towels to drain for 1 min. 100 μL avidin-HRP (diluted 1:6000) in blocking solution was then added to each well. Plates were covered and incubated at room temperature for 30 minutes. Plates were again washed 9 times by submersion in wash buffer. 100 μL TMB substrate was added to each well and plates were incubated at room temperature for 5 minutes. The reaction was stopped by the addition of 100 μL 0.1 M HCl to each well. The absorbance of each well was then read at 450 nm on a spectrophotometer.

*Immunoblotting for $\beta_6$ Expression*

After cervical dislocation, mice were perfused with sterile PBS through the left ventricle. ~50 mg of organs including liver, lung, kidney, heart, spleen, and subcutaneous tumors were minced with a razor blade. Each tissue was added to 500 μL RIPA buffer with 1X Roche Complete Protease Inhibitor Cocktail and homogenized using a Dounce homogenizer. The organ extracts were then sonicated using a probe sonicator 3 times in 2-

second bursts. The lysates were centrifuged at 16,000-x g for 15 minutes at 4°C, and the supernatants were collected as final tissue lysates. Total protein content was determined by standard BCA assay, and 20 µg protein was loaded onto a 8% SDS-PAGE gel. Gels were run at 100 mV for 1.5 hours before transferring to PVDF membranes at 35 mV for 1 hour. Membranes were blocked in PBS with 0.2% Tween-20 and 5% BSA, and β6 (C-19 from Santa Cruz Biotechnology 1:1000) and actin (clone AC-40 from Sigma Aldrich 1:1000) antibodies in PBS with 0.2% Tween-20 and 5% BSA and placed on an orbital shaker at 4°C overnight. Blots were washed with PBS with 0.2% Tween-20 3 times for 5 minutes at room temperature. Secondary antibodies (rabbit anti-goat + 800CW dye from Li-Cor for β6, rabbit anti-mouse + AF684 for actin) were diluted 1:15,000 in PBS with 0.2% Tween-20 and 5% BSA and incubated on the membranes for 1 hour, protected from light. Blots were then washed 4 times for 5 minutes with PBS with 0.2% Tween-20 and visualized on an Odyssey scanner from Li-Cor.

## Results

### *Internalization of Capped H2009.1 Tetramers into $\alpha_v\beta_6$–expressing NSCLC cells*

Assessment of the N-terminally modified H2009.1 peptides began *in vitro*. Our lab has established that the tetrameric H2009.1 peptide binds to the integrin $\alpha_v\beta_6$ with high affinity and triggers endocytosis into tumor cells [187, 212, 218-221]. It is essential that any modifications made to the peptide avoid interfering with this process. I evaluated internalization of the H2009.1 analogs into H2009 cells, a NSCLC cell line positive for $\alpha_v\beta_6$ expression by flow cytometry. Each modified, tetrameric H2009.1 peptide was directly

labeled with AlexaFluor 488 (AF488) at the tetrameric core. After incubation with labeled H2009.1 peptide at various concentrations, the H2009 cells were washed with PBS to remove free peptide. Because flow cytometry does not differentiate between intracellular and extracellular surface fluorescence, cells were then washed with a low pH buffer to remove surface bound peptide. This procedure is similar to that used in the original biopanning protocol. The amount of intracellular dye was then quantified and plotted against concentration to produce internalization curves. The results represent a combined measure of binding and internalization into H2009 cells and are summarized in Figure 4.1.

The majority of peptides in this library did not show significant changes in $EC_{50}$. Statistically significant loss of internalization was observed for the L-Leu capped peptide with a 3.4-fold increase in $EC_{50}$ ($p=0.003$). The D-Leu capped peptide also showed a 2.8-fold increase in $EC_{50}$. However, this was not significant by t-test ($p=0.09$). Interestingly, N-terminal acetylation of D-Leu H2009.1 appears to rescue the slight internalization efficiency loss caused by the addition of D-Leu alone. All of the peptides examined bind and internalize in the low nanomolar range, and the changes observed are minor. I conclude that all of the tested peptides are capable of delivering cargo efficiently to target cells *in vitro*. Therefore, all of the peptides in the library were advanced to the next stage of characterization.

*Serum Stability of Capped H2009.1 Peptides*

I then turned to the evaluation of *in vitro* half-life of the N-terminally capped H2009.1 peptides. After incubation of the H2009.1 tetrameric peptide in human plasma, serum proteins were removed by ethanol precipitation and the supernatants were analyzed by

A

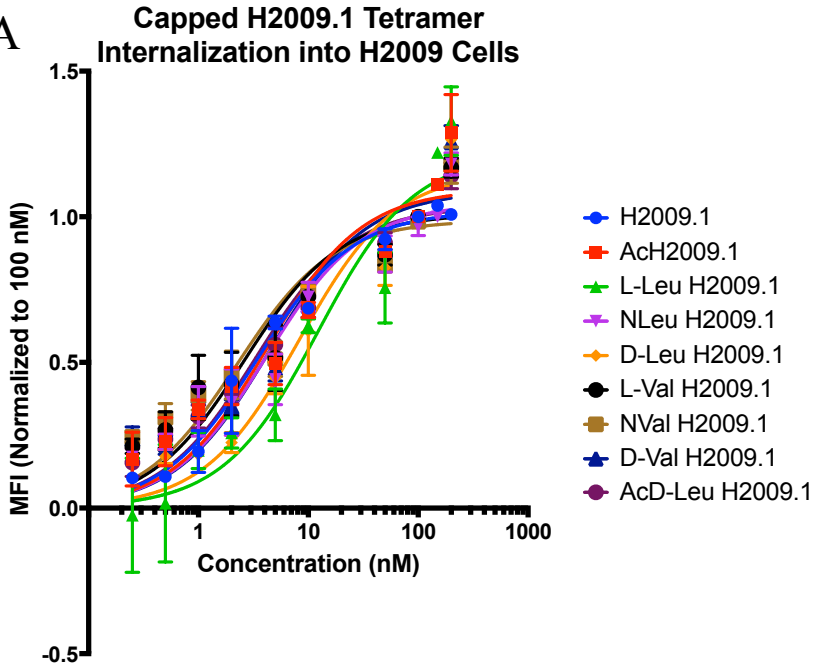


B

| Peptide | $EC_{50}$ (nM ± SEM) |
|---|---|
| H2009.1 | 3.6 ± 0.8 |
| AcH2009.1 | 5.4 ± 0.8 |
| L-Val H2009.1 | 3.4 ± 2.0 |
| N-Val H2009.1 | 2.5 ± 0.7 |
| D-Val H2009.1 | 4.5 ± 0.6 |
| L-Leu H2009.1 | 12.4 ± 1.1* |
| N-Leu H2009.1 | 3.7 ± 1.0 |
| D-Leu H2009.1 | 10.2 ± 2.9 |
| AcD-Leu H2009.1 | 3.4 ± 0.7 |

**Figure 4.1 Internalization of capped tetramers into H2009 cells**. AF488-labeled peptide was incubated with H2009 cells for 2 hours. Cells were washed with PBS followed by acid washes (pH 2.2) to remove un-internalized peptide. Levels of intracellular fluorescence were quantified by flow cytometry. Curves were plotted and ½ max internalization ($EC_{50}$) concentrations were calculated using GraphPad Prism. Representative curves are shown. N ≥ 3. *Indicates statistical significant difference from parental H2009.1 ($p<0.05$) by Student's t-test.

analytical HPLC on a C18 column. As shown in Figure 4.2, the parental H2009.1 peptide degrades rapidly in serum, with only 15.47% intact peptide remaining after 12 hours. The norleucine and norvaline caps improved *in vitro* serum stability of the H2009.1 peptide, more than doubling the percent of intact peptide after 12 hours. However, these amino acids are clearly degraded by serum peptidases, albeit at a slower rate than their natural counterparts. The N-acetylated and D-Val, D-Leu, and AcD-Leu capped H2009.1 peptides displayed significantly improved serum stability with 84%, 93%, 81%, and 84% of each peptide (respectively) remaining after 12 hours compared to 15% of the parental peptide.

In addition to significantly decreasing the rate of decomposition of the H2009.1 peptide, these caps also altered the modes by which the H2009.1 peptide degrades (Figures 4.3 and Appendix C). The uncapped H2009.1 tetramer degrades both by the rapid loss of residues from the N-terminus and by the slower process of losing entire monomeric chains from the tetramer. A complex mixture of degradation products is observed on the analytical HPLC chromatograms and MALDI spectra. N-terminally truncated H2009.1 peptides produced by N-terminal degradation are no longer capable of targeting cargo to $\alpha_v\beta_6$-expressing cells. In contrast, capped H2009.1 tetramers degrade almost entirely by loss of monomeric H2009.1 chains. The chromatograms and corresponding MALDI spectra demonstrate simple mixtures of tetrameric, trimeric, and dimeric peptides. This mode of degradation leaves a trimer or dimer of H2009.1 peptides. The PET imaging of the H2009.1 dimer indicates that these peptides are capable of delivery to $\alpha_v\beta_6$ –expressing tumors [105]. These serum stability results suggest that the N-acetylated, D-Leu, D-Val, and AcD-Leu capped H2009.1 peptides may show improved capacity to deliver long-lived cargo to $\alpha_v\beta_6$

expressing tumors in comparison to the parental peptide. These four peptides were deemed sufficiently promising targeting agents to move forward into the next stage of characterization.

A

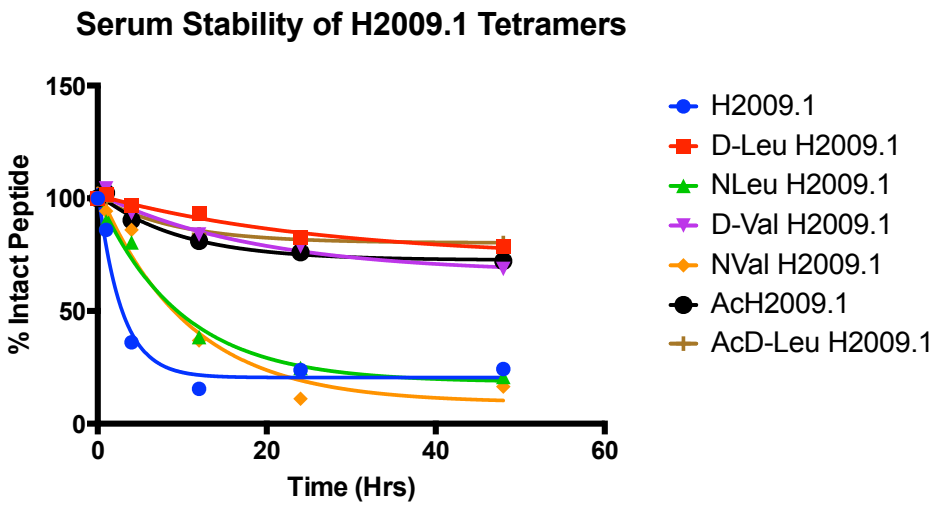


B

| Peptide | % Remaining Peptide at 12 Hrs |
|---|---|
| H2009.1 | 15.47 |
| AcH2009.1 | 81.07 |
| L-Val H2009.1 | CNR |
| N-Val H2009.1 | 36.88 |
| D-Val H2009.1 | 83.91 |
| L-Leu H2009.1 | CNR |
| N-Leu H2009.1 | 38.44 |
| D-Leu H2009.1 | 93.20 |
| AcD-Leu H2009.1 | 84.03 |

**Figure 4.2 Degradation of Capped H2009.1 Tetramers in Human Plasma.** A) Capped H2009.1 tetramer serum stability up to 48 Hrs. B) Summary of intact peptide remaining after 12 Hrs incubation at 37°C in human plasma CNR = Could not resolve.

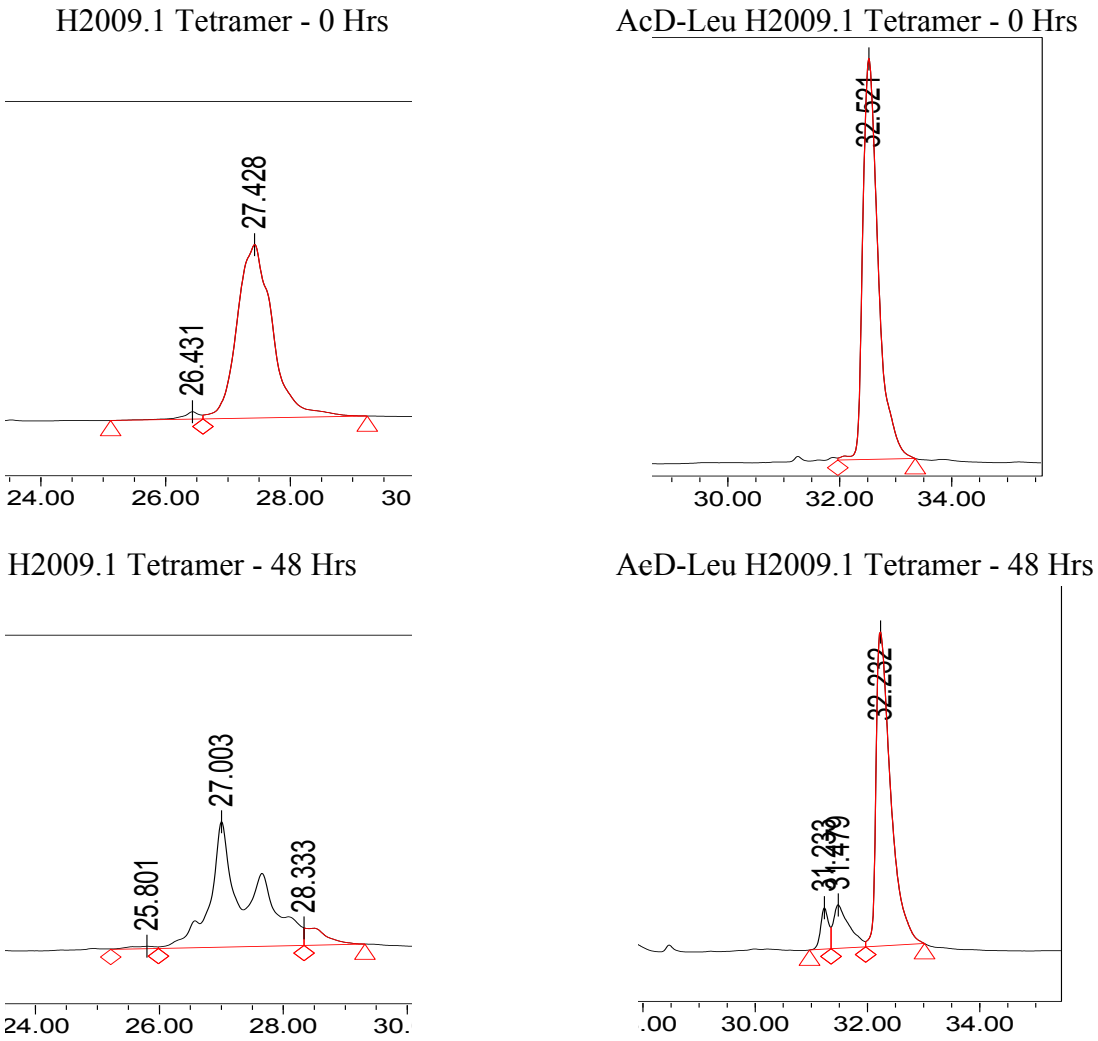


**Figure 4.3 Representative HPLC traces from Serum Stability Assays.** Traces illustrate the degradation patterns of parental and capped H2009.1 peptides during incubation in human plasma. The right-most peak of each trace represents intact peptide as determined by MALDI analysis. Uncapped H2009.1 tetramer is degraded both at the N-terminus and by reverse Michael addition to lose whole H2009.1 chains. AcD-Leu H2009.1 tetramer is degraded only by loss of monomeric H2009.1 chains.

As is seen in Figure 4.2, the rate of peptide degradation sharply decreases after 12 hours of incubation in plasma. This is likely due to degradation of the serum peptidases

themselves over long periods of time. The majority of targeting peptides currently under development are degraded in plasma in a matter of minutes as opposed to hours. Serum stability experiments rarely extend for more than 4 hours. The capped H2009.1 peptides are quite unique in the peptide field in their stability against serum metabolism.

This method of determining serum stability depends on analytical HPLC, which separates peptides based on their hydrophobicity. It is assumed in this experiment that the products of H2009.1 degradation in serum will have differ sufficiently in hydrophobicity to allow for separation into distinct peaks for quantification. Therefore, the quality of the data that can be produced by this assay depends on the identity of the degradation products. Degradation products of the L-Leu and L-Val capped H2009.1 peptides did not sufficiently separate to allow for reliable quantification, even when the gradient was significantly extended. These peptides were included in the library only as controls to allow for assessment of the effect of D-stereochemistry on the capping moieties, and were not investigated further.

*In Vivo Imaging and Biodistribution of Capped H2009.1 Peptides*

The most promising peptides, AcH2009.1, D-Leu H2009.1, D-Val H2009.1, and AcD-Leu H2009.1 were taken into NIRF imaging studies in order to assess their *in vivo* delivery capabilities and biodistribution. A dual tumor model was utilized to determine specific targeting to $\alpha_v\beta_6$ expressing tumors. Subcutaneous H2009 ($\alpha_v\beta_6$ positive) and H460 ($\alpha_v\beta_6$ negative) tumors were established on either flank of adult, female, NOD/SCID mice. 30 μg of Cy5-labeled peptide was injected intravenously. At 24, 48, and 72 hours, the mice were

sacrificed and their organs were imaged ex vivo to determine biodistribution (Figures 4.6-4.16 and Tables 4.2-4.4).

These studies focused on biodistribution of targeting peptide in tumors, kidney, liver, lungs, spleen, and heart. Tumors both positive and negative for $\alpha_v\beta_6$ were utilized to assess the ability of the H2009.1 peptide analogs to characterize tumors for $\alpha_v\beta_6$ expression and deliver cargo specifically to $\alpha_v\beta_6$ positive tumor cells. The kidneys were examined as a major focus of this project is reducing renal accumulation of the H2009.1 peptide. The spleen, heart, and liver are often affected by toxicity of chemotherapeutic agents. A major goal of the peptide-targeting field is the reduction of this toxicity. Therefore, accumulation of peptide-targeted cargo in these organs is to be avoided whenever possible. For imaging applications, low accumulation of the peptide in the lung and liver (the most common site of NSCLC metastasis) is also required to provide contrast between healthy and malignant cells. To simplify interpretation of the multi-dimensional nature of these studies, the results of these experiments are presented separately at each timepoint.

*Biodistribution of Capped H2009.1 Peptides - 24 HPI*

All of the peptides used in this study produced higher signal in H2009 tumors compared to H460 control tumors 24 HPI (Figures 4.6, 4.7, 4.8, and Table 4.2). The AcH2009.1 peptide showed increased H2009 signal compared to the parental peptide. A slight increase in H460 tumor signal was also observed for the AcH2009.1 peptide, resulting in a similar H2009/H460 targeting ratio (Table 4.2). Small increases in H2009 signal combined with

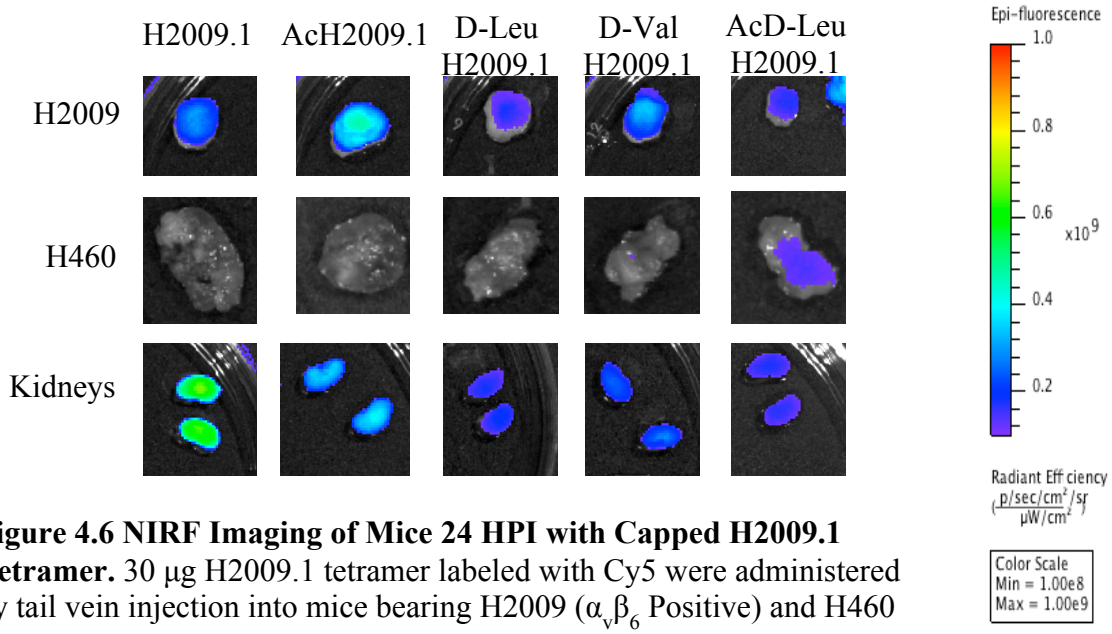


**Figure 4.6 NIRF Imaging of Mice 24 HPI with Capped H2009.1 Tetramer.** 30 µg H2009.1 tetramer labeled with Cy5 were administered by tail vein injection into mice bearing H2009 ($\alpha_v\beta_6$ Positive) and H460 ($\alpha_v\beta_6$ Negative) subcutaneous tumors. Mice were sacrificed and their organs were imaged *ex vivo*. N ≥ 6 Representative images are shown.

slight decreases in H460 signal produce improved targeting ratios for the D-Val and AcD-Leu capped H2009.1 tetramers.

Larger differences between the tetramers are seen in the kidneys. All of the capped peptides showed decreased accumulation in kidney compared to the uncapped H2009.1 peptide. Those peptides capped with D-Leu, D-Val, and AcD-Leu showed further improvement of kidney accumulation over simple N-terminal acetylation. These peptides reduced signal from the kidney by roughly 50% on average. As seen in Table 4.2, the AcD-Leu H2009.1 peptide gives the best tissue specificity at this timepoint, producing slightly higher signal in the H2009 tumor than in the kidneys. This is rare in the peptide-targeting

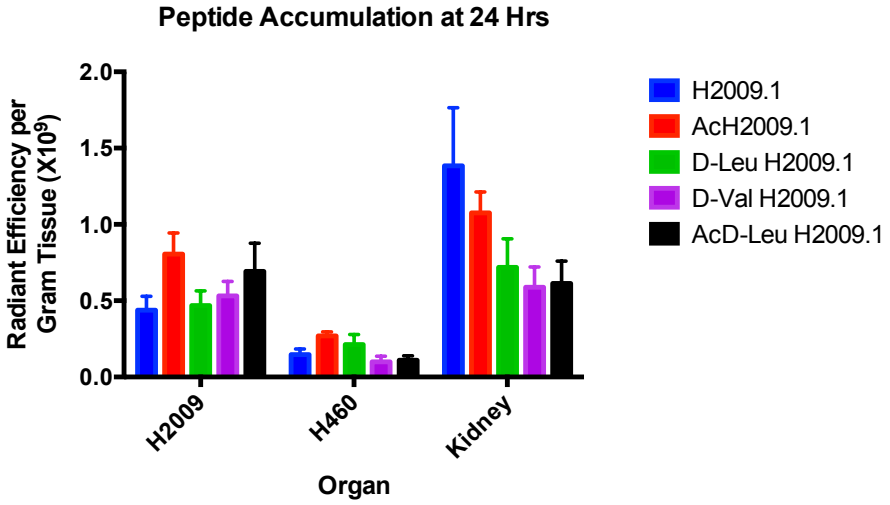


**Figure 4.7 NIRF Imaging of Mice 24 HPI with Capped H2009.1 Tetramer.** 30 μg H2009.1 tetramer labeled with Cy5 were administered by tail vein injection into mice bearing H2009 ($\alpha_v\beta_6$ Positive) and H460 ($\alpha_v\beta_6$ Negative) subcutaneous tumors. Mice were sacrificed and their organs were imaged *ex vivo*. N ≥ 6 All N-terminally capped H2009.1 peptide analogs showed decreased kidney signal at 24 HPI compared to parental H2009.1. Capped peptides produced specific signal in H2009 tumors. The AcD-Leu H2009.1 gives slightly higher tumor signal compared to parental H2009.1 along with very low H460 tumor and kidney signal.

field, and suggests that the AcD-Leu H2009.1 tetramer has great potential as a targeting ligand.

In these studies, the parental H2009.1 peptide suffers from a low tumor-to-lung signal ratio (Table 4.2). This would preclude the visualization of lung tumors due to lack of contrast. The capped tetramers, particularly the AcD-Leu H2009.1 peptide gave higher tumor-to-lung ratios. However, this improvement may not be sufficient for clinical applications. Levels of peptide accumulation in off-target organs are shown in Figure 4.8. Accumulation in cardiac tissue remained low for all of the peptides examined. Unexpectedly, all of the N-terminal modifications increase accumulation of the H2009.1 tetramer in the

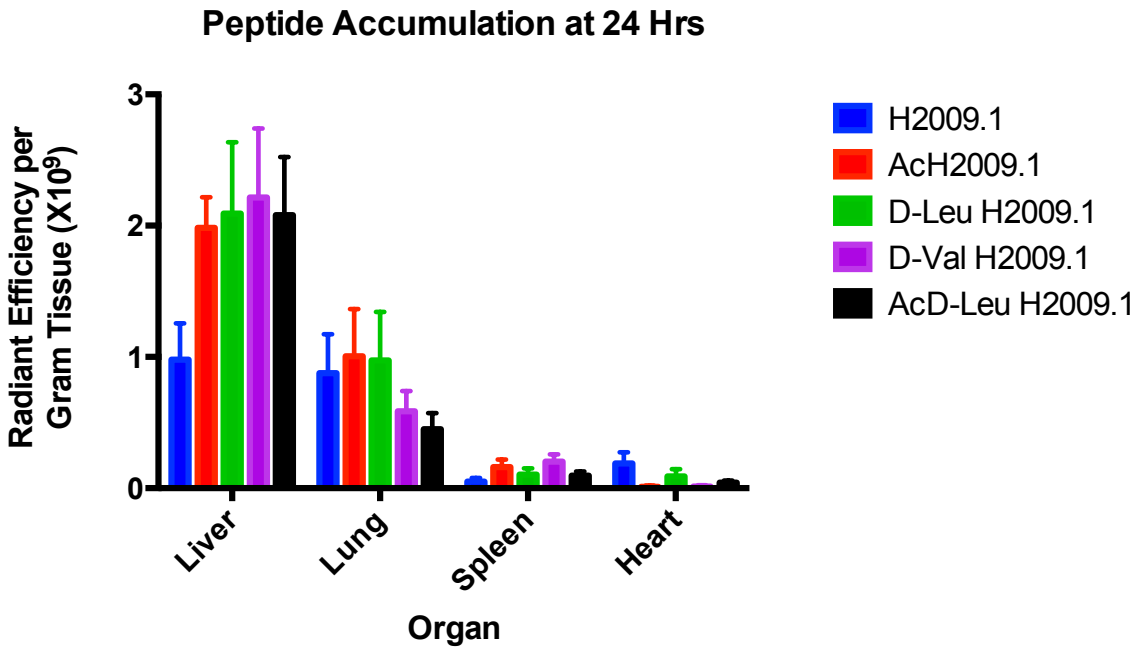


**Figure 4.8 Quantification of NIRF Imaging of Off-Target Organs 24 HPI with Capped H2009.1 Tetramer.**. N ≥ 6 Horizontal line denotes signal from H2009 tumor imaged with H2009.1 peptide. In all peptides, signal from normal lung and liver exceeds that from tumor tissue. While AcD-Leu H2009.1 gives the lowest lung signal, it is still too high to produce reliable contrast for imaging or therapeutic window. AcD-Leu H2009.1 also produces very high liver accumulation, similar to the other capped peptides.

liver 24 HPI. Small increases in spleen signal were also observed. Concurrent increases in signal from these organs could indicate a shift in the clearance mechanism followed by the capped H2009.1 analogs.

| Peptide | H2009/ H460 | H2009/ Kidney | H2009/ Liver | H2009/ Lung | H2009/ Spleen | H2009/ Heart |
|---|---|---|---|---|---|---|
| H2009.1 | 2.99 | 0.32 | 0.45 | 0.50 | 8.76 | 2.32 |
| AcH2009.1 | 2.99 | 0.75 | 0.41 | 0.80 | 5.02 | 69.03 |
| D-Leu H2009.1 | 2.20 | 0.65 | 0.22 | 0.48 | 4.51 | 5.20 |
| D-Val H2009.1 | 5.32 | 0.90 | 0.24 | 0.91 | 2.62 | 38.40 |
| AcD-LeuH2009.1 | 6.32 | 1.13 | 0.33 | 1.54 | 7.19 | 16.49 |

**Table 4.2 Ratios of Signal from Each Organ Relative to Target H2009 Tumors 24 HPI**

*Biodistribution of Capped H2009.1 Peptides - 48 HPI*

As shown in Figures 4.9, 4.10, 4.11, and Table 4.3, the parental H2009.1 peptide does not show any specificity for the H2009 tumor over the control H460 tumor at 48 HPI. However, all of the capped H2009.1 analogs maintain targeting to the $\alpha_v\beta_6$-expressing tumor at this timepoint. The D-Val H2009.1 peptide produces both the highest signal in the H2009 tumors and lowest signal in the H460 tumors, giving a significantly higher tumor-targeting ratio than the other modified peptides at this timepoint.

Surprisingly, the AcH2009.1 and D-Leu H2009.1 peptides give higher renal signal than the parental peptide, a sharp contrast to the data seen at 24 HPI. However, the tumor-to-kidney ratios still demonstrate an improvement in targeting over the uncapped H2009.1 tetramer. The D-Val and AcD-Leu capped peptides accumulate in the kidneys to a similar degree as the parental, producing favorable tumor-to-kidney tissue specificity ratios.

For reasons that are unclear, The D-Val H2009.1 tetramer produced high signal in the lung with large error at 48 HPI (Figure 4.11). The D-Leu and AcD-Leu capped tetramers also gave increased signal at this timepoint, producing similar tumor-to-lung ratios as the parental

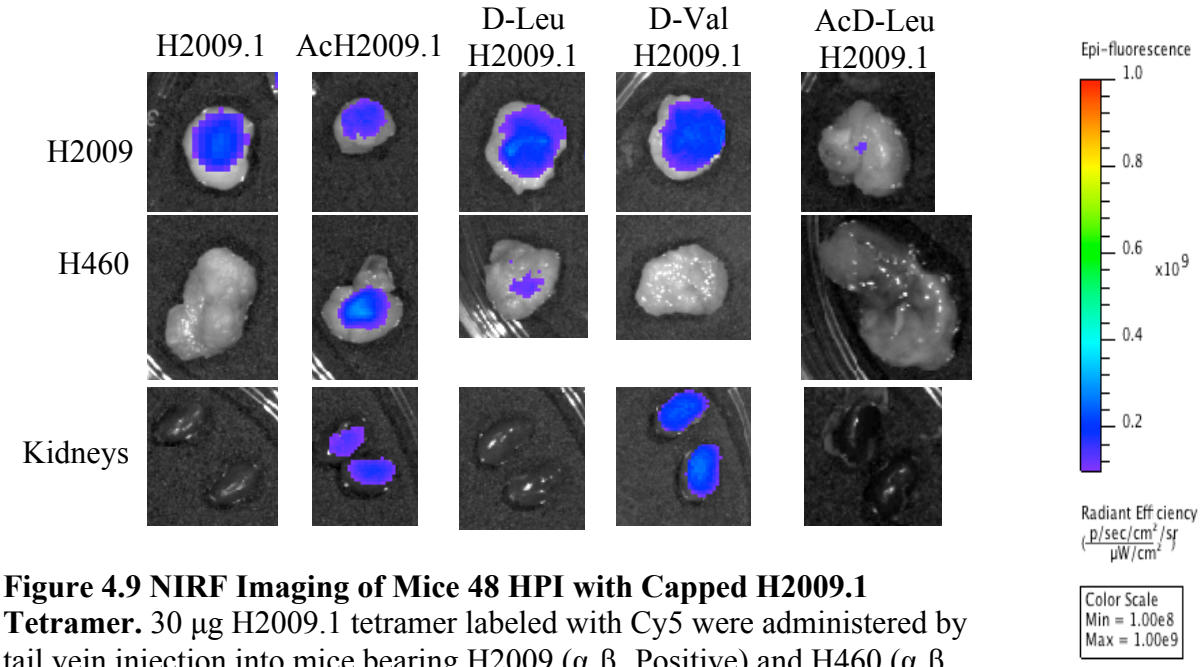


**Figure 4.9 NIRF Imaging of Mice 48 HPI with Capped H2009.1 Tetramer.** 30 µg H2009.1 tetramer labeled with Cy5 were administered by tail vein injection into mice bearing H2009 ($\alpha_v\beta_6$ Positive) and H460 ($\alpha_v\beta_6$ Negative) subcutaneous tumors. Mice were sacrificed and their organs were imaged *ex vivo*. N ≥ 5 Representative images are shown.

peptide. However, the AcH2009.1 gave nearly 2-fold accumulation in the H2009 tumor compared to healthy lung. As at 24 HPI, all of the capped peptides gave much higher signal in the liver and spleen than the parental H2009.1 tetramer. This was most obvious in the AcD-Leu H2009.1.

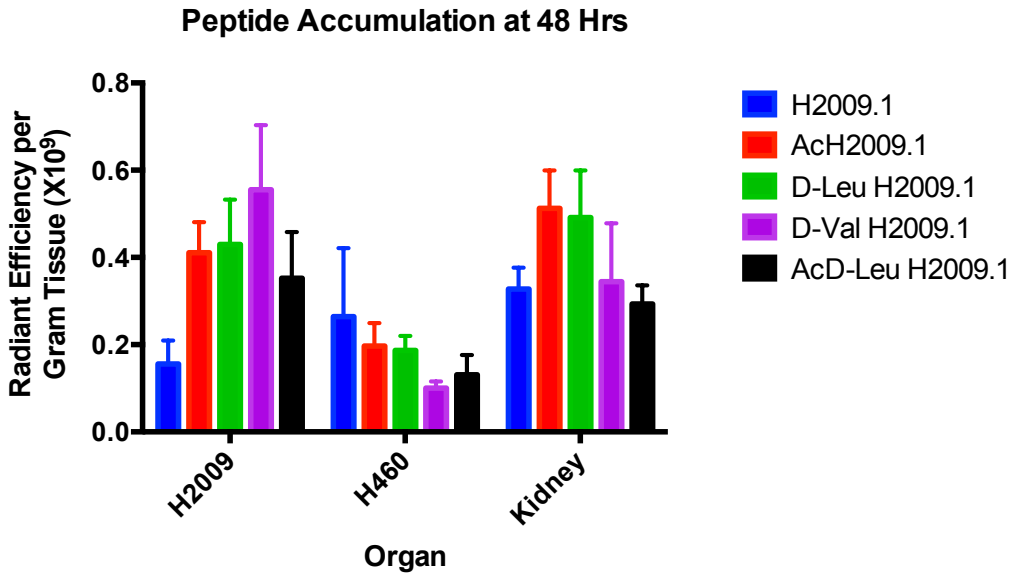


**Figure 4.10 NIRF Imaging of Mice 48 HPI with Capped H2009.1 Tetramer.** 30 μg H2009.1 tetramer labeled with Cy5 were administered by tail vein injection into mice bearing H2009 ($\alpha_v\beta_6$ Positive) and H460 ($\alpha_v\beta_6$ Negative) subcutaneous tumors. Mice were sacrificed and their organs were imaged *ex vivo*. N ≥ 5 At this timepoint, levels of the capped peptides are higher in the kidney than the uncapped peptide, with the exception of AcD-Leu H2009.1. However, the capped peptides maintain targeting to H2009 tumors over control H460 tumors.

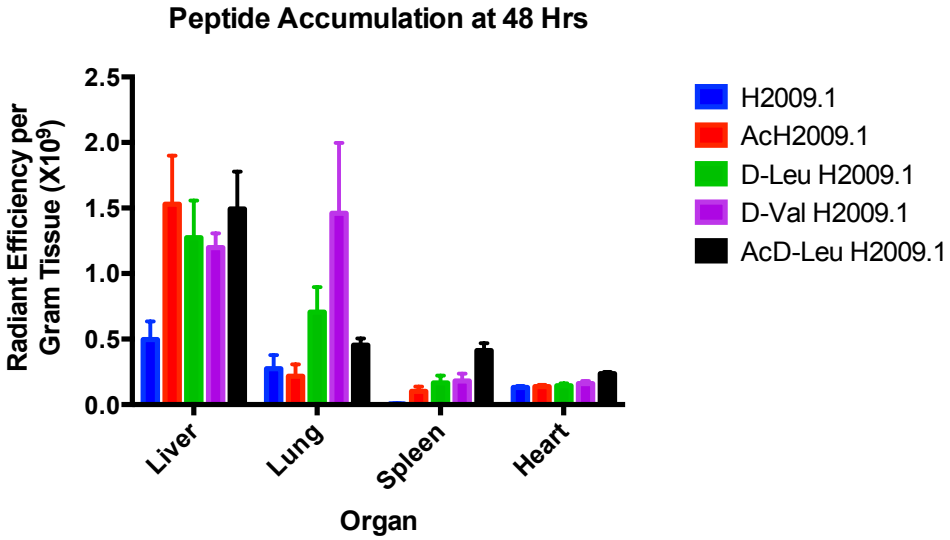


**Figure 4.11 Quantification of NIRF Imaging of Capped H2009.1 Tetramer in Off-Target Organs at 72 HPI.** N ≥ 6 Horizontal line indicates signal from H2009 tumor imaged with parental H2009.1 Tetramer + Cy5. In all peptides, signal from normal lung and liver is higher than that from tumor tissue. Levels of capped peptides, particularly the AcD-Leu H2009.1 peptide, are increased in spleen at this timepoint.

| Peptide | H2009/ H460 | H2009/ Kidney | H2009/ Liver | H2009/ Lung | H2009/ Spleen | H2009/ Heart |
|---|---|---|---|---|---|---|
| H2009.1 | 0.59 | 0.48 | 0.31 | 0.57 | 27.45 | 1.20 |
| AcH2009.1 | 2.09 | 0.80 | 0.27 | 1.90 | 4.06 | 2.99 |
| D-Leu H2009.1 | 2.30 | 0.88 | 0.34 | 0.61 | 2.59 | 2.98 |
| D-Val H2009.1 | 5.52 | 1.61 | 0.46 | 0.38 | 3.09 | 3.47 |
| AcD-LeuH2009.1 | 2.69 | 1.20 | 0.24 | 0.78 | 0.85 | 1.49 |

**Table 4.3 Ratios of Signal from Each Organ Relative to Target H2009 Tumors 48 HPI.**

*Biodistribution of Capped H2009.1 Peptides - 72 HPI*

The AcH2009.1, D-Leu H2009.1, and D-Val H2009.1 all showed increased signal in the H2009 target tumors 72 HPI (Figures 4.12, 4.13, 4.14 and Table 4.4). Low signal in off-target H460 tumors was also observed for these peptides. As seen in Table 4.4, these three tetramer analogs improved the tumor-targeting ratio. Curiously, the levels of the parental H2009.1 peptide rebound after significantly decreasing at 48 HPI. The reason for this is unknown, but may be due to differences in tumor mass between the mice used at each timepoint. The AcD-Leu H2009.1 tetramer produces similar signal to the parental peptide in both tumors.

The AcH2009.1, D-Leu H2009.1, and AcD-Leu H2009.1 tetramers show improvement in renal accumulation compared to uncapped peptide at this timepoint. Particularly, the D-Leu capped tetramer increases the tumor-to-kidney ratio more than 7-fold. The D-Val H2009.1 peptide, however, does not produce any improvement. As it does at the 48-hour timepoint, the D-Val cap does not decrease kidney signal relative to the parental peptide.

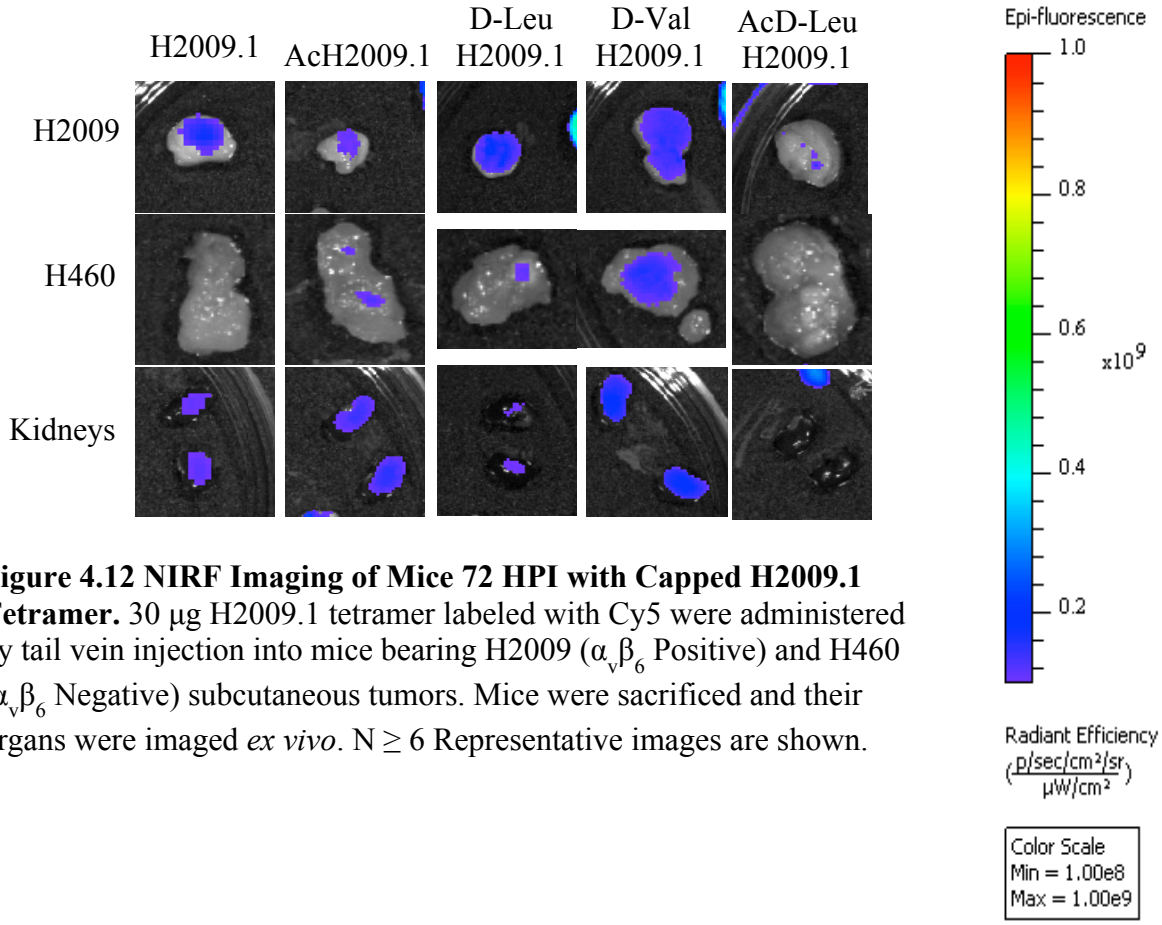


**Figure 4.12 NIRF Imaging of Mice 72 HPI with Capped H2009.1 Tetramer.** 30 µg H2009.1 tetramer labeled with Cy5 were administered by tail vein injection into mice bearing H2009 ($\alpha_v\beta_6$ Positive) and H460 ($\alpha_v\beta_6$ Negative) subcutaneous tumors. Mice were sacrificed and their organs were imaged *ex vivo*. N ≥ 6 Representative images are shown.

At this timepoint, the N-acetylated peptides both show significantly decreased accumulation in the lung (Figure 4.14). However, the low levels of AcD-Leu H2009.1 peptide in H2009 tumors at this timepoint, produces an unfavorable tumor-to-lung ratio. The AcH2009.1 tetramer gives the only favorable tumor-to-lung ratio at this timepoint at 1.51. At 72 HPI, the AcH2009.1 tetramer also gives by far the highest H2009-to-liver and H2009-to-spleen ratios of the peptides tested at 0.76 and 18.76, respectively. The AcD-Leu H2009.1

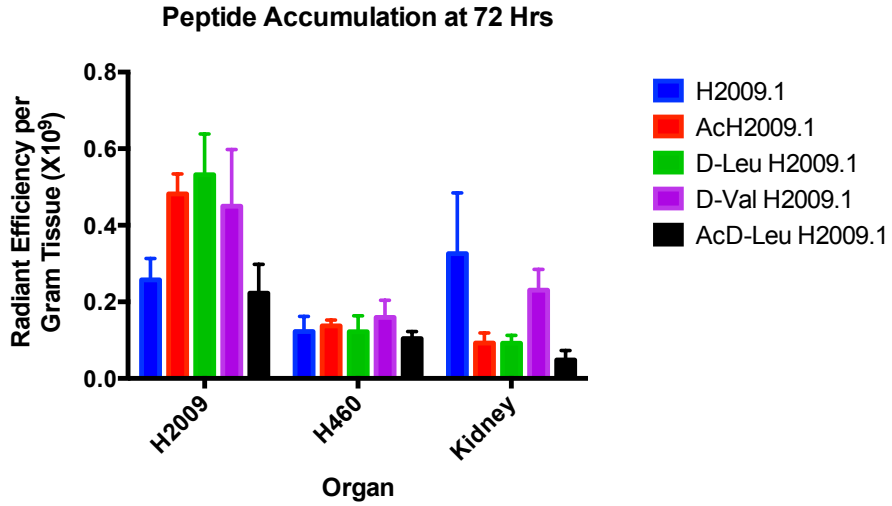


**Figure 4.13 NIRF Imaging of Mice 72 HPI with Capped H2009.1 Tetramer.** 30 μg H2009.1 tetramer labeled with Cy5 were administered by tail vein injection into mice bearing H2009 ($\alpha_v\beta_6$ Positive) and H460 ($\alpha_v\beta_6$ Negative) subcutaneous tumors. Mice were sacrificed and their organs were imaged *ex vivo*. N ≥ 6 AcH2009.1, D-Leu H2009.1, and D-Val H2009.1 maintained increased levels in H2009 tumors compared to parental and AcD-Leu H2009.1 peptides. At this timepoint, lower levels of AcH2009.1, D-Leu H2009.1, and AcD-Leu H2009.1 were observed in kidney while the D-Val H2009.1 peptide was retained to a similar degree as uncapped H2009.1.

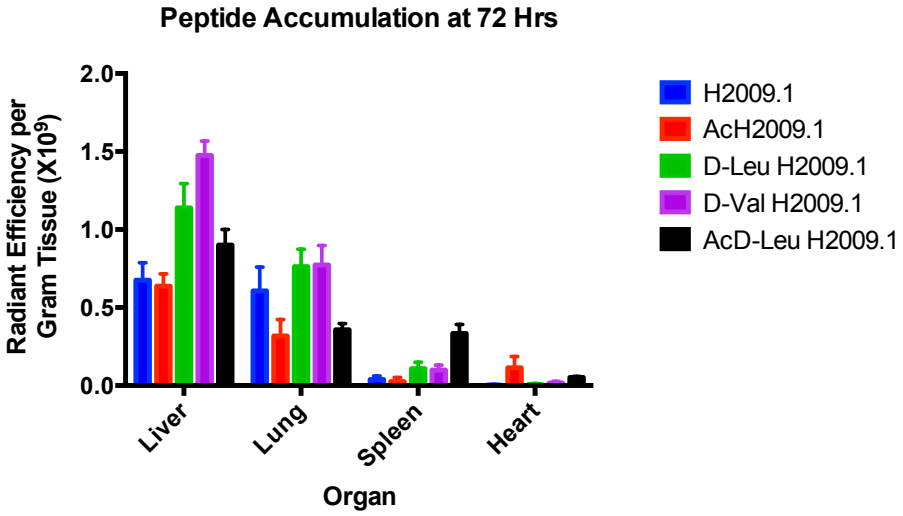


**Figure 4.14 Quantification of NIRF Imaging of Capped H2009.1 Tetramer in Off-Target Organs at 72 HPI.** N ≥ 6 Horizontal line indicates signal from H2009 tumor imaged with parental H2009.1 Tetramer + Cy5. In all peptides, signal from normal lung and liver is higher than that from tumor tissue. For reasons that are unclear, the D-Leu H2009.1 and AcD-Leu H2009.1 peptides also produce increased spleen signal at this timepoint.

| Peptide | H2009/ H460 | H2009/ Kidney | H2009/ Liver | H2009/ Lung | H2009/ Spleen | H2009/ Heart |
|---|---|---|---|---|---|---|
| H2009.1 | 2.10 | 0.79 | 0.38 | 0.42 | 6.58 | 65.62 |
| AcH2009.1 | 3.52 | 5.22 | 0.76 | 1.51 | 18.76 | 4.23 |
| D-Leu H2009.1 | 4.35 | 5.77 | 0.47 | 0.70 | 4.92 | 77.35 |
| D-Val H2009.1 | 2.82 | 1.95 | 0.31 | 0.58 | 4.50 | 26.52 |
| AcD-LeuH2009.1 | 2.14 | 4.63 | 0.25 | 0.62 | 0.67 | 4.29 |

**Table 4.4 Ratios of Signal from Each Organ Relative to Target H2009 Tumors 72 HPI.**

peptide, while it gives lower liver signal than the D-amino acid capped analogs, produces a clear spike in spleen accumulation at 72 HPI.

When signal in the H2009 tumors is examined over time, a distinct improvement in tumor targeting capacity can be observed (Figure 4.15). The parental H2009.1 peptide oddly decreases between 24 and 48 HPI, before rebounding at 72 HPI. The AcH2009.1 peptide appears to give a burst of signal early on before settling into a steady state. The D-Leu and D-Val H2009.1 peptides give similar signal to the parental peptide at 24 HPI, but signal does not decrease over the time course. The combined capping strategy of the AcD-Leu H2009.1 tetramer did not produce additive effects as hoped. Instead the peptide gave somewhat high signal at 24 HPI before clearly rapidly from all organs, including the H2009 tumors.

Improvements on the parental tetramer are also seen upon consideration of kidney signal over time (Figure 4.16). Uncapped H2009.1 tetramer accumulates to a high degree in the kidneys at 24 HPI, with roughly a quarter of that signal retained for long periods of time. In addition to the reduction in initial accumulation, the capped H2009.1 analogs are cleared from the kidneys throughout the experimental time course. This clearance is much slower in the D-Val capped peptide compared to the other modified tetramers.

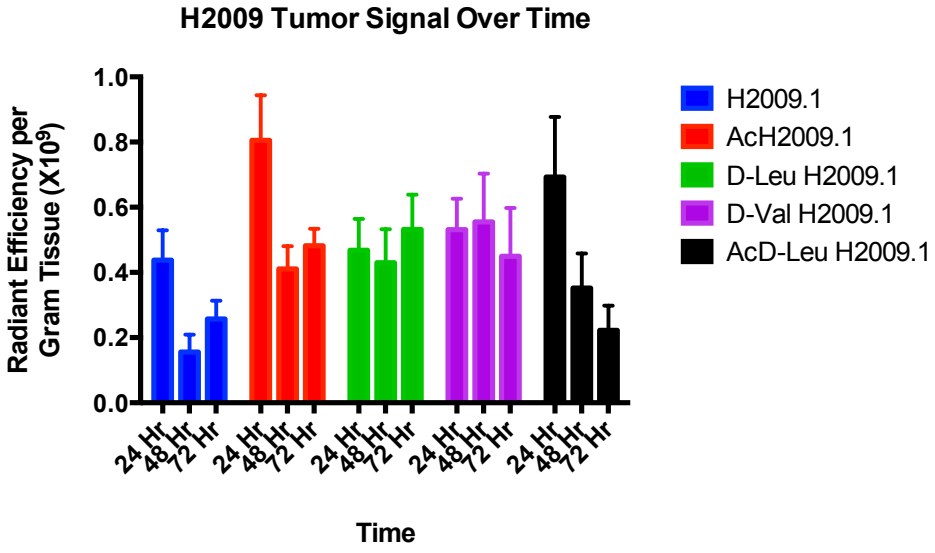


**Figure 4.15 Quantification of NIRF Imaging of Capped H2009.1 Tetramer in H2009 Tumors Over Time.** 30 µg H2009.1 tetramer labeled with Cy5 were administered by tail vein injection into mice bearing H2009 ($\alpha_v\beta_6$ Positive) and H460 ($\alpha_v\beta_6$ Negative) subcutaneous tumors. Mice were sacrificed and their organs were imaged *ex vivo*. N ≥ 5 at each timepoint. Tumor signal decreases over time for H2009.1 and AcD-Leu H2009.1 but is maintained for AcH2009.1, D-Leu H2009.1, and D-Val H2009.1 out to 72 HPI.

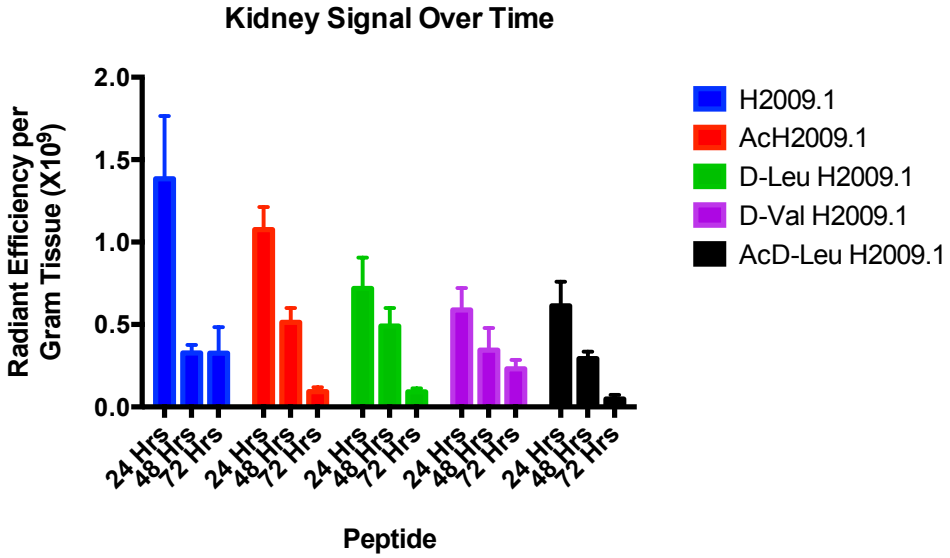


**Figure 4.16 Quantification of NIRF Imaging of Capped H2009.1 Tetramer in Kidneys Over Time.** 30 µg H2009.1 tetramer labeled with Cy5 were injected via tail vein into mice bearing H2009 ($\alpha_v\beta_6$ Positive) and H460 ($\alpha_v\beta_6$ Negative) subcutaneous tumors. Mice were sacrificed and organs were imaged *ex vivo*. N ≥ 3 at each timepoint. All capped peptides showed lower kidney signal compared to parental H2009.1 24 HPI and 72 HPI.

*Specificity of Capped H2009.1 Peptides for $\alpha_v\beta_6$ over $\alpha_v\beta_3$*

With such high accumulation of the tetramer H2009.1 peptides in liver and lung tissue, I wondered if the capped tetramers might bind to other cellular receptors in addition to $\alpha_v\beta_6$. The most likely candidate receptors for H2009.1 analogs are other RGD binding integrins including $\alpha_v\beta_3$ and $\alpha_5\beta_1$. Our group has previously shown that H2009.1 displays significant specificity for $\alpha_v\beta_6$ over these other integrins [105, 205, 206, 222-224]. However, it is possible that the N-terminal modifications may reduce this specificity. Therefore, I assessed the direct binding affinity of the most serum stable capped H2009.1 peptides against recombinant $\alpha_v\beta_6$ and $\alpha_v\beta_3$ by an ELISA-like assay (Figure 4.17). In this assay, recombinant integrins were adsorbed to ELISA plates overnight. Wells were incubated with biotinylated peptide followed by avidin-HRP conjugate. Standard TMB substrate was then used to produce the colorimetric signal of an ELISA.

The parental H2009.1 peptide binds to $\alpha_v\beta_6$ with a $K_D$ of 0.27 ± 0.5 nM, remarkably high affinity for a peptidic ligand. The AcH2009.1 and AcD-Leu H2009.1 bind with similarly low affinities. It appears that D-Leu interferes with binding as the D-Leu H2009.1 tetramer has a significantly higher $K_D$ of 1.6 ± 0.19 nM. However, N-acetylation of the D-Leu cap rescues this loss of affinity. This may indicate some minor repulsion of N-terminal cations or perhaps a weak hydrophobic interaction formed by the acetyl groups. These effects on binding affinity are quite small, as one would expect given structural data for ligand binding to $\alpha_v\beta_6$ (Figure 2.9).

Our ELISA experiments also demonstrated excellent specificity of the H2009.1 tetramer for $\alpha_v\beta_6$ over $\alpha_v\beta_3$. Reliable $K_D$s could not be calculated from our concentration

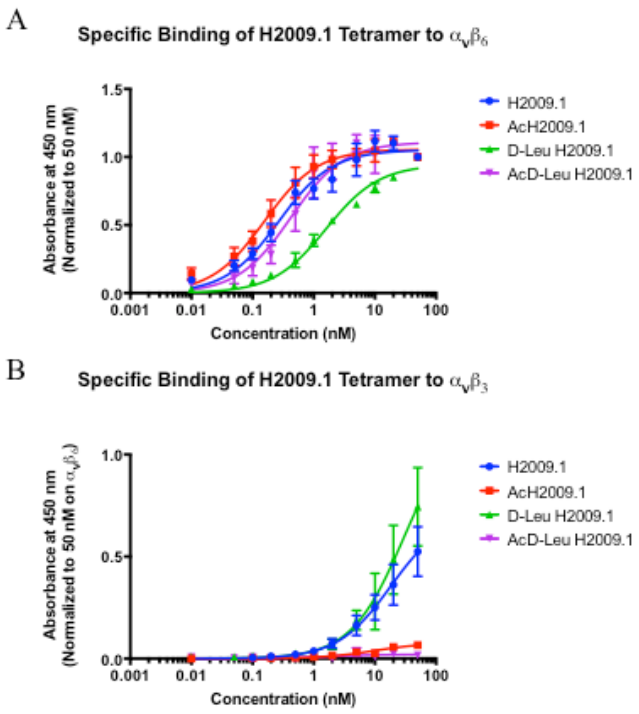


| Peptide | $K_D$ ± SEM (nM) |
|---|---|
| H2009.1 | 0.27 ± 0.05 |
| AcH2009.1 | 0.16 ± 0.04 |
| D-Leu H2009.1 | 1.6 ± 0.19 |
| AcD-Leu H2009.1 | 0.48 ± 0.09 |

**Figure 4.17 Direct binding of capped H2009.1 tetramers to recombinant integrins**. ELISAs were performed in 96 well plates coated with recombinant $\alpha_v\beta_6$ (A) or $\alpha_v\beta_3$ (B). Curves were normalized by 50 nM H2009.1 tetramer on $\alpha_v\beta_6$, plotted using GraphPad Prism, and binding affinities on $\alpha_v\beta_6$ were calculated (C). Binding affinities to $\alpha_v\beta_3$ could not be calculated and must be greater than 50 nM. N=3

curves, as saturation points were not reached. However, it can be predicted from our data that the $K_D$s of the parental and D-Leu capped tetramers must be at least 20 nM, producing minimum specificity ratios of 74- and 12.5-fold, respectively. Virtually no binding of the acetylated peptide to $\alpha_v\beta_3$ was observed up to 50 nM, indicating that the AcH009.1 peptide is highly specific for $\alpha_v\beta_6$.

## Discussion

New approaches are required to decrease accumulation of peptidic targeting ligands in renal tissue and increase serum stability. These modifications must maintain the affinity and targeting capacity of the peptide ligands while reducing re-absorption in the proximal tubules of the kidneys and protecting the peptide from serum metabolism. The development

of targeting ligands that meet these qualifications would substantially expand the therapeutic window available for the treatment of solid tumors by increasing concentrations of drug in the tumor while decreasing side effects such as nephrotoxicity. These studies present a simple and elegant strategy for overcoming both of these obstacles. By virtue of multimerization, the H2009.1 peptide was protected at the C-terminus via conjugation to a tri-lysine core [212]. We now explore capping strategies at the N-terminus with a library of peptides capped with unnatural amino acids or by N-acetylation.

First, I investigated the effects of each cap on binding and internalization into H2009 cells. This assay closely mimics the conditions of the original panning protocol by which the H2009.1 peptide was selected with a fluorescent label allowing for quantification of peptide uptake by flow cytometry. This approach allows for direct comparisons of the *in vitro* delivery capabilities of each member of the modified H2009.1 library. However, it is not a direct binding assay. Differences in signal could be caused changes in binding affinity or internalization dynamics, itself a complex process. Peptides that bind their target receptor with similar affinity, but internalize at lower rates, will produce the same results as a peptide that binds with low affinity but internalizes rapidly. Much of this depends on the endocytic pathway taken by a specific peptide ligand.

The results of this panel of experiments show that internalization efficiency is minimally affected upon N-terminal modification of the H2009.1 peptide. Only the L-Leu capped tetramer gave a statistically significant loss in $EC_{50}$, although the D-Leu H2009.1 peptide also trends in that direction. Interestingly, norleucine does not have any impact on EC50, and N-acetylation of the D-Leu H2009.1 peptide restore internalization efficiency to

parental levels. From this data, it cannot be determined whether these changes are dictated by variations in binding affinity or endocytic dynamics. However, the 3.4-fold increase in $EC_{50}$ between L-Leu H2009.1 and parental peptide should not be sufficient reduce targeting capabilities of the peptide *in vivo* as it is still in the low nanomolar range. I concluded that all of the peptides in this library are capable of *in vitro* delivery to target cells, and all of them were carried forward into the next stage of optimization.

Next, the modified peptides were evaluated on the basis of stability in human serum. As discussed in previous chapters, peptides are notoriously unstable in serum. Many agents that would benefit from peptide targeting survive in the bloodstream for much longer than the parental H2009.1. Assessments of serum stability must often be made in 10% or 50% solutions of plasma diluted in PBS to extend the half-life and allow for reliable quantification [225]. In 100% serum, peptides are often significantly degraded too quickly for current methods to detect. In this regard, the H2009.1 peptide is already notably stable in serum compared to many other peptides under development. I therefore extended the time course of these serum stability studies significantly beyond what is usually performed. This led to a rather surprising observation. After roughly 12 hours of incubation in serum, degradation essentially stopped completely. This is likely due to the degradation of the peptidases themselves by serum proteases. Despite this halt in degradation, clear differences between the modified peptides were apparent by the 12-hour timepoint. These results were then used to determine which peptides would be moved into i*n vivo* imaging studies.

Capping with norleucine and norvaline resulted in a noticeable increase in serum stability of the H2009.1 peptide. However these amino acids do appear to be susceptible to

degradation by amino peptidases, if at a lower rate than naturally occurring amino acids. In contrast, the acetylated and D-amino acid capped H2009.1 analogs remained largely stable in human serum and degraded into lower valency multimers of intact $\alpha_v\beta_6$ –binding peptides. This mode of degradation has significantly less impact on the targeting ability of the H2009.1 peptide than the loss of the N-terminal arginine residue. The H2009.1 trimer and dimer may bind and internalize into H2009 cells with lower efficiency than the tetrameric peptide. However, they are still capable of delivery to their target cells *in vitro* and *in vivo* [105, 212]. It is likely that this form of degradation is enzyme-independent cleavage of the thioether via thiol exchange [226]. Also, because the rate of degradation is so slow, the vast majority of the peptide would be cleared from the bloodstream before significant cleavage occurs. The results of these serum stability studies suggest that the D-amino acid capped and N-acetylated H2009.1 peptides have the most potential for extended targeting *in vivo*. The AcD-Leu H2009.1 peptide did not demonstrate any added stability over the N-acetylated peptide. However, it may exhibit improved biodistribution *in vivo*. All four of these capped peptides (AcH2009.1, D-Leu H2009.1, D-Val H2009.1, and AcD-Leu H2009.1) were remarkably stable *in vitro*. These peptides, along with the parental H2009.1 peptide as a control, were then carried forward into *in vivo* studies.

There are no established rules for predicting the biodistribution of a given targeting ligand. Therefore, the *in vivo* behavior of each peptide must be empirically determined. Near infrared fluorescence imaging (NIRF) was used to characterize the biodistribution of these peptides. This method provides reliable *in vivo* information without the added cost and complications of working with radioactive labels. The Cy5 near-infrared dye is shelf stable

and is not degraded by serum metabolism. Relatively large stocks of dye-labeled peptide can be manufactured at one time and used for several experiments without loss of signal. However, characterization NIRF is less directly quantitative than techniques that use radiolabeled peptides. Significant manipulation of the raw fluorescent signal is required to produce meaningful data as can be seen upon examination of the units. Additionally, auto-fluorescence of animal tissues can produce high background signal. The levels of auto-fluorescence can depend on a myriad of conditions such as the strain of animal in use, the type of chow the mice are fed, or the overall health of the mice. In the studies presented here, tumor-bearing, untreated control mice were imaged, and this background signal was subtracted to quantify dye-specific fluorescence.

As is the case with any biodistribution analysis regardless of technique, the signal quantified is the amount of the label itself. The detected fluorescence may be produced by intact peptide, products of peptide metabolism, or isolated dye that has been cleaved from the peptide ligand. Near IR dyes, including Cy5, are often highly hydrophobic and are likely to undergo metabolism in the liver. Hydroxylation and other modifications made by metabolic enzymes in the liver result in loss of fluorescent signal.

NIRF imaging is also less sensitive than radiolabeling techniques. Initial blood concentrations in the low micromolar range are required to produce sufficient signal for quantification. In contrast, the PET imaging with H2009.1 dimer discussed in Chapter 2 used a dose of 100 mCi, translating to a blood concentration of 280 pM. These differences in dose are likely to have significant impact on the *in vivo* behavior of peptide-targeted ligands. However, these properties can be used to aid development of peptide ligands for different

applications. The low concentrations used in PET imaging directly correspond to those used in clinical imaging. Higher dosages may be necessary to reach therapeutic levels of some drugs, and NIRF imaging provides more clinically relevant information in these cases. In the studies presented here, 30 μg of each peptide-dye conjugate was administered to mice, resulting in estimated blood concentrations of 1.5 μM.

These imaging experiments are multi-dimensional, and, therefore, produce complex results that are difficult to interpret. Levels of each peptide were assessed at three different timepoints in two subcutaneous tumor models and five off target organs. Due to wide variation in tumor and organ mass, the images themselves can be misleading. To solve this problem, the quantified signal is then normalized by organ mass. In order to simplify interpretation of these multifaceted experiments, the data is shown in several separate figures (4.6-4.16). In many cases, it is also helpful to examine the ratio of signal between the H2009 tumors and a specific off-target organ to determine the targeting capacity of a given peptide. These are presented in Tables 4.2-4.4.

Because the goal of this project is the optimization of the H2009.1 peptide, a simple way to interpret the data is to examine peptides in specific organs and eliminate those with unfavorable features, eventually leaving the peptides with best *in vivo* characteristics. This approach depends on the specific application intended for a peptide. Imaging and radiotherapy applications require high accumulation of a peptide in target tissue, low background in off-target organs, and rapid clearance from the organism. Peptides used to target chemotherapeutic agents should provide sustained accumulation in tumor tissue and

may be more flexible in terms of off-target accumulation. These peptides were assessed for their viability in both types of applications.

The first observation of the NIRF imaging data at 24 HPI is that all of the modified H2009.1 peptides examined accumulate in the H2009 ($\alpha_v\beta_6$ positive) tumor at least as well as the parental peptide. Therefore, it can be concluded that none of the modifications to the H2009.1 peptide reduce *in vivo* targeting to $\alpha_v\beta_6$-expressing tumors. This observation holds over time as shown in Figure 4.14. In fact, the AcH2009.1, D-Leu H2009.1, and D-Val H2009.1 tetramers all produce higher signal in the H2009 tumors than the parental peptide at both 48 and 72 HPI. Based on these observations, the pool of potential long-term targeting peptide ligands is reduced to these three peptides, dropping the parental and AcD-Leu capped peptides. However, these two peptides may still be useful for short-term targeting applications if they clear rapidly from other organs.

The surprising behavior of the AcD-Leu H2009.1 peptide indicates that stabilization of the H2009.1 peptide does not necessarily lead to increased retention in target tissue. The reasons for this are unknown. The AcD-Leu H2009.1 internalizes into H2009 cells *in vitro* with equal efficiency to the parental peptide, so it is unlikely the peptide is being washed out of the tumor tissue. Perhaps this modification alters the sub-cellular trafficking route followed by the other peptides, resulting in more rapid quenching of the fluorescent tag.

Turning attention to retention in the kidneys, a major goal of this project is to decrease the accumulation and retention of the H2009.1 peptide in renal tissue, presumably the proximal tubules, as discussed in Chapter 2. At 24 HPI, all of the capped peptides show decreased accumulation of fluorescence in the kidneys compared to the parental H2009.1

tetramer (Figure 4.6). However, at 48 HPI (Figure 4.9), this is not the case. The N-acetylated and D-Leu capped tetramers actually show an increase in kidney signal relative to uncapped H2009.1 while the D-Val and AcD-Leu capped peptides give no change. Moving out to 72 HPI (Figure 4.12), we see that AcH2009.1, D-Leu H2009.1, and AcD-Leu H2009.1 again show improvement over the parental peptide. These results are confusing until the accumulation of each peptide in the kidneys is examined over time. Viewing the data from this perspective, it can be observed that while the capped tetramers are steadily cleared from kidneys to low levels, the parental peptide is retained after an initial clearance period.

From this perspective, the AcD-Leu H2009.1 tetramer is the best performer as it gives low kidney signal at 24 HPI and clears the most rapidly. This peptide has already been eliminated as a potential long-term targeting agent on the basis of H2009 tumor retention, but this rapid clearance is highly valuable for short-term applications. The AcH2009.1 and D-Leu H2009.1 peptides also perform well in the kidneys, clearing to low levels by 72 HPI. The D-Val capped tetramer produces low renal signal at 24 HPI, but does not clear as quickly as the others. Rapid clearance from the kidneys is essential for any clinical application of peptide-targeted agents. For this reason, it is eliminated from further optimization studies.

It is unclear as to why some capped H2009.1 tetramers are retained in kidneys more than others. Previous studies have suggested that the number of charged residues or the distribution of these charges plays a significant role in the interaction between peptide ligands and these receptors [123]. Acetylation of H2009.1 removes four positive charges from the tetrameric peptide, and a corresponding decrease in renal accumulation is observed. However, even greater reduction in kidney accumulation was seen when the peptides were

capped with D-amino acids, leaving the positively charged N-terminus intact. It is possible that the high positive charge density of an N-terminal arginine residue may promote uptake into the kidneys, and capping with additional amino acids sufficiently re-distributes the positive charges to avoid this process. One study showed that D-amino acid caps stabilize small peptides against lysosomal degradation as well [115]. It may be possible that these peptides do not escape re-absorption, but survive the protein recycling process to be re-released back into circulation.

Differentiation between the xenograft tumor types is essential for peptides intended for use in diagnosis and characterization of tumors. All of the capped peptides accumulated at least two-fold higher in H2009 tumors over H460 tumors at all timepoints, as shown in Tables 4.2-4.4. Diagnostic applications are generally performed over short timespans, so the best peptide for these uses is most likely the AcD-Leu H2009.1 tetramer, which gives the best H2009/H460 ratio of 6.32 at 24 HPI.

At this point, the field of candidate peptide targeting agents has been reduced to the AcH2009.1, D-Leu H2009.1, and AcD-Leu H2009.1 tetramers. The AcD-Leu H2009.1 peptide provides the optimal combination of high targeting ability and low accumulation in the kidneys at 24 hrs, indicating it to be the best choice of targeting ligand in short term applications such as imaging of $\alpha_v\beta_6$-positive tumors. The data presented here show that the N-acetylated and D-Leu capped peptides successfully maintain levels in target tissue for extended periods of time. The AcH2009.1 and D-Leu H2009.1 peptides maintain high signal in the target tumor after clearing from the kidneys at 72 hrs. However, all of these peptide ligands exhibit problems with off-target accumulation, particularly in the lung and liver.

In previous PET imaging experiments with H2009.1 dimers, N-acetylation decreased accumulation in both the lungs and liver at 24 HPI. However, NIRF imaging with tetrameric H2009.1 peptides showed that N-acetylation increased liver accumulation and had no effect on lung signal at this timepoint. These differences could be due to the increased blood concentration required for NIRF imaging, or to the increase in peptide valency. Quantification of the impact of changes in blood concentration requires many more animals and would be time-consuming. However, further *in vitro* experiments may provide an explanation for differences produced by high valency. I hypothesized that increasing the valency of the H2009.1 peptide might result increase its binding affinity for other integrins in addition to $\alpha_v\beta_6$, the most likely candidate being $\alpha_v\beta_3$.

In order to test this hypothesis, the binding affinities of the parental and capped H2009.1 tetramers were measured by an ELISA-like assay [187]. This approach eliminates the complication of internalization dynamics and allows for direct quantification of binding. This assay replaces the primary and secondary antibodies used in standard ELISAs with biotinylated H2009.1 peptides and HRP-conjugated avidin. Binding can then be measured using the same colorimetric techniques of any ELISA. A control tetramer, with the same amino acid content as parental H2009.1 but with a scrambled sequence was also included. Signal generated by nonspecific binding of this scrambled peptide was subtracted from each of the other peptides to produce peptide specific binding curves.

This assay does have some disadvantages. The integrin receptors are removed from the context of the cell membrane. In order to maintain their native conformation in solution, the transmembrane domains of both the α and β subunits were removed, and their N-termini

are truncated to allow for stable formation of the heterodimer. These changes may have some impact on binding of the H2009.1 peptides. Also, coating the plate with solubilized protein produces a surface that is evenly distributed with proteins at random orientations. Many of the heterodimers will not adsorb in a manner that presents the full binding region for interaction with peptides. The even distribution of protein on the surface also removes any localization or clustering of the integrins that may be present in a cell membrane. Because each branch of the H2009.1 tetramer is theoretically capable of binding to a separate $\alpha_v\beta_6$ heterodimer, this distribution may impact binding affinity of the multimer. With these conditions in mind, comparisons between peptides within this assay may still be made. Because it has been previously shown that the parental H2009.1 tetramer is specific for $\alpha_v\beta_6$ over $\alpha_v\beta_3$, I included it as a control to assess the affinity and specificity of the capped peptides for $\alpha_v\beta_6$.

As shown in Figure 4.16A, all three capped tetramers maintain high affinity for $\alpha_v\beta_6$. Some loss of affinity is seen in the D-Leu capped H2009.1 tetramer, which corresponds to the loss of uptake into H2009 cells shown in Figure 4.1. Also consistent with the results of the previous assay, N-acetylation of the D-Leu H2009.1 tetramer rescues binding affinity to that of the parental peptide. This loss of binding affinity is not sufficient to impact *in vivo* targeting at the high dosages used in NIRF imaging. Interestingly, the patterns of the peptide binding affinities in the ELISA mirror those in the cell based binding/internalization assay. This would suggest that internalization of the H2009.1 peptide into H2009 cells is solely dependent on binding affinity. However, this may not be the case in other cell lines that exhibit different endocytic dynamics.

The ELISA demonstrates larger differences among the capped peptides when applied to $\alpha_v\beta_3$. The parental H2009.1 tetramer shows some binding to $\alpha_v\beta_3$ starting at 20 nM. The D-Leu capped tetramer shows binding to $\alpha_v\beta_3$ as low as 2 nM, and signal increases dramatically with concentration. Neither of the binding curves indicates saturation of the peptides on $\alpha_v\beta_3$, so binding affinities cannot be calculated. However, the $K_D$s for both the parental and D-Leu capped tetramers on $\alpha_v\beta_3$ must be at least 50 nM, and the tetramers bind $\alpha_v\beta_6$ with at least 185-fold and 30-fold specificity, respectively. Because the scrambled control tetramer is uncapped, it is possible that the high signal produced by the D-Leu capped peptide is a result of nonspecific interactions involving the hydrophobic cap itself. These interactions could lead to binding of the peptide to off-target receptors or the walls of the ELISA plate. In contrast, the AcH2009.1 and AcD-Leu H2009.1 peptides do not produce any observable binding up to 50 nM, thus showing an increase in specificity for $\alpha_v\beta_6$. These results indicate that a loss of specificity for $\alpha_v\beta_6$ is not the source of high off-target accumulation of the capped H2009.1 tetramers. While the D-Leu capped peptide does demonstrate significant loss of specificity, it performs as well as the highly specific N-acetylated H2009.1 tetramer in biodistribution studies.

The studies presented here were performed with the goal of optimizing the H2009.1 tetrameric peptide for clinical use in the characterization and treatment of $\alpha_v\beta_6$ –expressing NSCLCs. A library of N-terminally modified analogs was synthesized and characterized for serum stability, binding affinity, and targeting capacity both *in vitro* and *in vivo*. Of the peptides examined here, the optimal peptide for short-term targeting applications is the AcD-Leu H2009.1 as it accumulates well in target tumors and clears rapidly from both target and

off-target tissue. For long-term targeting, the AcH2009.1 and D-Leu H2009.1 peptides perform similarly. AcH2009.1 tetramer provides higher tumor-to-liver and tumor-to-lung ratios while D-Leu H2009.1 produces slightly better tumor-to kidney specificity. Therefore, the peptide of choice may depend on the intended cargo and its potential toxicities. However, all of these peptides demonstrate a high degree of accumulation in liver and lung. For this reason, further optimization was required to obtain a tissue specific targeting agent. These studies are outlined in the next chapter of this dissertation.

# CHAPTER FIVE
# OPTIMIZATION OF THE H2009.1 DIMERIC PEPTIDE FOR IN VIVO APPLICATIONS

## Introduction

Tetrameric H2009.1 delivers cargo to $\alpha_v\beta_6$ expressing tumor cells both *in vitro* and *in vivo*. The previous chapter presented modifications to this peptide that extend the lifetime of *in vivo* targeting and reduce accumulation of the peptide in kidneys. As shown in Figures 4.7, 4.11, and 4.14, the newly stabilized peptides accumulate and are retained in healthy liver and lung tissue. The next step in the optimization of the H2009.1 peptide was to reduce this off target accumulation while maintaining the improvements made in tumor targeting and kidney retention.

As discussed in previous chapters, PET Imaging studies demonstrated that the dimeric H2009.1 peptide is capable of targeting to $\alpha_v\beta_6$ –positive tumors in mice, at least out to 24 HPI [105]. In these studies, accumulation of the H2009.1 dimer in liver and lung relative to tumors was much lower. The tumor-to-lung ratio of the parental dimer was 1.87 at 24 HPI as opposed to 0.5 for the tetramer. Additionally, N-acetylation of the dimer was observed to decrease liver accumulation, producing a tumor-to-liver ratio of 1.24 (compared to 0.22 for the parental dimer and 0.41 for the N-acetylated tetramer). These results suggest that the H2009.1 dimer may demonstrate improved tissue specificity over the tetrameric peptide.

However, the targeting capacity and *in vivo* behavior of the H2009.1 dimer had not been examined at longer timepoints or higher concentrations. I therefore sought to further

optimize the dimeric H2009.1 peptide to extend targeting capacity and improve tissue specificity. I hypothesized that capping the dimer with D-amino acids could further reduce kidney accumulation of the dimeric H2009.1, as it had for the tetramer. Toward this end, dimeric versions of the AcH2009.1, D-Leu H2009.1, and AcD-Leu H2009.1 peptides were synthesized and characterized for their *in vitro* and *in vivo* targeting abilities.

## Methods

The methods used in these experiments are similar to those presented in chapter 4 of this dissertation with the following differences.

### *Internalization into H2009 Cells*

H2009 cells were seeded at 50,000 cells per well in 24-well plates with 0.5 mL RPMI + 5% FBS and allowed to adhere overnight. Solutions of dimeric H2009.1 peptides at concentrations ranging from 0.5 nM to 500 nM were made in RPMI + 5% FBS and incubated on cells for 2 hours. After washing with PBS and acid wash as described previously, the adherent cells were collected by trypsinization, pelleted by centrifugation, and re-suspended in PBS for analysis on a BD Accuri C6 flow cytometer. Mean fluorescence intensity was calculated using the Accuri C6 software. Curves and $EC_{50}$ values were then calculated using GraphPad Prism.

*ELISA for Binding of Peptides to Recombinant Integrins*

NuncMaxiSorp ELISA plates were coated with 0.25 μg/ml of either $\alpha_v\beta_6$ or $\alpha_v\beta_3$ integrin at 100 μL/well. Biotinylated H2009.1 dimers were diluted to 0.01-50 nM in blocking buffer. Avidin-HRP conjugate from Rockland Inc. was diluted 1:60,000 in blocking buffer. Upon addition of TMB, plates were incubated at room temperature for 10 minutes before quenching the colorimetric reaction with 0.1 M HCl.

*Serum Stability Assays*

These studies were performed as previously described. However the analytical HPLC gradient ran from 0-100% acetonitrile in water over 60 minutes on a Shimadzu HPLC system and degradation products were analyzed on an Applied Biosystems Sciex MALDI/TOF/TOF.

*Near IR Fluorescence Imaging for Peptide Biodistribution In Vivo*

These studies were performed at two different institutions. All protocols were approved by their respective institutions' Institutional Animal Care and Use committees. Those using a dose of 30 μg dimeric H2009.1 peptides were performed at UT Southwestern Medical Center (Animal Welfare Assurance Number A3472-01) under the animal protocol number 2010-0280. These studies were performed in NOD/SCID mice bearing H2009 and H460 xenograft tumors established as previously described in chapter 4. Three mice were included in each experimental group. Those using 15 μg H2009.1 peptides were done at SRI International under the animal protocol number 14008. These experiments involved J/Nu mice purchased from Jackson Laboratories. Xenograft tumors were implanted following a

similar protocol, increasing the number of injected cells to 5 million for both H2009 and H460 tumors. Animals were anesthetized by isoflurane inhalation and sacrificed by cervical dislocation. Three mice were included in each experimental group, with the exception of the D-Leu H2009.1 group at 24 HPI with two mice and the AcD-Leu H2009.1 group at 24 HPI with 4 mice.

*Immunoblotting for $\beta_6$ Expression*

After cervical dislocation, mice were perfused with sterile PBS through the left ventricle. ~50 mg of organs including liver, lung, kidney, heart, spleen, and subcutaneous tumors were minced with a razor blade. Each tissue was added to 500 µL lysis buffer (50 mM Tris-HCl, pH 7.4, 1% NP-40, 0.5% Na-deoxycholate, 0.1% sodium dodecyl sulfate, 150 mM NaCl, 2 mM EDTA, 50 mM NaF, 1X Roche Complete Protease Inhibitor Cocktail) and homogenized using a Dounce homogenizer. The organ extracts were then sonicated using a probe sonicator 3 times in 2-second bursts. The lysates were centrifuged at 16,000-x g for 15 minutes at 4°C, and the supernatants were collected as final tissue lysates. Total protein content was determined by standard BCA assay, and 20 µg protein was loaded onto a 8% SDS-PAGE gel. Gels were run at 100 mV for 1.5 hours before transferring to PVDF membranes at 35 mV for 1 hour. Membranes were blocked in PBS with 0.2% Tween-20 and 5% BSA, and β6 (C-19 from Santa Cruz Biotechnology 1:1000) and actin (clone AC-40 from Sigma Aldrich 1:1000) antibodies in PBS with 0.2% Tween-20 and 5% BSA and placed on an orbital shaker at 4°C overnight. Blots were washed with PBS with 0.2% Tween-20 3 times for 5 minutes at room temperature. Secondary antibodies (rabbit anti-goat + 800CW dye

from Li-Cor for β6, rabbit anti-mouse + AF684 for actin) were diluted 1:15,000 in PBS with 0.2% Tween-20 and 5% BSA and incubated on the membranes for 1 hour, protected from light. Blots were then washed 4 times for 5 minutes with PBS with 0.2% Tween-20 and visualized on an Odyssey scanner from Li-Cor.

**Results**

*Internalization of Capped H2009.1 Dimers into $\alpha_v\beta_6$–expressing NSCLC cells*

As we did with the H2009.1 tetramers, the dimeric H2009.1 peptide analogs were characterized for their ability to deliver cargo to H2009 cells *in vitro*. The results of these experiments indicate that capping the H2009.1 dimer does not significantly interfere with binding and internalization of the peptide (Figure 5.1). Surprisingly, there is no statistical difference between the internalization efficiency of the dimeric H2009.1 peptides and their tetrameric counterparts. Because previous results had indicated that the dimer binds with 20-fold lower affinity, we expected to see a corresponding decrease in *in vitro* delivery. However, these two assays are fundamentally different. The previously reported results are a specific measure of binding affinity. These binding curves were obtained by blocking internalization of H2009.1-displaying bacteriophages with free H2009.1 peptide. The internalized phages were then collected and titered following established methods [212]. The data presented here is a direct measure of internalized synthetic peptide by flow cytometry. Therefore, it is unsurprising that the results of these assays do not agree. It is theoretically possible that the dimer could bind with lower affinity, but internalize more quickly, resulting in similar levels of uptake into target cells. However, this seems unlikely.

A

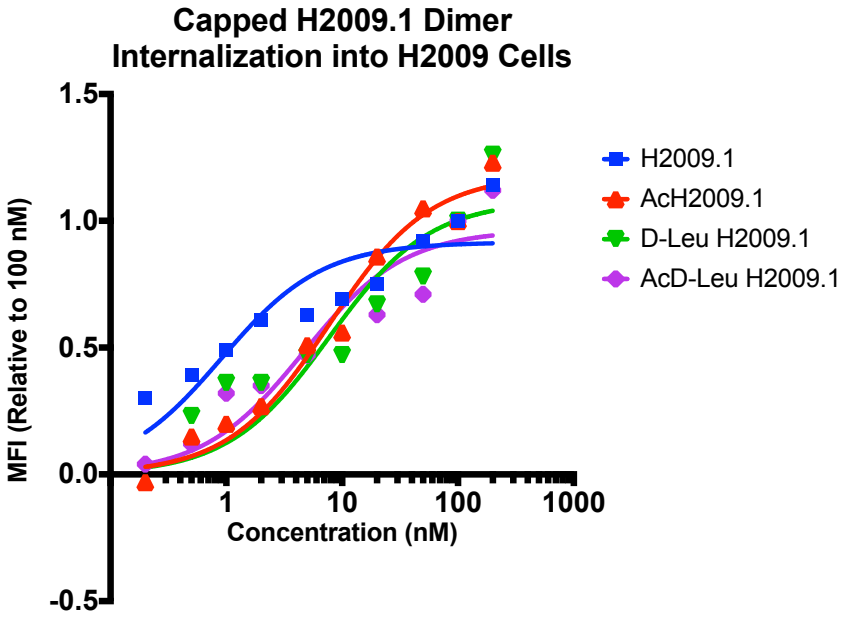


B

| Peptide | $EC_{50}$ ± SEM (nM) |
|---|---|
| H2009.1 | 6.2 ± 1.3 |
| AcH2009.1 | 12 ± 4.5 |
| D-Leu H2009.1 | 22 ± 6.9 |
| AcD-Leu H2009.1 | 17 ± 4.8 |

**Figure 5.1 Internalization of capped dimers into H2009 cells**. AF488-labeled peptide was incubated with H2009 cells at appropriate concentrations for 2 hours. Cells were washed with PBS followed by acid washes (pH 2.2) to remove un-internalized peptide. The level of fluorescence in the cells was quantified by flow cytometry. Curves were plotted and ½ max internalization ($EC_{50}$) concentrations were calculated using GraphPad Prism. Representative curves are shown. .

*Binding Affinity and Specificity of Dimeric H2009.1 Peptides for $\alpha_v\beta_6$*

Quantification of integrin binding of H2009.1 dimers by ELISA allowed for the re-examination of the previous affinity data, as well as the determination of the affinity and

specificity of the modified H2009.1 dimers. The parental H2009.1 dimer binds to recombinant $\alpha_v\beta_6$ with a $K_D$ of 140 pm (Figure 5.2). This affinity is much higher than was anticipated from previous phage blocking data. The capped dimers follow similar trends as

A

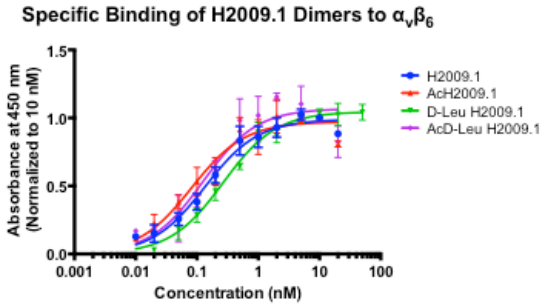


B

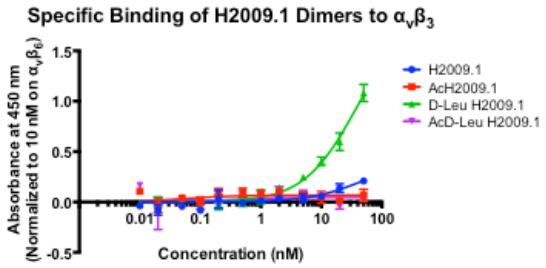


C

| Peptide | $K_D$ ± SEM (nM) |
|---|---|
| H2009.1 | 0.14 ± 0.02 |
| AcH2009.1 | 0.07 ± 0.02 |
| D-Leu H2009.1 | 0.25 ± 0.06 |
| AcD-Leu H2009.1 | 0.15 ± 0.04 |

**Figure 5.2 Direct binding of capped H2009.1 dimers to recombinant integrins**. ELISAs were performed in 96 well plates coated with recombinant $\alpha_v\beta_6$ (A) or $\alpha_v\beta_3$ (B). Curves were normalized by 10 nM H2009.1 dimer on $\alpha_v\beta_6$, plotted using GraphPad Prism, and binding affinities (C) on $\alpha_v\beta_6$ were calculated. Binding affinities to $\alpha_v\beta_3$ could not be calculated and must be greater than 20 nM. N=3

their corresponding tetramers. Some loss of affinity is observed with the D-Leu capped dimer ($p=0.001$), and this loss is rescued by N-acetylation. The capped dimers also interact with $\alpha_v\beta_3$ in a similar manner as the tetramers. Binding of the uncapped H2009.1 dimer is observed at high concentrations. This signal is dramatically increased in the D-Leu capped peptide, and decreased below the detection threshold in both acetylated dimers. Surprisingly, the dimeric peptide binds with slightly higher affinity than the tetrameric peptide. While the parental and N-acetylated peptides do not demonstrate statistical significance in binding affinity between the two valencies, the D-Leu H2009.1 dimer shows 6.4-fold increase in

affinity over its corresponding tetramer. The AcD-Leu H2009.1 dimer also gives a 3.2-fold increase in affinity compared to the tetrameric peptide.

*Serum Stability of Capped H2009.1 Dimers*

Before moving the capped H2009.1 dimers into animal imaging studies, we assessed their metabolic stability in plasma. As expected, all of the capped dimers demonstrated significantly higher serum stability than the uncapped parental peptide (Figure 5.3). In this instance, the acetylated peptides display higher serum stability than the D-Leu capped dimer. This was not observed in the tetramers where D-Leu H2009.1 was the most stable peptide examined (Figure 4.2). Once again, the capped peptides degraded almost exclusively by loss of whole H2009.1 peptide branches rather than stepwise degradation of the termini. Changes in molecular mass between the intact peptide and the degradation products suggest a loss of the multimeric core (See Appendix D). For this to occur, both branches of the dimer would have to undergo a reverse Michael addition, and the newly free thiols would have to oxidize to form a disulfide bond between the H2009.1 monomers. In a clinical situation, this mode of degradation could result in loss of targeting. However, the rate of degradation is slow enough, particularly for the AcH2009.1 and AcD-Leu H2009.1 dimers, that biodistribution may not be significantly affected. Therefore, all of the peptides were advanced to NIRF imaging in animals.

A

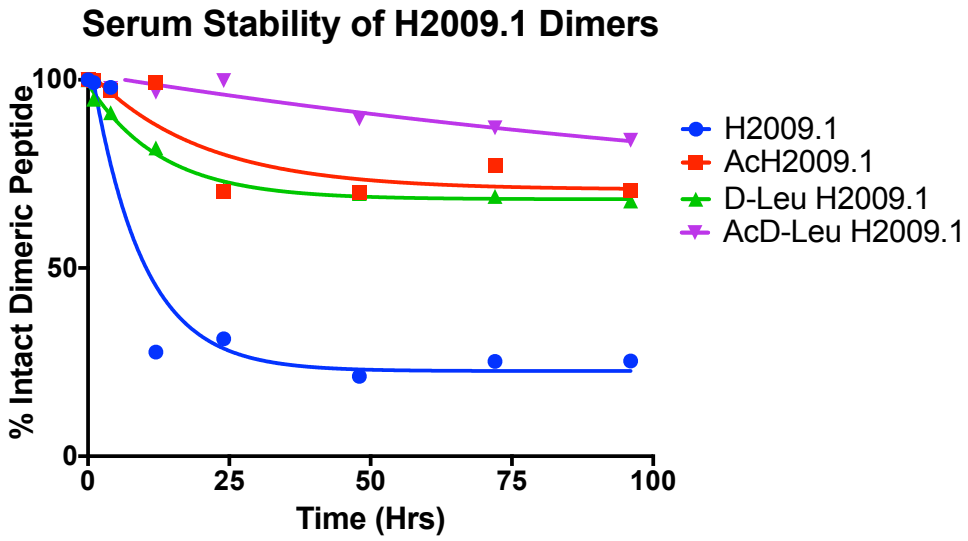


B

| | % Intact Peptide at 12 Hrs |
|---|---|
| H2009.1 | 27.68 |
| AcH2009.1 | 99.31 |
| D-Leu H2009.1 | 81.89 |
| AcD-Leu H2009.1 | 99.71 |

**Figure 5.3 Degradation of Capped H2009.1 Dimers in Human Plasma.** A) Capped H2009.1 dimer serum stability up to 96 Hrs. B) Summary of intact peptide remaining after 12 Hrs incubation at 37°C in human plasma. All capped peptides demonstrated significant improvements in serum stability.

*In Vivo Imaging and Biodistribution of Capped H2009.1 Dimers*

*In vivo* targeting and biodistribution of the modified H2009.1 dimers were assessed using NIRF imaging methods, as described in Chapter 4. Two dosages of dimeric peptide were examined. A dose of 15 µg peptide provides similar blood concentrations of the Cy5 dye as the previous experiments with tetrameric H2009.1. For this dosage, 24 Hr and 72 Hr

timepoints were chosen as to give information on both short-term and long-term *in vivo* behavior. We also examined the effects of increasing the peptide dose to 30 µg to produce the same blood concentration of available $\alpha_v\beta_6$ binding moieties.

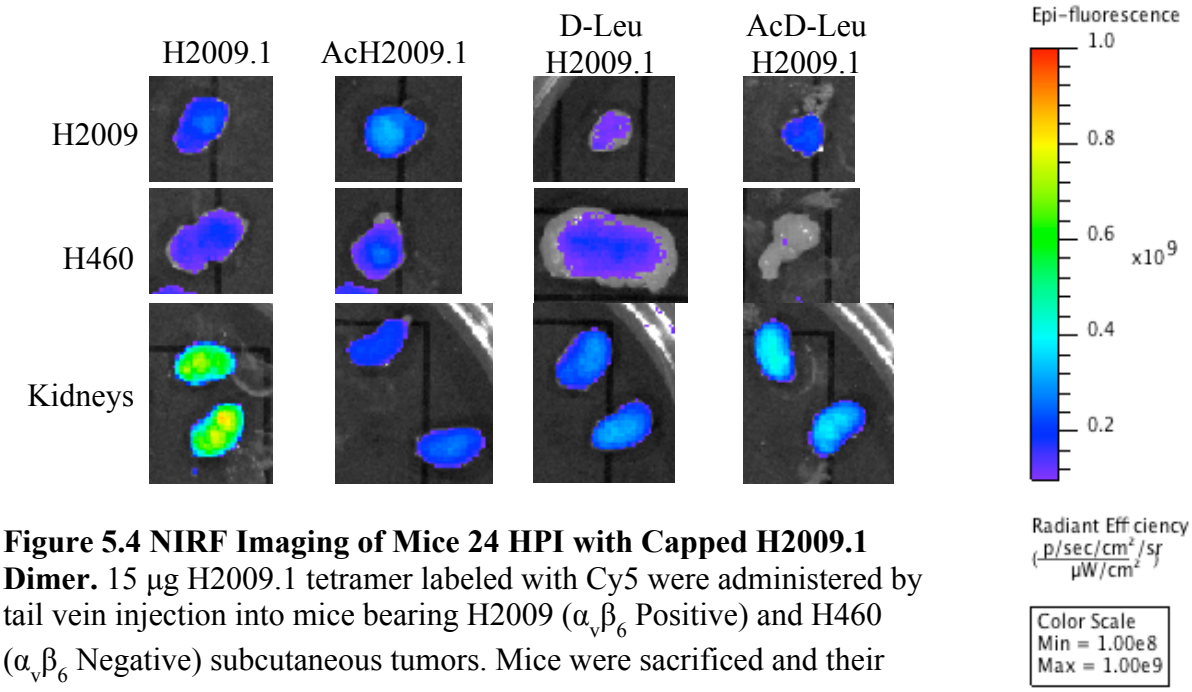


**Figure 5.4 NIRF Imaging of Mice 24 HPI with Capped H2009.1 Dimer.** 15 µg H2009.1 tetramer labeled with Cy5 were administered by tail vein injection into mice bearing H2009 ($\alpha_v\beta_6$ Positive) and H460 ($\alpha_v\beta_6$ Negative) subcutaneous tumors. Mice were sacrificed and their organs were imaged *ex vivo*. N ≥ 2 Representative images are shown.

*Biodistribution of Capped H2009.1 Dimers - 24 HPI, 15 ug Dose*

As can be observed in Figures 5.4 and 5.5, all four H2009.1 dimers examined accumulate in H2009 tumors at 24 HPI. The AcH2009.1 dimer shows a slight increase in signal in H2009 tumors compared to the parental dimer while the D-Leu and AcD-Leu capped dimers show a slight decrease. However, examination of H460 accumulation reveals the opposite pattern. As seen in Figure 5.4 and Table 5.1, the H2009-to-H460 ratio is decreased for the AcH2009.1 peptide (1.34) compared to uncapped H2009.1 dimer (2.26), while it is increased for D-Leu H2009.1 (7.09) and AcD-Leu H2009.1 (3.83) due to low

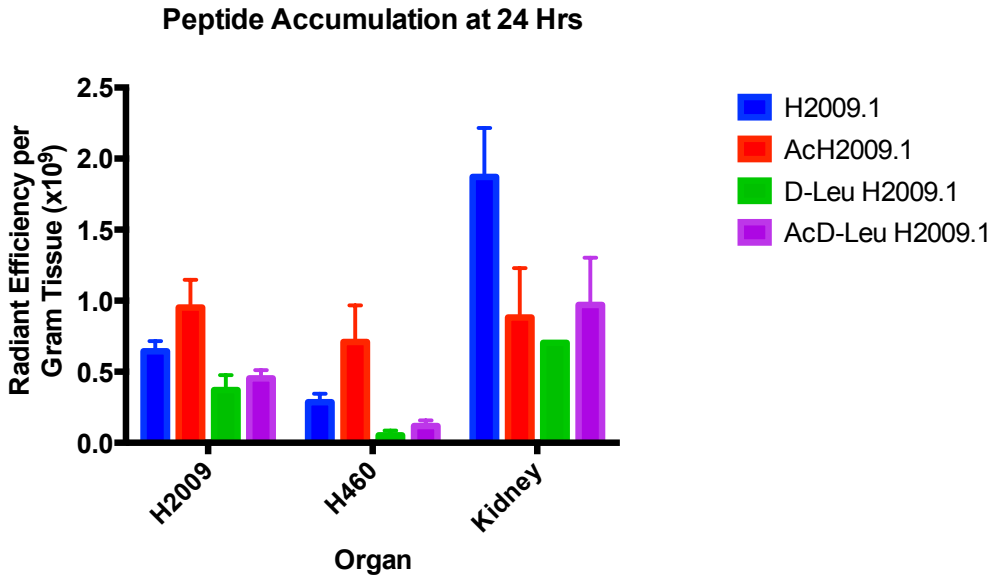


**Figure 5.5 NIRF Imaging of Tumors and Kidneys in Mice 24 HPI with Capped H2009.1 Dimer.** 15 µg H2009.1 tetramer labeled with Cy5 were administered by tail vein injection into mice bearing H2009 ($\alpha_v\beta_6$ Positive) and H460 ($\alpha_v\beta_6$ Negative) subcutaneous tumors. Mice were sacrificed and their organs were imaged *ex vivo*. N ≥ 2

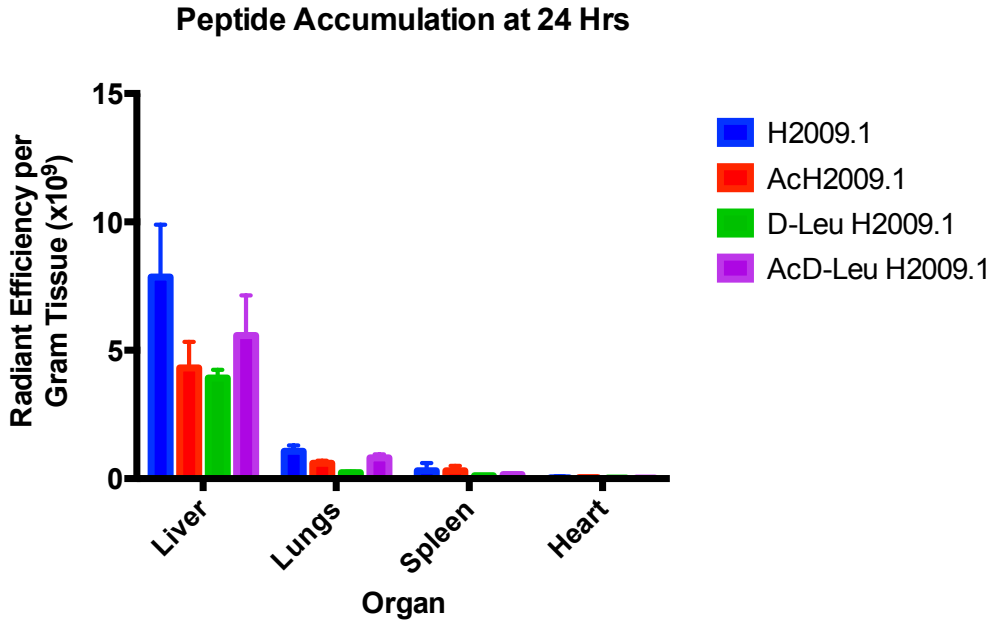


**Figure 5.6 NIRF Imaging of Off Target Organs in Mice 24 HPI with Capped H2009.1 Dimer.** 15 µg H2009.1 tetramer labeled with Cy5 were administered by tail vein injection into mice bearing H2009 ($\alpha_v\beta_6$ Positive) and H460 ($\alpha_v\beta_6$ Negative) subcutaneous tumors. Mice were sacrificed and their organs were imaged *ex vivo*. N ≥ 2

accumulation in H460 tumors. The D-Leu H2009.1 dimer performs particularly well at this timepoint with a 3-fold increase in specificity between the $\alpha_v\beta_6$ positive and negative tumors relative to the parental H2009.1 dimer.

| Peptide | H2009/ H460 | H2009/ Kidney | H2009/ Liver | H2009/ Lung | H2009/ Spleen | H2009/ Heart |
|---|---|---|---|---|---|---|
| H2009.1 | 2.26 | 0.34 | 0.82 | 0.61 | 2.10 | 17.74 |
| AcH2009.1 | 1.34 | 1.08 | 0.22 | 1.59 | 3.10 | 23.02 |
| D-Leu H2009.1 | 7.09 | 0.52 | 0.09 | 2.60 | 3.24 | 14.13 |
| AcD-LeuH2009.1 | 3.83 | 0.46 | 0.08 | 0.56 | 2.87 | 17.80 |

**Table 5.1 Ratios of Signal from Each Organ Relative to Target H2009 Tumors 24 HPI.**

In agreement with previous PET studies, N-acetylation of the H2009.1 peptide decreases the levels of accumulation in renal tissue. In contrast to the NIRF imaging of the tetramers, capping the N-terminus with a D-amino acid does not produce any further benefit. All three capped peptides accumulated to similar levels in the kidneys at 24 HPI. Accumulation in spleen and heart was consistent across all peptides examined in these studies. The AcH2009.1 and D-Leu H2009.1 dimers showed decreases in lung accumulation 24 HPI while the AcD-Leu H2009.1 performed similarly to the parental peptide.

All of the N-terminal modifications also decrease liver accumulation of the dimeric H2009.1 peptide as well. Curiously, this is the opposite result of the tetrameric H2009.1 peptide at 24 HPI (Figure 4.6). However, the overall accumulation of dimer in the liver was much higher than what was observed in imaging of the tetrameric peptide with an 8-fold increase in signal for the parental H2009.1 and a 2-2.5-fold increase for the capped peptides. This surprising difference may result from strain differences in the mice used in these studies.

*Biodistribution of Capped H2009.1 Dimers - 72 HPI, 15 ug Dose*

At 72 HPI, the AcH2009.1 and D-Leu H2009.1 dimers both demonstrate increased retention in target H2009 tumors over the unmodified H2009.1 peptide Figures 5.7 and 5.8. The AcD-Leu capped dimer does not demonstrate any benefit over the parental dimer at this timepoint. By 72 HPI, little signal remains in the H460 tumors, producing high tumor targeting ratios for all of the peptides, particularly AcH2009.1 and D-Leu H2009.1. In fact, the level of fluorescence signal from the H460 tumors in all three mice in the AcH2009.1 was below that of negative control mice. This prevents quantification of tumor specificity. However, we can assume it is much higher than those of the other peptides examined.

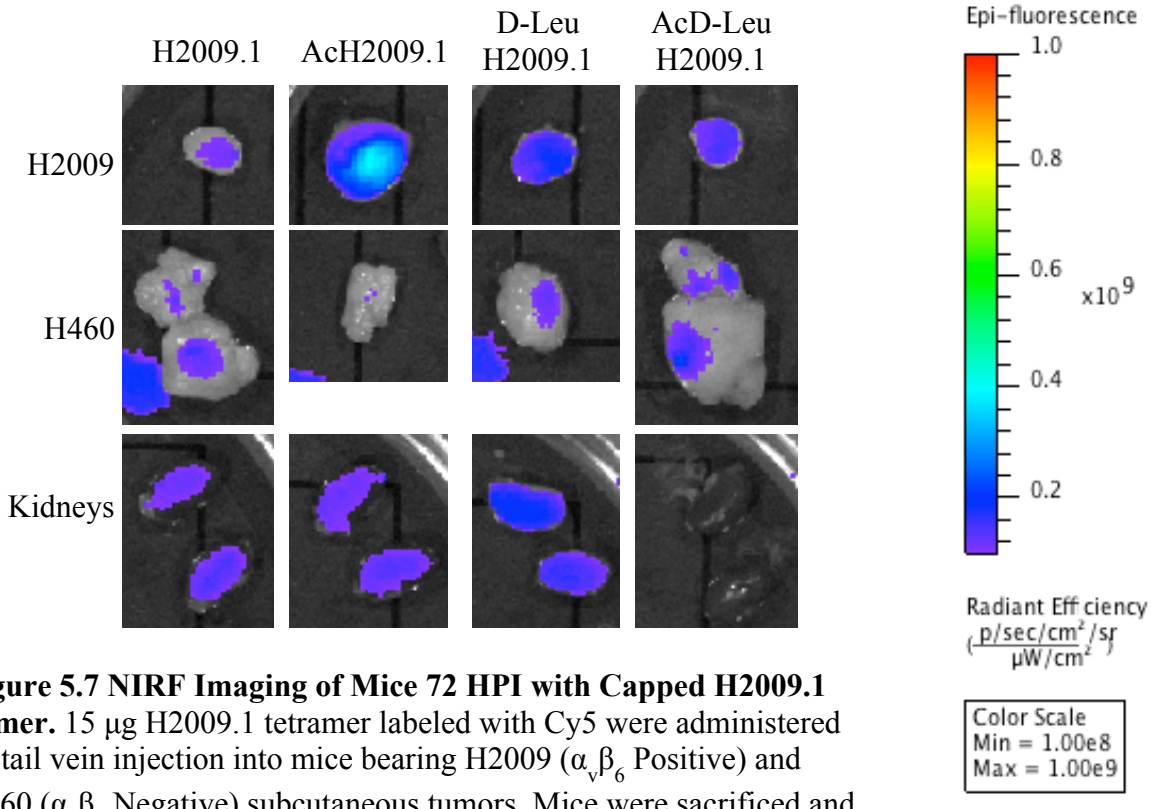


**Figure 5.7 NIRF Imaging of Mice 72 HPI with Capped H2009.1 Dimer.** 15 µg H2009.1 tetramer labeled with Cy5 were administered by tail vein injection into mice bearing H2009 ($\alpha_v\beta_6$ Positive) and H460 ($\alpha_v\beta_6$ Negative) subcutaneous tumors. Mice were sacrificed and their organs were imaged *ex vivo*. N ≥ 3 Representative images are shown.

While the AcH2009.1 dimer is at high levels in H460 tumors 24 HPI, by 72 HPI the peptide is virtually gone. The levels of fluorescent signal in these tumors are below that detected from negative control mice. The peptide is retained in H2009 tumors, producing the highest signal at this timepoint. One tumor in the AcH2009.1 group produced significantly higher signal than the other two. However, the peptide levels in all of the other organs were similar to the rest of the group, and thus the animal was included in the data. While this does result in a large amount of error, all three replicates produced higher signal than parental H2009.1 tumor. In the off-target organs, the AcH2009.1 dimer performs similarly to the parental peptide at 72 HPI.

Similar levels of kidney retention are observed for the parental, N-acetylated, and D-Leu capped H2009.1 dimers at 72 HPI. However, the increased retention of AcH2009.1 dimer in target tumors results in an improved tumor-to-kidney ratio. The AcD-Leu H2009.1 dimer gives reduced accumulation at this timepoint compared to the others, but its concurrent decrease in H2009 tumor retention produces a similar tumor-to-kidney ratio to the parental and D-Leu H2009.1 dimers.

By this timepoint, much of the dimeric peptide has cleared from the liver (Figure 5.9). However, signal is still higher than what was observed for the tetrameric H2009.1 analogs. This is likely the result of differences in metabolism between the two strains of mice. The parental H2009.1 dimer produces lower liver signal than the D-Leu and AcD-Leu capped peptides, indicating that it clears more rapidly from the liver than the modified dimers. Accumulation of the N-acetylated H2009.1 dimer is roughly equal to that of the parental

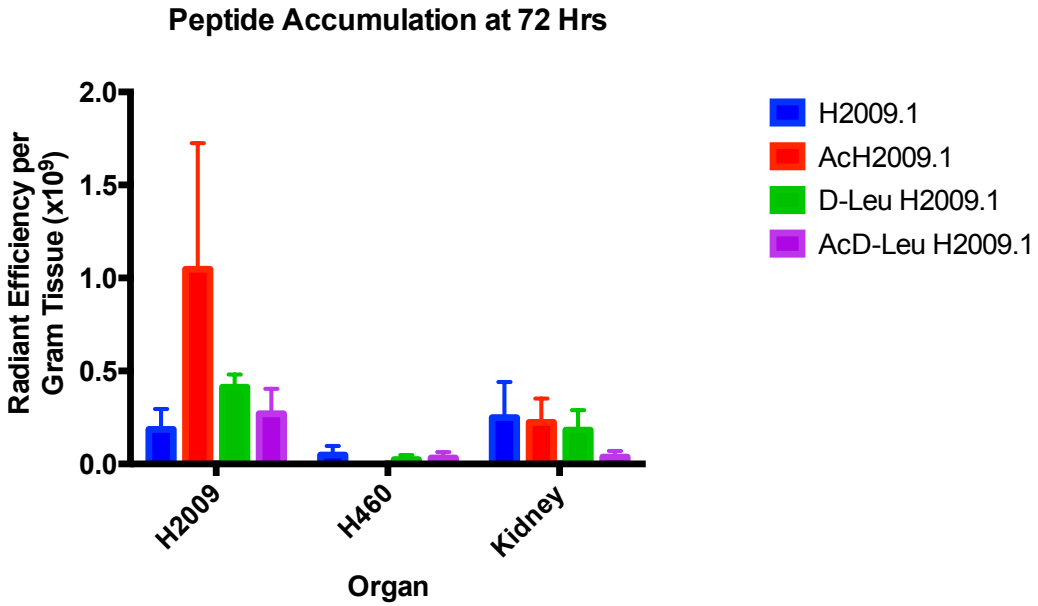


**Figure 5.8 NIRF Imaging of Tumors and Kidneys in Mice 72 HPI with Capped H2009.1 Dimer.** 15 µg H2009.1 tetramer labeled with Cy5 were administered by tail vein injection into mice bearing H2009 ($\alpha_v\beta_6$ Positive) and H460 ($\alpha_v\beta_6$ Negative) subcutaneous tumors. Mice were sacrificed and their organs were imaged *ex vivo*. N ≥ 3

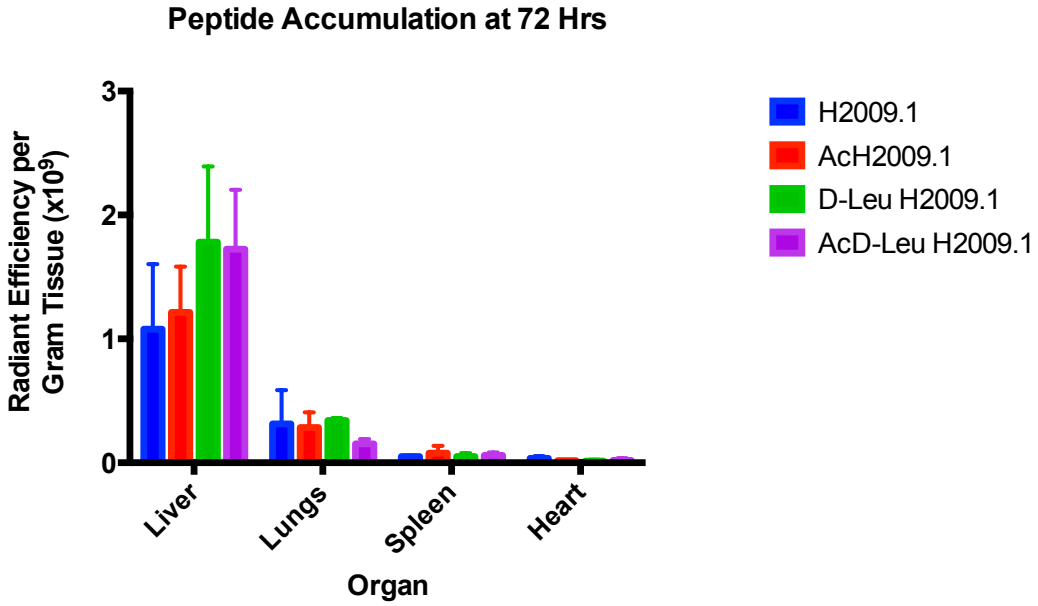


**Figure 5.9 NIRF Imaging of Off Target Organs in Mice 72 HPI with Capped H2009.1 Dimer.** 15 µg H2009.1 tetramer labeled with Cy5 were administered by tail vein injection into mice bearing H2009 ($\alpha_v\beta_6$ Positive) and H460 ($\alpha_v\beta_6$ Negative) subcutaneous tumors. Mice were sacrificed and their organs were imaged *ex vivo*. N ≥ 3

peptide at 72 HPI. However, its increased retention in the H2009 tumor tissue produces a significantly improved tumor-to-liver specificity ratio.

Unlike the 24 Hr timepoint, the AcH2009.1 and D-Leu H2009.1 dimers do not demonstrate any decrease in lung tissue at 72 HPI. The AcD-Leu H2009.1 does show some improvement. Due to low retention at this timepoint, all of the capped dimers produce much improved tumor-to-lung specificity compared to the parental dimer, and to the tetrameric H2009.1 peptides. All four dimers show little retention in the spleen and heart, with no differences observed among the capped peptides.

| Peptide | H2009/ H460 | H2009/ Kidney | H2009/ Liver | H2009/ Lung | H2009/ Spleen | H2009/ Heart |
|---|---|---|---|---|---|---|
| H2009.1 | 3.85 | 0.74 | 0.17 | 0.59 | 3.71 | 5.32 |
| AcH2009.1 | * | 4.68 | 0.86 | 3.67 | 13.41 | 61.63 |
| D-Leu H2009.1 | 17.08 | 2.26 | 0.23 | 1.21 | 8.16 | 29.31 |
| AcD-LeuH2009.1 | 8.49 | 7.26 | 0.16 | 1.77 | 4.59 | 14.60 |

**Table 5.2 Ratios of Signal from Each Organ Relative to Target H2009 Tumors 72 HPI.** *Indicates that a ratio could not be calculated. All mice in this group produced H460 tumor signal that was lower than negative control.

When signal in the H2009 tumors is plotted over time (Figure 5.10), it is observed that the N-acetylated and D-Leu capped analogs are retained in target tissue while the parental dimer is cleared over time. Tumor accumulation of the AcD-Leu capped dimer decreases slightly over the time course. Examination of kidney retention over time (Figure 5.11) shows that the benefits of N-terminally capping the H2009.1 dimer to not extend to long-term targeting. However, this appears to be more of a result of good clearance of the parental dimer after 72 Hrs rather than retention of the capped peptides.

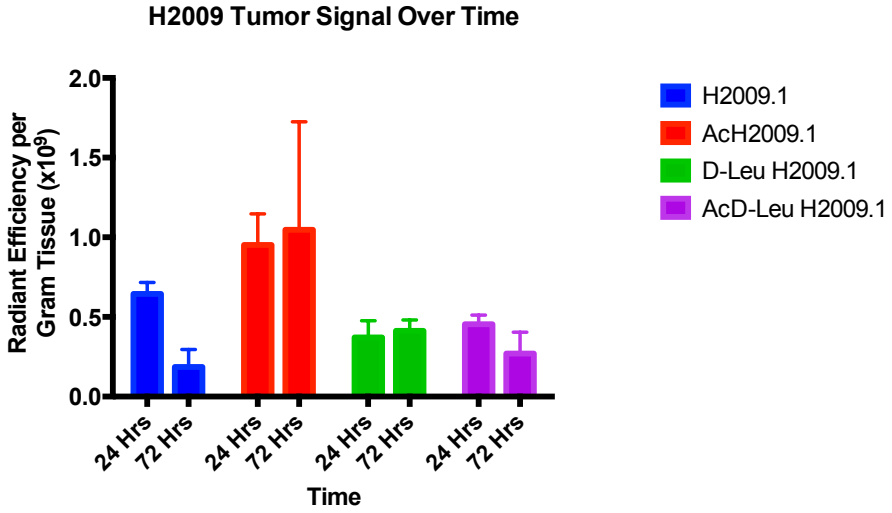


**Figure 5.10 Quantification of NIRF Imaging of Capped H2009.1 Dimer in H2009 Tumors Over Time.** 15 µg H2009.1 tetramer labeled with Cy5 were administered by tail vein injection into mice bearing H2009 ($\alpha_v\beta_6$ Positive) and H460 ($\alpha_v\beta_6$ Negative) subcutaneous tumors. Mice were sacrificed and their organs were imaged *ex vivo*. N ≥ 2 at each timepoint. Tumor signal decreases over time for H2009.1 and AcD-Leu H2009.1 but is maintained for AcH2009.1 and D-Leu H2009.1 out to 72 HPI.

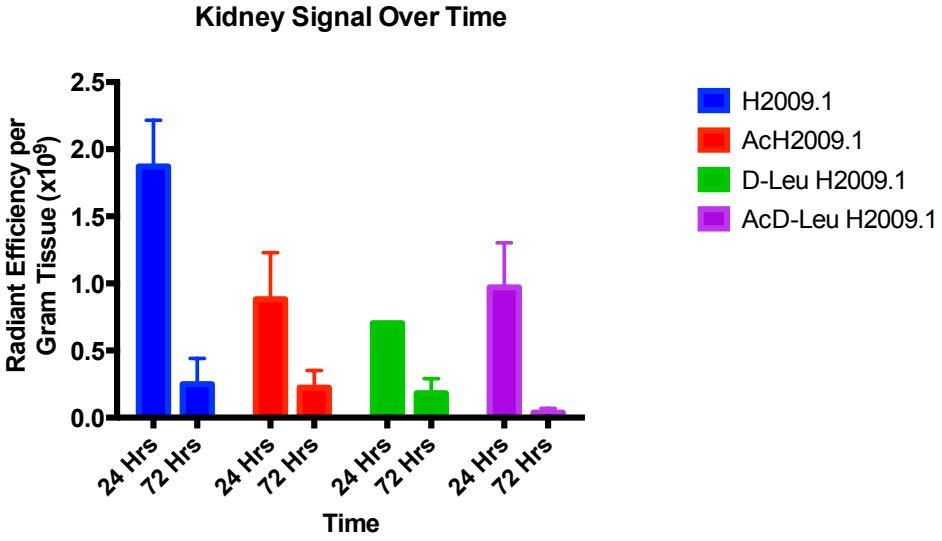


**Figure 5.11 Quantification of NIRF Imaging of Capped H2009.1 Tetramer in Kidneys Over Time.** 15 µg H2009.1 tetramer labeled with Cy5 were administered by tail vein injection into mice bearing H2009 ($\alpha_v\beta_6$ Positive) and H460 ($\alpha_v\beta_6$ Negative) subcutaneous tumors. Mice were sacrificed and their organs were imaged *ex vivo*. N ≥ 2 at each timepoint. All capped peptides showed lower kidney signal compared to parental H2009.1 24 HPI and 72 HPI.

*Biodistribution of Capped H2009.1 Dimers – 24 HPI, 30 µg Dose*

We also examined the biodistribution of peptide dosed at the same mass of 30 µg to produce the same concentration of available $\alpha_v\beta_6$ binding peptides. Under these conditions, all of the peptides accumulated to a similar degree in nearly all organs (Figures 5.12-5.14). The only exceptions were observed with the D-Leu capped H2009.1 dimer, which produced decreased in accumulation in the H2009 tumor and increased accumulation in the lung. This decrease in H2009 signal is consistent with the results of the low dose dimer imaging. However, the 15 ug dose of D-Leu H2009.1 produced lower signal in the lung compared to parental peptide. Overall, these data show that increasing the benefits of N-terminal capping the dimer decrease as dosage increases.

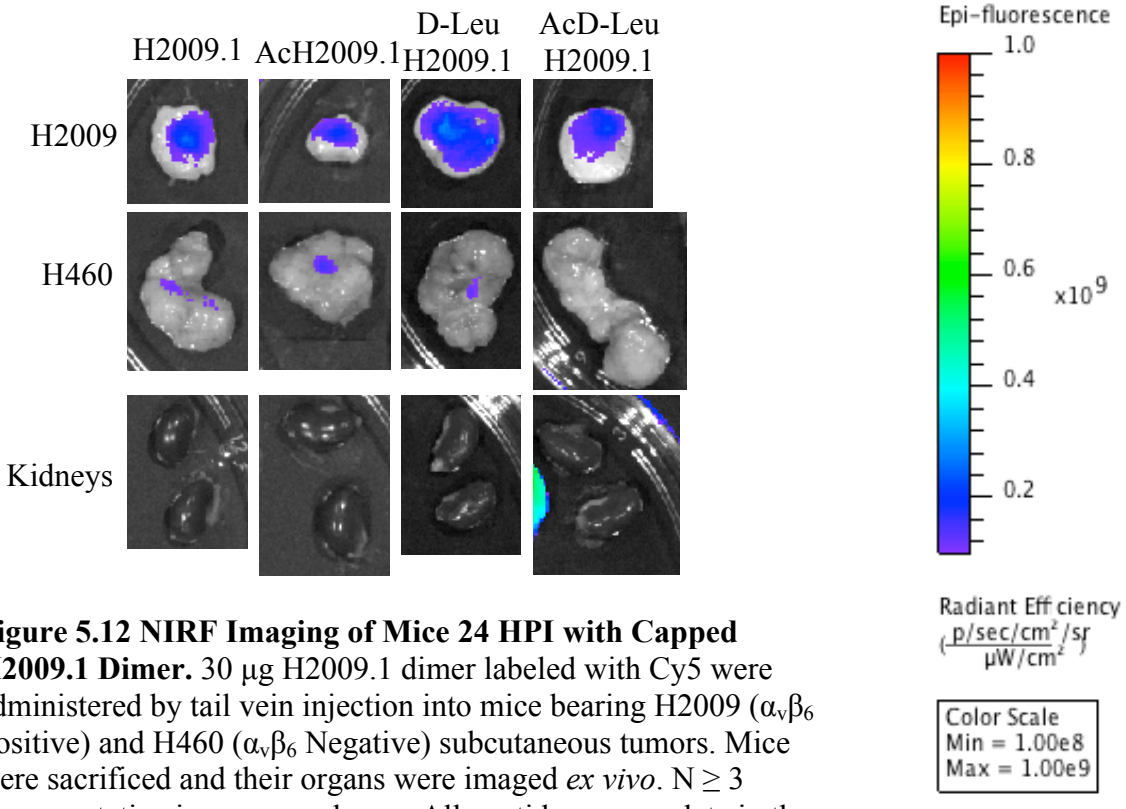


**Figure 5.12 NIRF Imaging of Mice 24 HPI with Capped H2009.1 Dimer.** 30 µg H2009.1 dimer labeled with Cy5 were administered by tail vein injection into mice bearing H2009 ($\alpha_v\beta_6$ Positive) and H460 ($\alpha_v\beta_6$ Negative) subcutaneous tumors. Mice were sacrificed and their organs were imaged *ex vivo*. N ≥ 3 Representative images are shown. All peptides accumulate in the H2009 tumor to a similar degree and specificity.

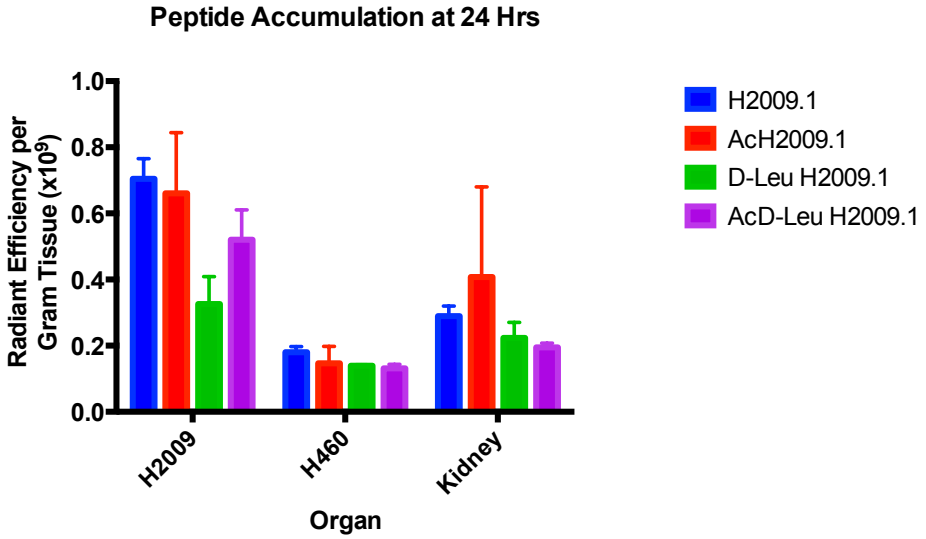


**Figure 5.13 Quantification of NIRF Imaging of Organs and Kidneys in Mice 24 HPI with Capped H2009.1 Dimer.** 30 µg H2009.1 dimer labeled with Cy5 were administered by tail vein injection into mice bearing H2009 ($\alpha_v\beta_6$ Positive) and H460 ($\alpha_v\beta_6$ Negative) subcutaneous tumors. Mice were sacrificed and their organs were imaged *ex vivo*. N ≥ 3 All peptides accumulate in the H2009 tumor to a similar degree and specificity. No significant differences were observed in the biodistribution of these peptides.

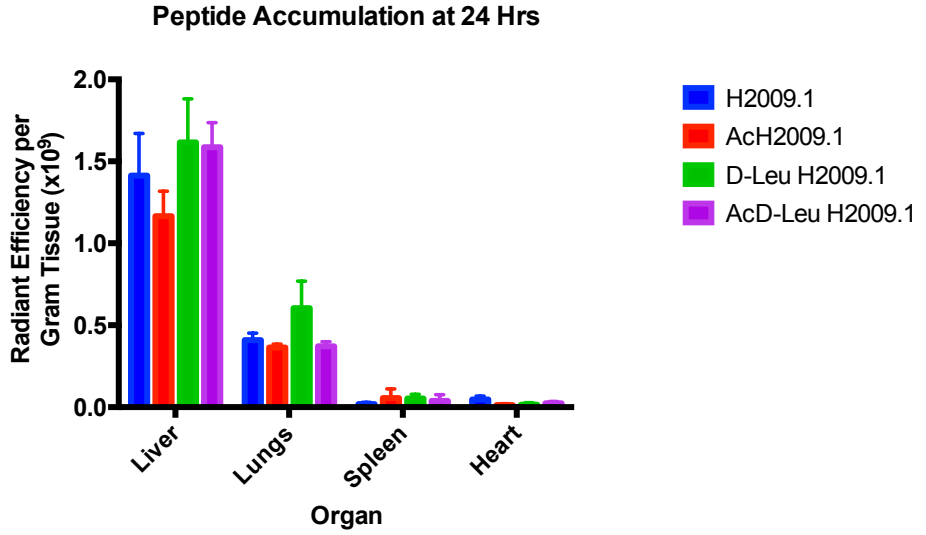


**Figure 5.14 Quantification of NIRF Imaging of Off Target Organs in Mice 24 HPI with Capped H2009.1 Dimer.** 30 µg H2009.1 dimer labeled with Cy5 were administered by tail vein injection into mice bearing H2009 ($\alpha_v\beta_6$ Positive) and H460 ($\alpha_v\beta_6$ Negative) subcutaneous tumors. Mice were sacrificed and their organs were imaged *ex vivo*. N ≥ 3 All peptides accumulate in the H2009 tumor to a similar degree and specificity. No significant differences were observed in the biodistribution of these peptides.

| Peptide | H2009/ H460 | H2009/ Kidney | H2009/ Liver | H2009/ Lung | H2009/ Spleen | H2009/ Heart |
|---|---|---|---|---|---|---|
| H2009.1 | 3.91 | 2.43 | 0.50 | 1.72 | 36.85 | 15.14 |
| AcH2009.1 | 4.5 | 1.62 | .57 | 1.82 | 11.91 | 50.40 |
| D-Leu H2009.1 | 2.33 | 1.46 | 0.20 | 0.54 | 6.21 | 20.87 |
| AcD-LeuH2009.1 | 3.96 | 2.67 | 0.32 | 1.40 | 13.71 | 22.41 |

**Table 5.3 Ratios of Signal from Each Organ Relative to Target H2009 Tumors 24 HPI.**

*Expression of Integrin $\alpha_v\beta_6$ in Mouse Tissue*

The high degree of accumulation of the H2009.1 peptides in mouse lung and liver, despite clear specificity for $\alpha_v\beta_6$, suggests that levels of the integrin in these tissues may be higher than anticipated. It is often stated in the literature that the $\beta_6$ subunit is only expressed during fetal development and wound healing [149, 188, 200, 227, 228]. However, many of these studies are based solely on PCR results demonstrating an absence of $\beta_6$ mRNA. Our group has used immunohistochemistry to demonstrate low levels of $\beta_6$ protein in normal human lung [157] while other groups have done the same in liver tissue [229, 230]. However, the $\beta_6$ expression profiles of the specific mouse strains used in our imaging studies were unknown. Western blot analysis of collected murine tissues demonstrated significant expression of $\beta_6$ integrin in both the liver and the lung (Figure 5.15). Levels of the integrin in lung were quantified at 61.0% of those in the target H2009 tumor in J/Nu mice, while those in NOD/SCID mice were much lower at 27.0% of H2009 tumor expression. In contrast, relative liver expression of $\beta_6$ was nearly three-fold higher in the NOD/SCID mice (29.2%) than in the J/Nu mice (11.5%). This is unexpected, as the NIRF imaging data indicates much higher levels of H2009.1 peptide accumulation in the livers of J/Nu mice. These results suggest that accumulation of the peptide in the liver is not a function of specific peptide-

receptor interactions. Importantly, little $\alpha_v\beta_6$ expression was observed in kidney, spleen, or heart J/Nu mice. Similar results were observed in NOD/SCID tissues. Unfortunately, sample degradation prevented the normalization of loading, and precludes accurate data quantification.

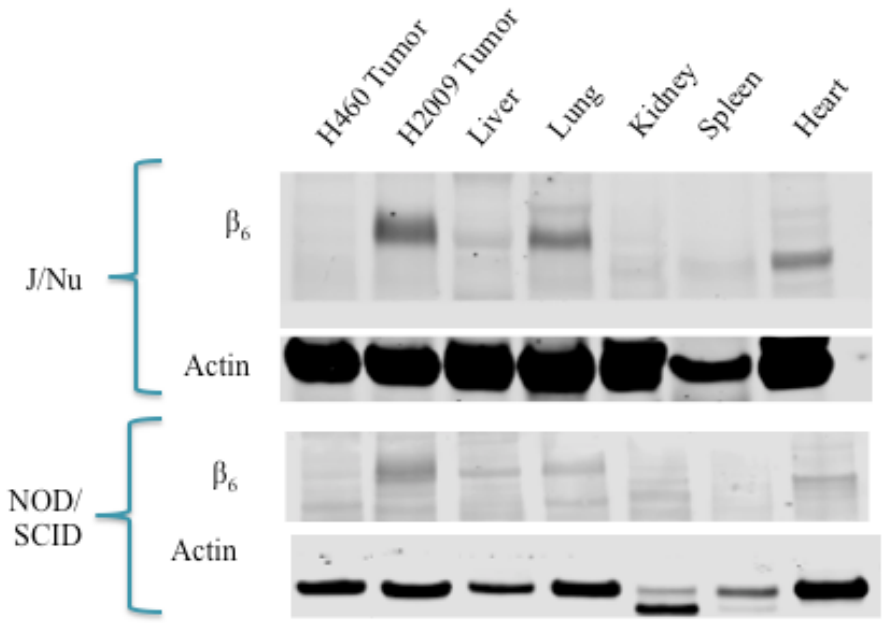


| | Expression of $\beta_6$ (% H2009 Tumor Levels) | |
|---|---|---|
| Organ | J/Nu Mice | NOD/SCID Mice |
| H460 Tumor | 0.9% | 0.9% |
| H2009 Tumor | 100% | 100% |
| Liver | 11.5% | 29.2% |
| Lung | 61.0% | 27.0% |
| Kidney | 3.3% | NA |
| Spleen | 0.5% | NA |
| Heart | 4.4% | 0.4% |

**Figure 5.15 Analysis of Integrin $\beta_6$ Expression by Western Blot.** A mouse bearing H2009 and H460 tumors was sacrificed and perfused with PBS. Organs were collected, tissue was homogenized in lysis buffer, and analyzed by SDS-PAGE and Western blot for expression of β6 and actin/tubulin. Quantified expression levels are normalized against actin levels in each sample. (Blot on J/Nu tissues performed by Chinying Chung in our lab.)

**Discussion**

The studies presented in this chapter describe the optimization the H2009.1 dimeric peptide for *in vivo* applications. Previous work detailed in Chapter 4 of this dissertation revealed N-terminal capping of the H2009.1 tetramer extended targeting capacity while decreasing retention in the kidneys. However, further improvement was required to decrease off-target accumulation of the peptide in kidney, liver, and lung. I then strove to identify an analog of the H2009.1 peptide with the optimal properties to differentiate between target tumors and these off-target tissues. Previous PET imaging studies indicated that the H2009.1 dimer is capable of delivering cargo to tumors and that N-acetylation improves tissue specificity of the dimeric peptide (Figures 2.10-2.11). However, the behavior of these dimeric peptides at longer timepoints was unknown. I therefore sought to thoroughly characterize the in vitro and in vivo targeting capabilities of the dimeric H2009.1 peptide. D-Leu and AcD-Leu capped dimers were also investigated as these caps proved beneficial to biodistribution of the tetrameric peptide.

As described in the previous chapter, the capped H2009.1 dimers were assessed in vitro to characterize their binding affinity, specificity, and internalization into $\alpha_v\beta_6$–positive cells. In vitro, the dimeric peptides behave remarkably similar to their tetrameric counterparts. All of the peptides demonstrate high affinity and specificity for $\alpha_v\beta_6$. The D-Leu capped dimer appears to bind to $\alpha_v\beta_3$ with higher affinity than the other peptides. However, as signal did not saturate within the concentration curve, we can only estimate the binding affinity at greater than 20 nM. This indicates that the D-Leu H2009.1 dimer still binds to $\alpha_v\beta_6$ with at least 80-fold specificity.

Both the tetramer and dimer show increased binding to $\alpha_v\beta_3$ when capped with D-Leu. There are a couple of possible explanations for this. The hydrophobic D-Leu residue could participate in binding to the $\alpha_v$ subunit. Cilengitide, a cyclic peptide that binds selective to $\alpha_v\beta_3$ bears a Val residue at the position immediately N-terminal to the RGD sequence. This seems unlikely as the AcD-Leu capped peptides show virtually no binding to $\alpha_v\beta_3$. It is more likely that the extension of the N-terminal amine by another residue promotes binding in some way. The structural data (Figure 2.9) indicates that the termini of the peptides extend away from the integrin heterodimer. However, the peptide might be sufficiently flexible to allow interaction of the termini with the $\alpha_v$ subunit.

In the ELISA, not only do the dimers follow the same patterns relative to each other, they also demonstrate surprisingly similar binding affinities to the tetramer H2009.1 analogs. I expected that, in accordance with previous binding affinity data, the H2009.1 dimer would bind $\alpha_v\beta_6$ with about 20-fold lower affinity than the tetramer. In fact, the D-Leu H2009.1 and AcD-Leu H2009.1 bind with significantly higher affinity. This implies that the addition of extra binding moieties actually hinders binding, at least in the context of the ELISA. Steric hindrance or interactions between the branches of the tetramer would have this effect, or the decrease in binding affinity could simply be caused by the increased entropic cost of binding a larger molecule without a compensating increase in enthalpy.

As discussed in the previous chapter, the ELISA takes binding out of the context of the cell membrane. The integrin heterodimers are immobilized on a plate, distributed evenly, and at random orientation. These conditions may obscure the benefits of increasing the valency of H2009.1 peptides. It is possible that, in the context of a cell membrane, the

tetrameric peptide may bind more tightly to clustered integrins such as those localized to focal adhesions. Alternatively, the tetramer peptide might contribute to clustering of integrins, perhaps triggering internalization into the cell. This would explain the disagreement between the results of the ELISA and the phage blocking assay.

I therefore extended the *in vitro* characterization of the H2009.1 peptides to examine internalization into H2009 cells by flow cytometry. Once again, the N-terminally modified dimers followed the same pattern as their tetrameric counterparts. Surprisingly, the results of the cellular uptake assay agreed with the ELISA in that no significant difference was observed between the H2009.1 multimers. This disagrees with the previous phage blocking experiments, and the basis of this disagreement is unknown. However, because flow cytometry and ELISAs are more direct measurements than phage blocking, these results take precedence.

The *in vitro* serum stability of the H2009.1 dimer analogs was also examined. As expected, N-terminal capping stabilizes the H2009.1 dimer against serum metabolism. In the case of the dimeric peptides, the acetylated peptides appear to be more stable than the D-Leu capped dimer. The reasons for this are unclear, as the capping moieties are quite distant from the point of degradation, the thioether linkage to the lysine core. However, all of the capped peptides are significantly more stable in human serum than the parental H2009.1 dimer.

However, one major difference was observed in the degradation patterns between the dimeric and tetrameric H2009.1 peptides. As the capped H2009.1 dimers degraded, the molecular weights of the products demonstrated a loss of 700 Daltons. The loss of mass is the same for the AcH2009.1, D-Leu H2009.1, and AcD-Leu H2009.1, suggesting that all

three peptides are degrading at their common C-termini rather than their unique N-termini. During degradation of the H2009.1 tetramers, whole chains of targeting peptides were lost by reverse Michael addition, producing un-saturated tetrameric core with two or three intact targeting H2009.1 sequences. I believe that the dimeric peptides are degrading in the same manner. However, because the dimeric peptides only have two monomeric chains to lose, the lysine cores are being entirely stripped of their H2009.1 peptides. The free cysteines at the H2009.1 C-termini are then oxidizing to form disulfide dimers of the H2009.1 peptide. Indeed, re-examination of the tetramer degradation products supports this hypothesis. After incubation in serum, peaks corresponding to disulfide dimers of each peptide (Parental and capped) are observed in the MALDI spectra. This could be further validated by treatment of these samples with reducing agents and observing dissociation of the dimers.

This has significant implications for the *in vivo* behavior of drugs conjugated to the H2009.1 dimer. Because cargo is loaded at the C-termini of the lysine core module, targeting is lost when both H2009.1 branches are lost. Because this process is slow, particularly for the AcH2009.1 and AcD-Leu H2009.1 dimers, short-term targeting is unlikely to be significantly effected. However, long-lived agents could lose targeting at long timepoints.

Bearing these potential caveats in mind, the capped H2009.1 dimers were assessed by NIRF imaging in mice. Altering the valency of the H2009.1 multimer changes the ratio of binding ligands to dye molecules. In order to compare these data with imaging studies done with the tetrameric peptide, the biodistribution of two different dosages of H2009.1 dimers were examined, 30 μg and 15 μg. The 30 μg dose produces a blood concentration of Cy5 dye of ~3 μM, assuming a total blood volume of 2 mL. This is double what was used in imaging

of the tetrameric peptides. Because each branch of an H2009.1 multimer is capable of binding a separate $\alpha_v\beta_6$ heterodimer, this dose maintains similar concentrations of $\alpha_v\beta_6$ binding peptides. A dose of 15 μg produces equivalent concentrations of Cy5 and allows for more direct comparisons between the two multimers.

At a dose of 15 μg, the results of NIRF imaging of the H2009.1 dimers at 24 HPI are similar to the results of the tetramers. All peptides accumulate in the H2009 tumors, and capping the N-terminus decreases kidney accumulation at this timepoint. The AcH2009.1 and D-Leu H2009.1 peptides also showed decreased liver and lung accumulation compared to the parental peptide. However, both of these peptides present disadvantages as well. The AcH2009.1 dimer showed a significant increase in H460 accumulation while the D-Leu H2009.1 dimer gave decreased H2009 delivery compared to parental peptide. Overall, the D-Leu capped dimer produces excellent specificity for H2009 tumor over both the H460 tumor and normal lung, giving it the advantage over the AcH2009.1 dimer at this timepoint.

The examination of the 72 Hr data provides useful insight in this matter. By this time, the AcH2009.1 has cleared from most off-target organs while being retained in the H2009 tumor. On the other hand, the AcD-Leu H2009.1 dimer produces the lowest overall signal in every off-target organ except for the liver, but also clears from the H2009 tumors. Overall, at this timepoint the AcH2009.1 dimer produces the highest tissue specificity of any peptide examined in this dissertation. This is likely to translate into a wide therapeutic window, facilitating improved delivery of therapeutics with extended lifetimes.

At a dose of 30 μg at 24 HPI, none of the N-terminal modifications produced significant benefit to either targeting or tissue specificity (Figures 5.12-5.14). However, all of

the dimers outperformed the AcD-Leu H2009.1 tetramer, the best peptide previously observed at this timepoint (Figure 5.4). Previously, the tetrameric H2009.1 demonstrated superiority over the dimer when compared *in vitro* [219]. However, the dimer produces the same levels of signal in H2009 tumors, with lower accumulation in liver and kidney. This clearly shows that extensive *in vitro* optimization does not necessarily translate into the best peptides *in vivo*.

Indeed, the *in vitro* studies presented here do not allow for prediction of biodistribution of the various H2009.1 constructs. All of the peptides have similar affinity for $\alpha_v\beta_6$ and internalize into $\alpha_v\beta_6$ –expressing cells efficiently, and differences in serum stability alone do not explain the differences in observed *in vivo* behavior. This emphasizes the importance of empirical examination of peptide biodistribution *in vivo*. Capping the H2009.1 peptide with D-Leu appears to increase its affinity for other RGD-binding integrins while N-acetylation and the AcD-Leu cap decrease binding to other integrins. One would expect from these results that the AcH2009.1 and AcD-Leu H2009.1 peptides would show much higher tissue specificity than the D-Leu H2009.1 peptide. Yet this is not the case. The D-Leu capped peptide avoids accumulation in H460 tumors (which express $\alpha_v\beta_3$ in their vasculature) in both tetrameric and dimeric formats. Both the AcH2009.1 dimer and tetramer shows increased accumulation in H460 tumors at 24 HPI. This suggests that tissue specificity is not a function of receptor specificity. This is typical of the peptide targeting field and emphasizes the importance of empirical *in vivo* characterization of targeting ligands. One cannot currently predict the biodistribution of a given ligand based on in vitro data.

The imaging of H2009.1 dimers at the 15 μg dose was performed using J/Nu mice while the 30 μg imaging was done in NOD/SCID mice. The H2009 and H460 cells used to establish xenograft tumors are from the same stocks of cell lines, and thus should be consistent. However, differences were observed between the two strains of mice. Tumor take rates were significantly decreased in J/Nu mice, necessitating a 5-fold increase in the number of injected cells to reliably produce tumors. Additionally, as shown in Figures 5.6 and 5.9, levels of peptide accumulation in liver are consistently much higher in these mice. Levels of $\alpha_v\beta_6$ expression in the liver are relatively low. Therefore, this increase is likely due to differences in liver metabolism between these two strains. It is possible, for example, that the peptide-dye conjugate is degraded more slowly in the livers of J/Nu mice, resulting in an increase in signal. These results have important implications for the use of H2009.1 peptides in humans. The H2009.1 dimer would produce much higher tissue specificity in a patient with rapid liver metabolism. Therefore, a simple metabolic panel can then be performed to determine which patients are most likely to benefit from $\alpha_v\beta_6$ –targeting imaging and therapy.

Levels of $\alpha_v\beta_6$ in each tissue may also vary between mouse strains. Until recently, expression of $\beta_6$ in normal adult tissue had not been detected in either mice or humans. With the availability of new antibodies against $\beta_6$, low levels have been observed in healthy epithelia in humans. However, the $\beta_6$ expression profiles for either strain of mouse could not be found in the literature. I therefore analyzed expression levels of $\alpha_v\beta_6$ in mouse organs by Western blot. Tumor bearing mice from each strain bearing both H2009 and H460 tumors were sacrificed and perfused with sterile PBS. Tissue extracts were made and protein content was normalized by BCA assay.

While Western blot analysis is ubiquitous throughout biology and considered standard, examination of membrane protein expression in multiple organs can problematic. The polyclonal antibody used in this analysis was raised against a peptide from the intracellular C-terminus of human $\beta_6$ and is known to react against $\beta_6$ from mouse and several other species. This allows for the direct comparison between murine tissue and human xenograft H2009 and H460 tumors. However, this antibody does not differentiate between variable glycosylation patterns. The molecular weight of the $\beta_6$ polypeptide is 88 kD. As a membrane protein, $\beta_6$ is heavily glycosylated, and bands from tumor cell lysates consistently run at ~110 kD. A band is observed in the heart sample from J/Nu mice just under 100 kD, and could indicate the presence of $\beta_6$ in heart tissue. However, because accumulation of H2009.1 peptides is consistently low in the heart, I discounted this as a non-specific band produced by the polyclonal antibody.

Despite these obstacles, the Western blot analysis did provide useful information. No detectable levels of $\beta_6$ are present in kidney. Thus, the renal signal observed in NIRF imaging is not the result of specific interactions between the H2009.1 tetramers and their target integrin. Levels of $\beta_6$ in H460 tumors, spleen, and heart are also below the detection threshold. Expression of the integrin is observed in both lung and liver tissue. This expression is almost certainly the cause of H2009.1 peptide accumulation in the lungs, especially in the J/Nu mice. However, this is not likely to be the case in the liver. Examination of the NIRF imaging alone would suggest that J/Nu mice express higher levels of $\beta_6$ in liver tissue than NOD/SCID mice, as significantly higher liver accumulation was observed in this strain. In fact, NOD/SCID mice express nearly triple the levels of $\beta_6$ in liver.

This suggests that accumulation of H2009.1 peptides in the liver is not a function of $\beta_6$ levels, and supports the hypothesis that NIRF signal from the liver is dependent on the metabolic profile of the animals.

From these studies, the optimal peptide at 24 HPI is likely to be the AcD-Leu dimer. While this peptide does not accumulate in H2009 tumors as well as other peptides examined, it differentiates clearly between $\alpha_v\beta_6$ positive and negative tumors and demonstrates the lowest retention in off-target organs. For long-term targeting of therapeutics, the AcH2009.1 dimer high and persistent accumulation in H2009 tumors with low accumulation in normal tissue. Both of these peptides warrant further investigation as clinical targeting peptides.

# CHAPTER SIX
# CONCLUSIONS AND FUTURE DIRECTIONS

Lung cancer is a persistent global health problem, and new tools and strategies are required to improve diagnosis and treatment of this disease. In recent decades, the move to classify tumors and target tumors according to their molecular biomarkers has led to the development of a variety of new chemotherapeutics, but this technology has not yet reached its full potential. The identification of molecular biomarkers also allows for improved use of general chemotherapeutics by allowing targeted delivery of these compounds specifically to malignant cells. Potent cytotoxins can be conjugated to targeting agents that bind specifically to tumor-restricted biomarkers, resulting in accumulation of the targeted drug in tumor tissue and decreased toxicity to healthy cells. The targeting of imaging agents can also improve diagnosis and characterization by improving contrast between malignant and normal tissue. Targeted imaging can also be used to profile the expression of known molecular biomarkers in a given tumor, providing guidance towards effective courses of treatment.

While monoclonal antibodies have seen the most success as targeting agents, peptides are uniquely suited for delivery to tumor cells. Peptides are small enough to distribute throughout tumor tissue despite high interstitial pressure, can be made synthetically in high yield and purity, are compatible with a wide variety of conjugation chemistries for loading cargo, and are capable of binding their target receptors with high affinity. Peptides can also be developed without prior knowledge of specific target receptors using phage display biopanning.

The Brown lab has identified a suite of 13 peptides capable of binding and internalizing into NSCLC cells while avoiding normal human lung cells. The H2009.1 peptide, selected on H2009 adenocarcinoma cells, was found to bind to the integrin $\alpha_v\beta_6$. Our subsequent work has established that $\alpha_v\beta_6$ is over-expressed in roughly half of NSCLCs and correlates with poor prognosis, indicating its potential as a molecular marker for the characterization and treatment of these tumors. While $\alpha_v\beta_6$ is expressed at low levels in normal human epithelia, many groups have confirmed over-expression of the integrin in many epithelial derived tumors including head and neck, breast, prostate, pancreatic, and colorectal cancers. Little is known about the role of $\alpha_v\beta_6$ in these cancers, and the development of the H2009.1 as an $\alpha_v\beta_6$ –specific ligand may facilitate research into its oncological functions in addition to the clinical applications of the peptide.

Extensive *in vitro* optimization of the H2009.1 peptide was performed before I joined the project. The peptide was conjugated to a multimeric scaffold to better mimic its presentation to $\alpha_v\beta_6$ in the context of phage display and increase affinity. The peptide sequence was also reduced to its 10 N-terminal residues, further improving affinity while reducing molecular weight and manufacturing costs. These studies produced the tetrameric H2009.1 peptide with a binding sequence of RGDLATLRQL. This peptide was used to target several chemotherapeutic drugs, either by direct conjugation or by modification of drug loaded nanoparticles. Addition of the H2009.1 tetramer consistently expanded the therapeutic window of these compound *in vitro*. However, the peptide-targeted drug performed similarly to free drug when used to treat xenograft tumors in animals, regardless

of context. I hypothesized that this was a result of rapid degradation of the peptide ligand by serum peptidases.

A dimeric H2009.1 peptide had also been utilized to target PET imaging agents to $\alpha_v\beta_6$-positive tumors in animals. These studies indicated that the peptide has significant potential as a clinical imaging agent, but additional in vivo optimization was required. As is common with peptide targeting agents, significant accumulation and retention in the kidneys was observed. Many therapeutics used to treat NSCLC produce nephrotoxicity in their free, un-targeted state. Therefore, increased renal concentrations produced by conjugation to a peptide targeting ligand should be minimized.

Using the results of the PET imaging experiments as a guide, a library of modified H2009.1 tetrameric peptides was synthesized and characterized for their ability to specifically deliver cargo to $\alpha_v\beta_6$ –expressing cells both *in vitro* and *in vivo*. Evaluation of in vitro serum stability and internalization in H2009 cells narrowed the field of potential H2009.1 analogs down to N-acetylated and D-amino acid capped tetramers dubbed AcH2009.1, D-Leu H2009.1, D-Val H2009.1, and AcD-Leu H2009.1. The *in vivo* behavior of these peptides was then assessed using NIRF imaging to obtain biodistribution data at 24, 48, and 72 hours after systemic administration of Cy5 labeled tetramer. These studies indicated that N-terminal capping does extend tumor targeting and decrease accumulation and retention in the kidneys. However, the reduction in renal accumulation was not as significant as was hoped, and the capped H2009.1 tetramers also accumulated to a high degree in the liver.

Because significant liver accumulation was not observed in PET imaging experiments, I chose to reduce the valency of the H2009.1 tetramer back to the dimer. The *in vitro* functionality of the capped H2009.1 dimers were verified before these peptides were assessed by NIRF imaging. The H2009.1 dimers delivered their fluorescent cargo to tumors as well as their tetrameric counterparts and differentiated between $\alpha_v\beta_6$ - positive and negative tumors effectively. Interpretation of the dimer imaging data is complicated by differences in the strains of mouse utilized in these experiments. However, these differences also provide valuable insight into the clinical use of these peptides. The biodistribution of these peptides, particularly their accumulation in liver, is likely to depend heavily on the metabolic profile of the patient.

In the *in vivo* studies presented here, the dimeric H2009.1 peptides outperformed the tetrameric analogs, and for most clinical applications, these would be the targeting ligands of choice. Dimeric peptides do not appear to demonstrate any disadvantages in delivery of cargo to tumors and are smaller and would diffuse against the high interstitial pressure of tumor tissue more efficiently. Additionally, the dimeric peptides are less expensive to manufacture. There may, however, be instances in which the tetrameric peptide would be preferable to the dimeric peptide. For example, one application of the H2009.1 peptide might be the delivery of cargo with an extremely long circulation time, such as heparin-coated or PEGylated nanoparticles, which may remain in the bloodstream for several days. In this case, the tetramer may prove useful simply because more advanced degradation is required to destroy the targeting capabilities of the higher valency ligand. However, conjugation of the capped

H2009.1 peptides to a nanoparticle would drastically affect the biodistribution of these agents as most nanoparticles do not filter in the kidneys and are cleared through the liver and spleen.

I conclude from these experiments that, in most cases, the optimal peptide for long-term targeting of therapeutics to $\alpha_v\beta_6$ –positive NSCLCs is the AcH2009.1 dimer as it gives the highest accumulation and retention in target tumors while avoiding kidney and lung tissue. The best peptide of this set for imaging applications is the AcD-Leu H2009.1 dimer, which differentiates well between $\alpha_v\beta_6$–positive and negative tumors and clears rapidly from the animal. This rapid clearance also indicates that the AcD-Leu H2009.1 dimer would be the optimal peptide for targeting of short-lived therapies such as radiotherapeutics. However, additional optimization is required to decrease liver accumulation of the peptide.

The next step in the optimization of the H2009.1 peptide as a clinical targeting agent is to move the peptides with the highest potential into more quantitative biodistribution studies using radiolabeled peptide. For evaluation of the AcH2009.1 dimer as a long-term targeting agent, I would recommend labeling the peptide directly with radioactive isotopes of iodine rather than conjugating to a chelator. The Tyr residue C-terminal to the $PEG_{(11)}$ allows for direct labeling of the peptide without interfering with peptide binding. The γ-emitter $^{125}I$ has a half-life 59 days and could be used for extended studies of H2009.1 dimer levels. Because γ counters have a wide linear range, quantitative biodistribution could be obtained for peptides dosed at multiple concentrations, depending on the half-life of the peptide's intended cargo. Further characterization of the AcD-Leu H2009.1 dimer as an imaging agent can easily be achieved through our lab's collaboration with Xiankai Sun's group at UT

Southwestern. The lab has extensive experience with both PET and SPECT imaging, and the protocols for those imaging experiments are already in place.

Alternatively, additional modifications to the H2009.1 peptide could be made to further improve biodistribution. For example, the RQL sequence at the C-terminus of the peptide is not directly involved in binding. Elimination of these residues would remove an additional positive charge from each branch of the H2009.1 dimer and reduce manufacturing costs. Deletion of these amino acids resulted in a slight decrease in binding affinity, likely to do decreased spacing between the peptide and the multimeric core. I substituted three Gly residues for the RQL sequence and observed a complete loss of internalization into H2009 cells (data not shown). It is possible that the GGG sequence disrupts the α-helical structure of the adjacent LATL residues. Perhaps a substitution of AAA would stabilize this α-helix, restore binding, and positively impact biodistribution of the H2009.1 dimer.

To improve long-term targeting, the AcH2009.1 dimer could be modified to include serum albumin binding sequences. These short peptide sequences could be added at the C-terminus of the lysine core of the peptide construct, and significantly increase *in vivo* serum stability of peptides by associating with serum albumin. Because the albumin binding sequences are short, the addition would not likely be sufficient to prevent penetration of the peptide through tumor tissue. However, albumin-bound peptides would likely be filtered in the kidneys at a much lower rate, increasing the overall circulation time of peptide-targeted agents.

Additional modifications to the N-terminus could also be made. Replacement of the present N-terminal caps with a short PEG polymer may also prevent degradation in serum

without interfering with the delivery functions of the peptide. PEGylation would reduce overall hydrophobicity, potentially decreasing liver accumulation. However, there is little data in the literature on the effects of these types of modifications and PEG polymers of specific length are much more expensive than amino acids.

One major lesson of this dissertation is that the choice of model is critical for biodistribution studies. Data from our lab and others indicates that levels of $\alpha_v\beta_6$ are low in human lung epithelial cells. However, the lungs of both strains of mice used in these studies express much higher levels of $\alpha_v\beta_6$ than those observed in humans. One study in C57B/6 mice indicated minimal expression of the integrin in these mice. It is possible that expression of $\alpha_v\beta_6$ is increased only in immune-deficient mice. Several NSCLC lines originating in mouse have been established. However, the $\alpha_v\beta_6$ expression status of these cell lines is unknown. If an $\alpha_v\beta_6$ –positive mouse NSCLC cell line could be obtained, more clinically relevant biodistribution data could be obtained.

These studies also emphasize the importance of crosstalk between *in vitro* and *in vivo* experiments during development of peptide ligands. Our lab has many other tumor targeting peptides at earlier stages of development. The experiences of this project suggest that in vivo characterization of these peptides should be included as early as possible in the optimization process. As discovered with the tetrameric H2009.1 peptide, the optimal peptide in vitro does not necessarily translate into a better targeting ligand in vivo. Even experiments aimed at finding the minimum binding sequence of a peptide can have major impact on the biodistribution of a peptide as hydrophobicity, stability, and size all depend heavily on the sequence and length of a peptide targeting ligand. The removal of charged residues may

reduce kidney accumulation, the most common obstacle preventing peptides from clinical use. N-terminal capping may not benefit all peptides. If the terminus of a peptide participates in receptor binding, modification would likely decrease or completely abolish delivery to tumor cells. However, other modifications, such as the addition of albumin binding sequences may prove beneficial in these instances.

The H2009.1 peptide is a promising targeting ligand for the characterization and treatment of NSCLC. The goal of this project was to move the H2009.1 peptide closer to clinical use by improving its in vivo targeting capabilities. N-terminal capping and reduction of the peptide valency to a dimeric peptide ligand extended targeting to $\alpha_v\beta_6$ expressing tumors while decreasing accumulation and retention in off-target organs. These modifications also introduced a branch point from which the peptide can be optimized for both long-term and short-term applications. While further work is necessary to bring the H2009.1 peptide into clinical use, the results and experiences of this thesis project have provided critical insights into the *in vivo* optimization of this and many other peptide targeting ligands.

# APPENDIX A
# ANALYTICAL HPLC OF SYNTHESIZED PEPTIDES

| Targeting Sequence | Valency and Label | % Purity | Chromatogram |
|---|---|---|---|
| Biotin Dimer Core | | | |
| Biotin Tetramer Core | | | |
| Cysteine Dimer Core | | | |
| Cysteine Tetramer Core | | | |
| H2009.1 | Monomer | | |
| | Dimer | | Figure 1 |
| | Biotinylated Dimer | | Figure 2 |
| | AF488 Dimer | | Figure 3 |
| | Cy5 Dimer | | Figure 4 |
| | Tetramer | | Figure 5 |
| | Biotinylated Tetramer | | |
| | AF488 Tetramer | | |
| | Cy5 Tetramer | | |
| Scrambled H2009.1 | Monomer | | |
| | Dimer | | |
| | Biotinylated Dimer | | |
| | Tetramer | | |
| | Biotinylated Tetramer | | |
| AcH2009.1 | Monomer | | |
| | Dimer | | Figure 6 |
| | Biotinylated Dimer | | Figure 7 |
| | AF488 Dimer | | Figure 8 |
| | Cy5 Dimer | | Figure 9 |
| | Tetramer | | Figure 10 |
| | Biotinylated Tetramer | | |
| | AF488 Tetramer | | |
| | Cy5 Tetramer | | |
| L-Leu H2009.1 | Monomer | | |
| | Tetramer | | |
| | AF488 Tetramer | | |
| D-Leu H2009.1 | Monomer | | |
| | Dimer | | Figure 11 |
| | Biotinylated Dimer | | Figure 12 |
| | AF488 Dimer | | Figure 13 |
| | Cy5 Dimer | | Figure 14 |
| | Tetramer | | Figure 15 |
| | Biotinylated Tetramer | | |

| | | | |
|---|---|---|---|
| | AF488 Tetramer | | |
| | Cy5 Tetramer | | |
| N-Leu H2009.1 | Monomer | | |
| | Tetramer | | |
| | AF488 Tetramer | | |
| L-Val H2009.1 | Monomer | | |
| | Tetramer | | |
| | AF488 Tetramer | | |
| D-Val H2009.1 | Monomer | | |
| | Tetramer | | |
| | Biotinylated Tetramer | | |
| | AF488 Tetramer | | |
| | Cy5 Tetramer | | |
| N-Val H2009.1 | Monomer | | |
| | Tetramer | | |
| | AF488 Tetramer | | |
| AcD-Leu H2009.1 | Monomer | | |
| | Dimer | | |
| | Biotinylated Dimer | | Figure 16 |
| | AF488 Dimer | | Figure 17 |
| | Cy5 Dimer | | Figure 18 |
| | Tetramer | | Figure 19 |
| | Biotinylated Tetramer | | |
| | AF488 Tetramer | | |
| | Cy5 Tetramer | | |
| H2009.1 GGG | Monomer | | |
| | Biotinylated Dimer | | |
| HCC15.1 | Monomer | | |
| | AF488 Tetramer | | |
| ScrHCC15.1 | Monomer | | |
| | Biotinylated Tetramer | | |
| HCC15.2 | Monomer | | |
| | Biotinylated Tetramer | | |
| ScrHCC15.2 | Monomer | | |
| | Biotinylated Tetramer | | |
| H1299.2 | AF488 Tetramer | | |
| ScrH1299.2 | Monomer | | |
| | Biotinylated Tetramer | | |
| ScrH460.1 | Monomer | | |
| | Biotinylated Tetramer | | |

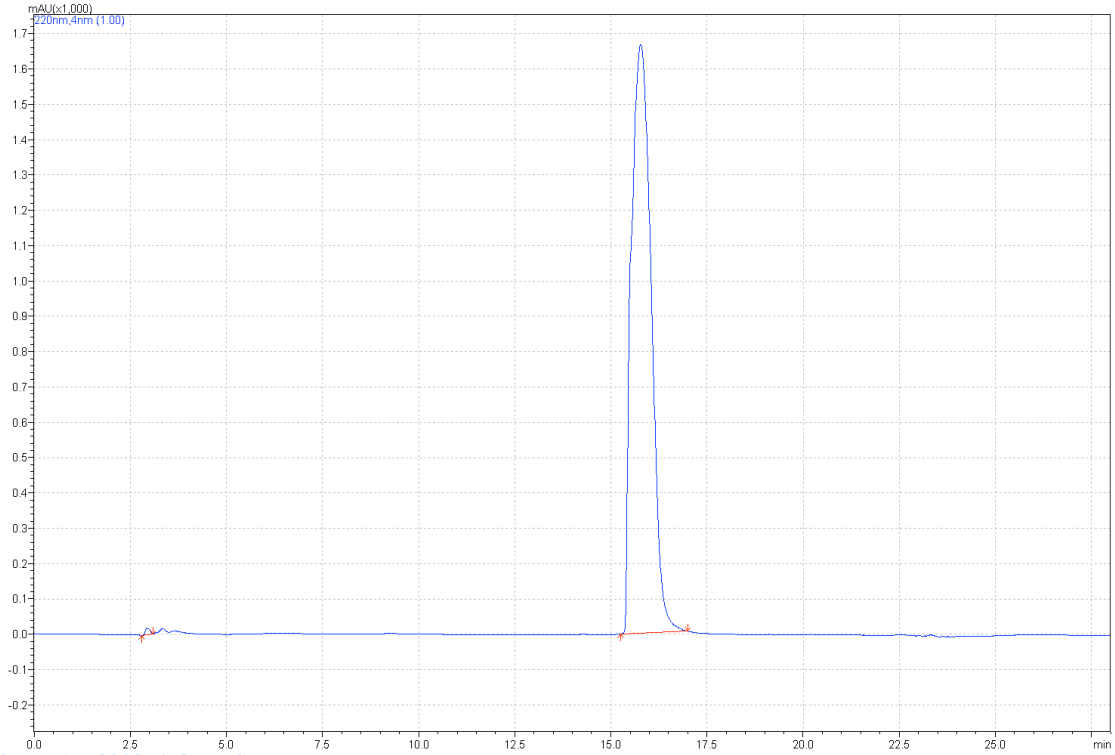


**Figure 1 H2009. 1 Cys Dimer**

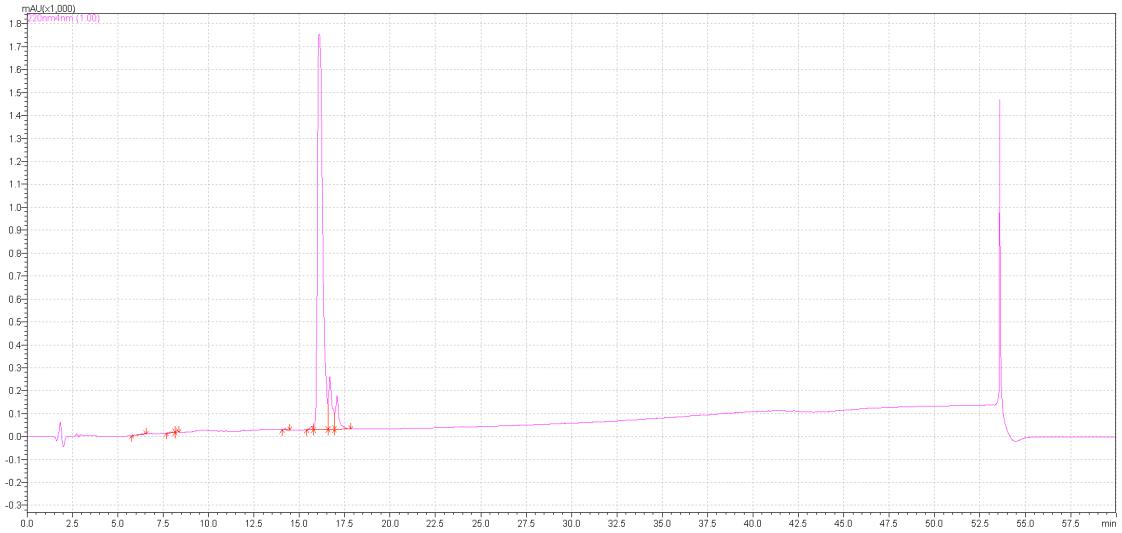


**Figure 2 H2009.1 Biotinylated Dimer**

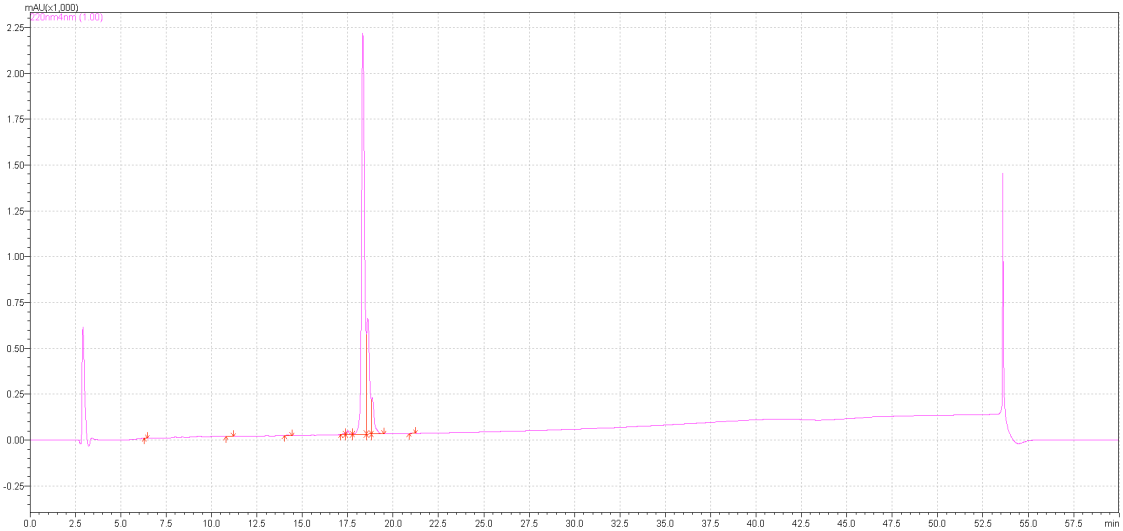


Figure 3 H2009.1 Dimer + AF488


Figure 4 H2009.1 Dimer + Cy5

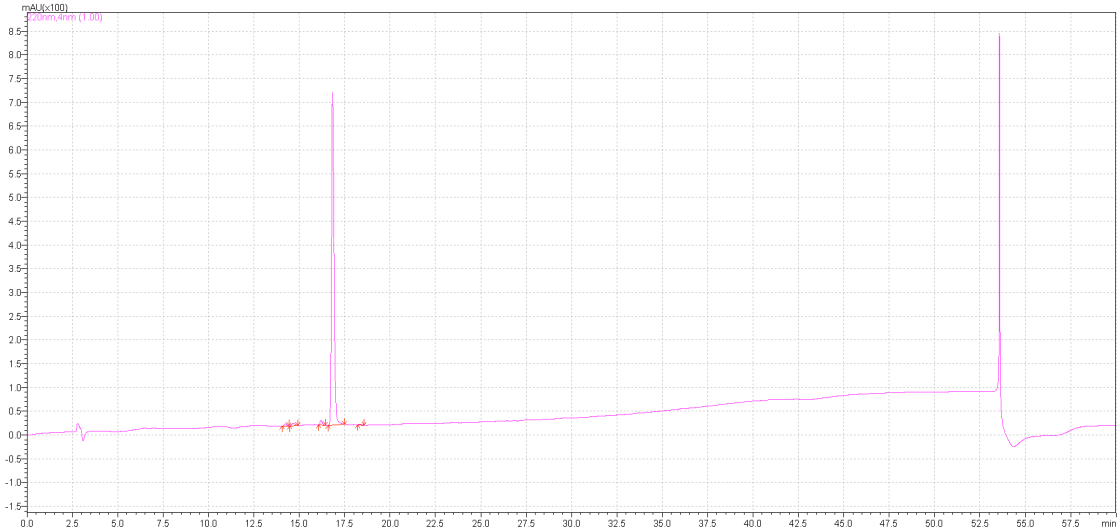


**Figure 5 H2009.1 Cys Tetramer**

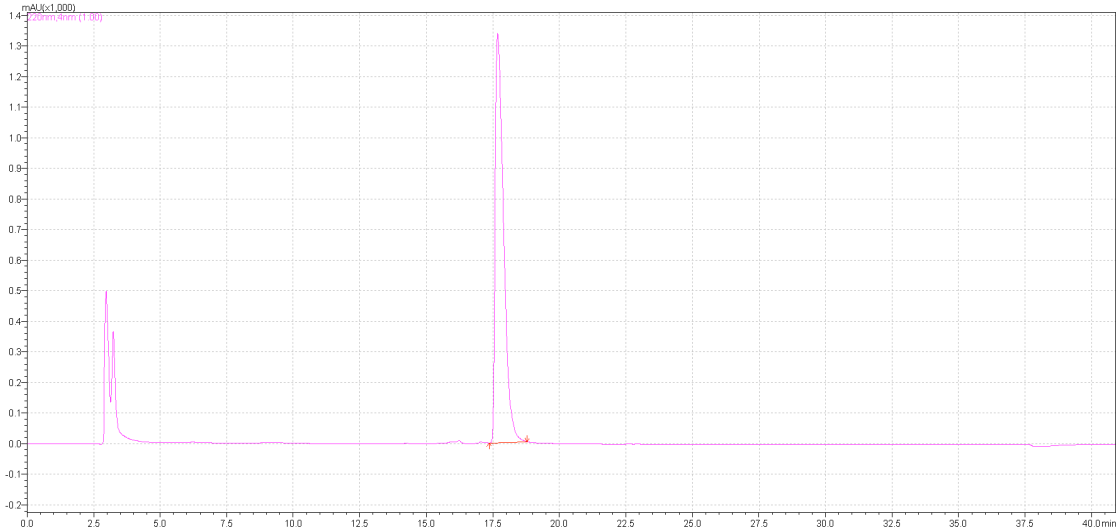


**Figure 6 AcH2009.1 Cysteine Dimer**

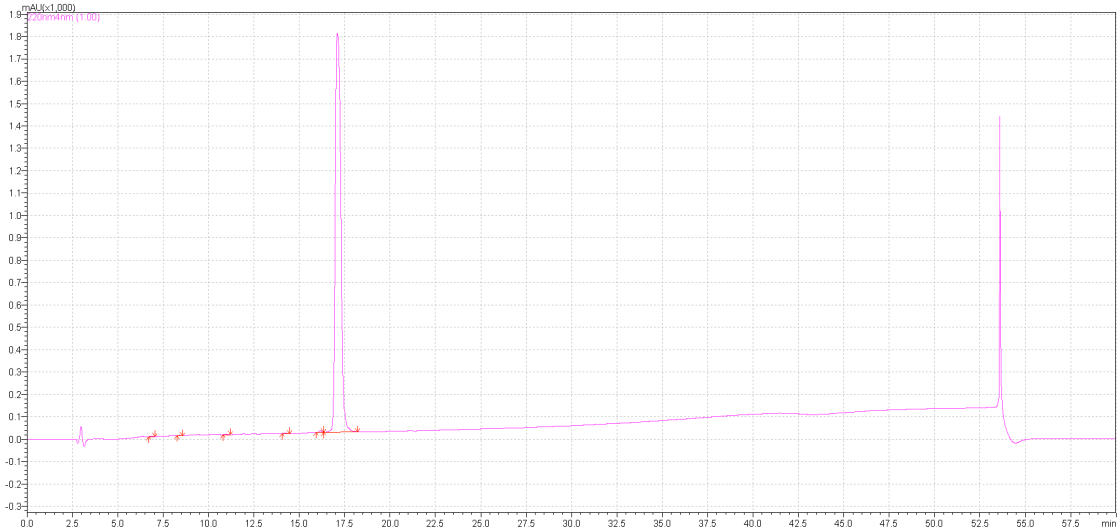


**Figure 7 AcH2009.1 Biotinylated Dimer**

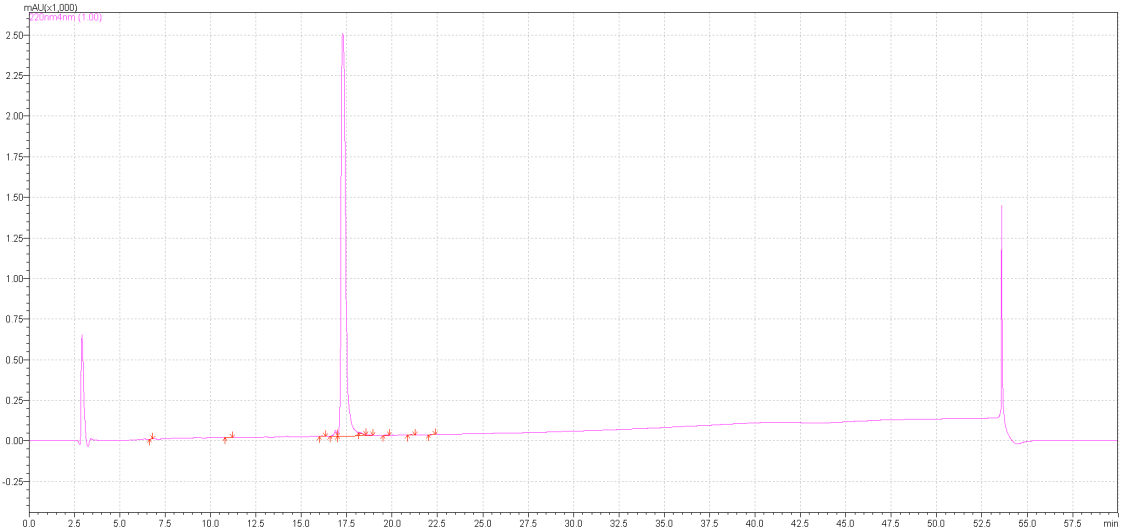


**Figure 8 AcH2009.1 Dimer + AF488**

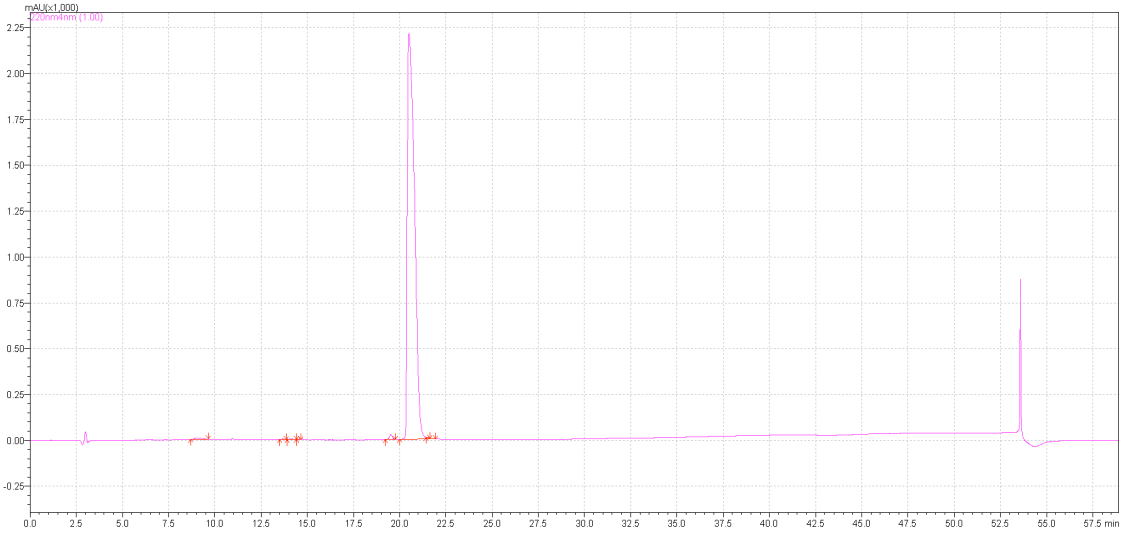


**Figure 9 AcH2009.1 Dimer + Cy5**

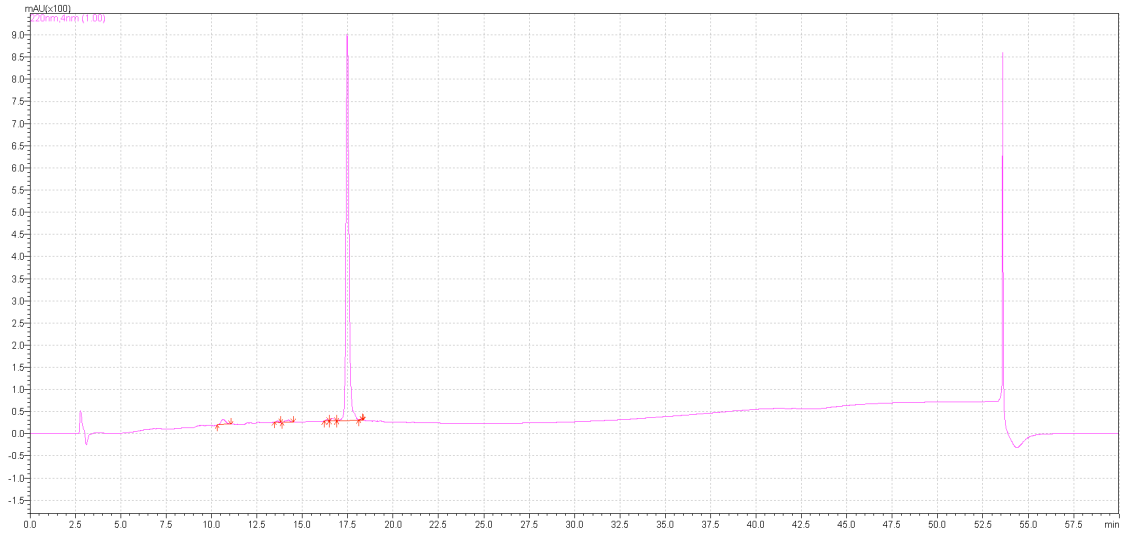


**Figure 10 AcH2009.1 Cysteine Tetramer**

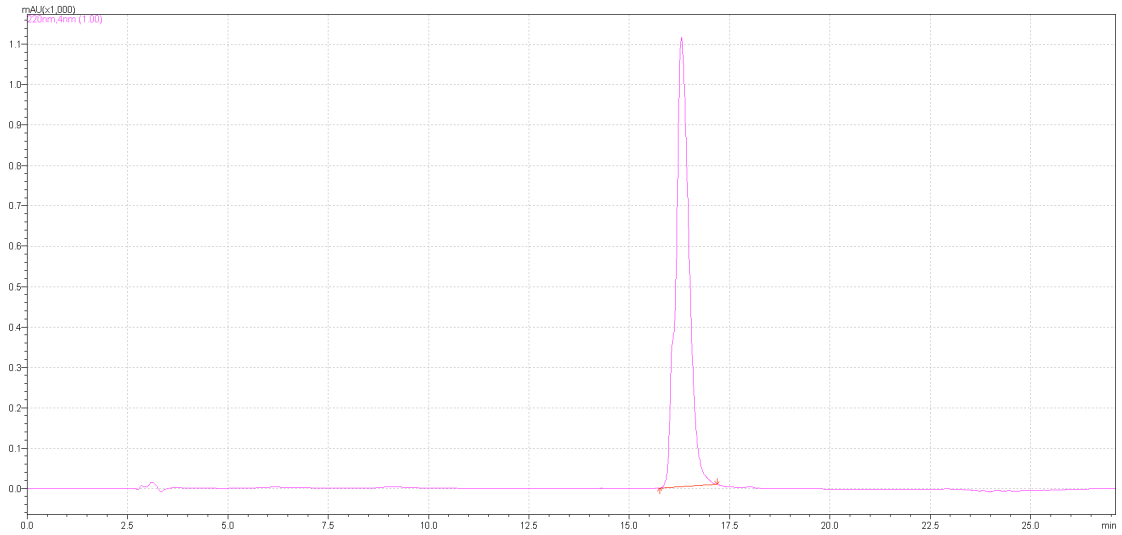


**Figure 11 D-Leu H2009.1 Cysteine Dimer**

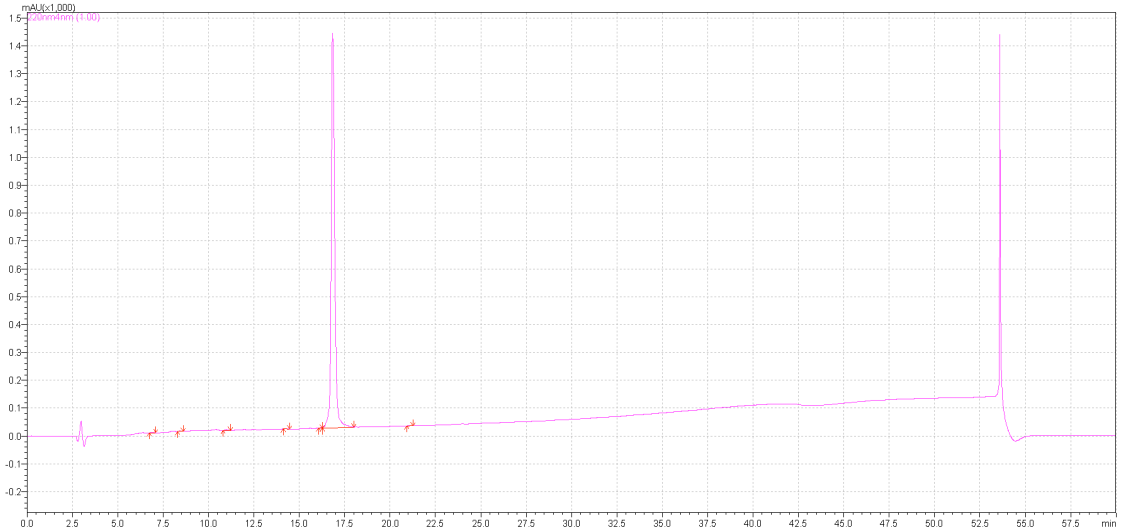


**Figure 12 D-Leu H2009.1 Biotinylated Dimer**

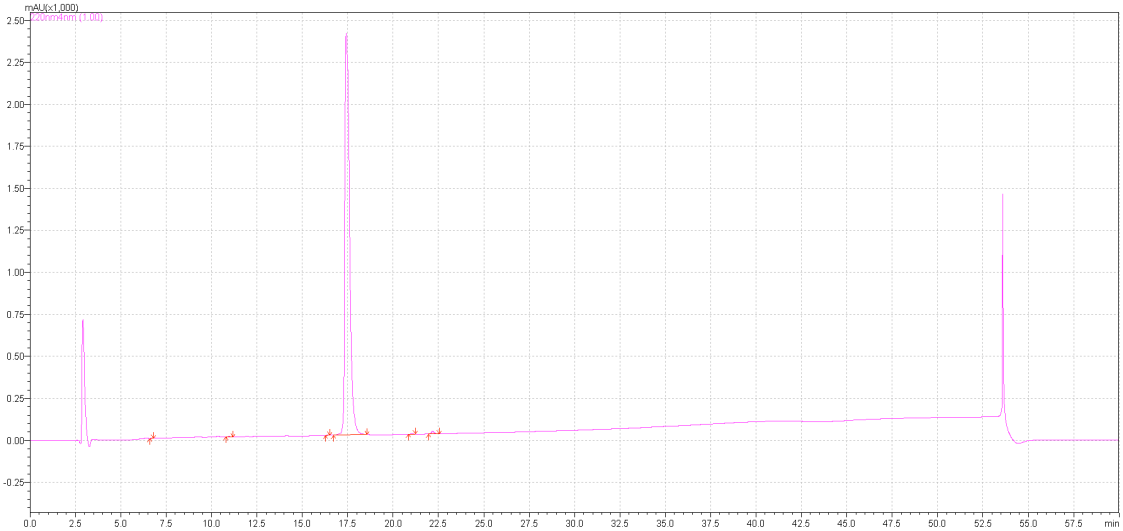


**Figure 13 D-Leu H2009.1 Dimer + AF488**

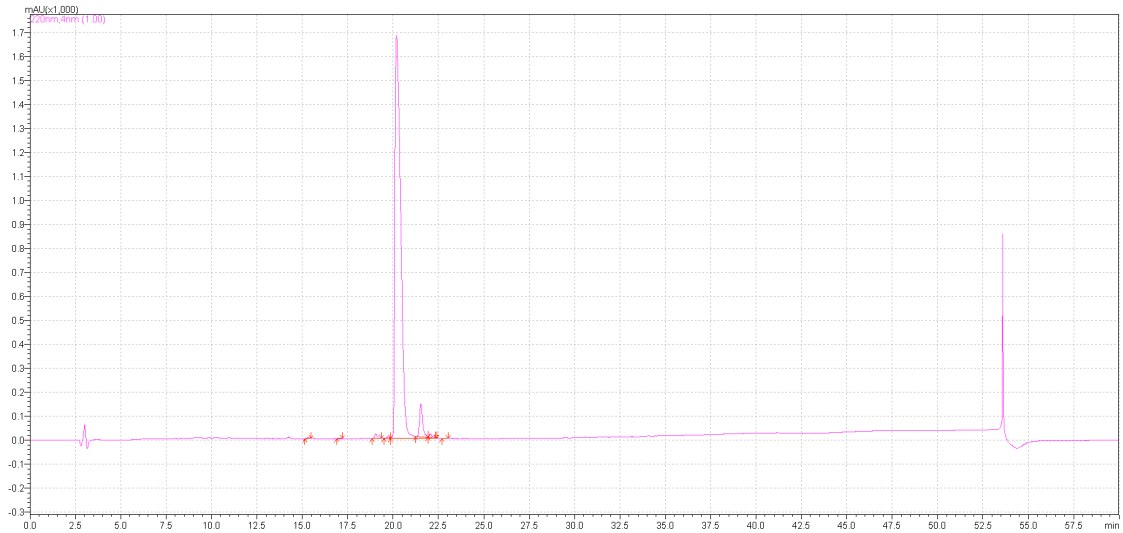


**Figure 14 D-Leu H2009.1 Dimer + Cy5**

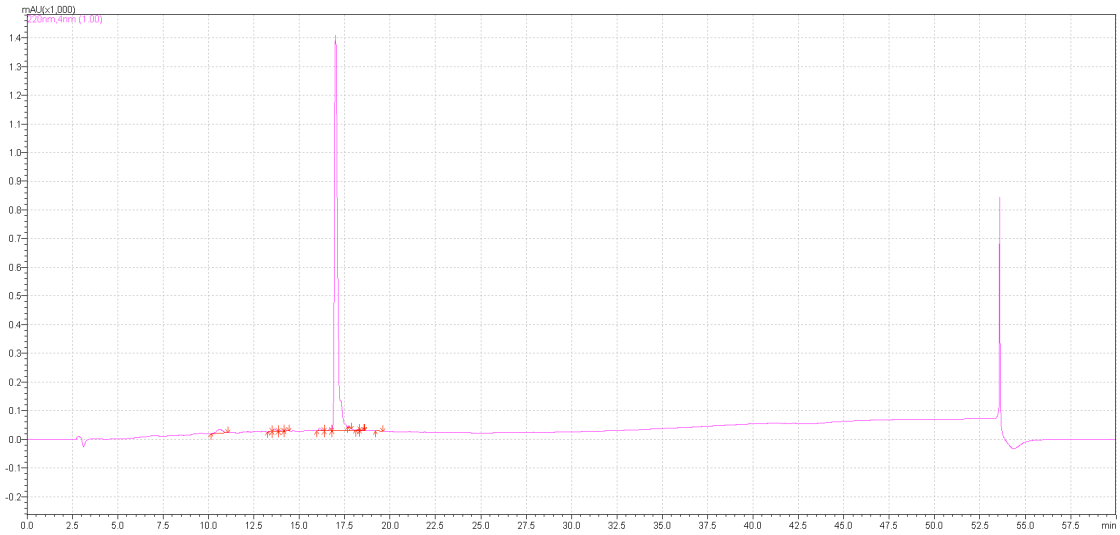


Figure 15 D-Leu H2009.1 Cysteine Tetramer

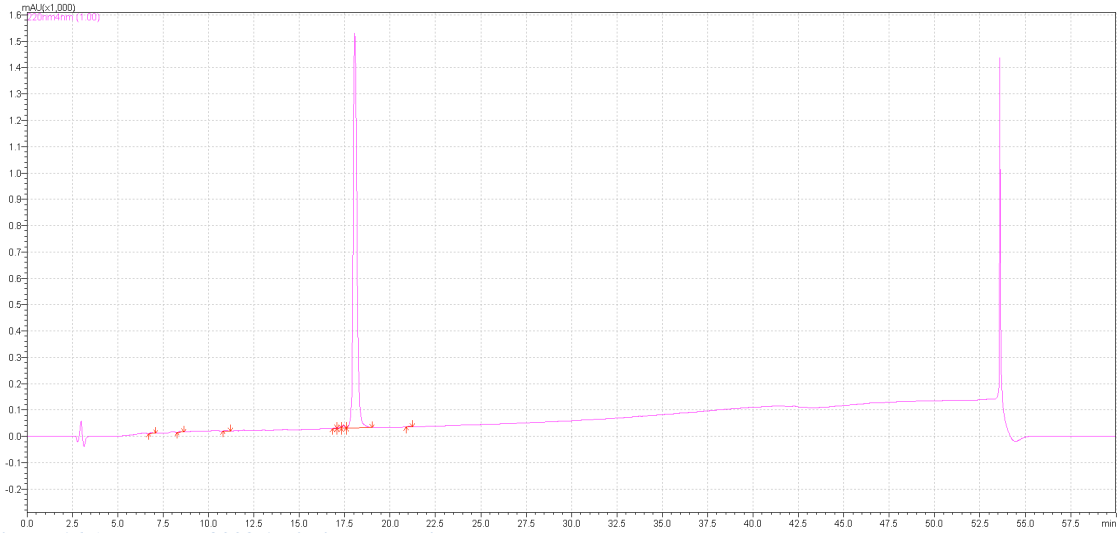


Figure 16 AcD-Leu H2009.1 Biotinylated Dimer

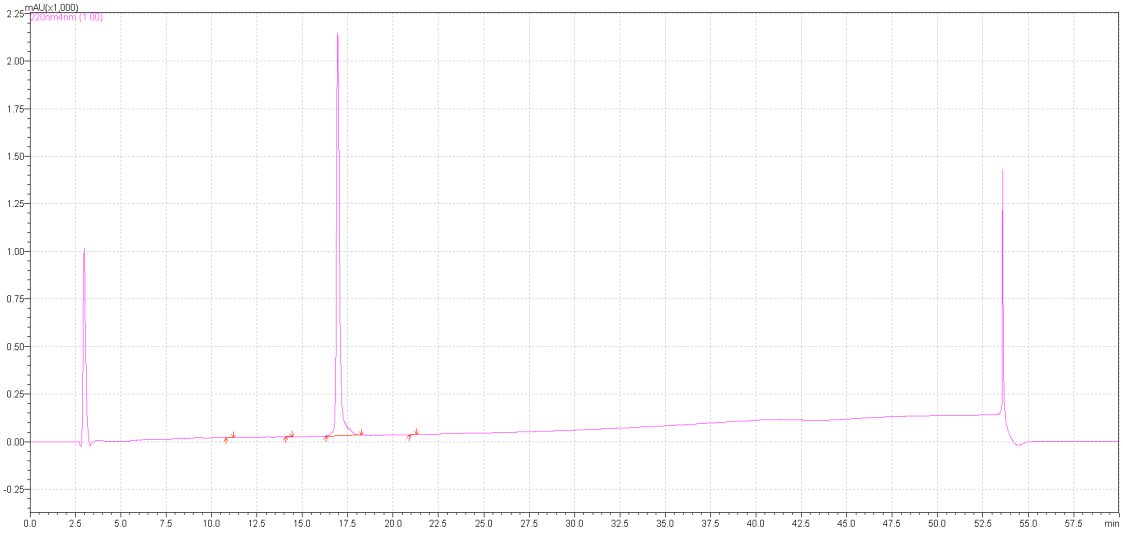


**Figure 17 AcD-Leu H2009.1 Dimer + AF488**

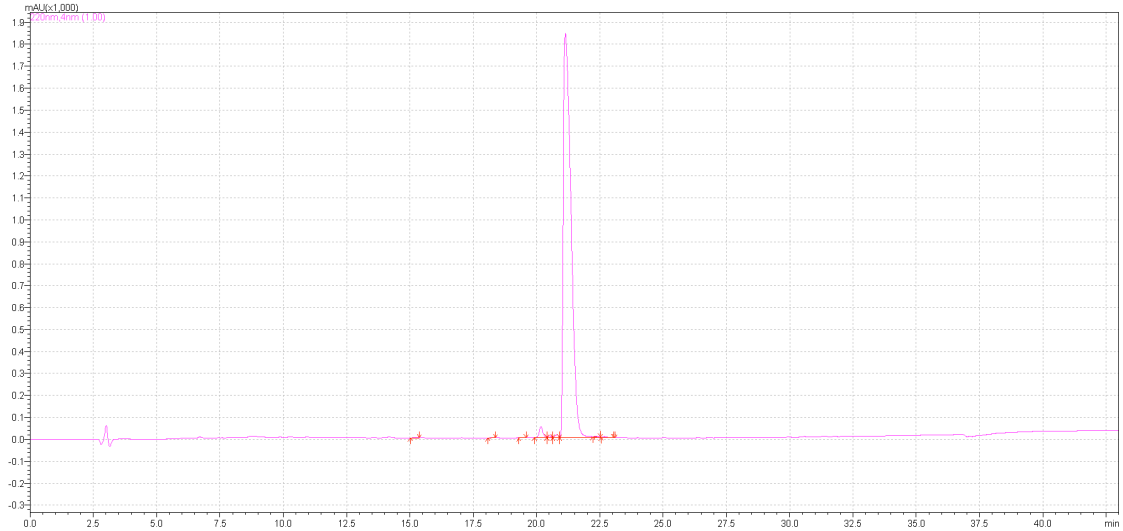


**Figure 18 AcD-Leu H2009.1 Dimer + Cy5**

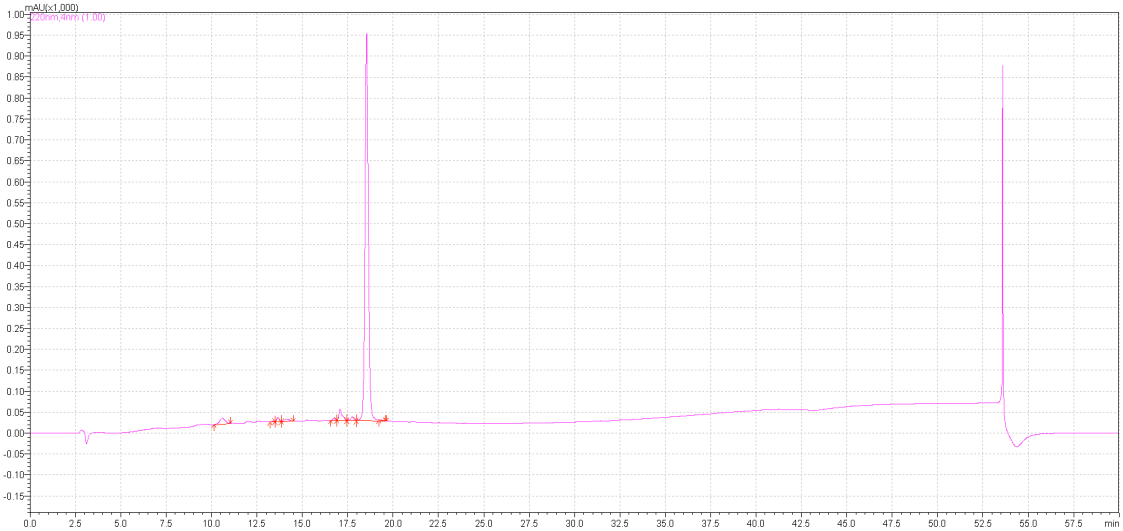


**Figure 19 AcD-Leu H2009.1 Cysteine Tetramer**

# APPENDIX B
# MALDI ANALYSIS OF SYNTHESIZED PEPTIDES

| Targeting Sequence | Valency and Label | Expected MW | MALDI |
|---|---|---|---|
| Biotin Dimer Core | | 1075 | |
| Biotin Tetramer Core | | 1634 | |
| Cysteine Dimer Core | | 693 | |
| Cysteine Tetramer Core | | 1252 | |
| H2009.1 | Monomer | 2006 | |
| | Dimer | 4705 | |
| | Biotinylated Dimer | 5087 | |
| | AF488 Dimer | 5347 | |
| | Cy5 Dimer | 5239 | |
| | Tetramer | 9276 | |
| | Biotinylated Tetramer | 9658 | |
| | AF488 Tetramer | 9918 | |
| | Cy5 Tetramer | 9810 | |
| Scrambled H2009.1 | Monomer | 2006 | |
| | Dimer | 4705 | |
| | Biotinylated Dimer | 5087 | |
| | Tetramer | 9276 | |
| | Biotinylated Tetramer | 9658 | |
| AcH2009.1 | Monomer | 2050 | |
| | Dimer | 4793 | |
| | Biotinylated Dimer | 5175 | |
| | AF488 Dimer | 5435 | |
| | Cy5 Dimer | 5327 | |
| | Tetramer | 9452 | |
| | Biotinylated Tetramer | 9834 | |
| | AF488 Tetramer | 10094 | |
| | Cy5 Tetramer | 9986 | |
| L-Leu H2009.1 | Monomer | 2121 | |
| | Tetramer | 9736 | |
| | AF488 Tetramer | 10378 | |
| D-Leu H2009.1 | Monomer | 2121 | |
| | Dimer | 4935 | |
| | Biotinylated Dimer | 5317 | |
| | AF488 Dimer | 5577 | |
| | Cy5 Dimer | 5469 | |
| | Tetramer | 9736 | |

| | | | |
|---|---|---|---|
| | Biotinylated Tetramer | 10118 | |
| | AF488 Tetramer | 10378 | |
| | Cy5 Tetramer | 10270 | |
| N-Leu H2009.1 | Monomer | 2121 | |
| | Tetramer | 9736 | |
| | AF488 Tetramer | 10378 | |
| L-Val H2009.1 | Monomer | 2106 | |
| | Tetramer | 9676 | |
| | AF488 Tetramer | 10318 | |
| D-Val H2009.1 | Monomer | 2106 | |
| | Tetramer | 9676 | |
| | Biotinylated Tetramer | 10058 | |
| | AF488 Tetramer | 10318 | |
| | Cy5 Tetramer | 10210 | |
| N-Val H2009.1 | Monomer | 2106 | |
| | Tetramer | 9676 | |
| | AF488 Tetramer | 10318 | |
| AcD-Leu H2009.1 | Monomer | 2164 | |
| | Dimer | 5021 | |
| | Biotinylated Dimer | 5402 | |
| | AF488 Dimer | 5663 | |
| | Cy5 Dimer | 5555 | |
| | Tetramer | 9908 | |
| | Biotinylated Tetramer | 10290 | |
| | AF488 Tetramer | 10550 | |
| | Cy5 Tetramer | 10442 | |
| H2009.1 GGG | Monomer | 1780 | |
| | Biotinylated Dimer | 4634 | |
| HCC15.1 | Monomer | 2991 | |
| | AF488 Tetramer | 13858 | |
| ScrHCC15.1 | Monomer | 2991 | |
| | Biotinylated Tetramer | 13598 | |
| HCC15.2 | Monomer | 2065 | |
| | Biotinylated Tetramer | 9894 | |
| ScrHCC15.2 | Monomer | 2065 | |
| | Biotinylated Tetramer | 9894 | |
| H1299.2 | AF488 Tetramer | 10154 | |
| ScrH1299.2 | Monomer | 2206 | |
| | Biotinylated Tetramer | 10458 | |
| ScrH460.1 | Monomer | 3003 | |
| | Biotinylated Tetramer | 13646 | |

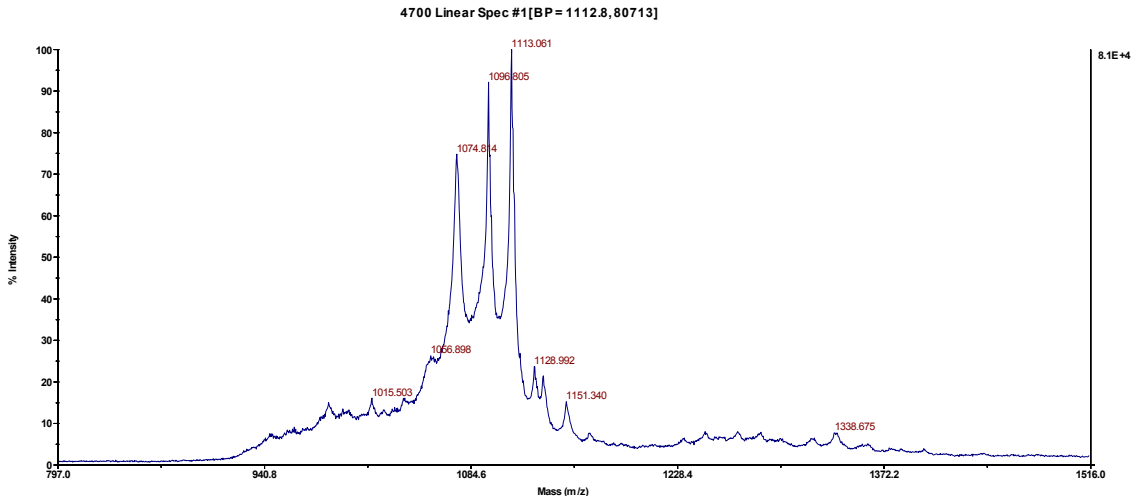


**Figure 20 Biotinylated Dimer Core**

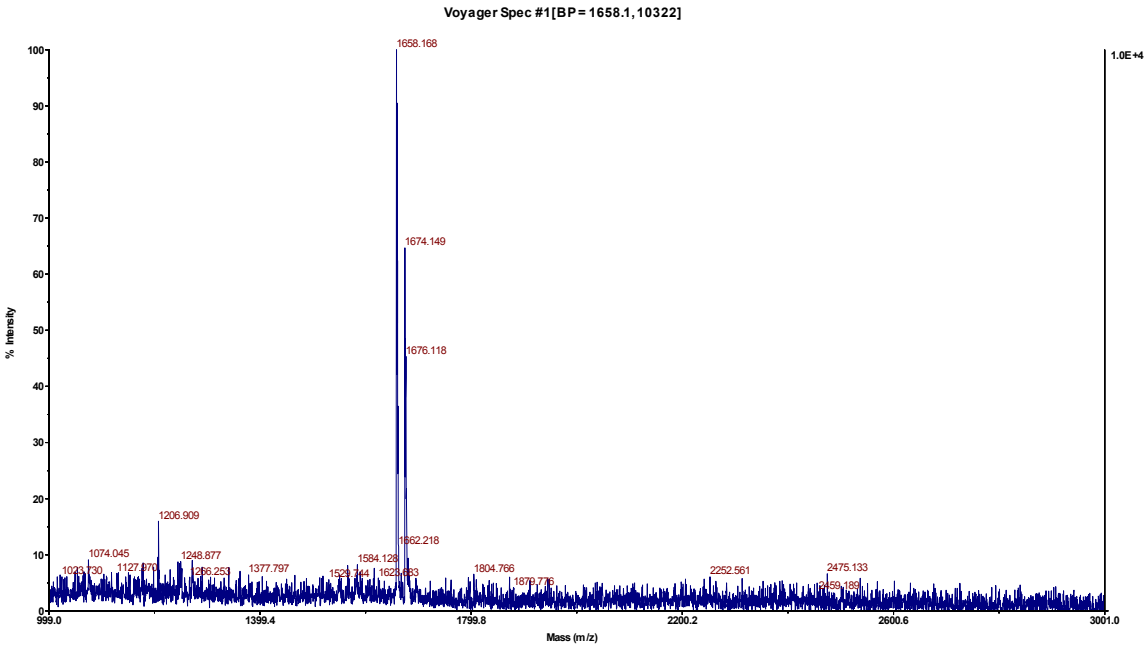


**Figure 21 Biotinylated Tetramer Core**

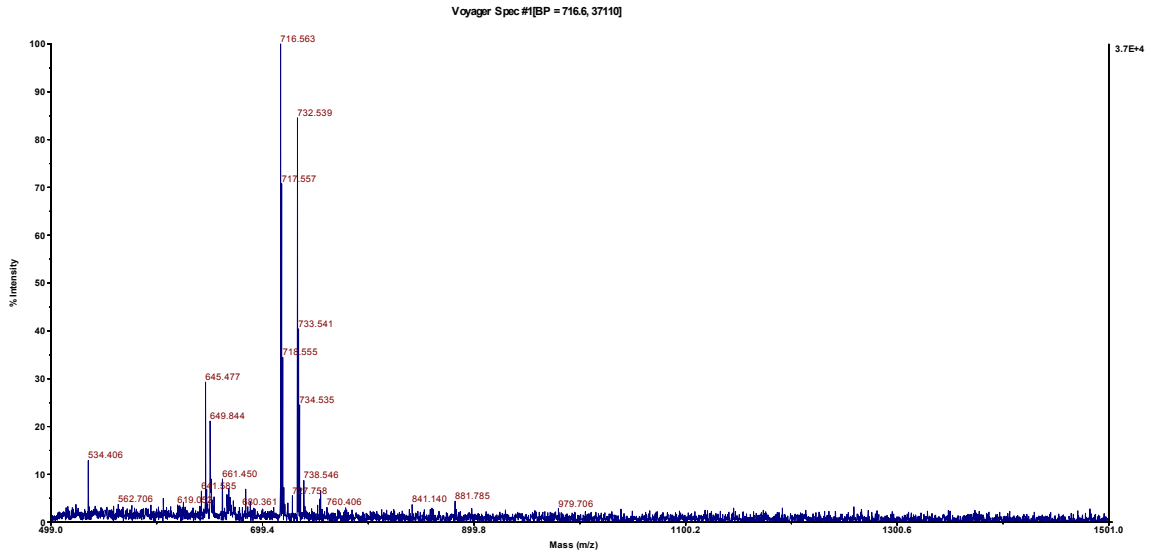


Figure 22 Cysteine Dimer Core

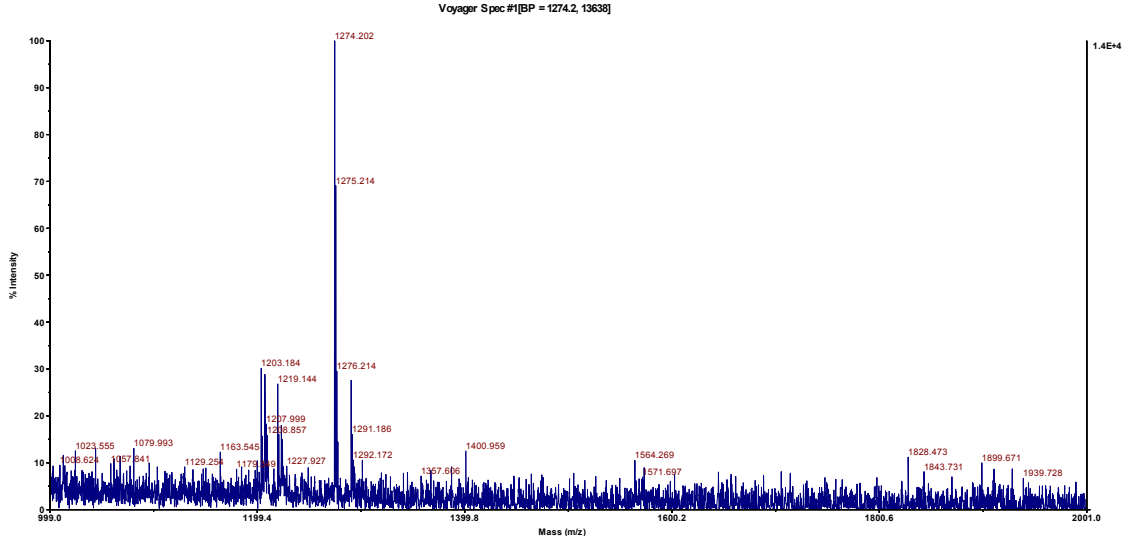


Figure 23 Cysteine Tetramer Core

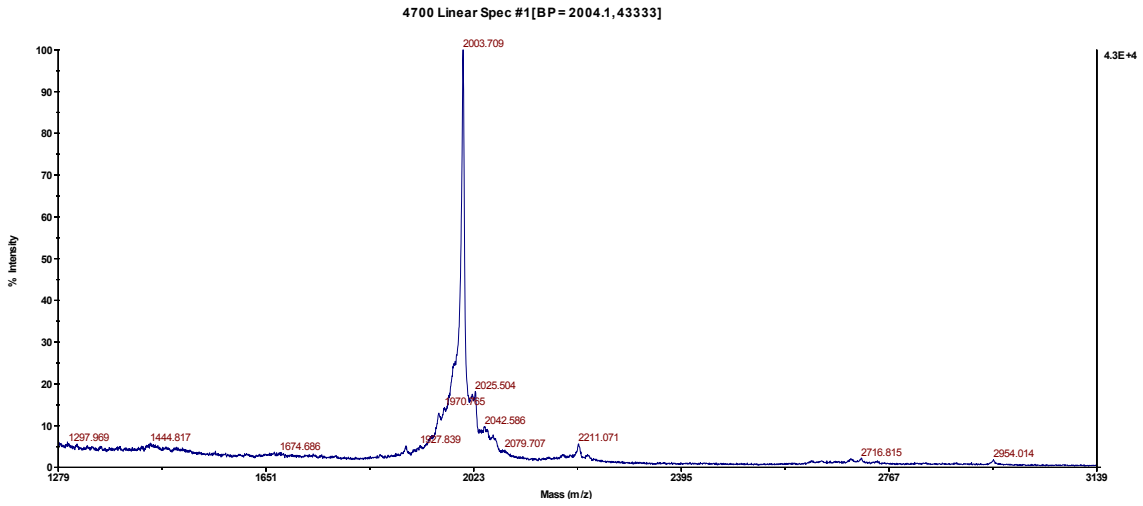


Figure 24 H2009.1 Monomer

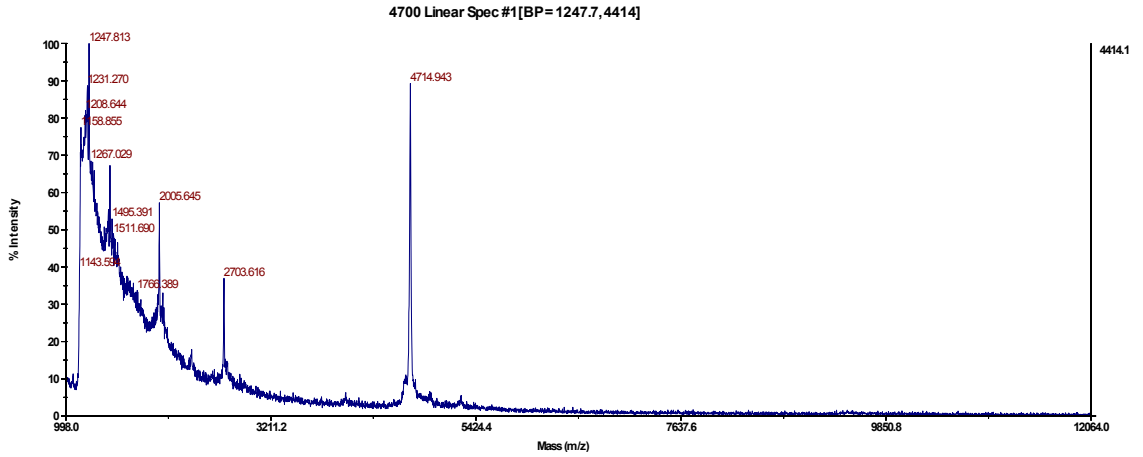


Figure 25 H2009.1 Cys Dimer

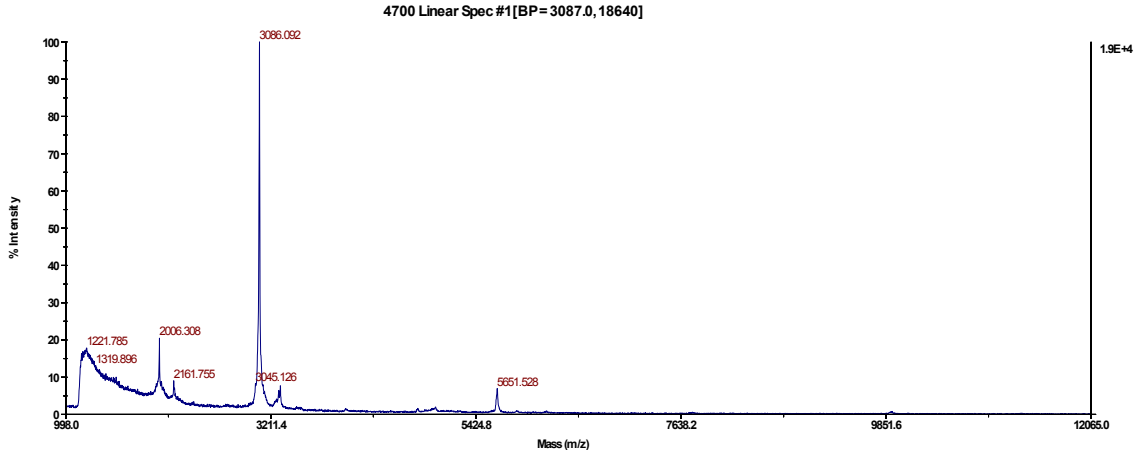


Figure 26 H2009.1 Biotinylated Dimer

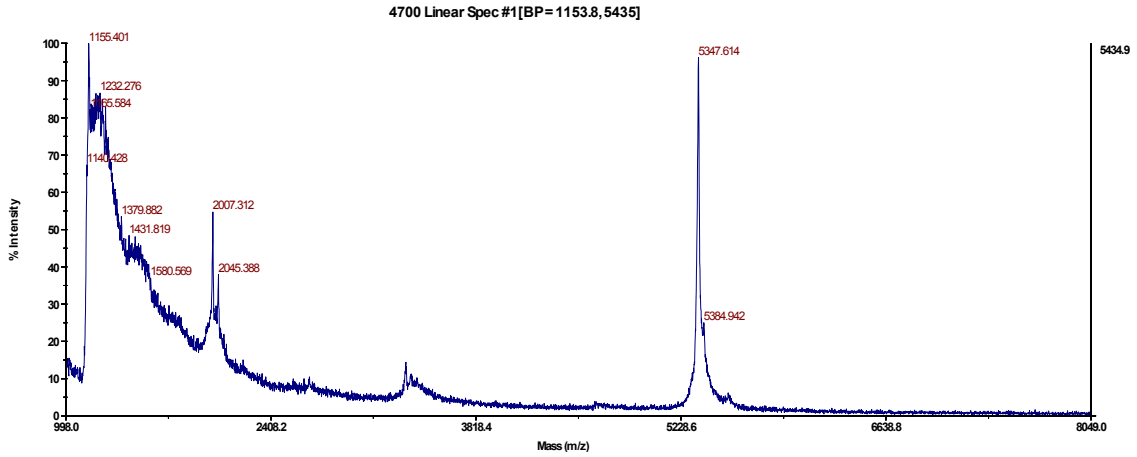


Figure 27 H2009.1 Dimer + AF488

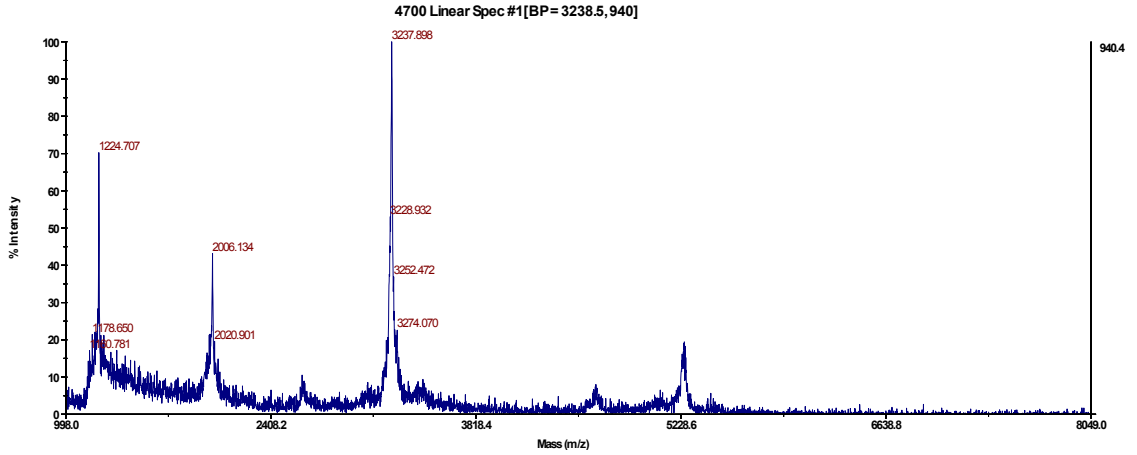


Figure 28 H2009.1 Dimer + Cy5

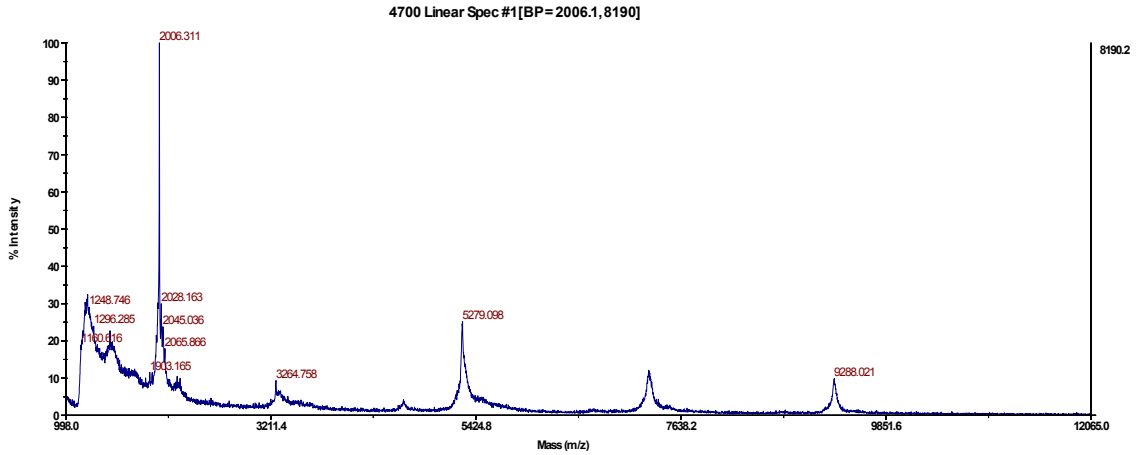


Figure 29 H2009.1 Cys Tetramer

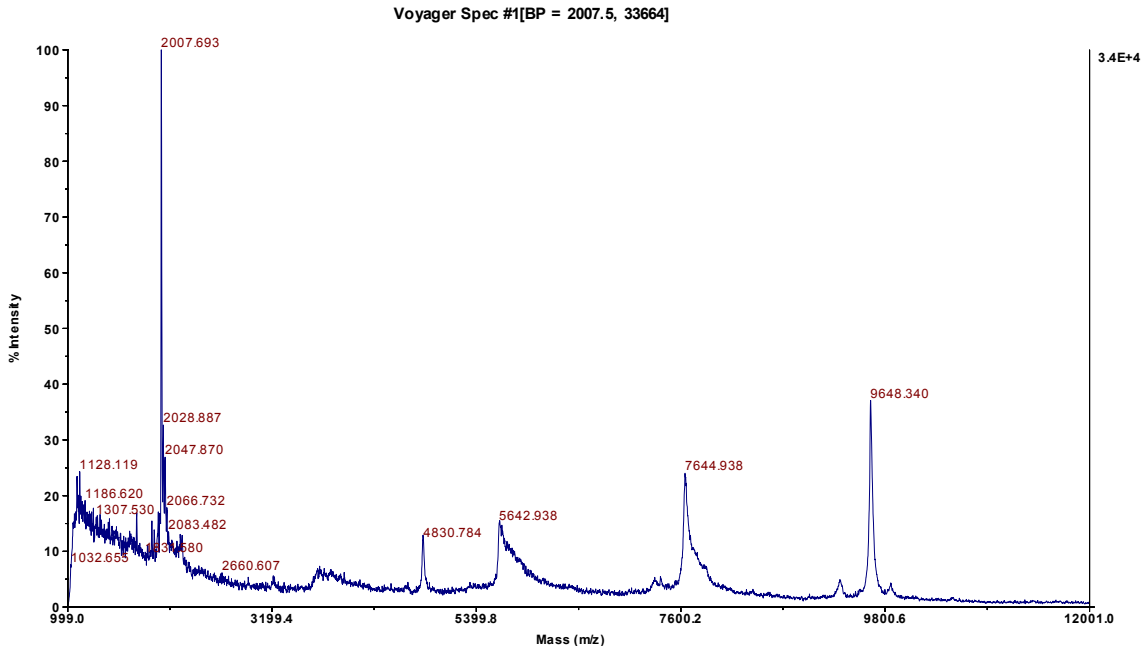


**Figure 30 H2009.1 Biotinylated Tetramer**

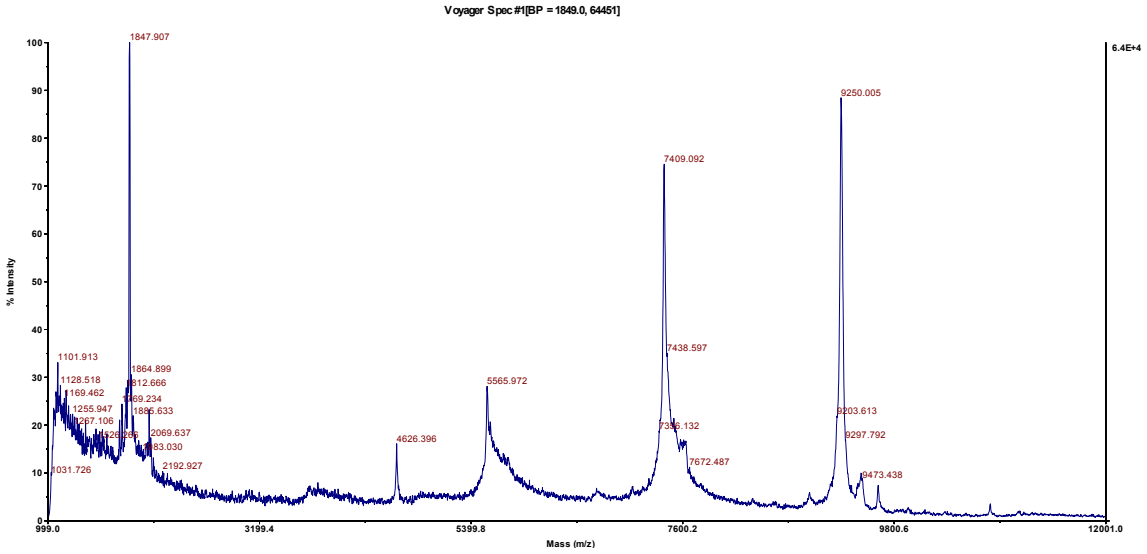


**Figure 31 H2009.1 Tetramer + AF488**

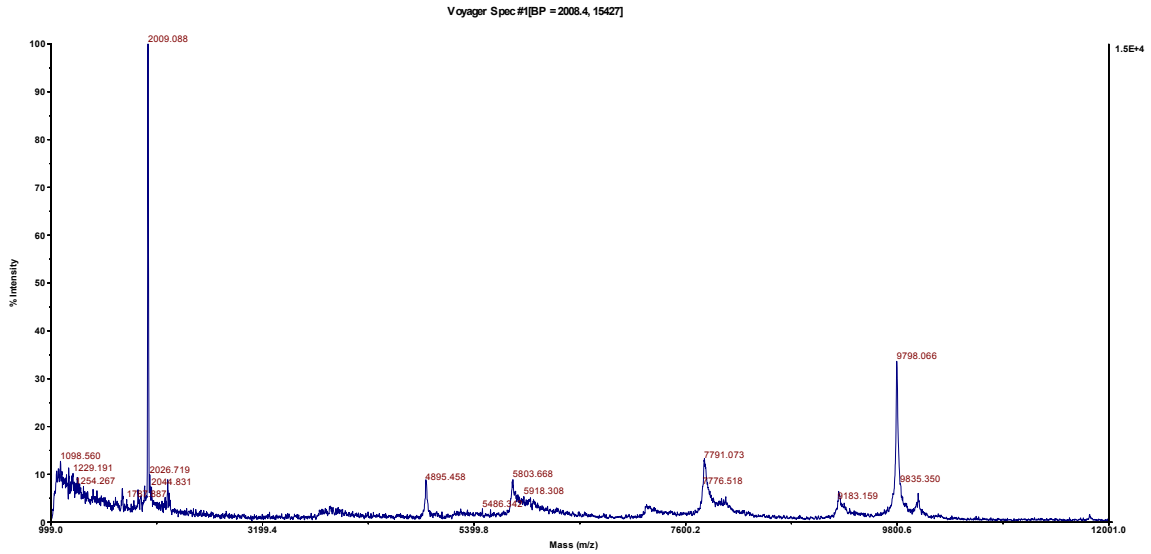


Figure 32 H2009.1 Tetramer + Cy5

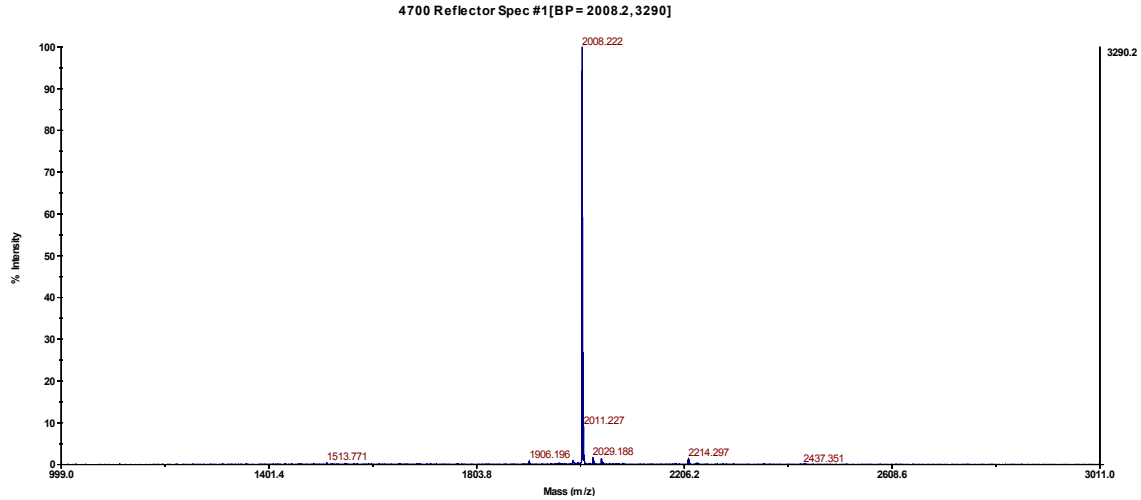


Figure 33 ScrH2009.1 Monomer

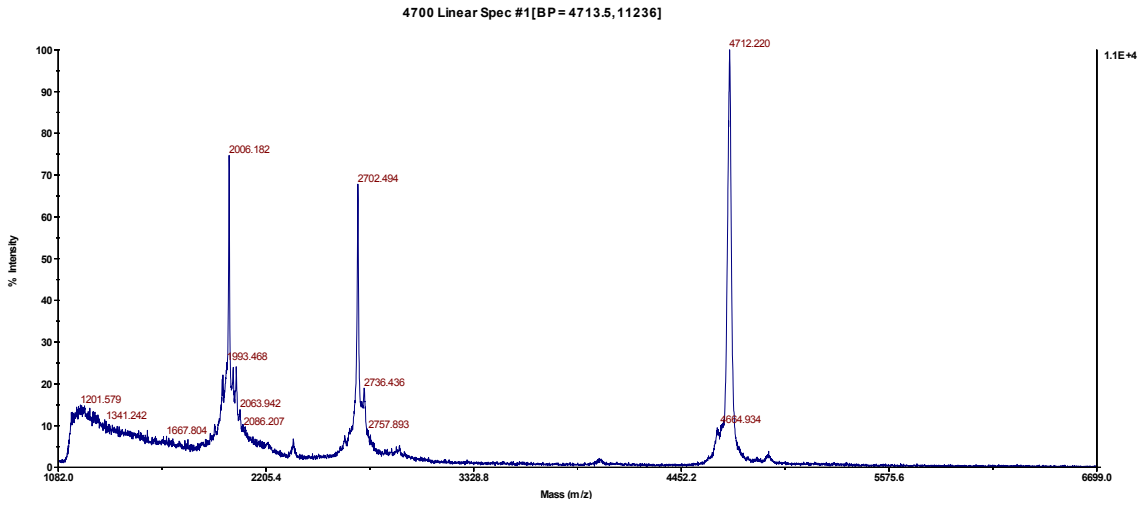


Figure 34 ScrH2009.1 Cys Dimer

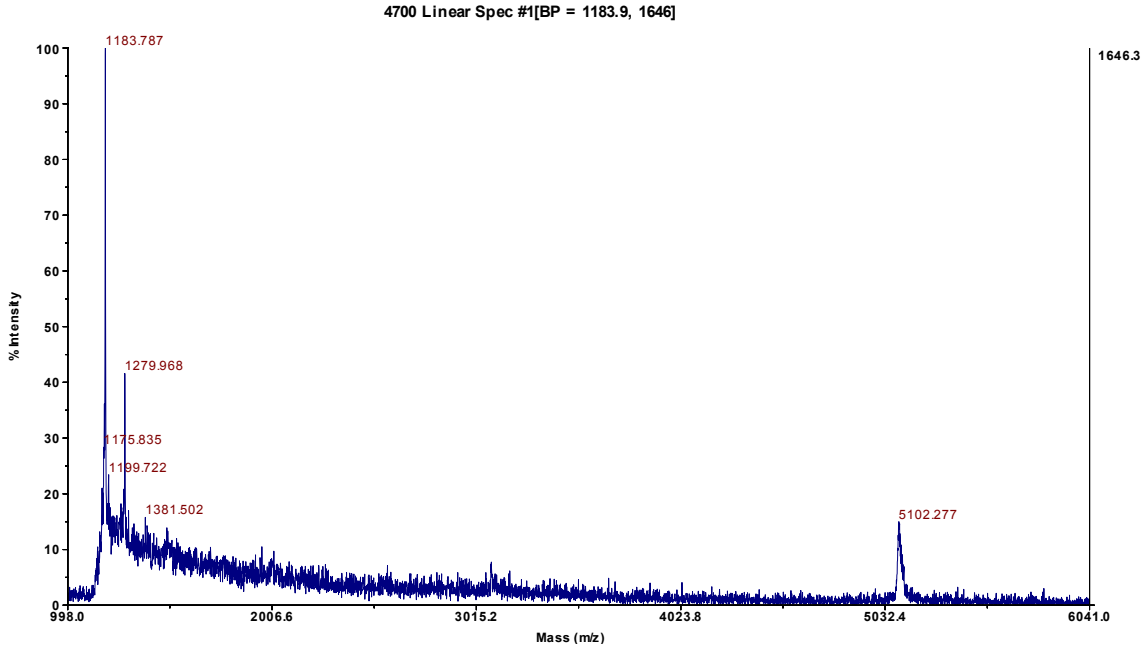


Figure 35 ScrH2009.1 Biotinylated Dimer

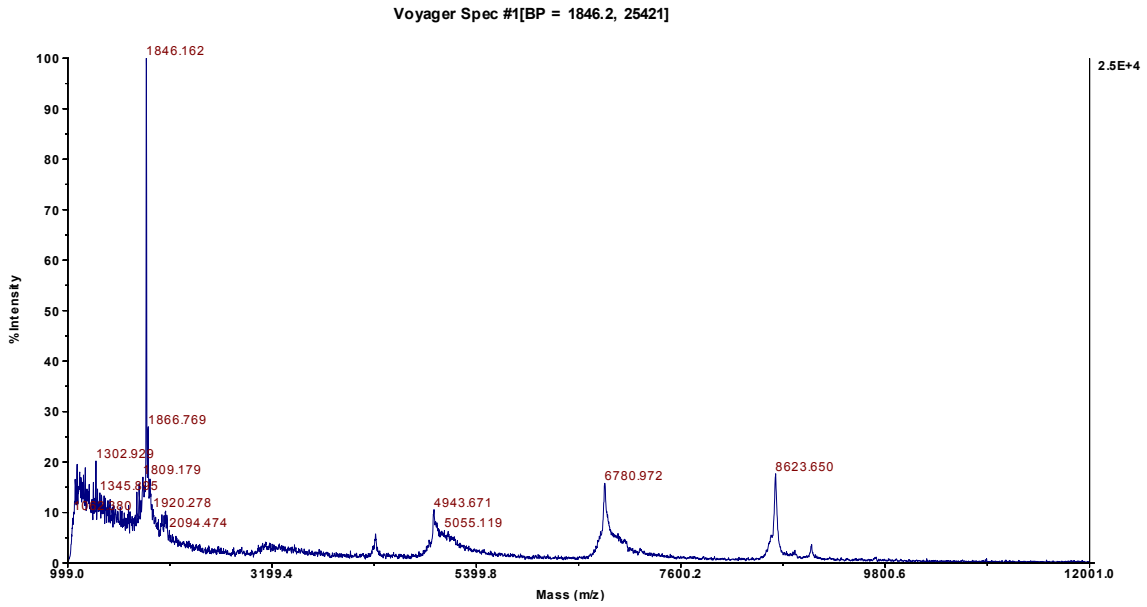


Figure 36 ScrH2009.1 Cys Tetramer

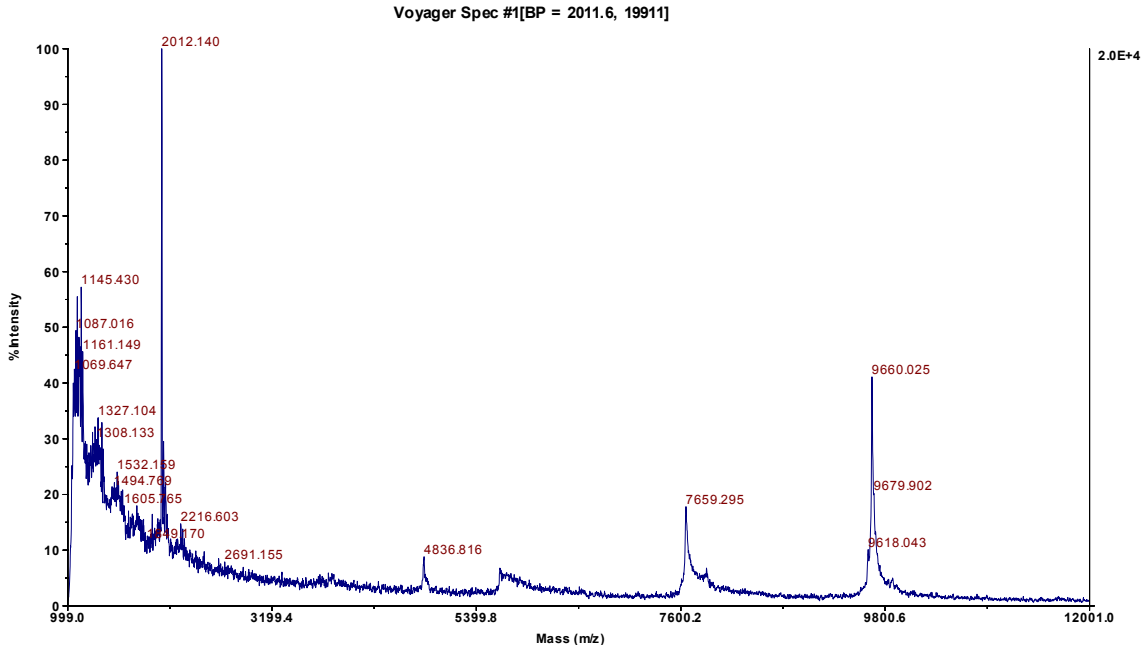


Figure 37 ScrH2009.1 Biotinylated Tetramer

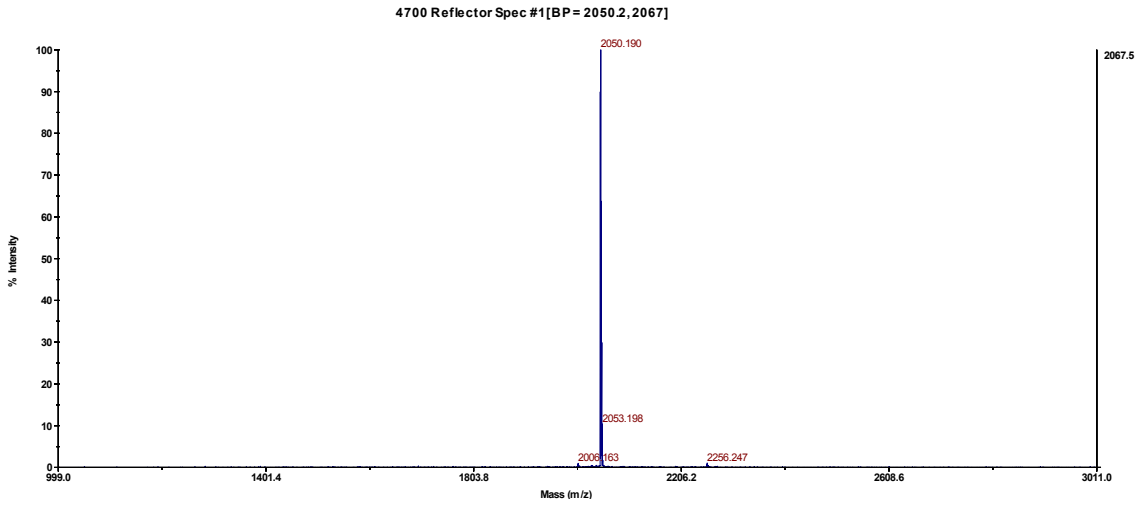


Figure 38 AcH2009.1 Monomer

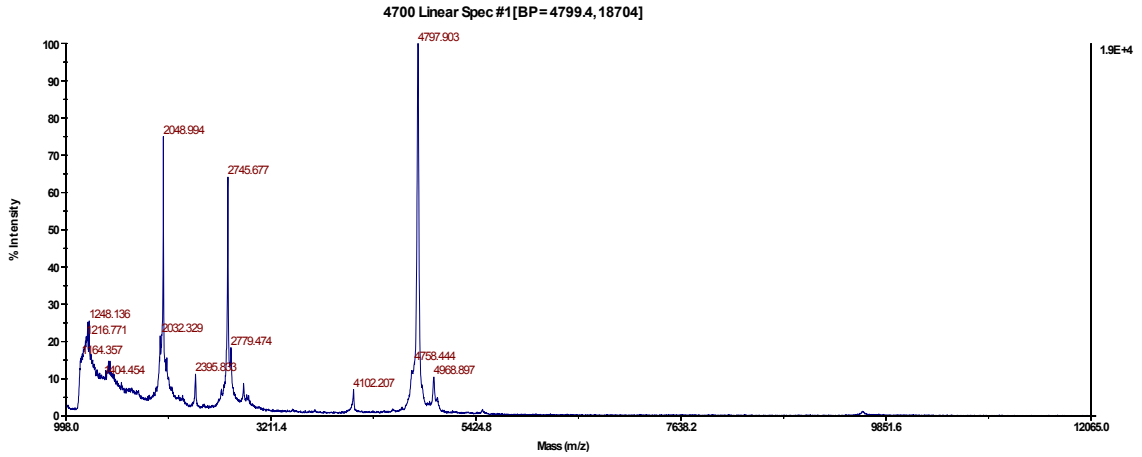


Figure 39 AcH2009.1 Cys Dimer

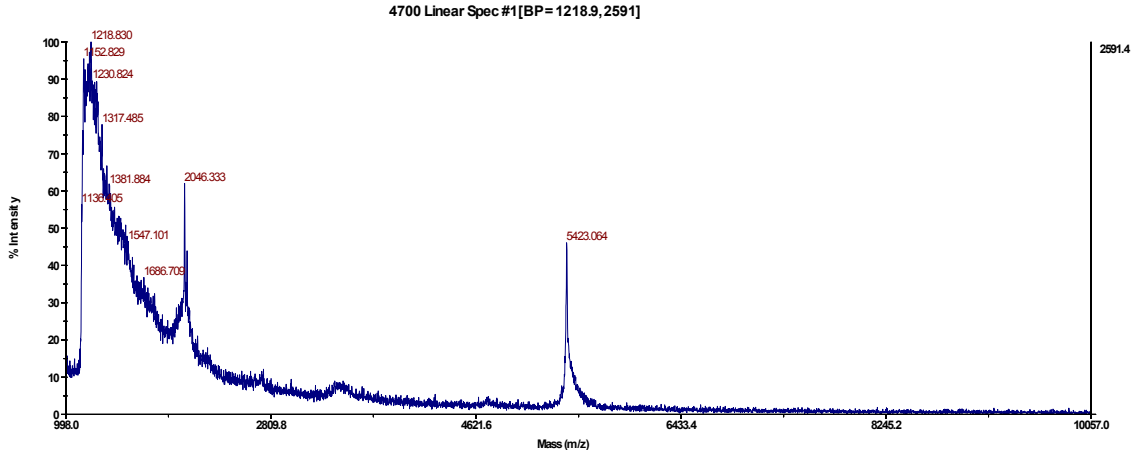


Figure 40 AcH2009.1 Dimer + AF488

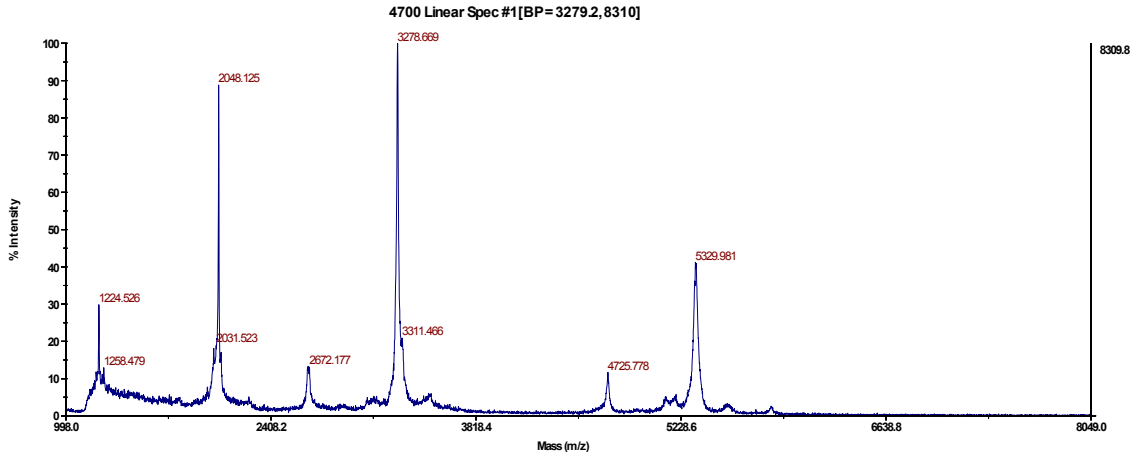


Figure 41 AcH2009.1 Dimer + Cy5

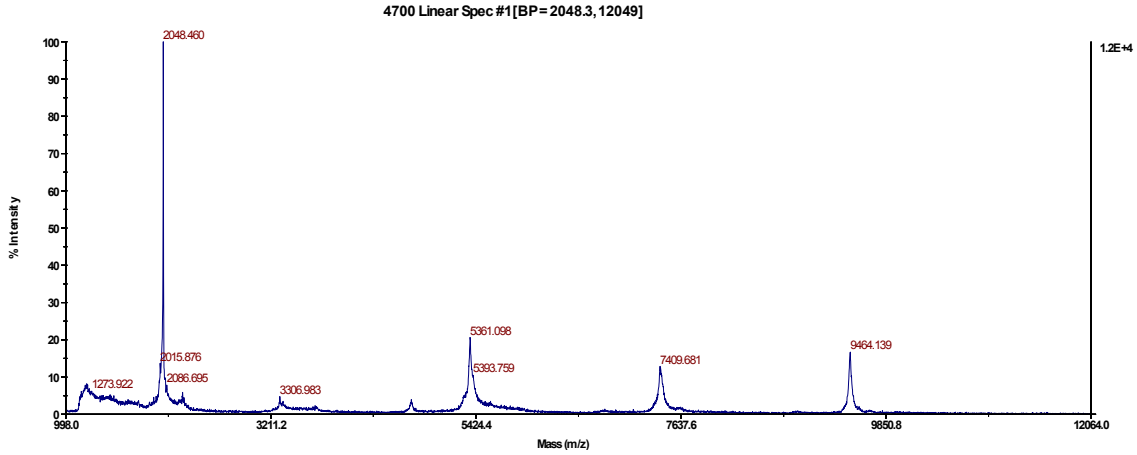


Figure 42 AcH2009.1 Cys Tetramer

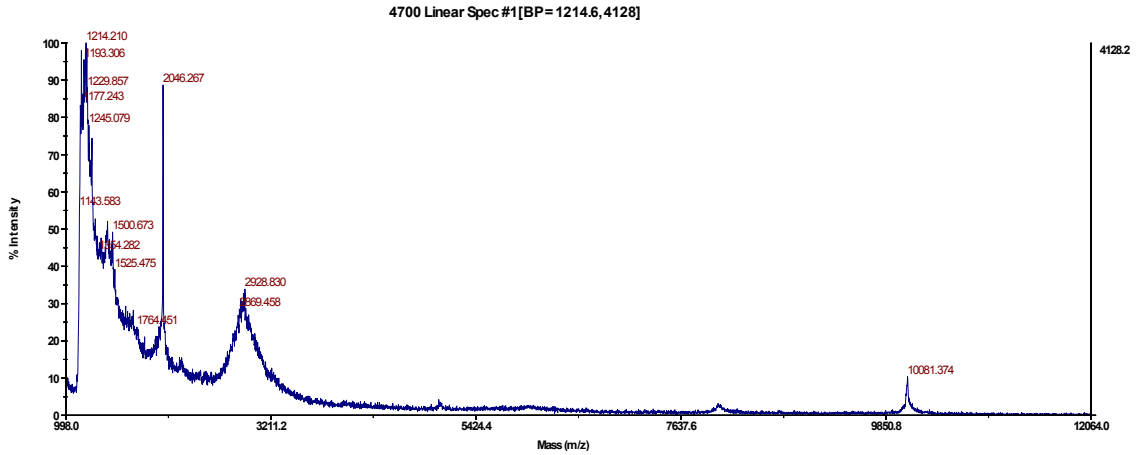


Figure 43 AcH2009.1 Tetramer + AF488

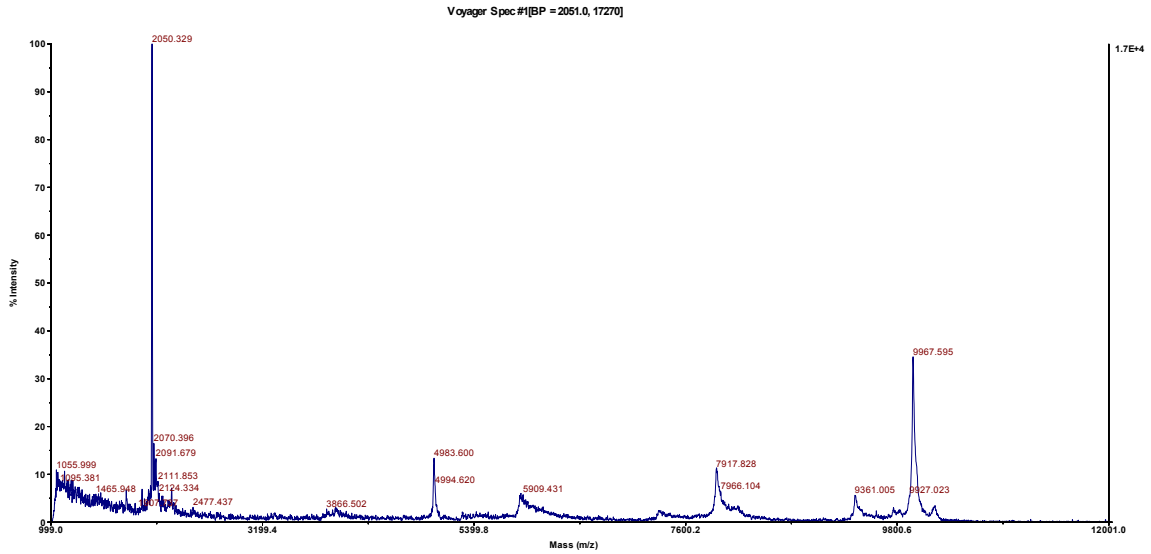


**Figure 44 AcH2009.1 Tetramer + Cy5**

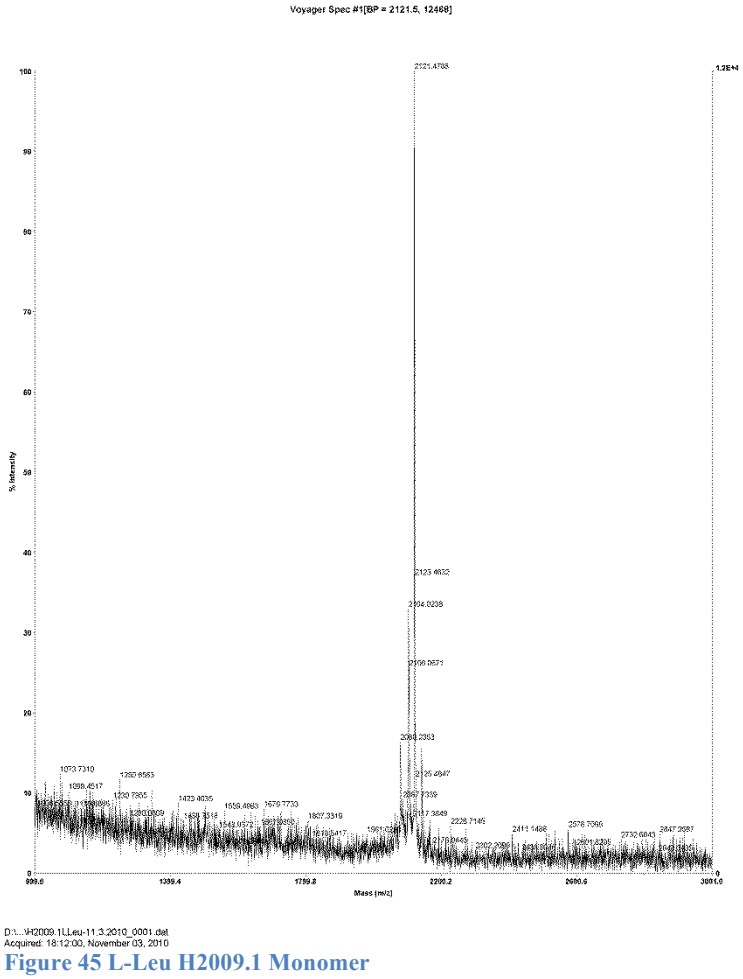


**Figure 45 L-Leu H2009.1 Monomer**

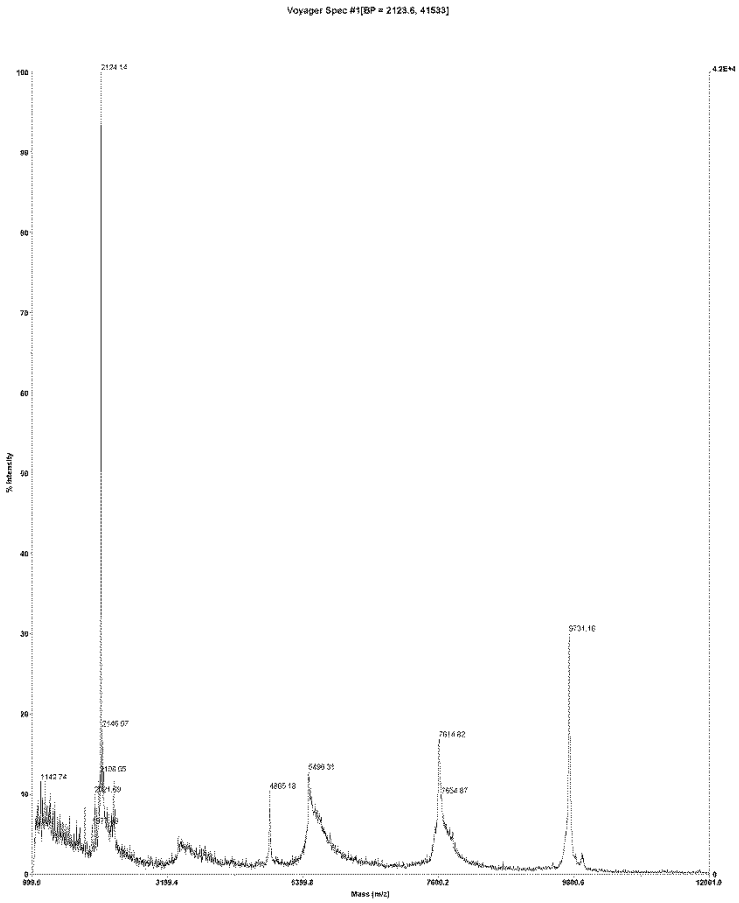


D:\...\H2009.1LLeuTetramer11.12.2010_0001.dat
Acquired: 17:03:00, November 12, 2010

**Figure 46 L-Leu H2009.1 Cys Tetramer**

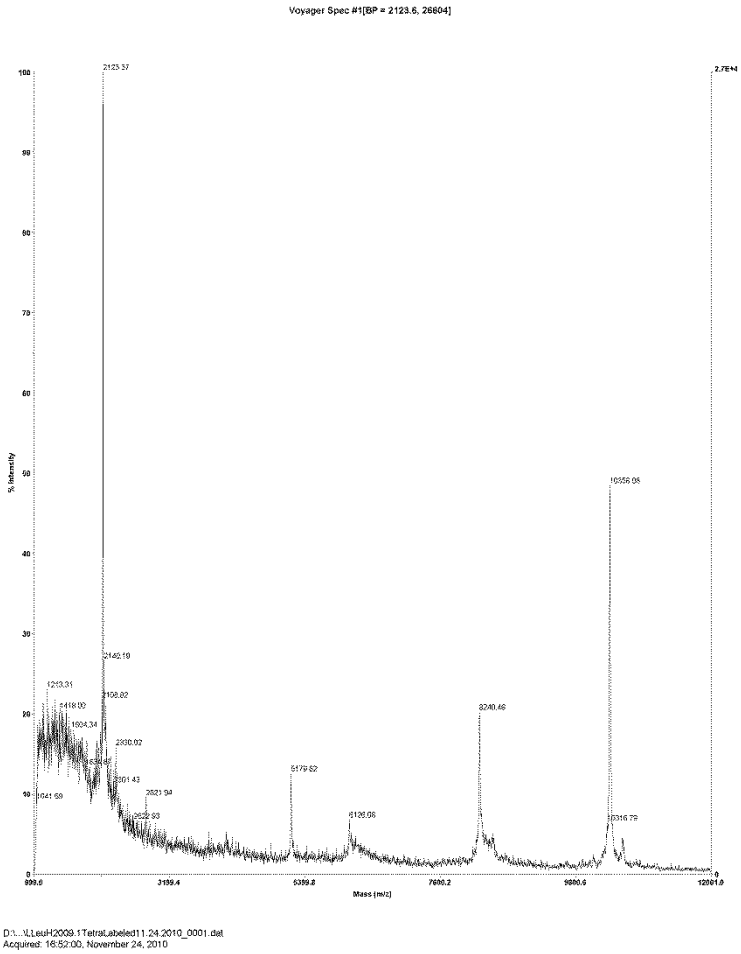


**Figure 47 L-Leu H2009.1 Tetramer + AF488**

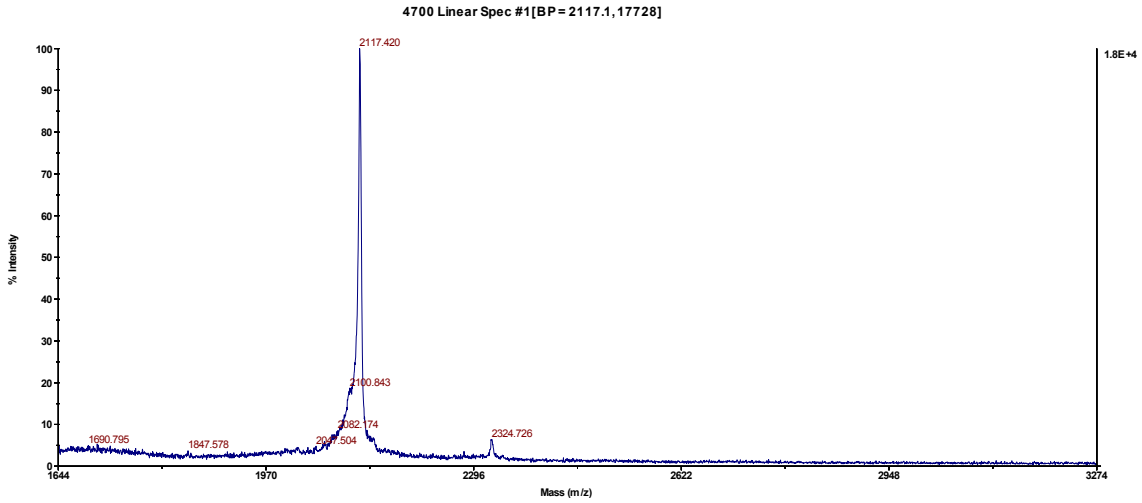


**Figure 48 D-Leu H2009.1 Monomer**

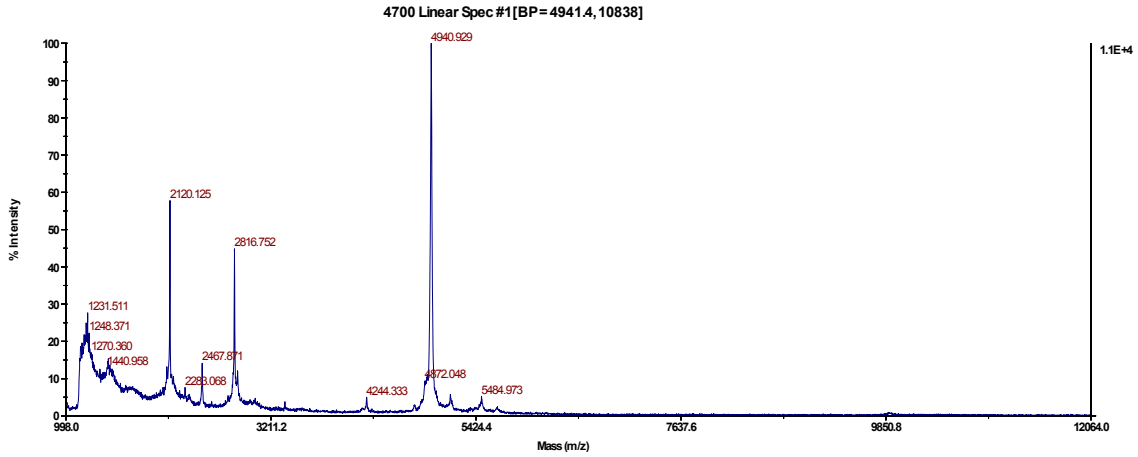


**Figure 49 D-Leu H2009.1 Cys Dimer**

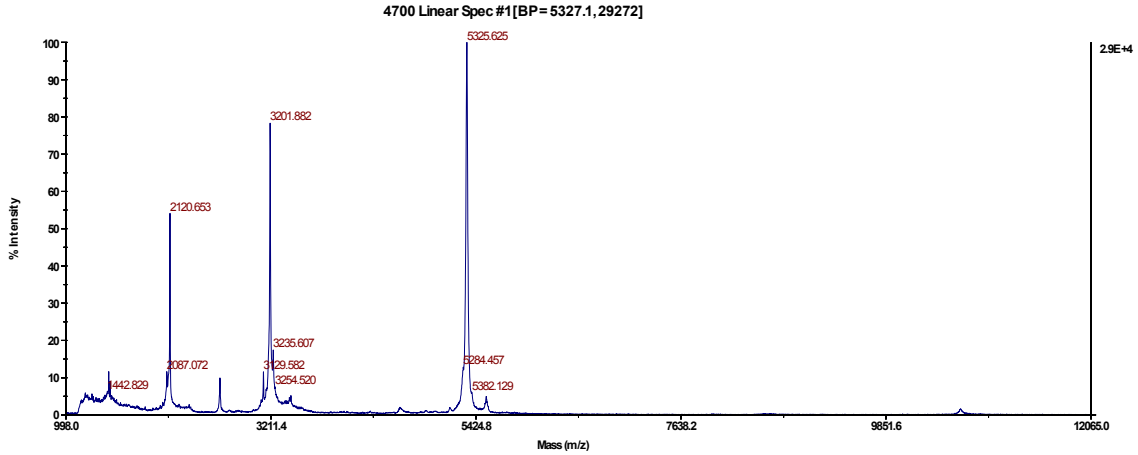


**Figure 50 D-Leu H2009.1 Biotinylated Dimer**

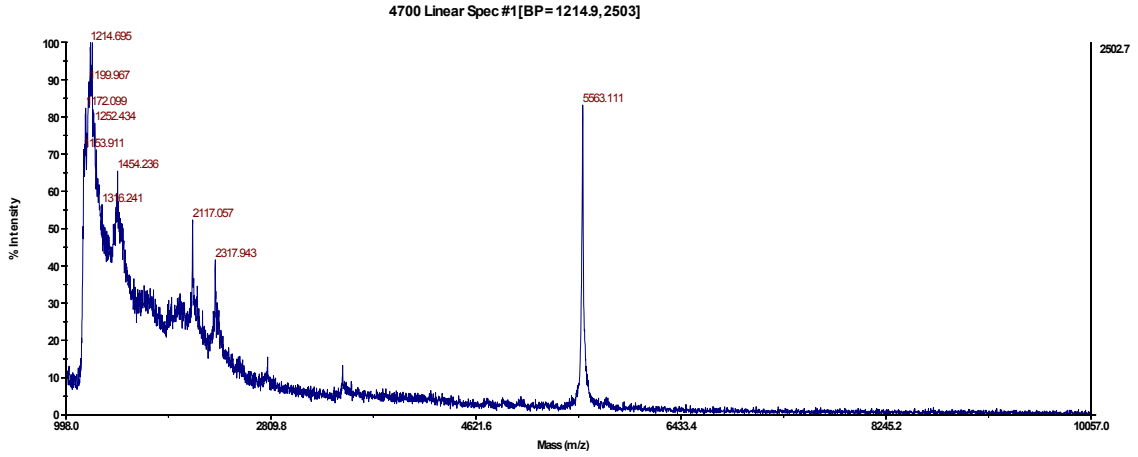


**Figure 51 D-Leu H2009.1 Dimer + AF488**

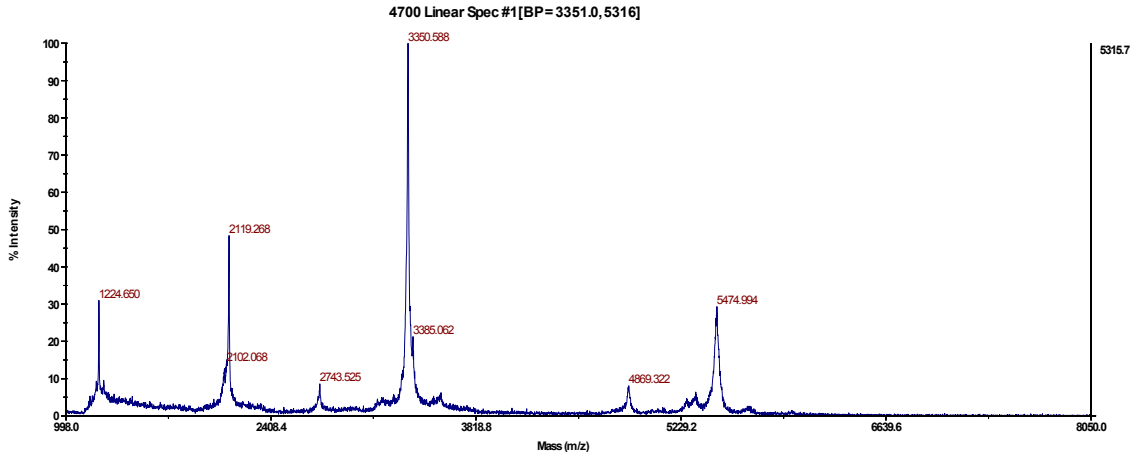


Figure 52 D-Leu H2009.1 Dimer + Cy5

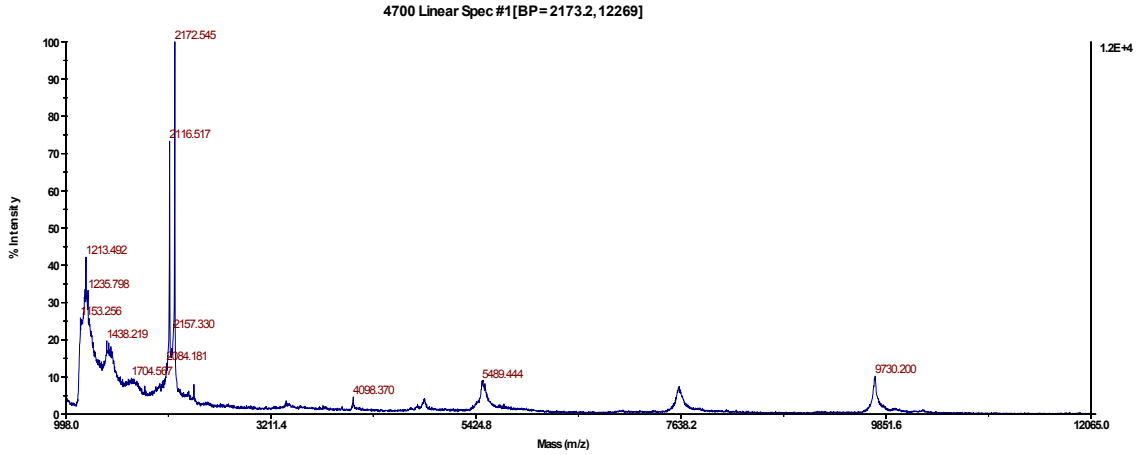


Figure 53 D-Leu H2009.1 Cys Tetramer

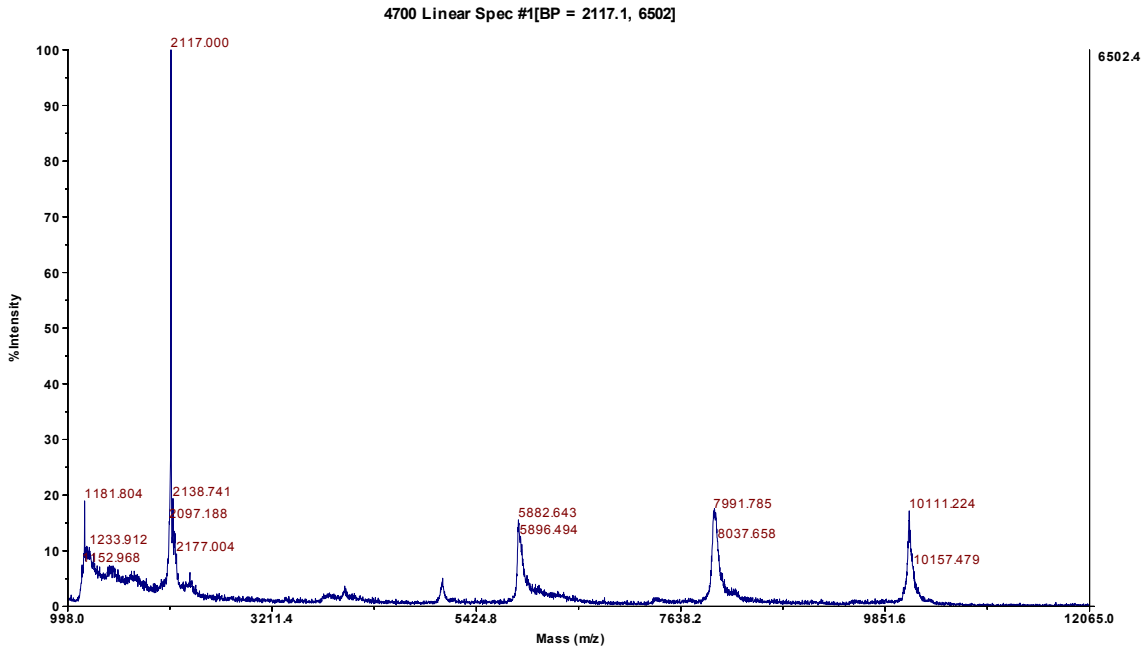


**Figure 54 D-Leu H2009.1 Biotinylated Tetramer**

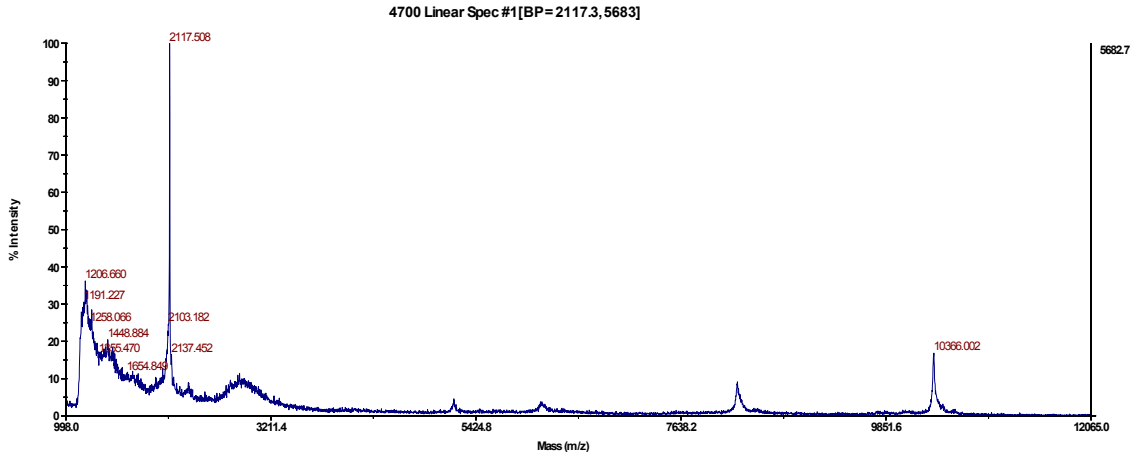


**Figure 55 D-Leu H2009.1 Tetramer + AF488**

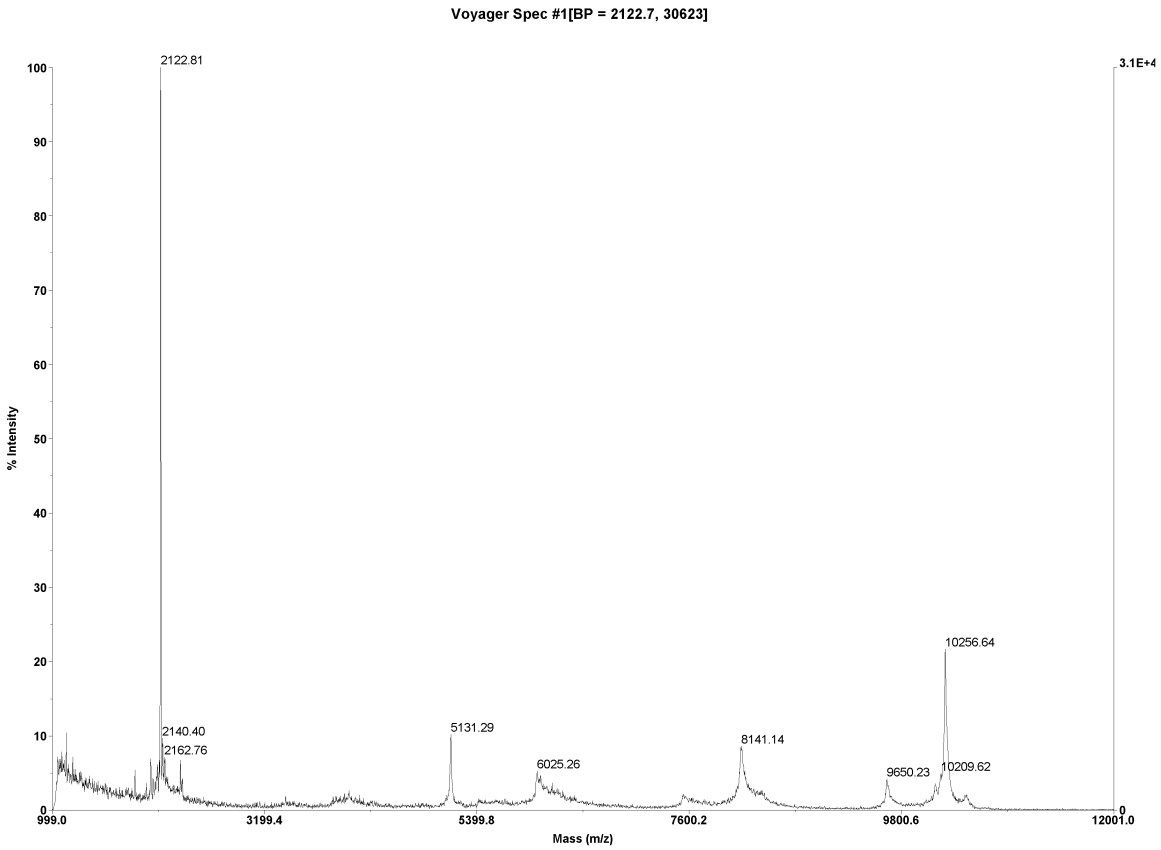


D:\...\DLeu Tetramer + Cy5_0002.dat
Acquired: 13:23:00, July 03, 2012

**Figure 56 D-Leu H2009.1 Tetramer + Cy5**

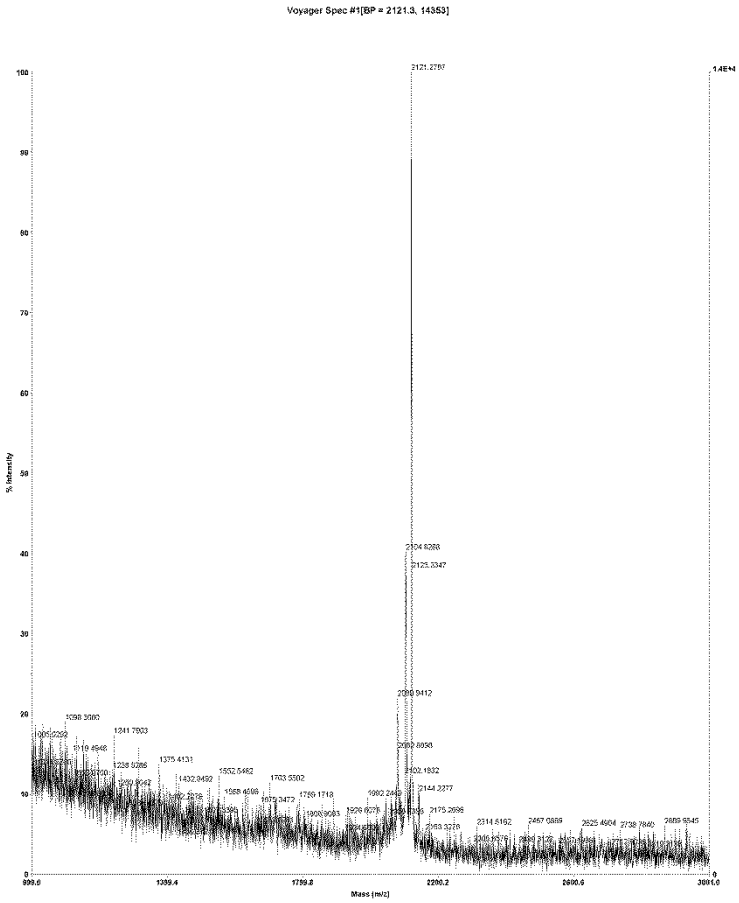


D:\...\H2009.1NLeu-11.9.2010_0001.dat
Acquired: 16:47:00, November 09, 2010

**Figure 57 NLeu H2009.1 Monomer**

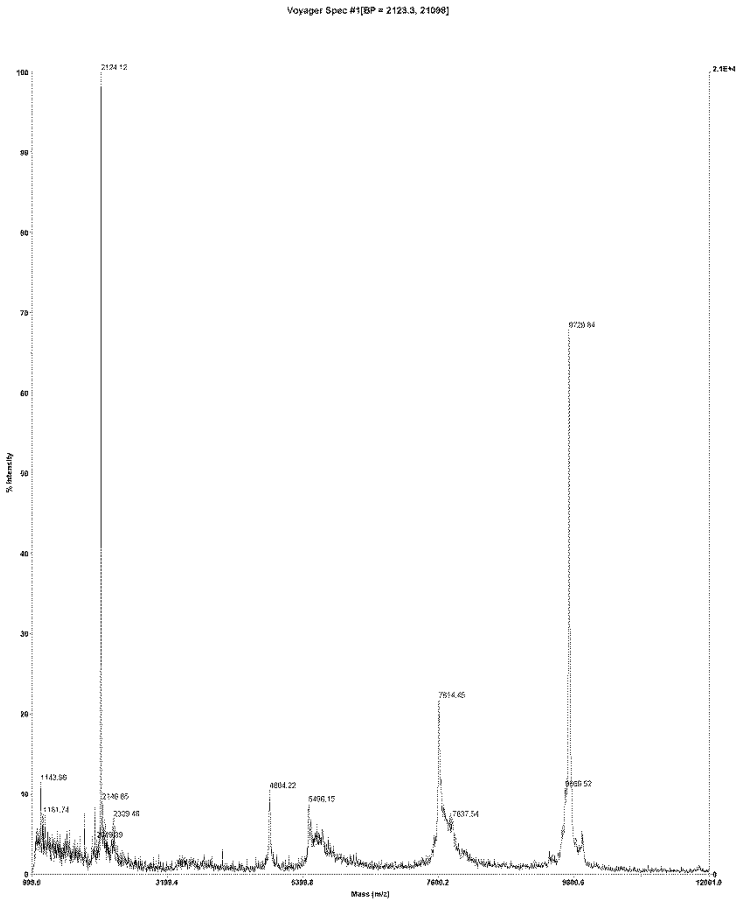


**Figure 58 NLeu H2009.1 Cys Tetramer**

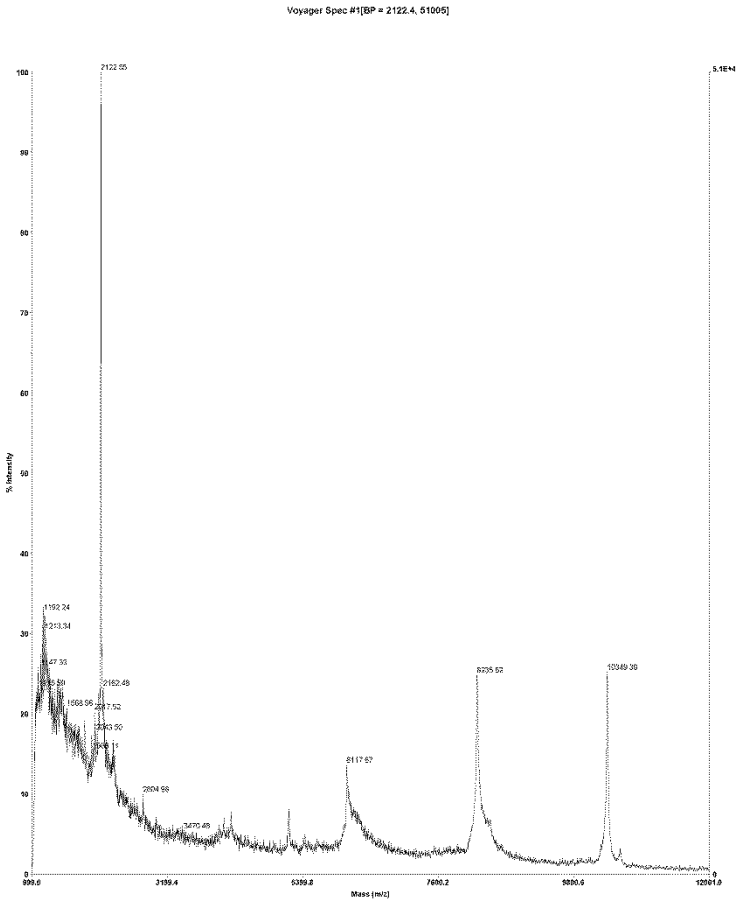


D:\...\NLeuH2009.1TetraLabeled11.23.2010_0001.dat
Acquired: 19:14:00, November 23, 2010

**Figure 59 NLeu H2009.1 Tetramer + AF488**

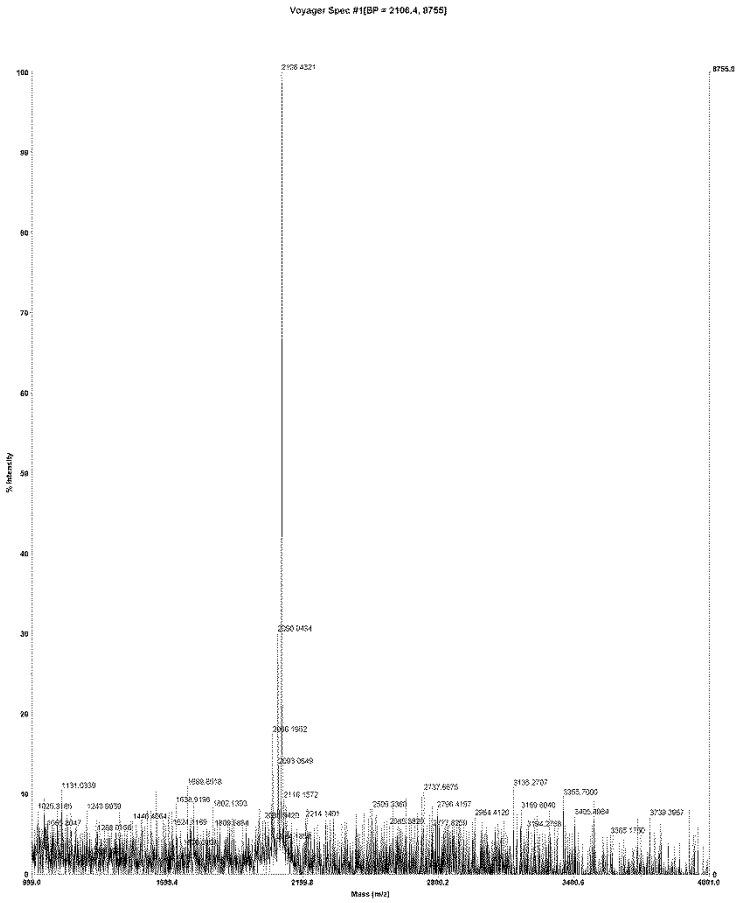


D:\...\H2009.1LVal\11.18.2010_0001.dat
Acquired: 17:34:00, November 18, 2010

**Figure 60 LVal H2009.1 Monomer**

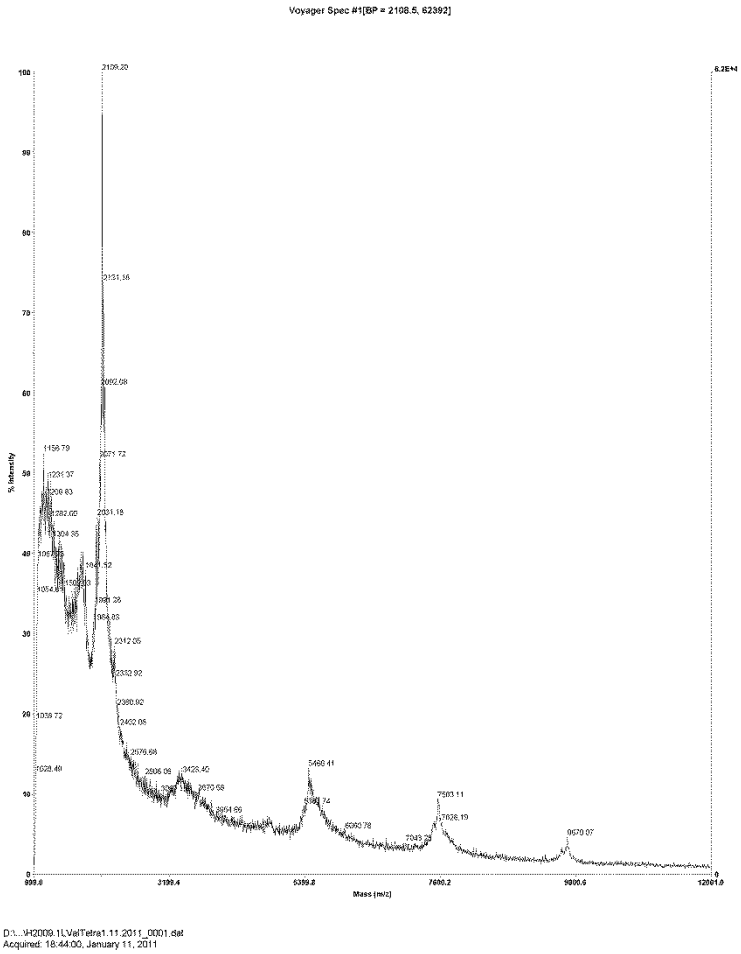


D:\...\H2009.1LValTetra1.11.2011_0001.dat
Acquired: 18:44:00, January 11, 2011

**Figure 61 L-Val H2009.1 Cys Tetramer**

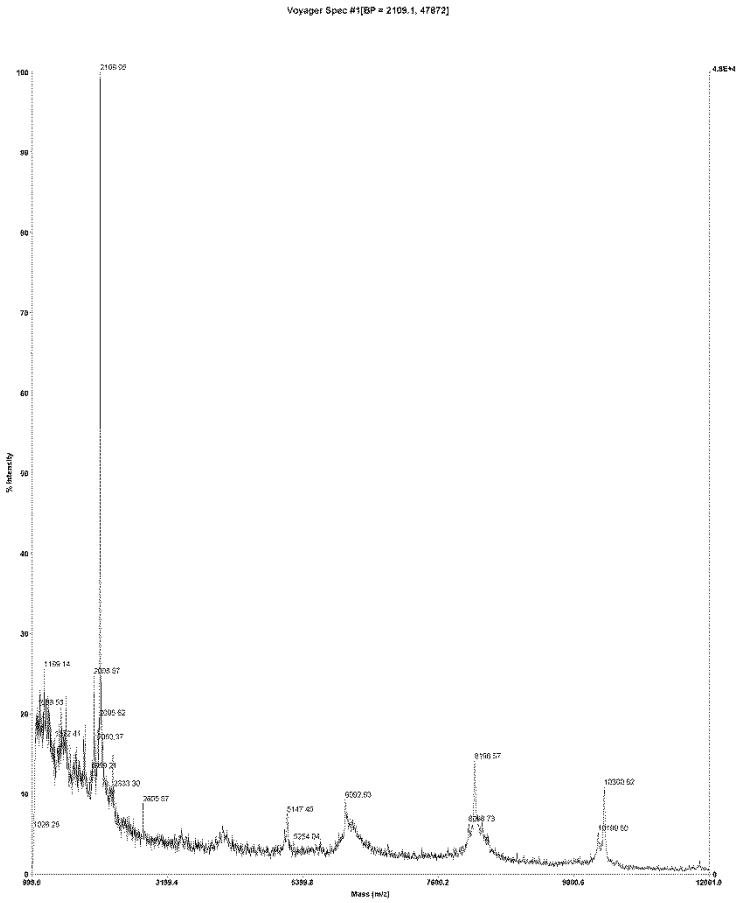


D:\...\H2009.1LValTetraAF1.19.2011_0002.dat
Acquired: 19:04:00, January 19, 2011

**Figure 62 L-Val H2009.1 Tetramer + AF488**

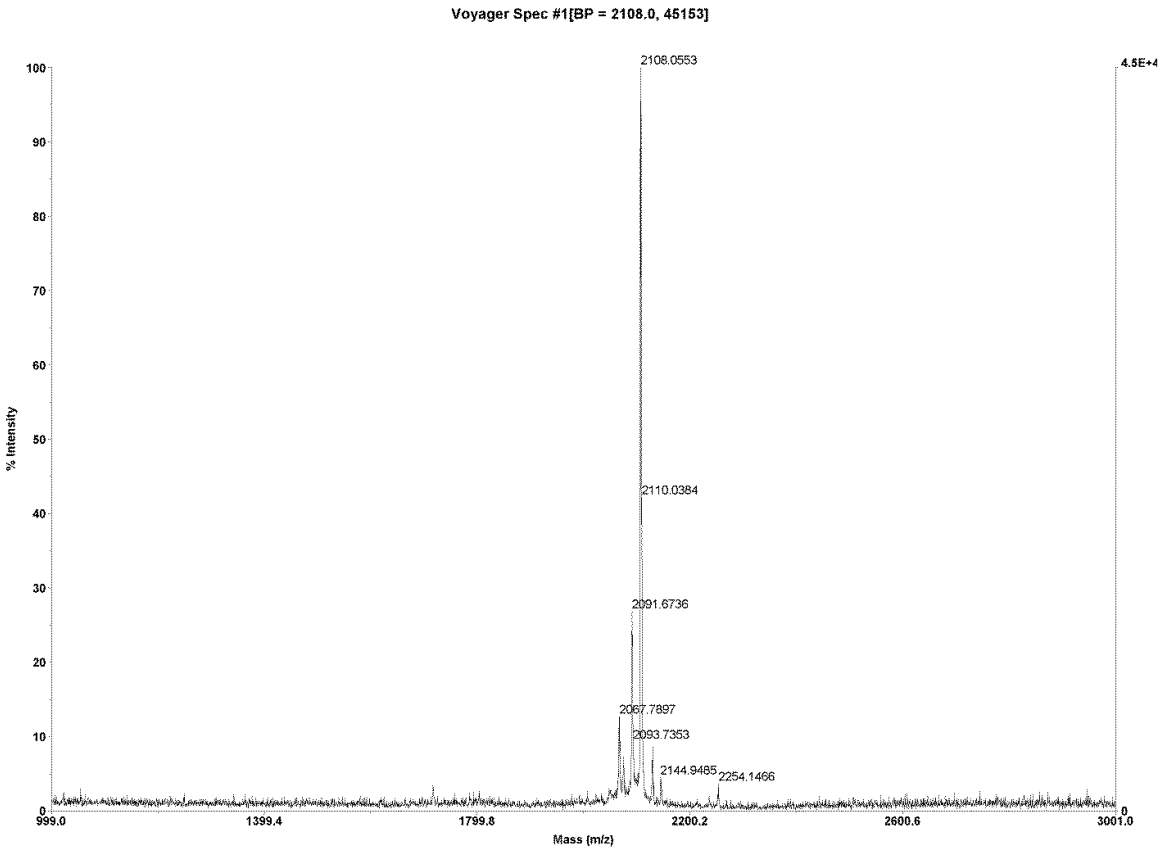


**Figure 63 D-Val H2009.1 Monomer**

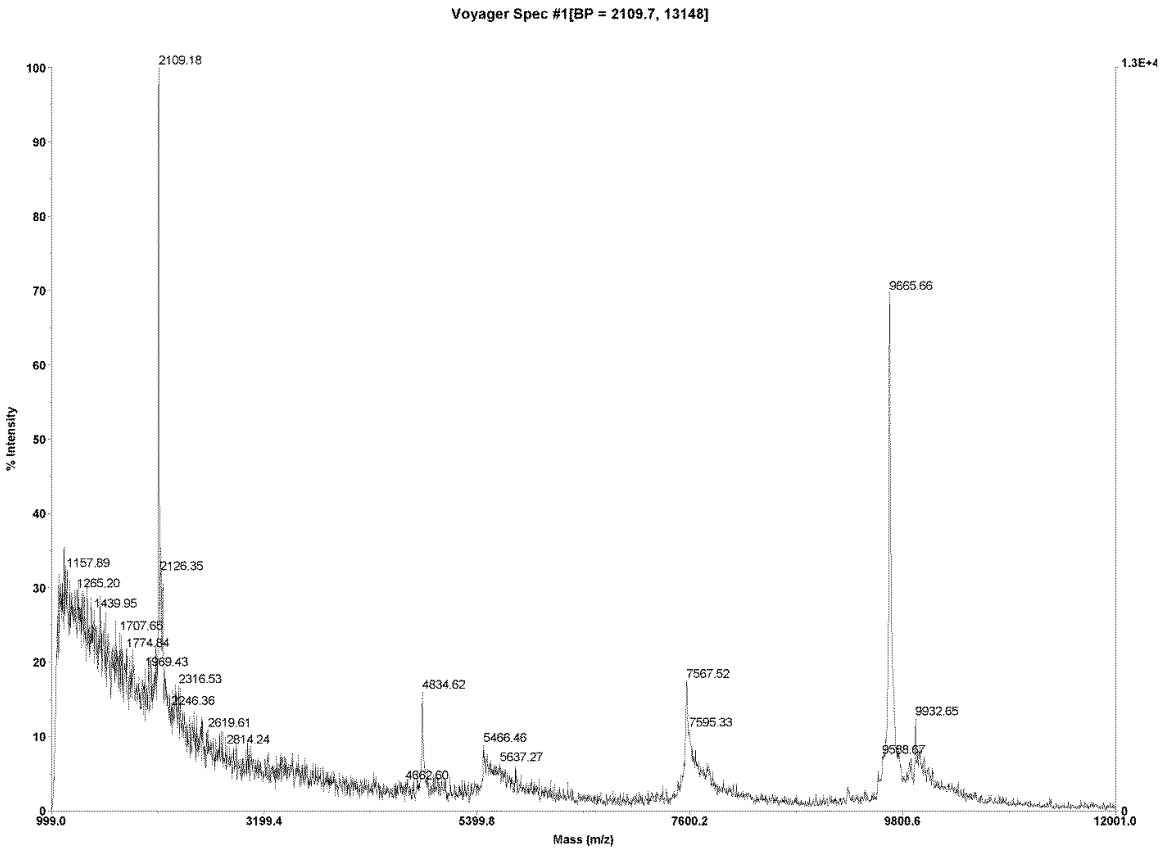


D:\...\DVal Tetramer 6.6.2012_0002.dat
Acquired: 17:43:00, June 06, 2012

**Figure 64 D-Val H2009.1 Cys Tetramer**

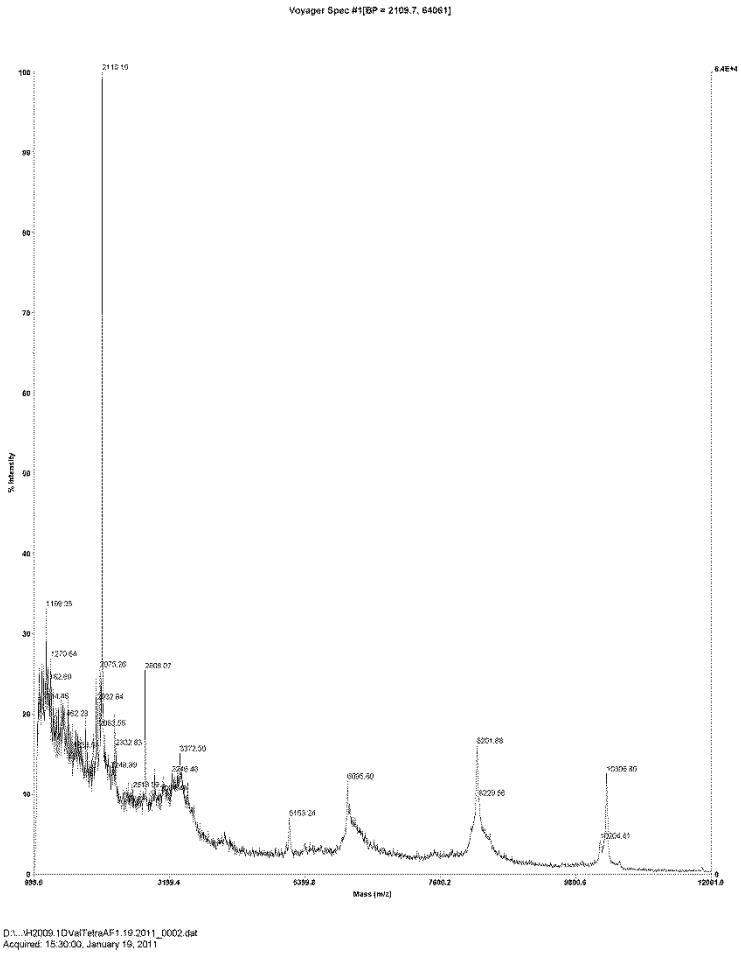


**Figure 65 D-Val H2009.1 Tetramer + AF488**

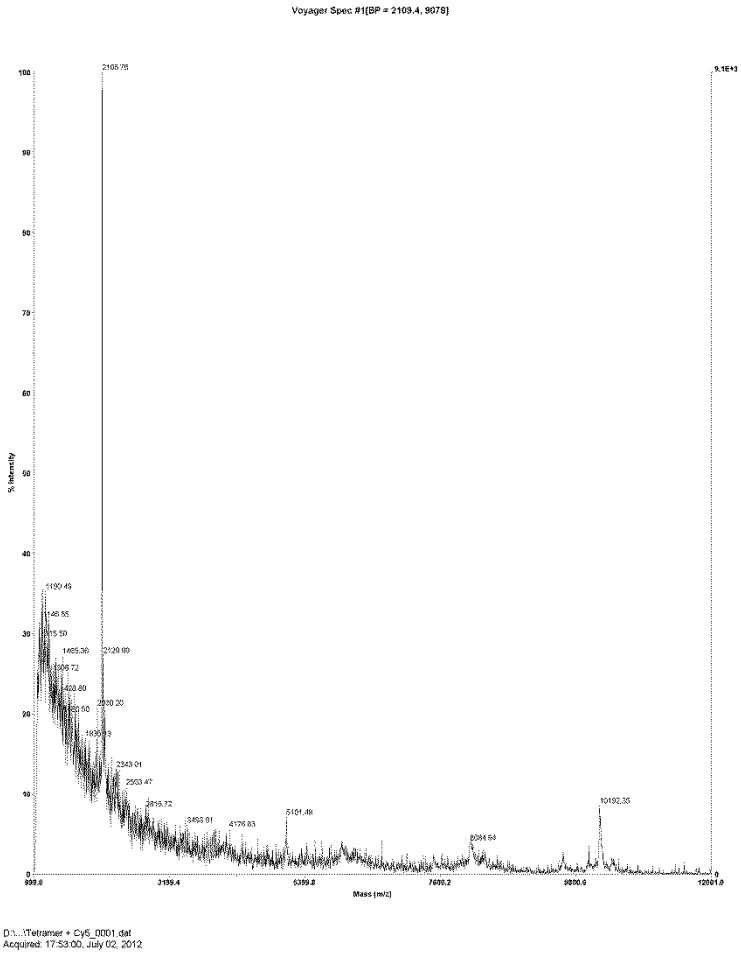


D:\...\Tetramer + Cy5_0001.dat
Acquired: 17:53:00, July 02, 2012

**Figure 66 D-Val H2009.1 Tetramer + Cy5**

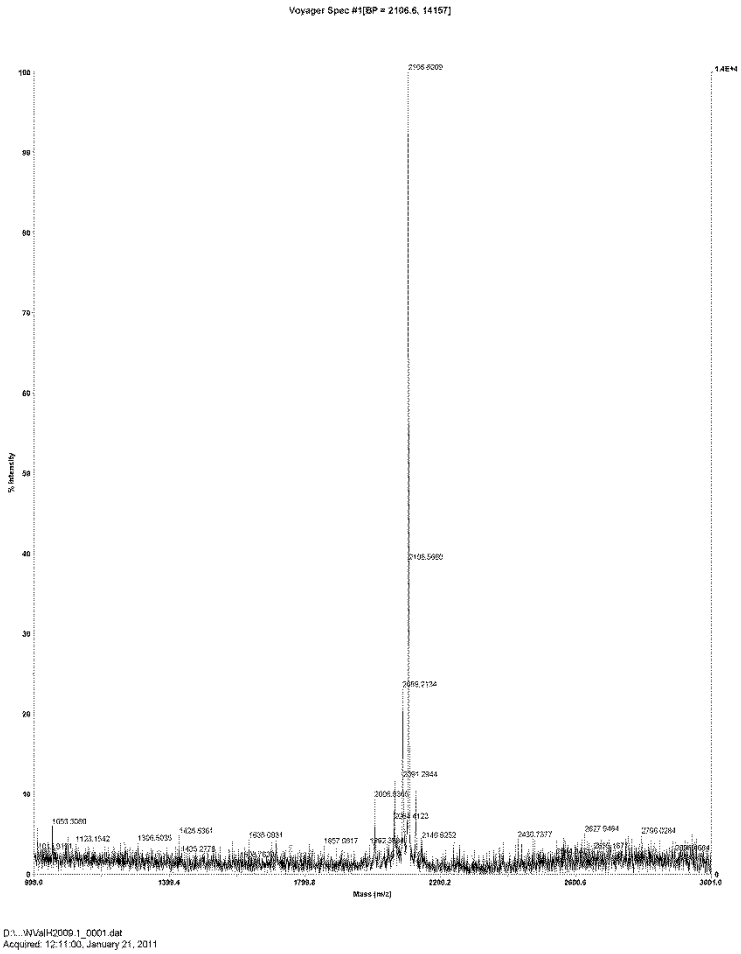


**Figure 67 NVal H2009.1 Monomer**

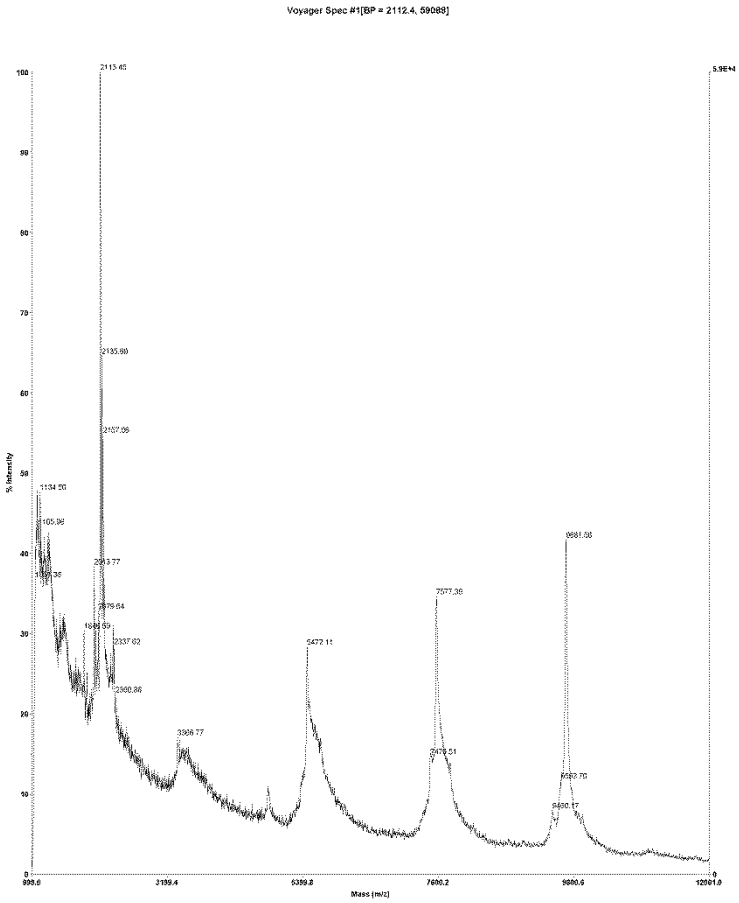


D:\...\NValH2009.1Tetra_0003.dat
Acquired: 19:00:00, February 03, 2011

**Figure 68 NVal H2009.1 Cys Tetramer**

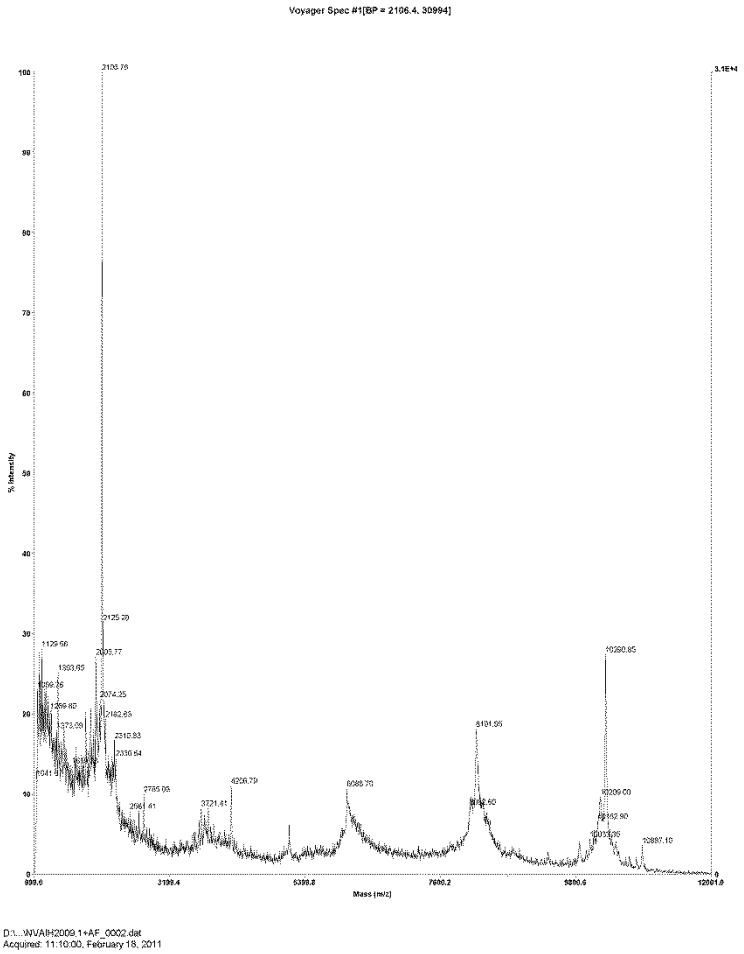


**Figure 69 NVal H2009.1 Tetramer + AF488**

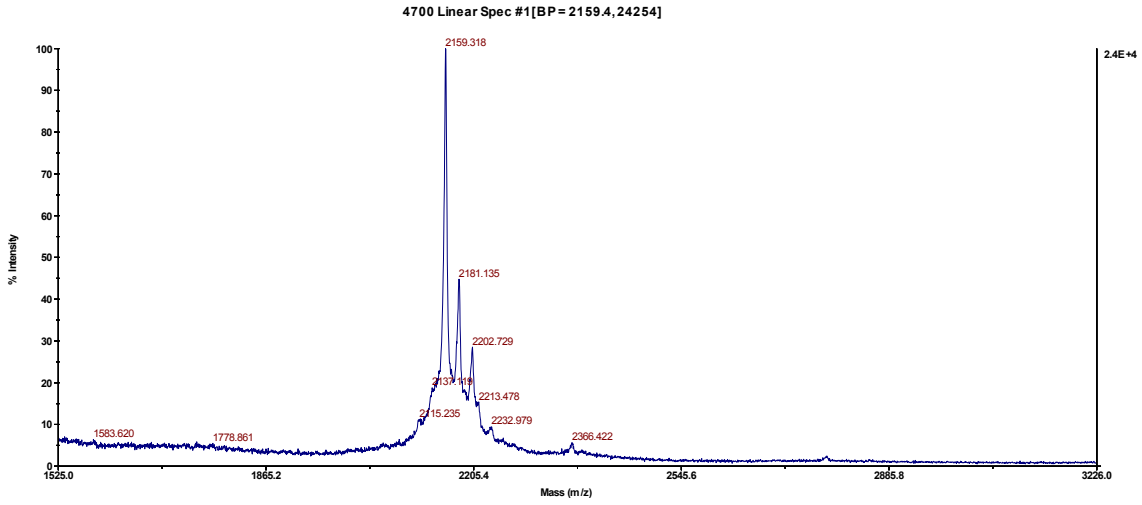


**Figure 70 AcD-Leu H2009.1 Monomer**

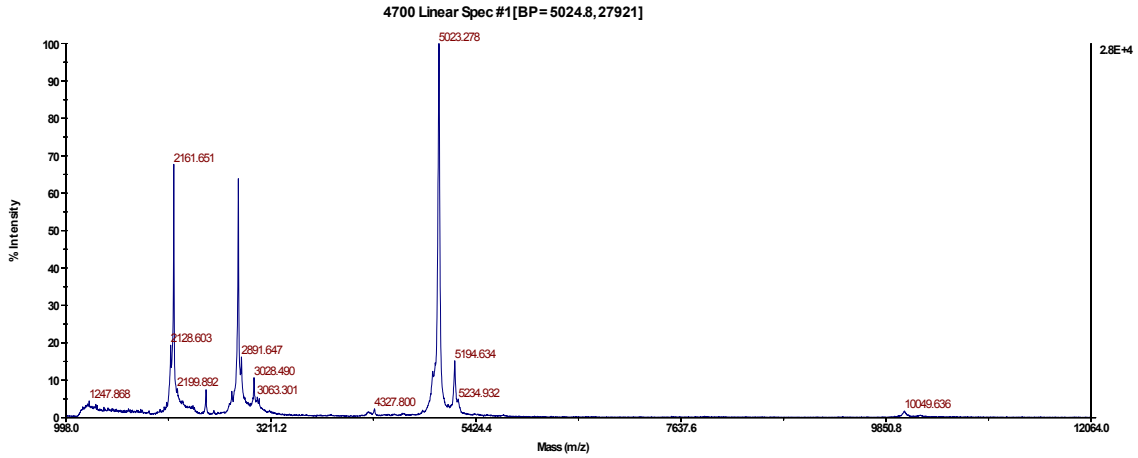


Figure 71 AcD-Leu H2009.1 Cysteine Dimer

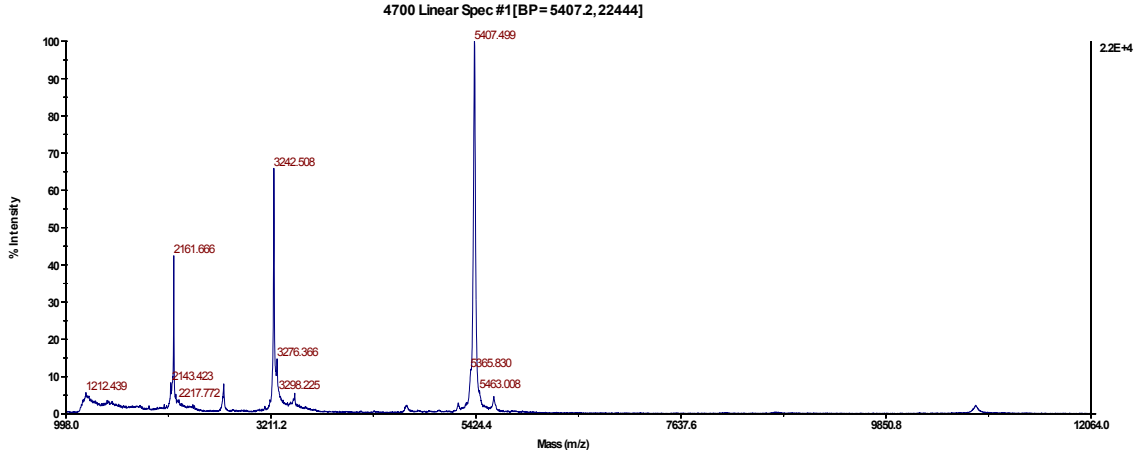


Figure 72 AcD-Leu H2009.1 Biotinylated Dimer

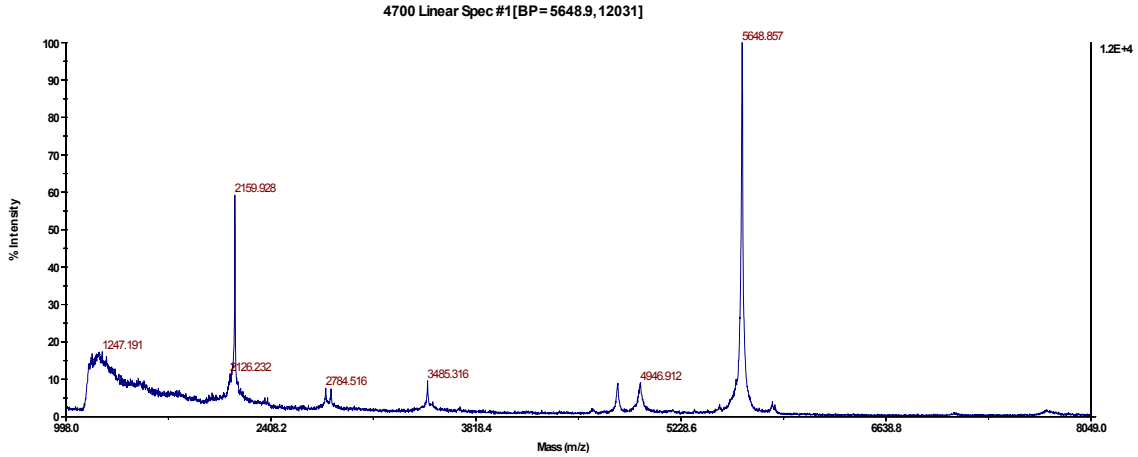


Figure 73 AcD-Leu H2009.1 Dimer + AF488

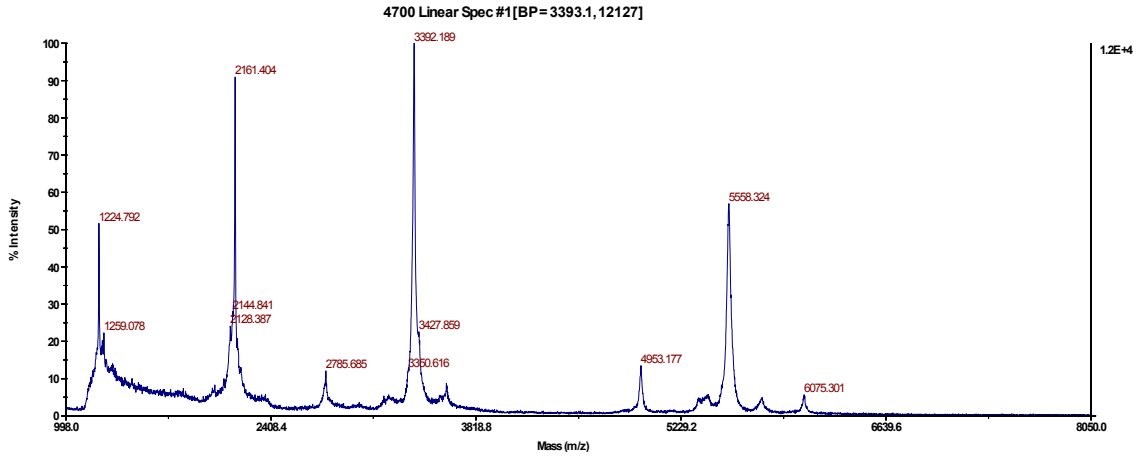


Figure 74 AcD-Leu H2009.1 Dimer + Cy5

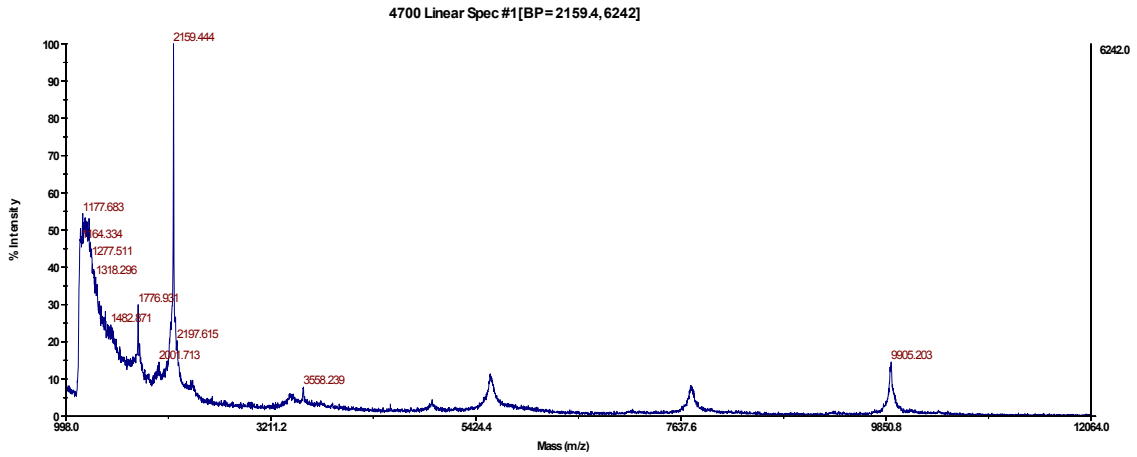


Figure 75 AcD-Leu H2009.1 Cysteine Tetramer

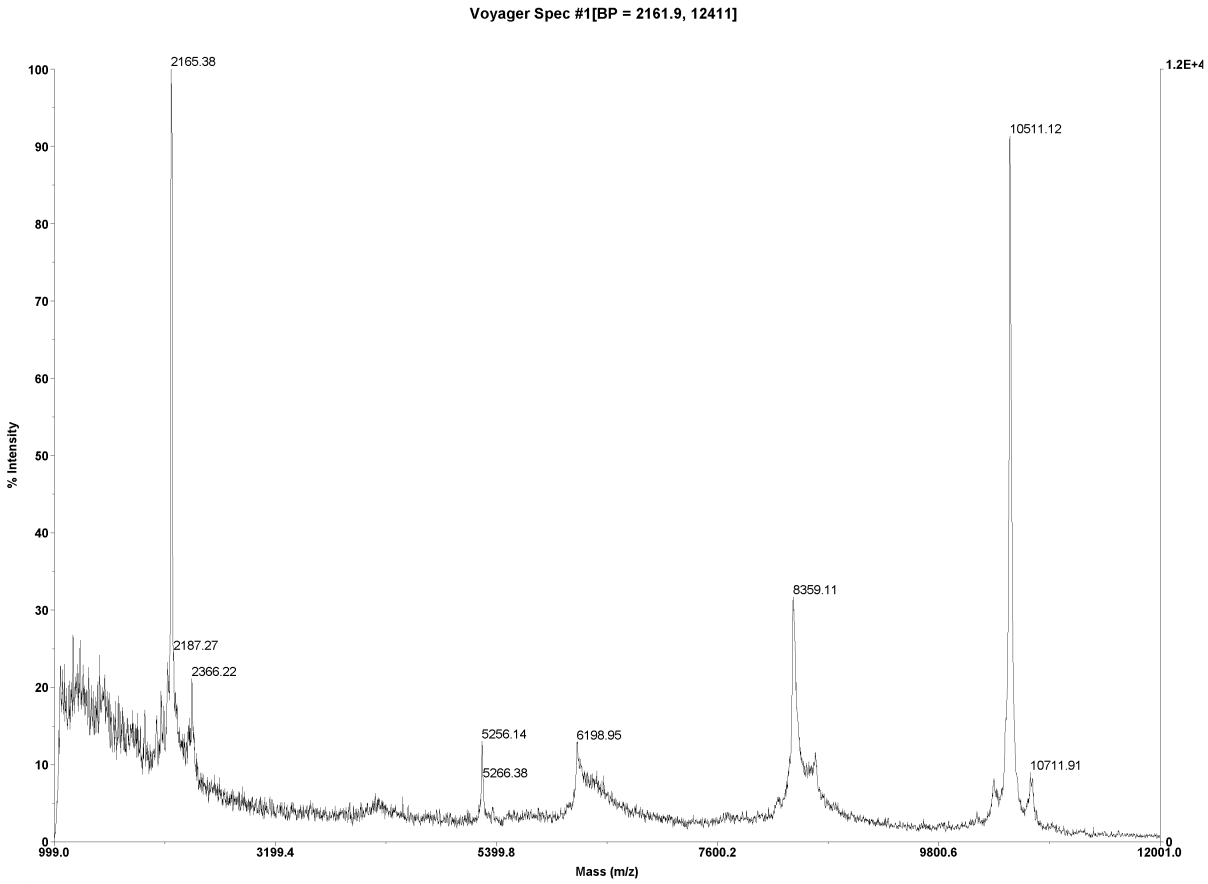


**Figure 76 AcD-Leu H2009.1 Tetramer + AF488**

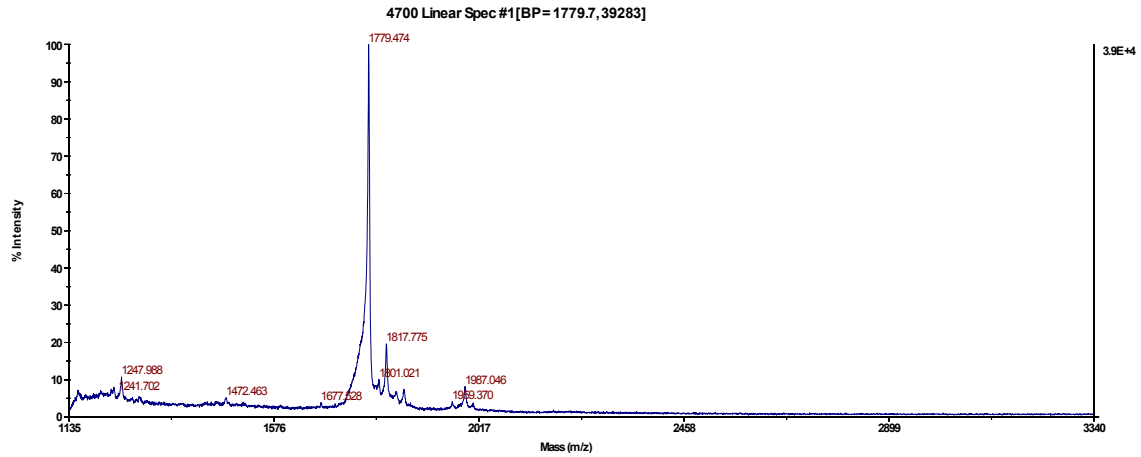


**Figure 77 H2009.1 GGG Monomer**

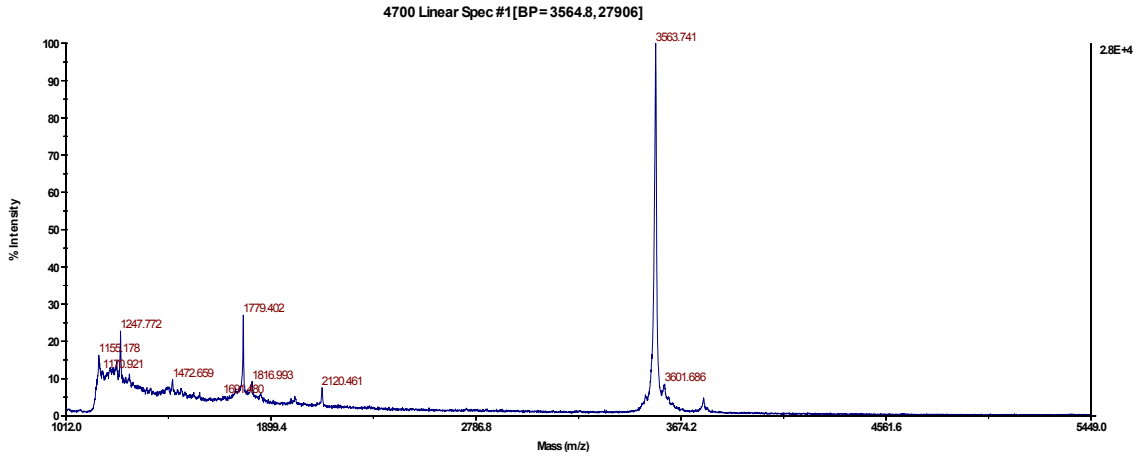


**Figure 78 H2009.1 GGG Biotinylated Dimer**

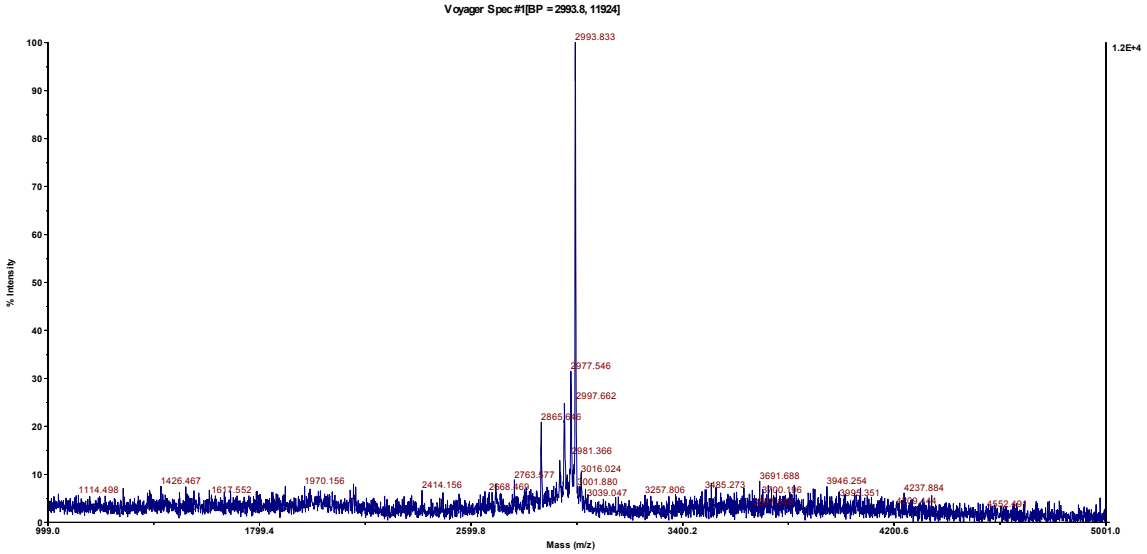


**Figure 79 HCC15.1 Monomer**

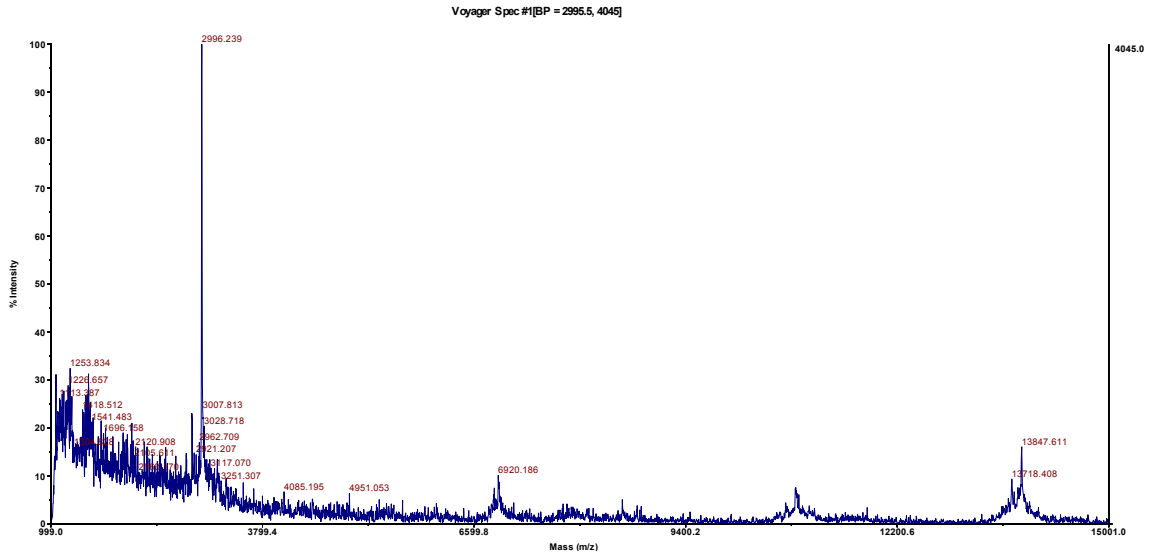


**Figure 80 HCC15.1 Tetramer + AF488**

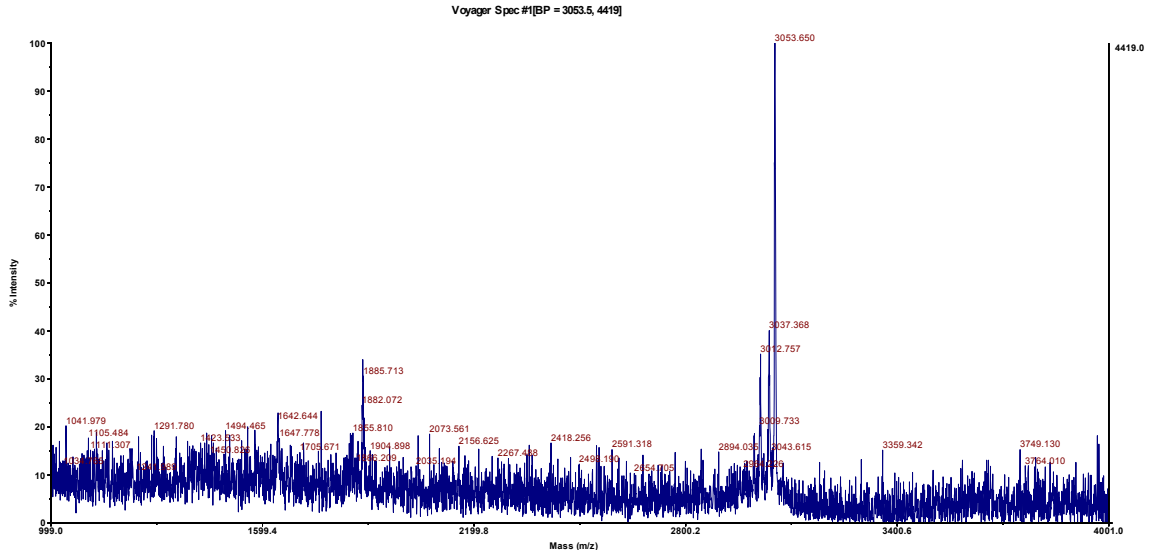


**Figure 81 ScrHCC15.1 Monomer**

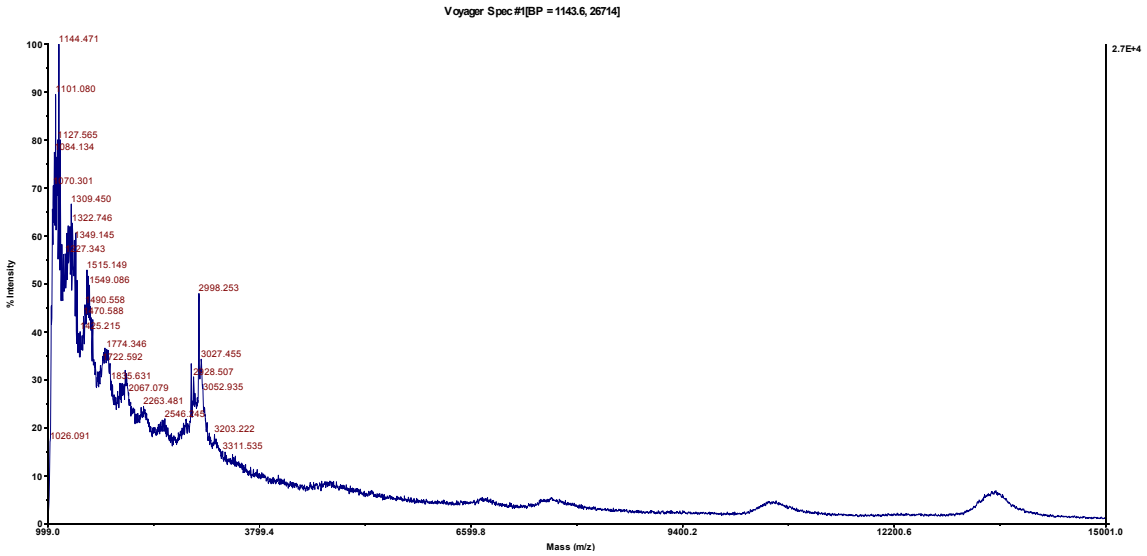


**Figure 82 ScrHCC15.1 Biotinylated Tetramer**

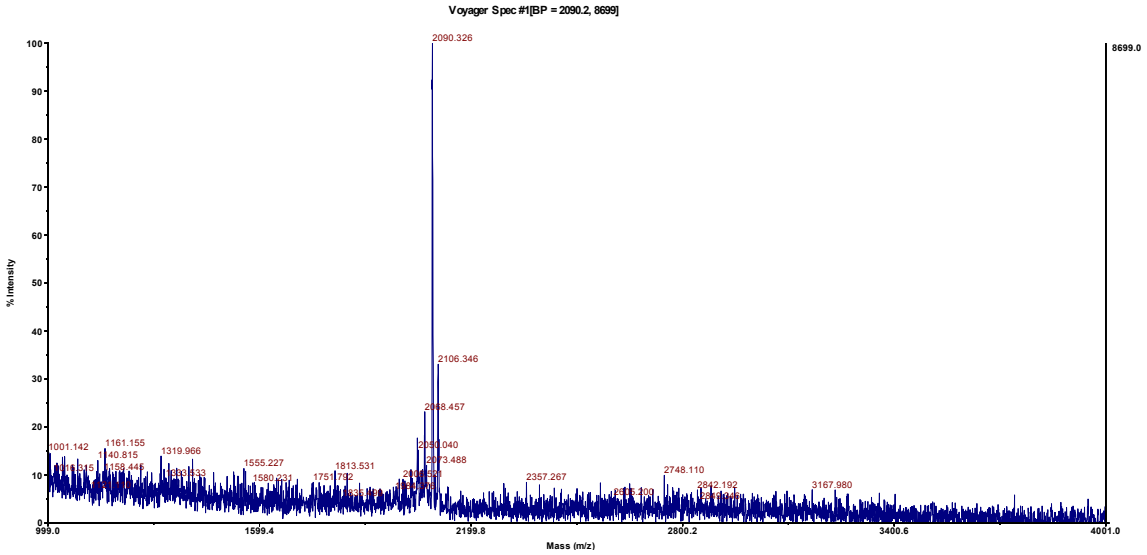


**Figure 83 HCC15.2 Monomer**

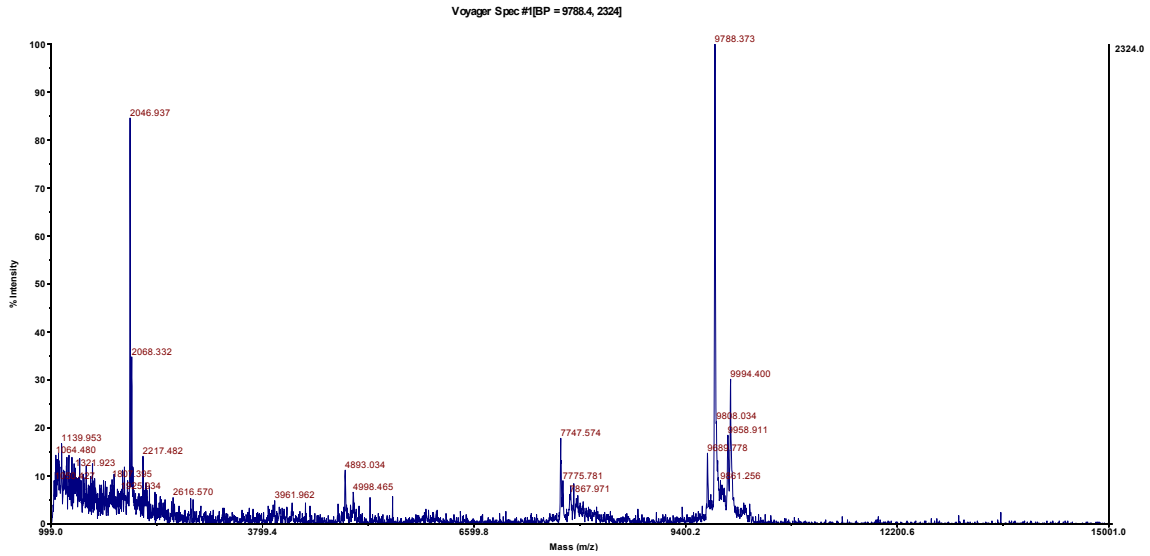


**Figure 84 HCC15.2 Biotinylated Tetramer**

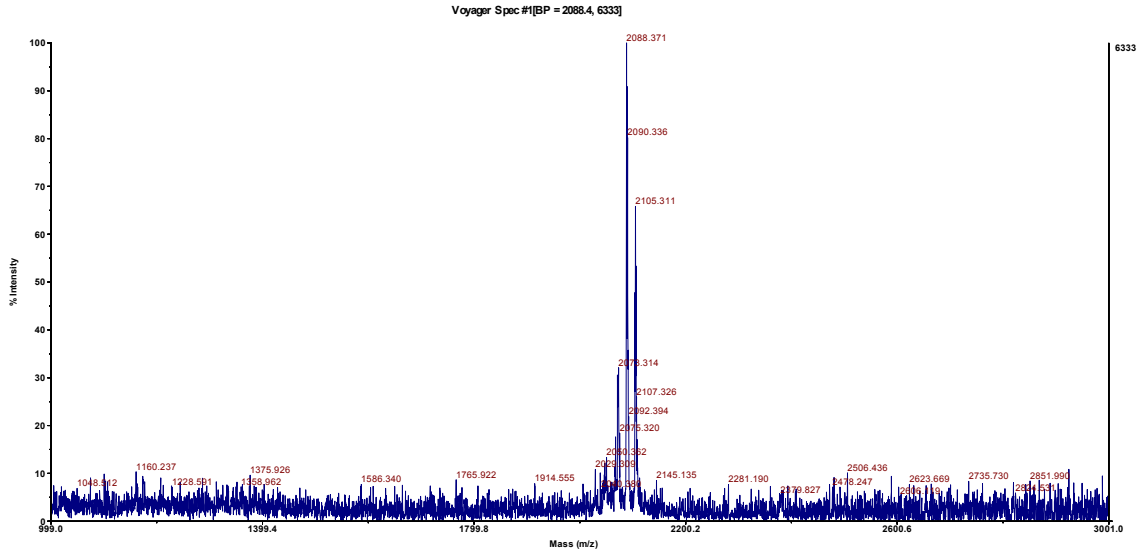


**Figure 85 ScrHCC15.2 Monomer**

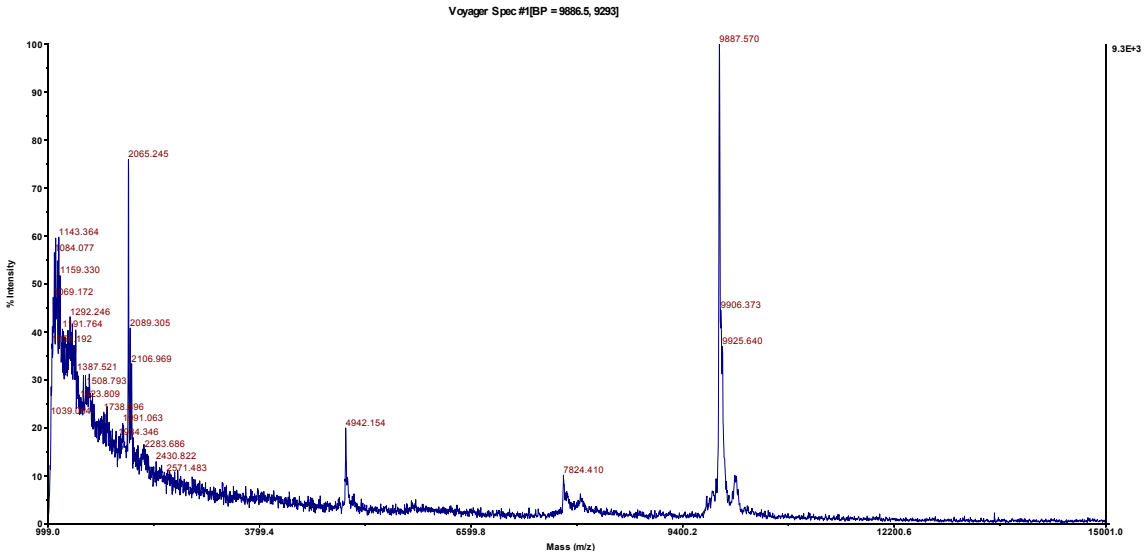


**Figure 86 ScrHCC15.2 Biotinylated Tetramer**

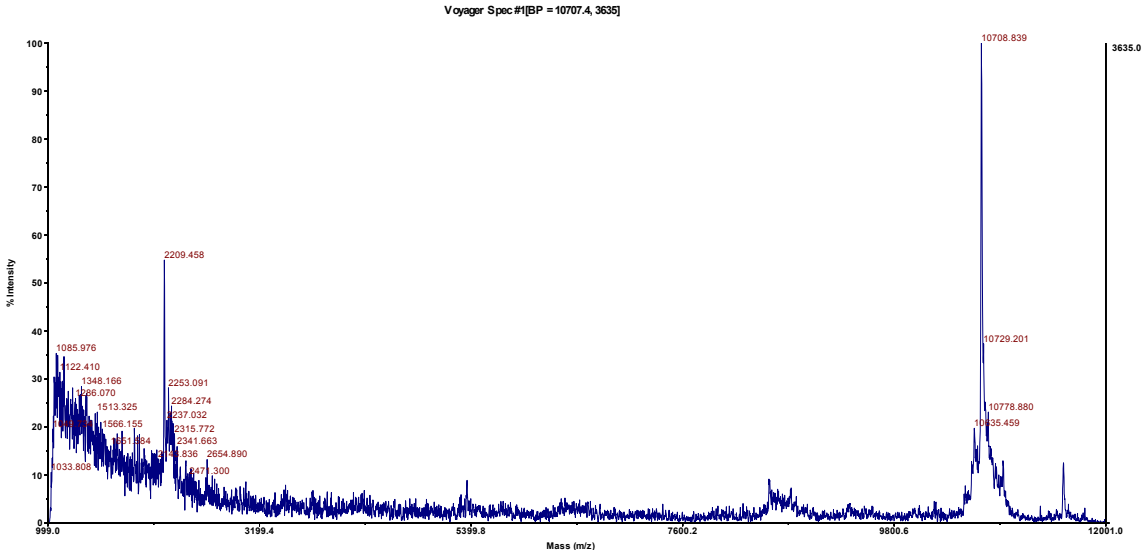


**Figure 87 H1299.2 Tetramer + AF488**

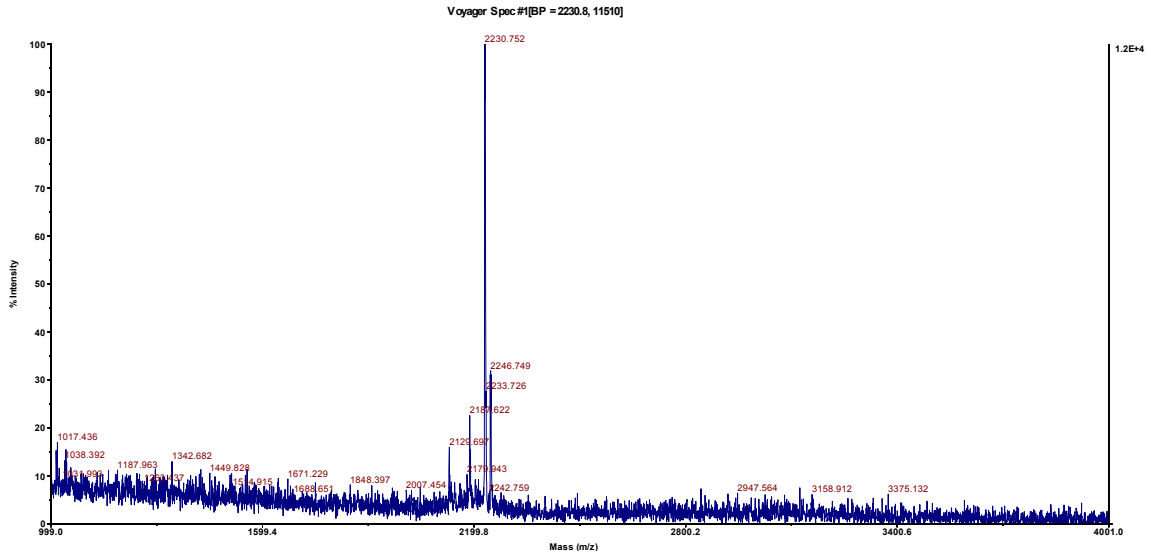


**Figure 88 ScrH1299.2 Monomer**

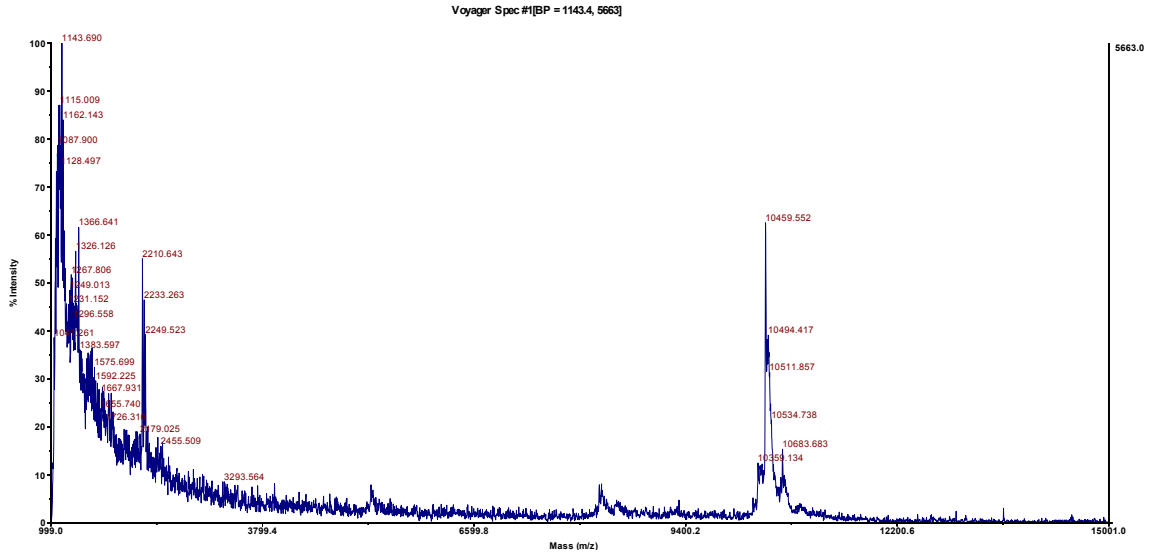


**Figure 89 ScrH1299.2 Biotinylated Tetramer**

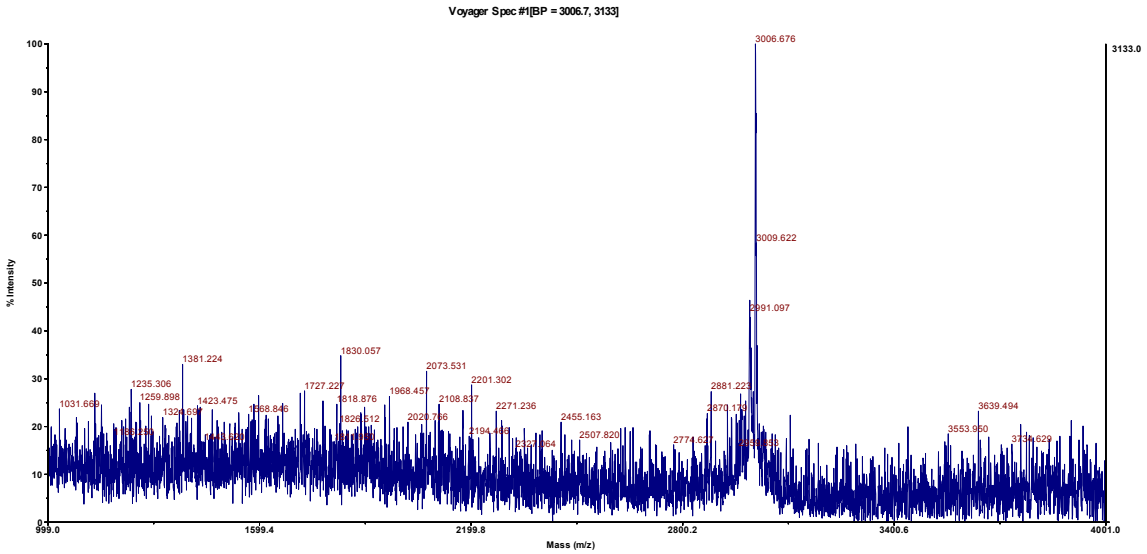


**Figure 90 ScrH460.1 Monomer**

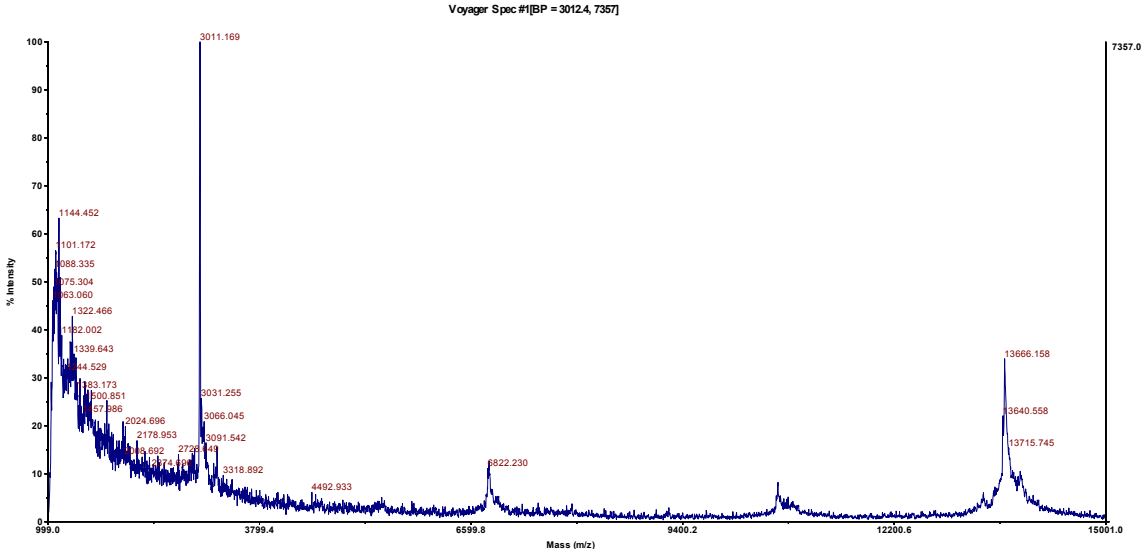


**Figure 91 ScrH460.1 Biotinylated Tetramer**

# APPENDIX C
# MALDI ANALYSIS OF H2009.1 TETRAMER SERUM STABILITY

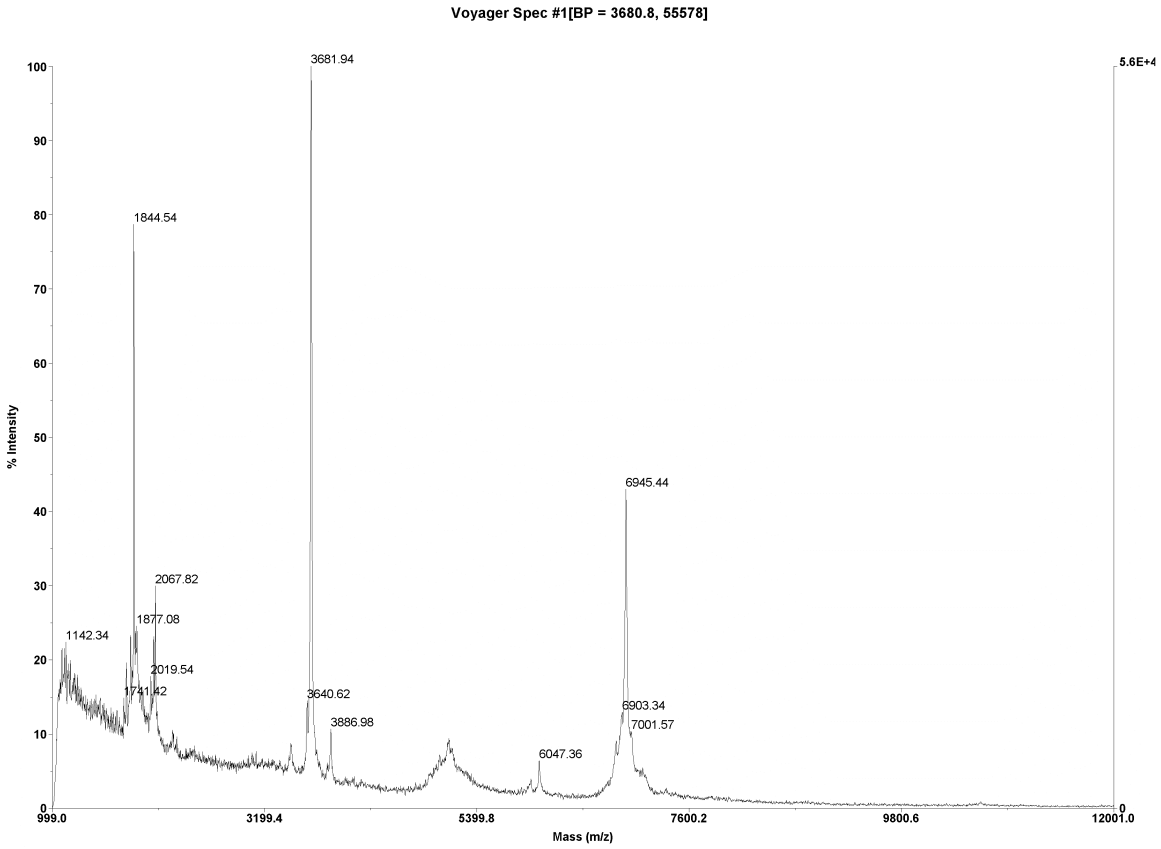


D:\...\Fraction1_0001.dat
Acquired: 10:08:00, April 22, 2011

**Figure 77 H2009.1 4 Hr Fraction 1**

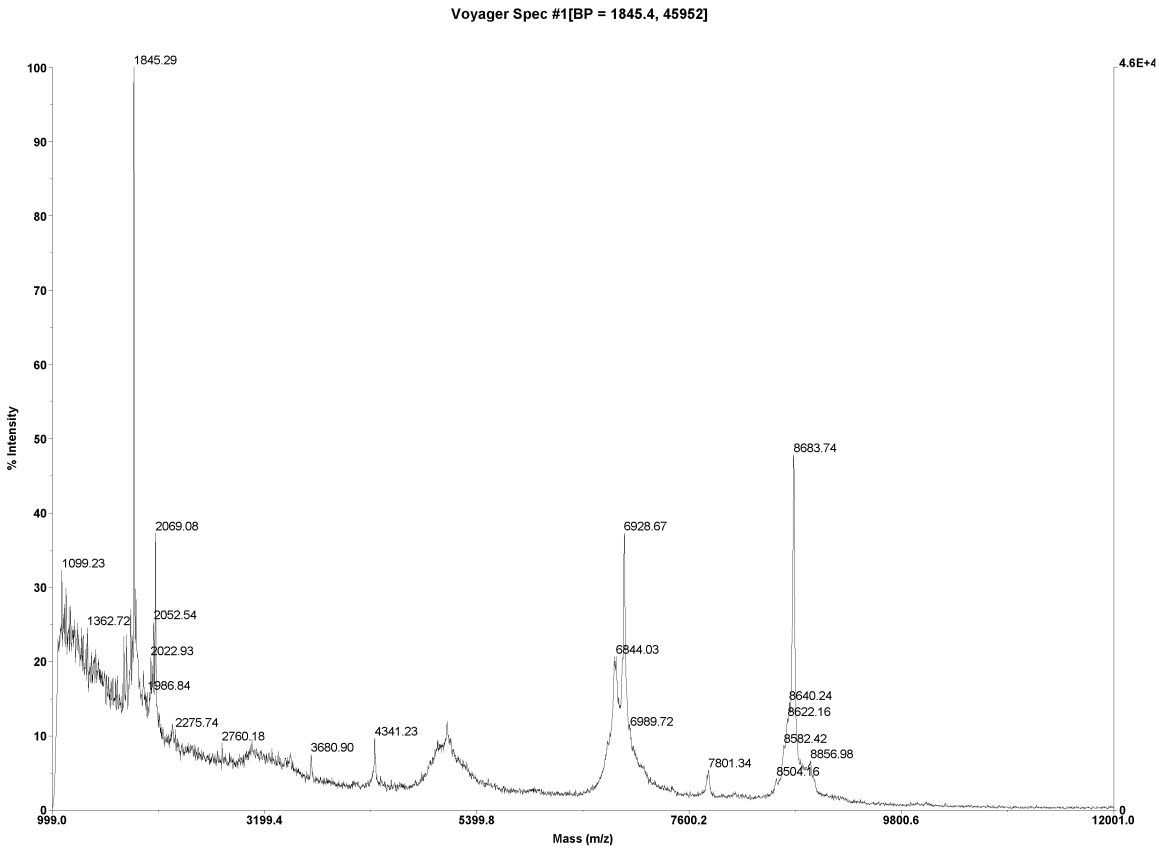


D:\...\Fraction2_0001.dat
Acquired: 10:09:00, April 22, 2011

**Figure 78 H2009.1 4 Hr Fraction 2**

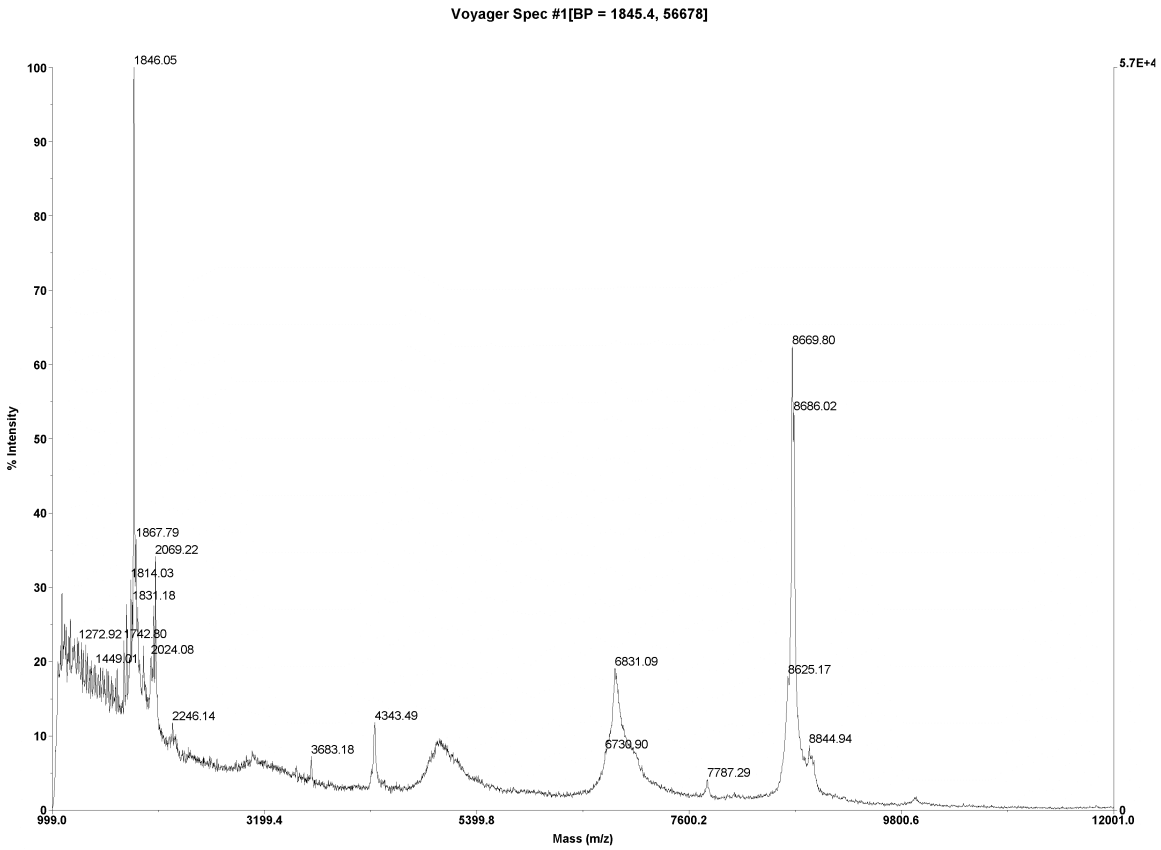


D:\...\Fraction3_0001.dat
Acquired: 10:09:00, April 22, 2011

**Figure 79 H2009.1 4 Hr Fraction 3**

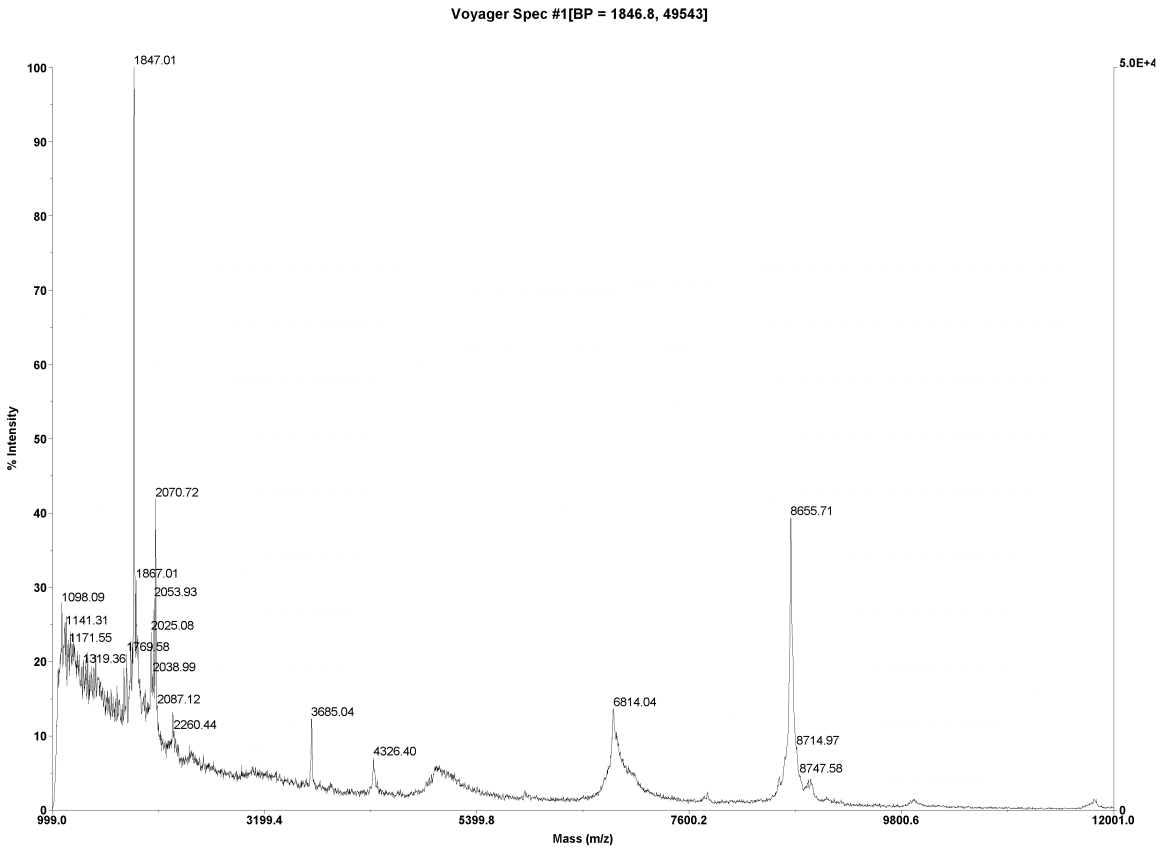


**Figure 80 H2009.1 4 Hr Fraction 4**

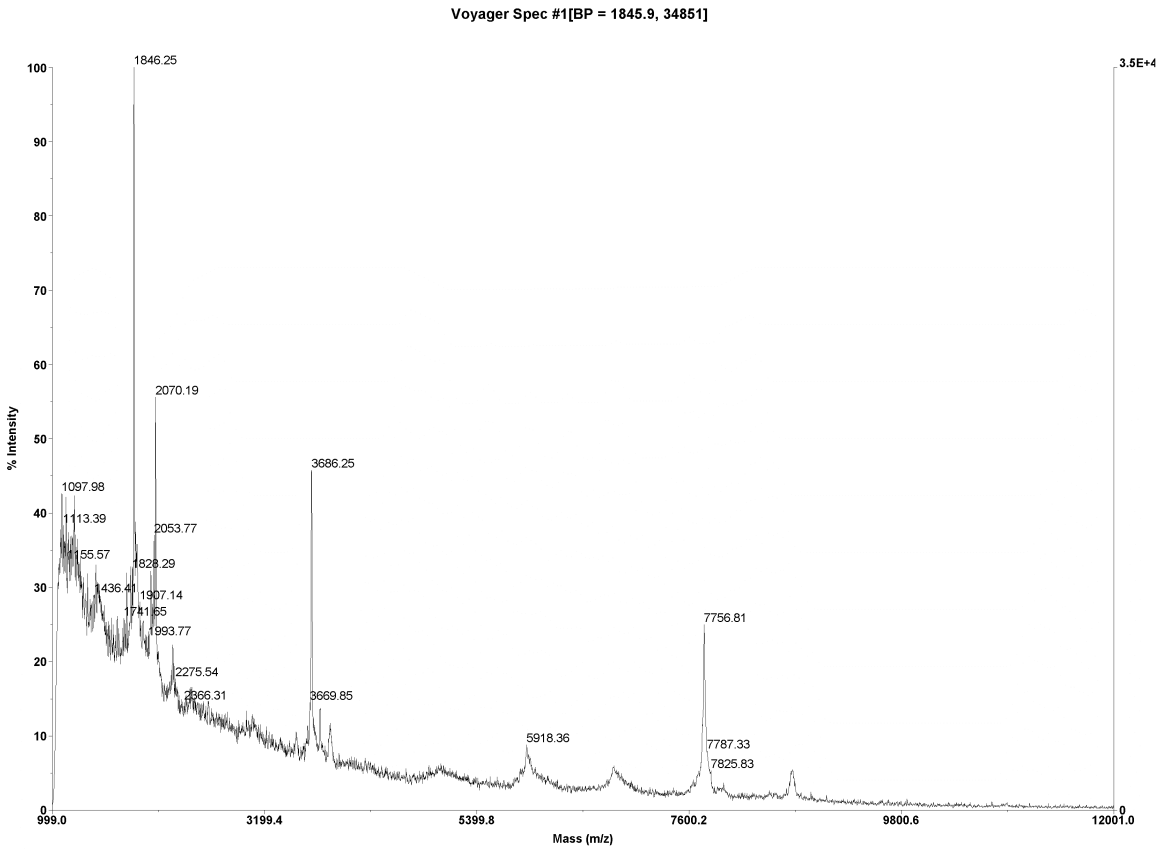


**Figure 81 H2009.1 4 Hr Fraction 5**

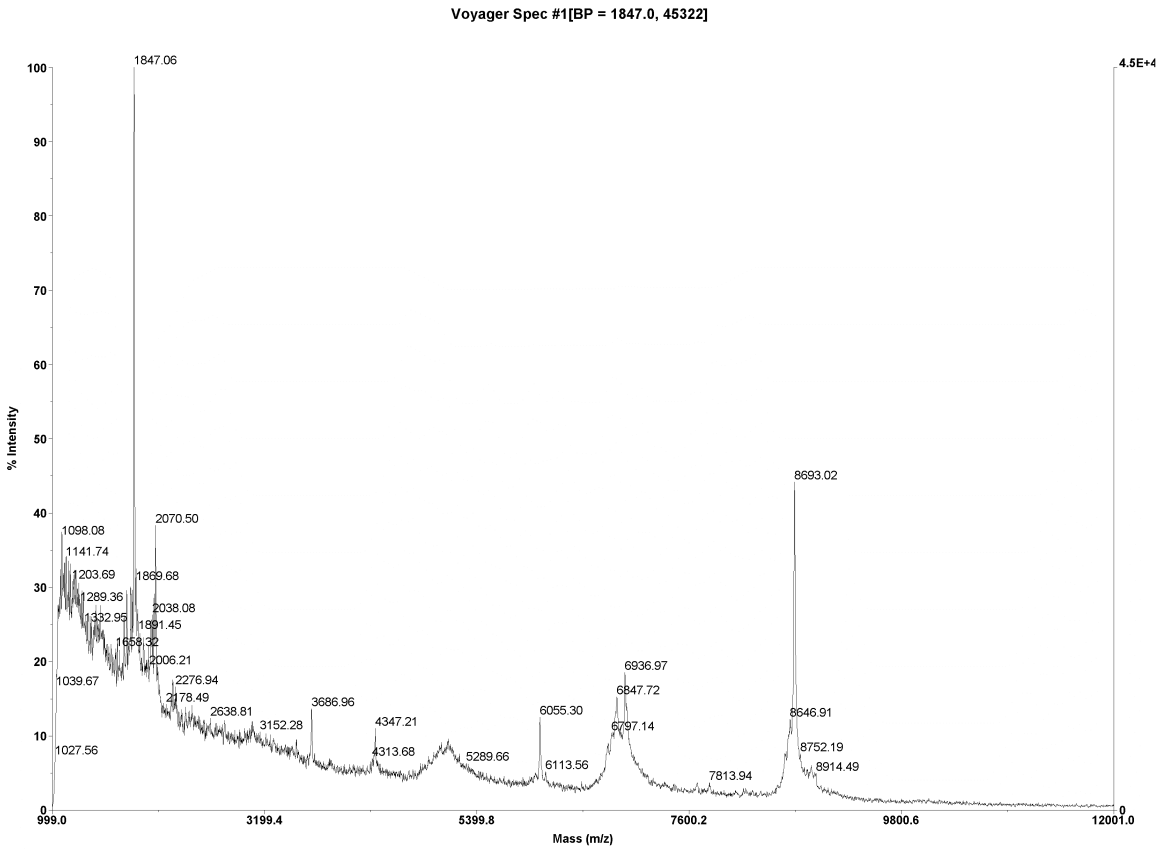


D:\...\Fraction1_0001.dat
Acquired: 10:11:00, April 22, 2011

**Figure 82 H2009.1 24 Hr Fraction 1**

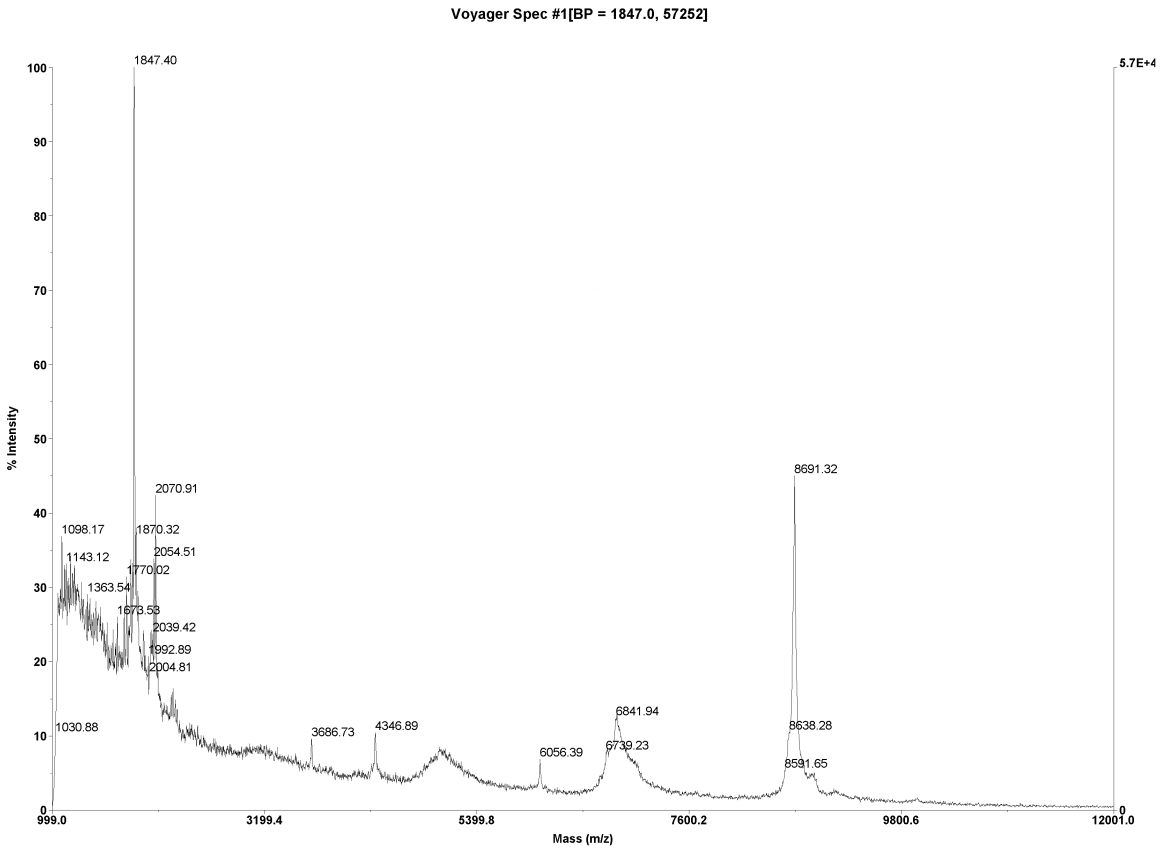


D:\...\Fraction2_0001.dat
Acquired: 10:11:00, April 22, 2011

**Figure 83 H2009.1 24 Hr Fraction 2**

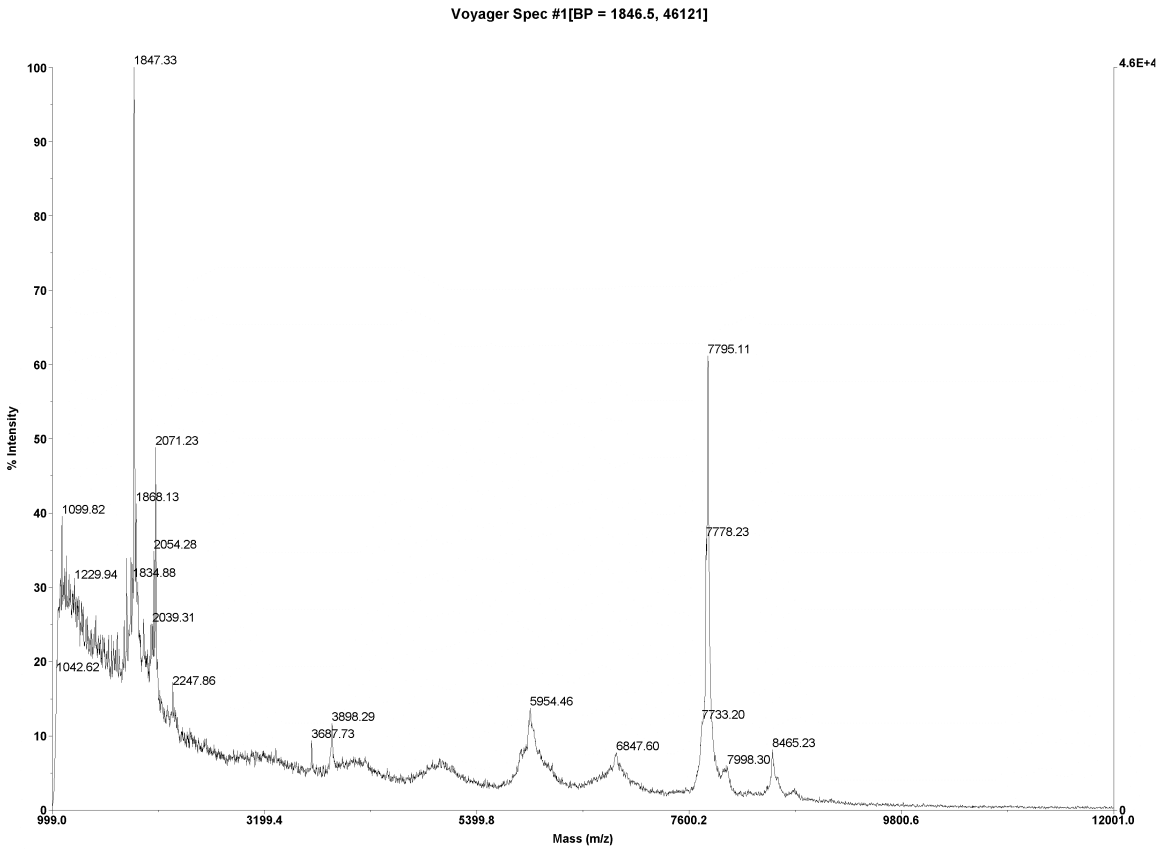


D:\...\Fraction3_0001.dat
Acquired: 10:12:00, April 22, 2011

**Figure 84 H2009.1 42 Hr Fraction 3**

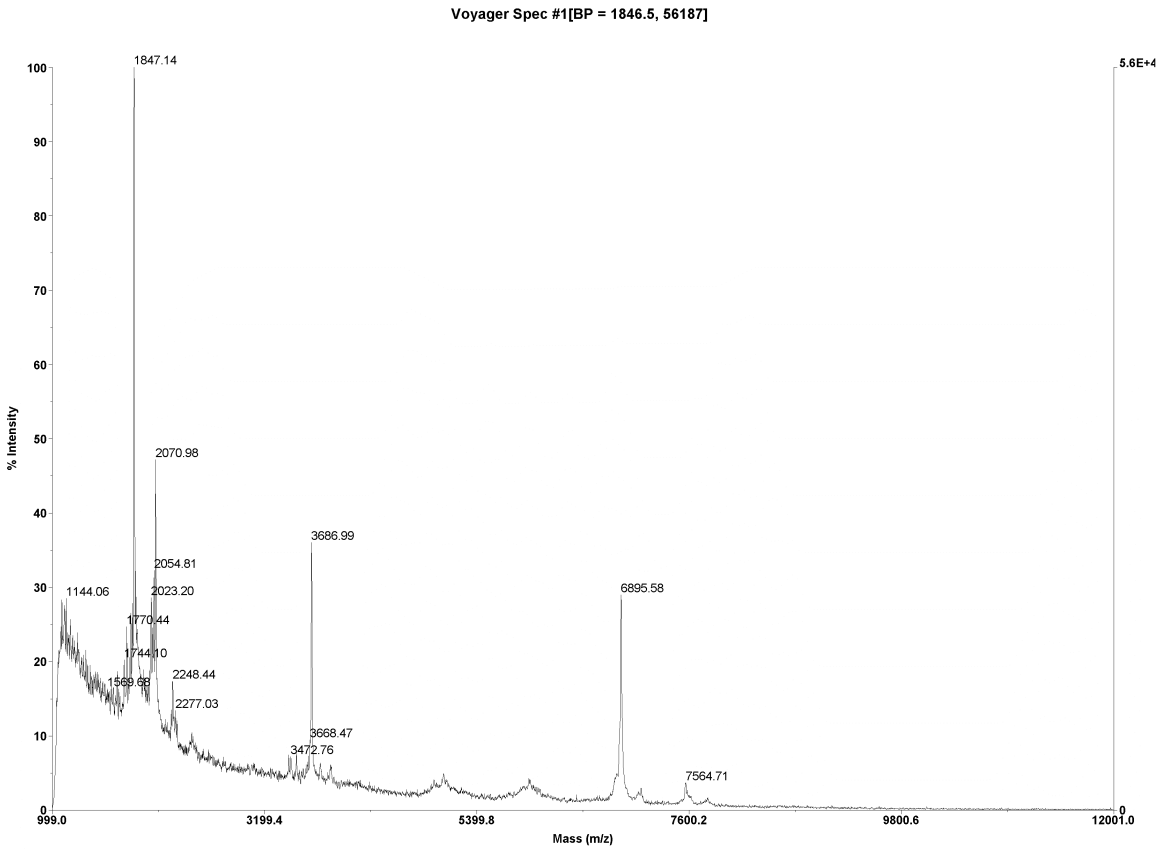


D:\...\Fraction4_0001.dat
Acquired: 10:12:00, April 22, 2011

**Figure 85 H2009.1 24 Hr Fraction 4**

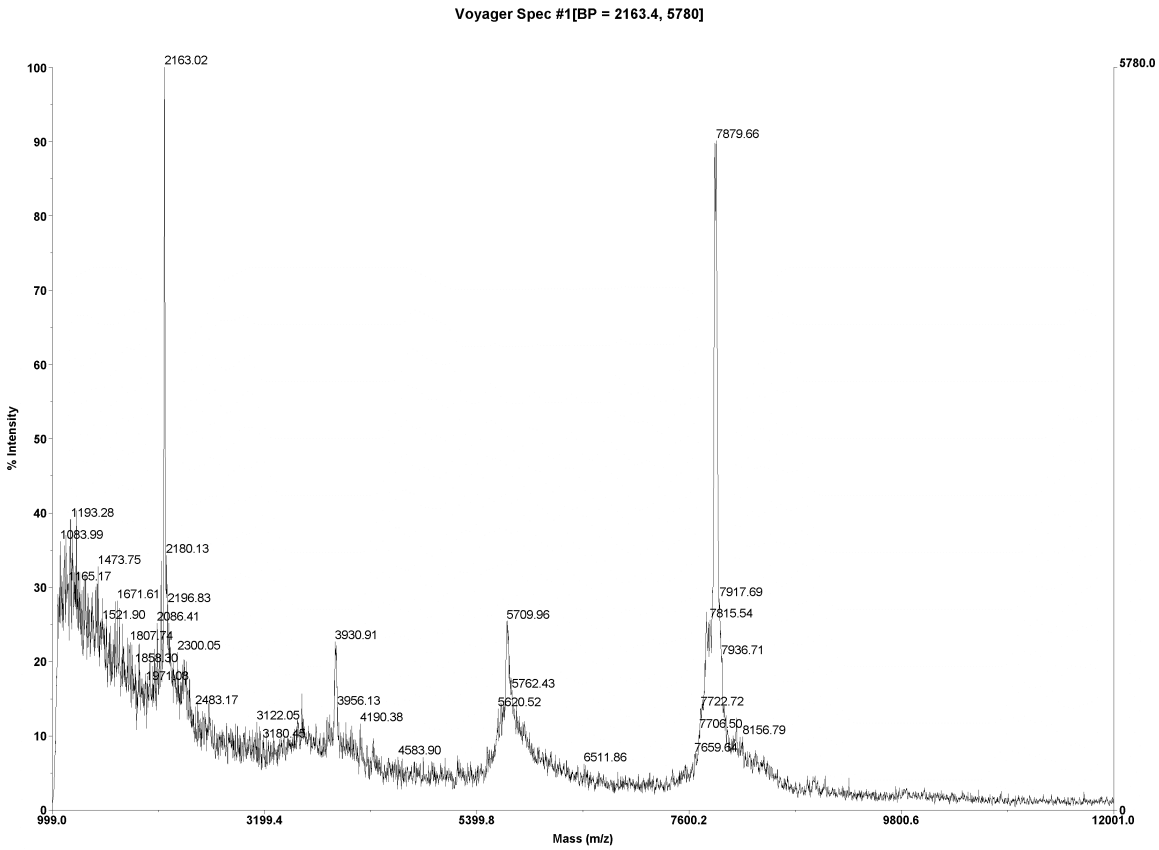


D:\...\4 Hr 4.27.2013_0001.dat
Acquired: 15:00:00, April 28, 2013

**Figure 86 AcD-Leu H2009.1 4 Hr Fraction 1**

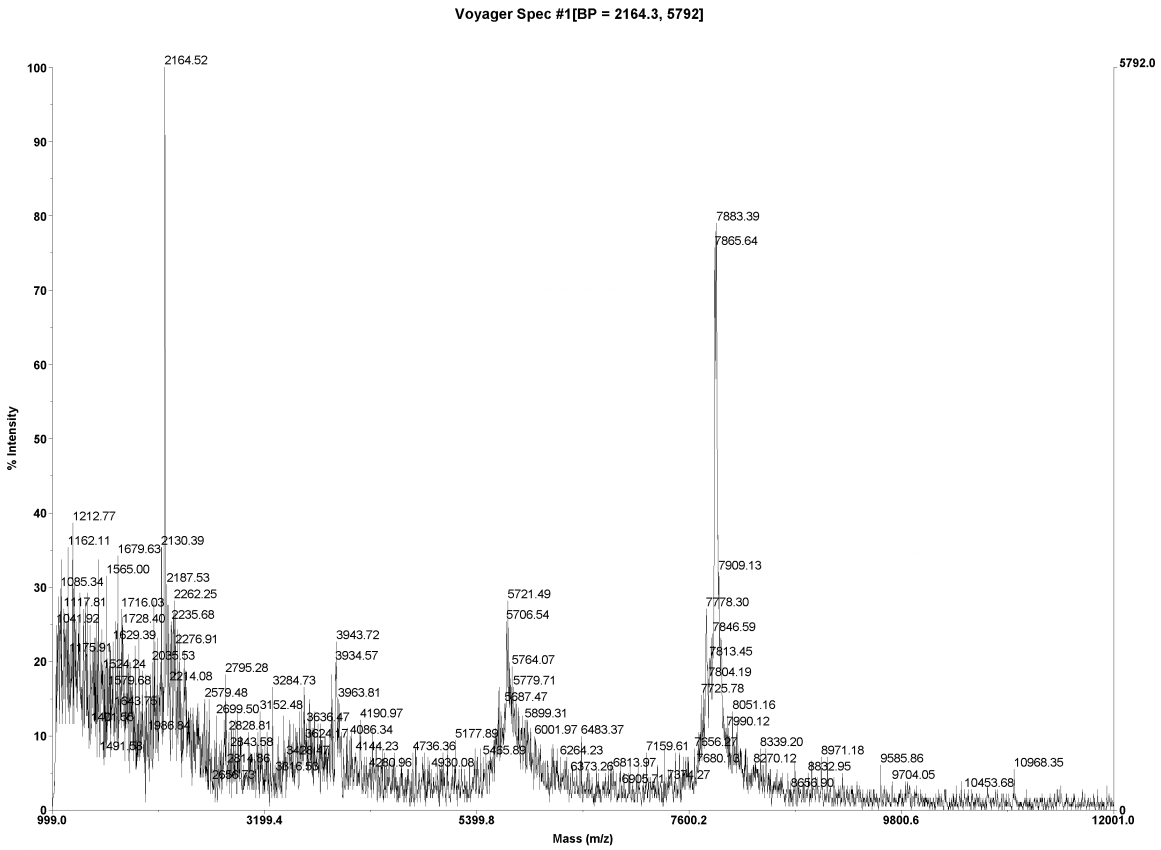


D:\...\4 Hr 4.27.2013_0002.dat
Acquired: 15:00:00, April 28, 2013

**Figure 87 AcD-Leu H2009.1 4 Hr Fraction 2**

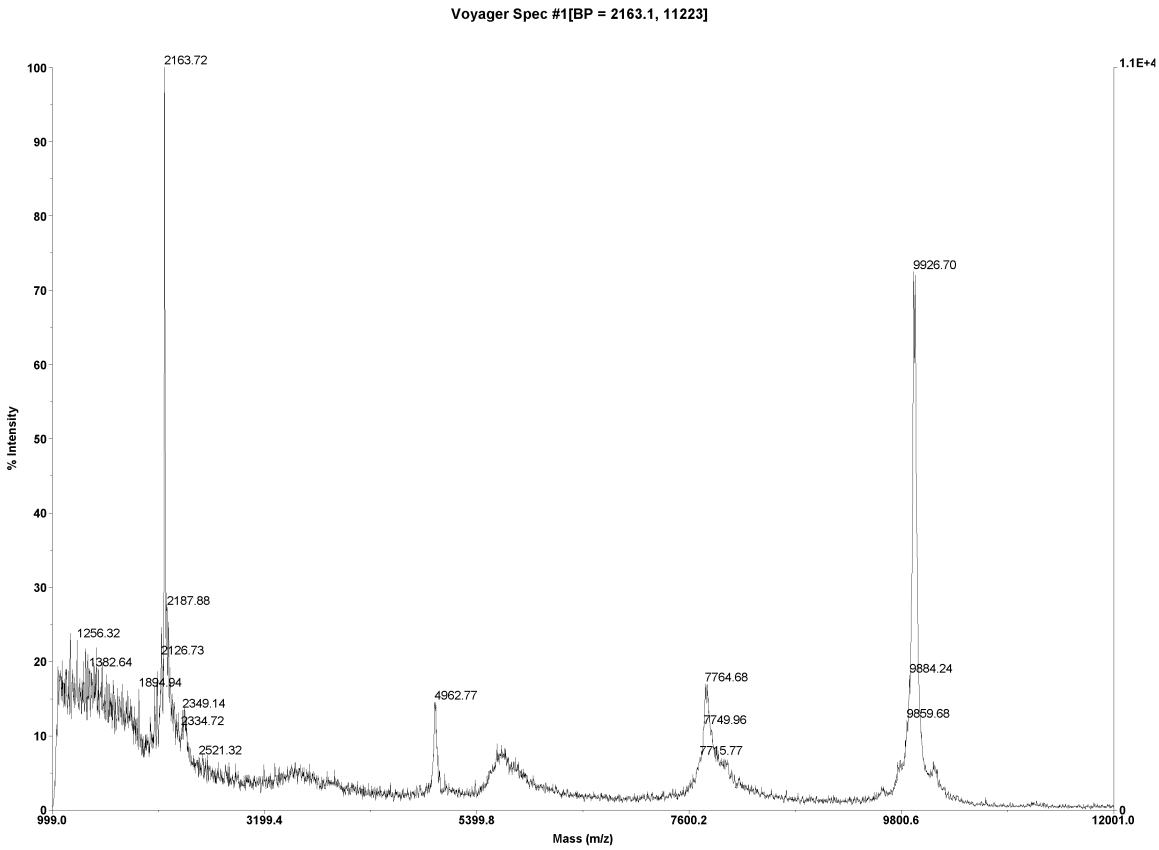


D:\...\4 Hr 4.27.2013_0003.dat
Acquired: 15:01:00, April 28, 2013

**Figure 88 AcD-Leu H2009.1 4 Hr Fraction 3**

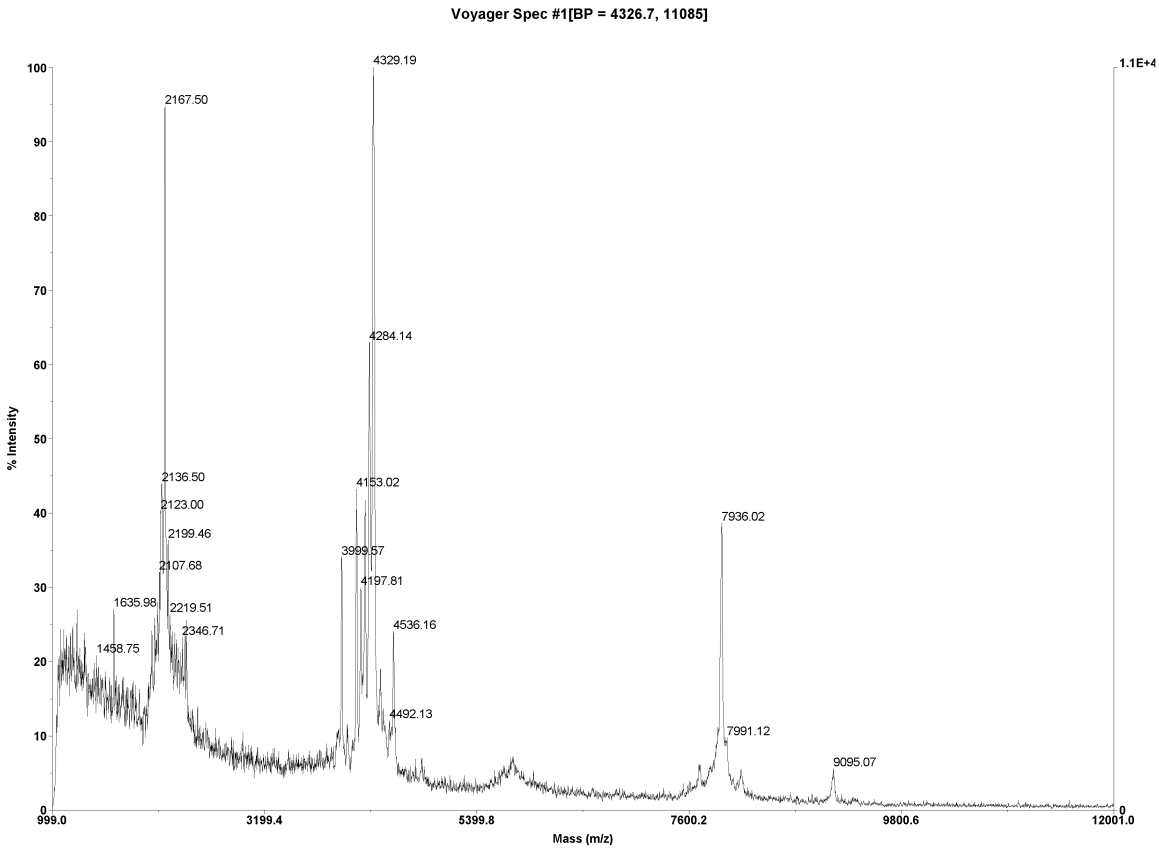


**Figure 89 AcD-Leu H2009.1 24 Hr Fraction 1**

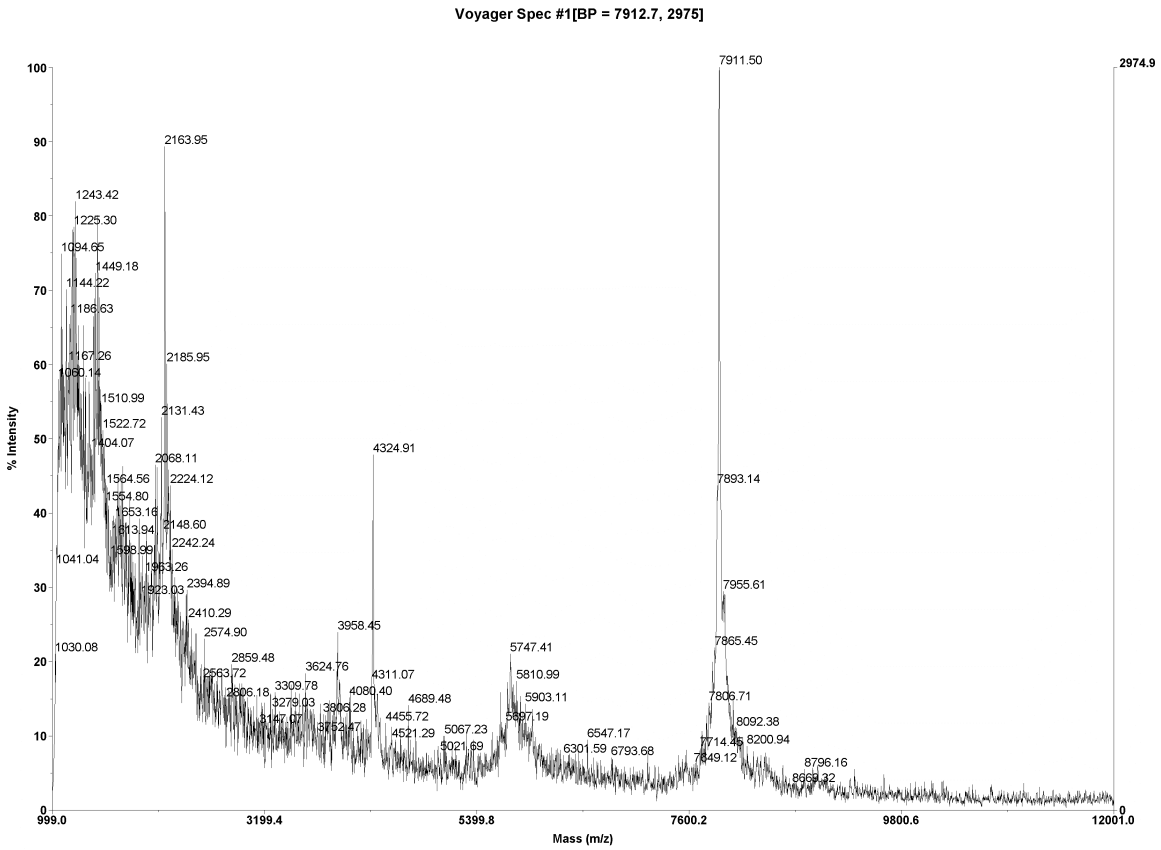


**Figure 90 AcD-Leu H2009.1 24 Hr Fraction 2**

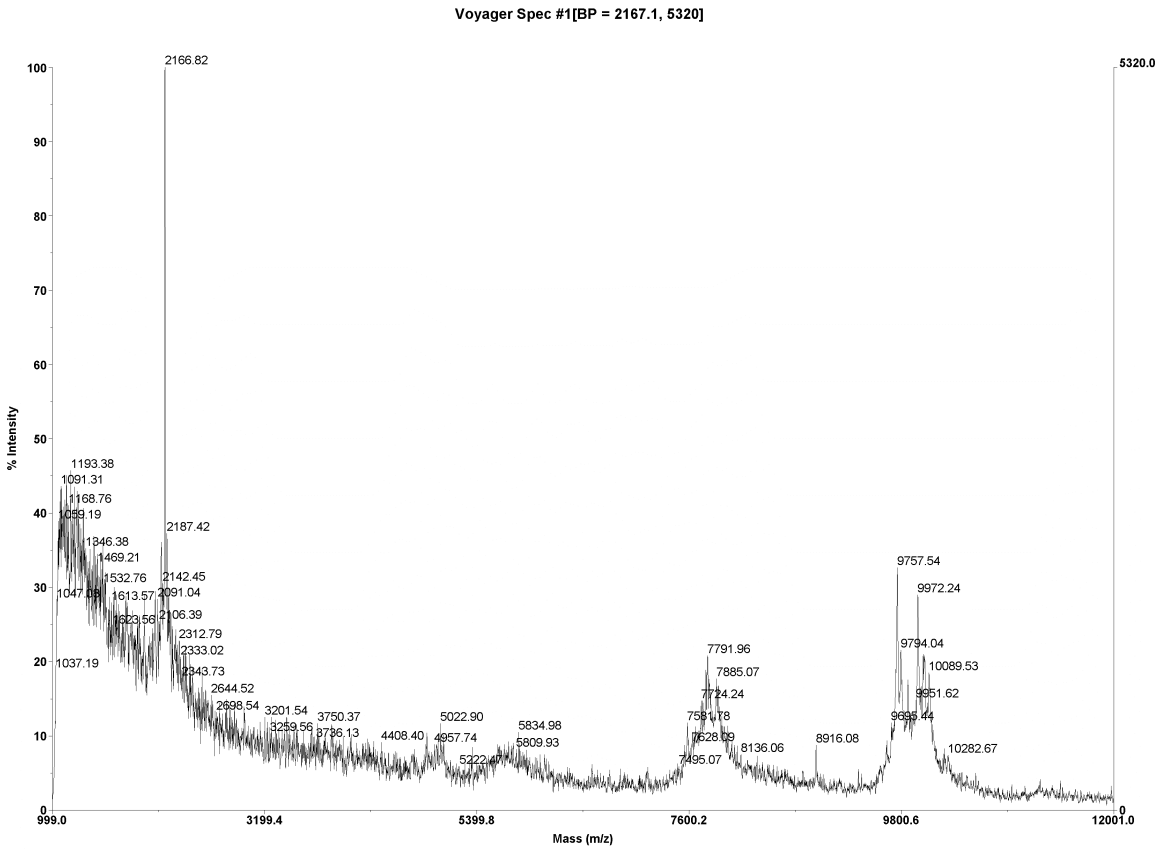


**Figure 91 AcD-Leu H2009.1 24 Hr Fraction 3**

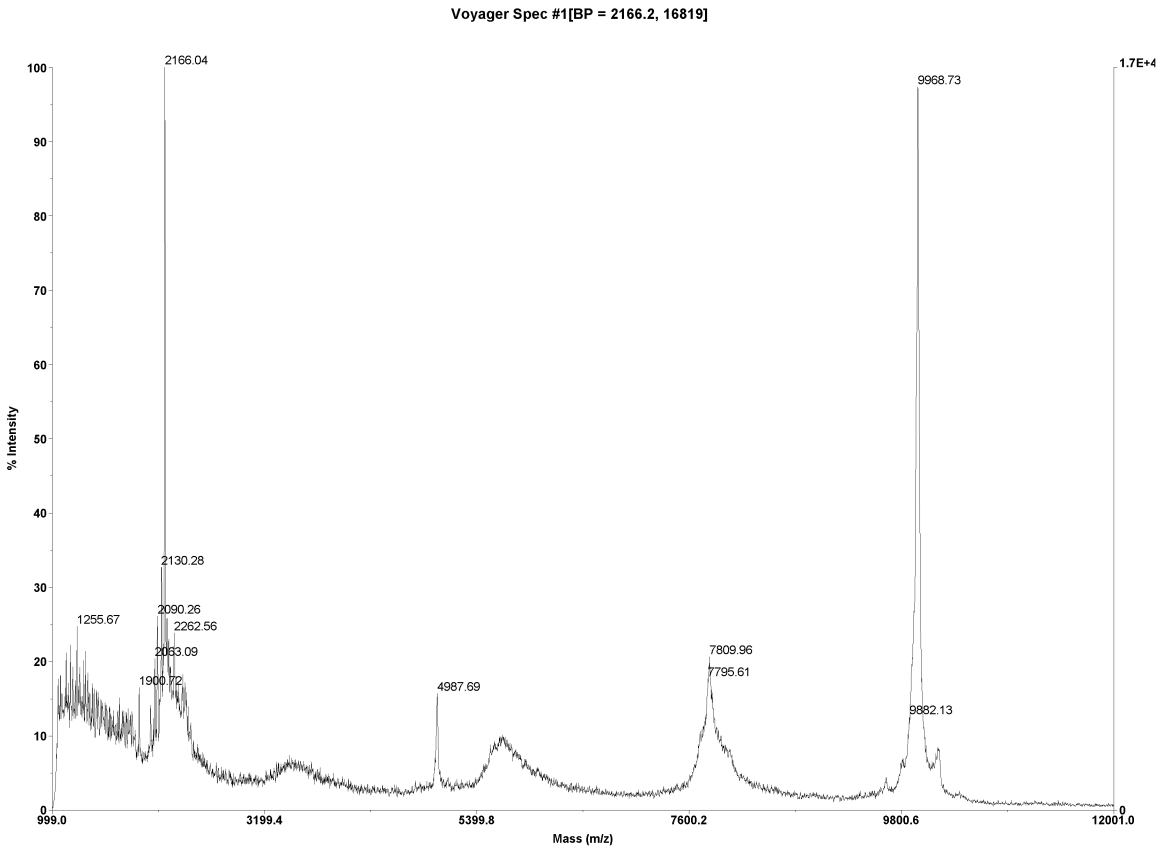


**Figure 92 AcD-Leu H2009.1 24 Hr Fraction 4**

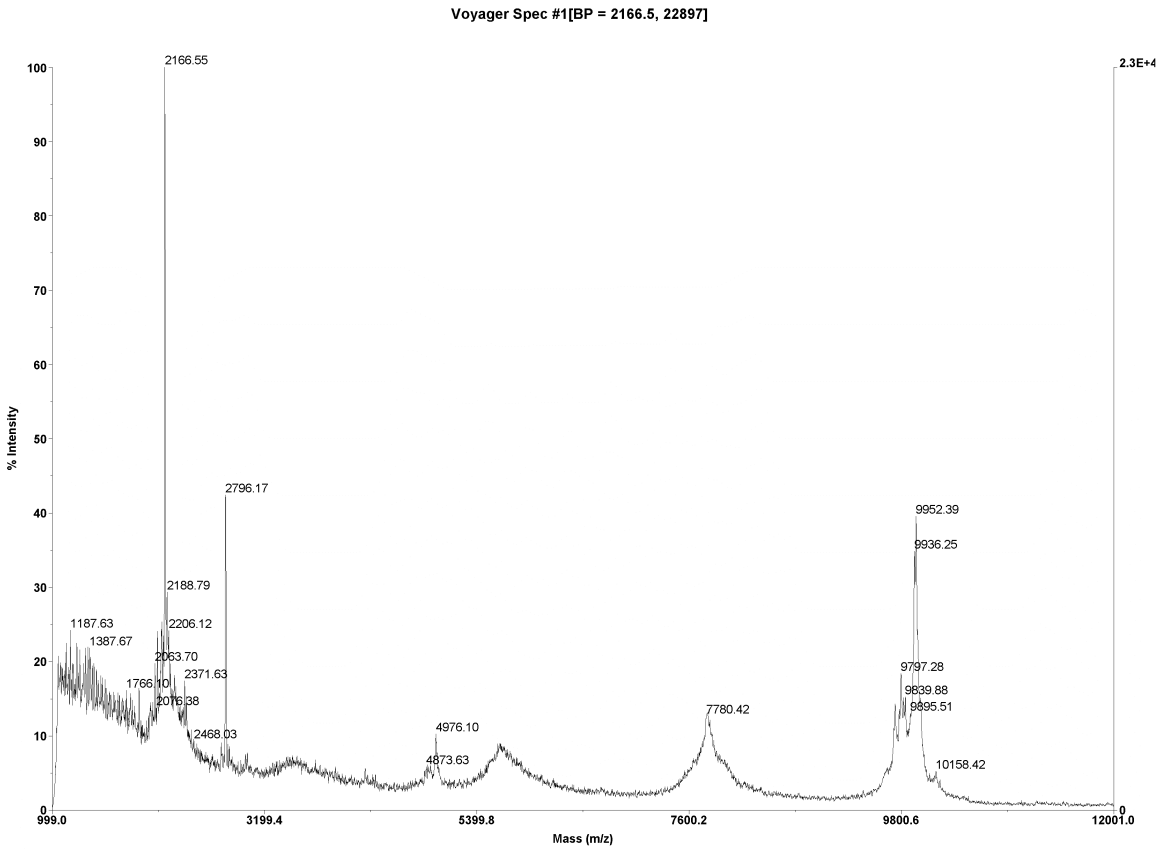


**Figure 93 AcD-Leu H2009.1 24 Hr Fraction 5**

# APPENDIX D
# ANALYTICAL HPLC AND MALDI ANALYSIS OF H2009.1 DIMER SERUM STABILITY

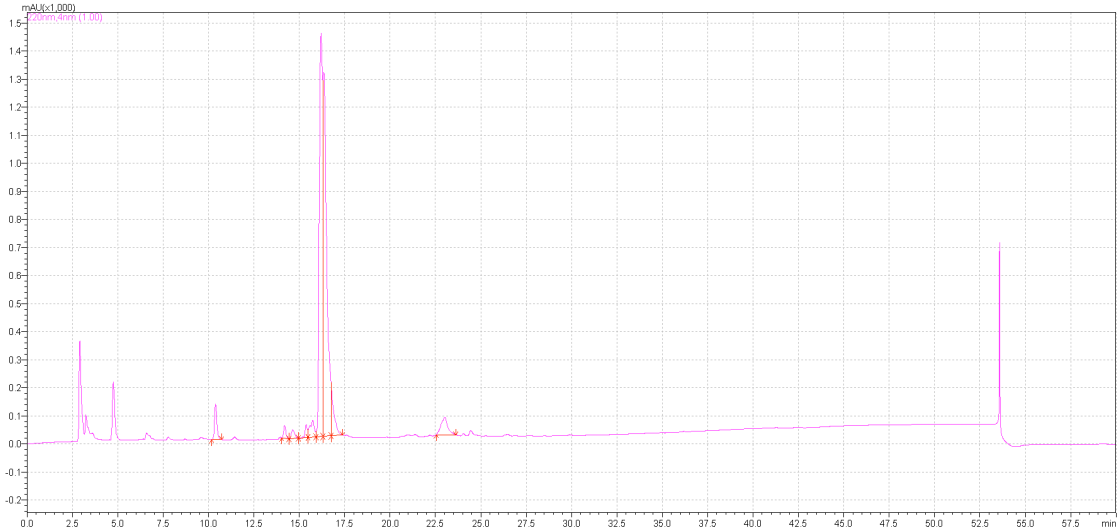


Figure 94 H2009.1 0 Hr

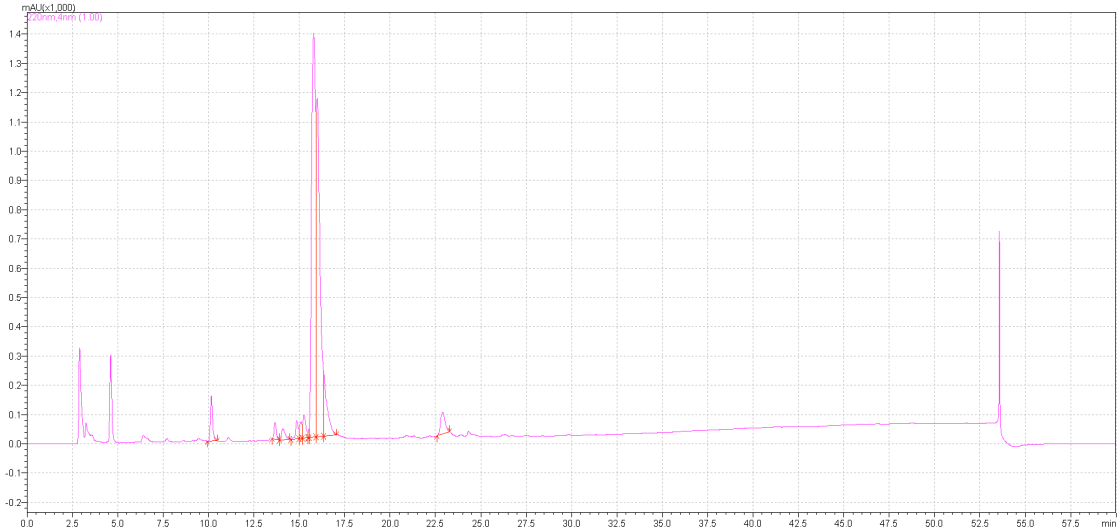


Figure 95 H2009.1 1 Hr

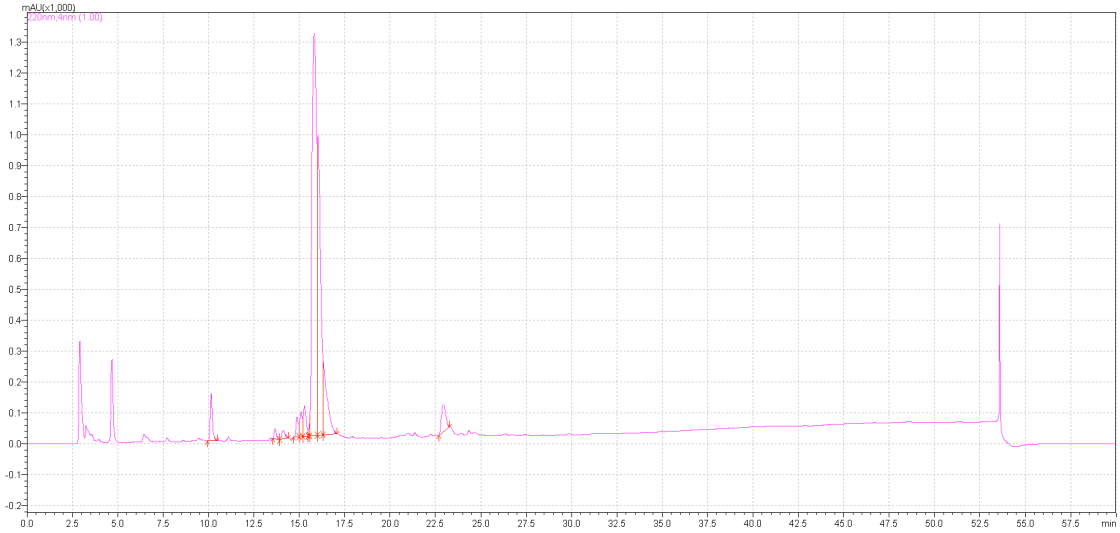


**Figure 96 H2009.1 4 Hr**

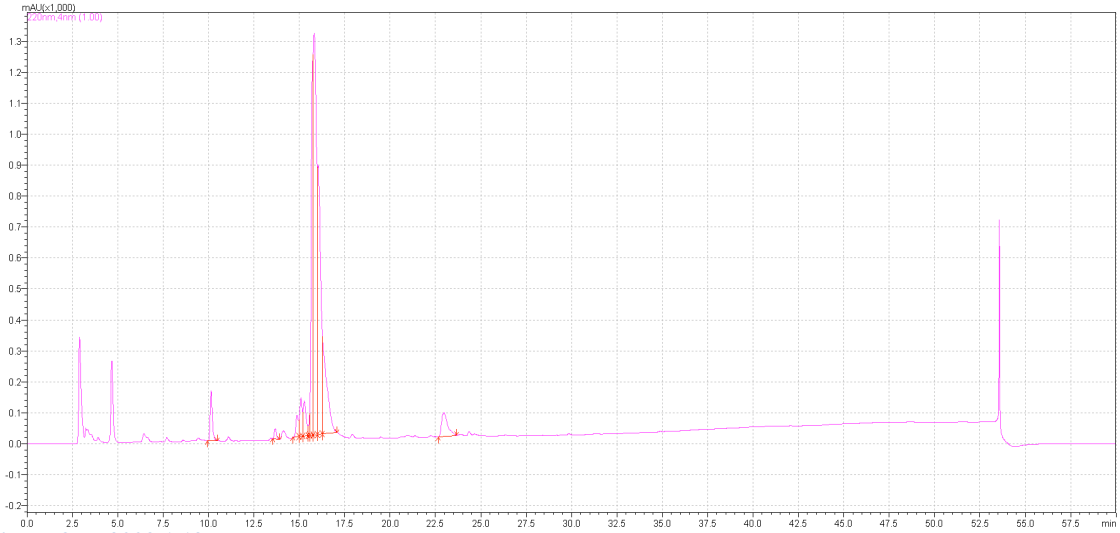


**Figure 97 H2009.1 12 Hr**

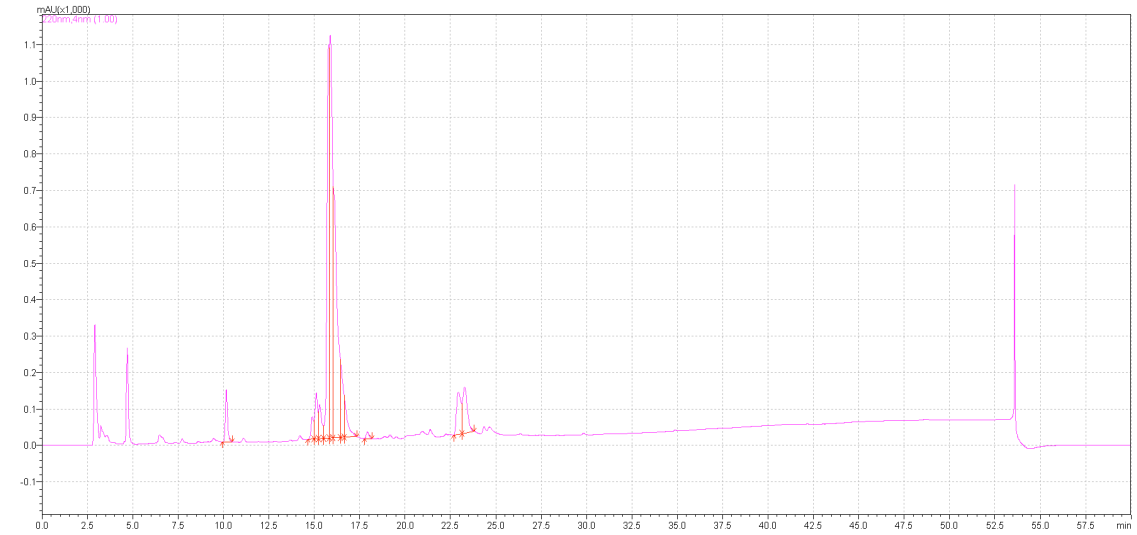


Figure 98 H2009.1 24 Hr

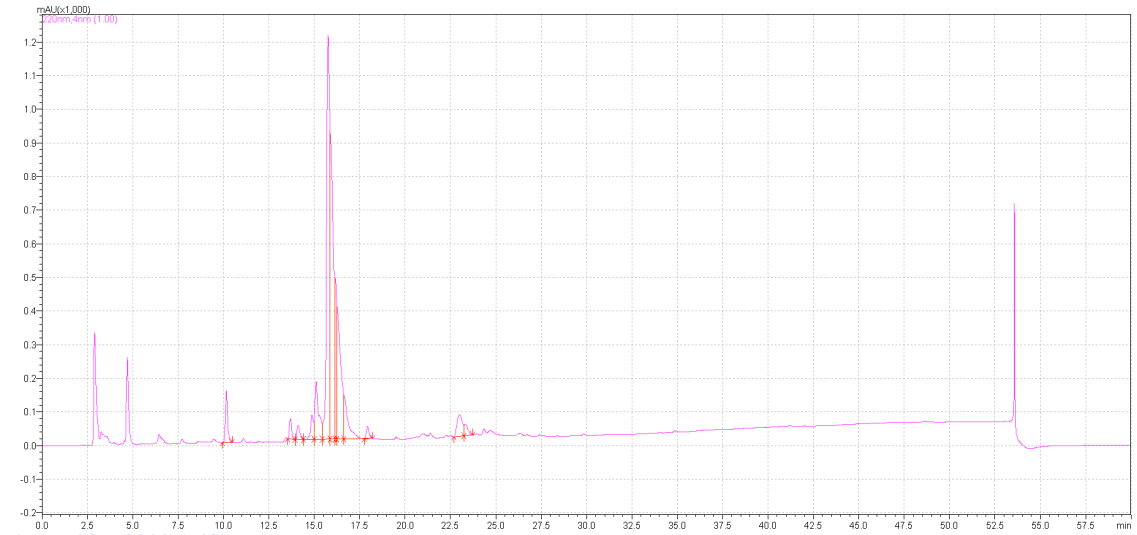


Figure 99 H2009.1 48 Hr

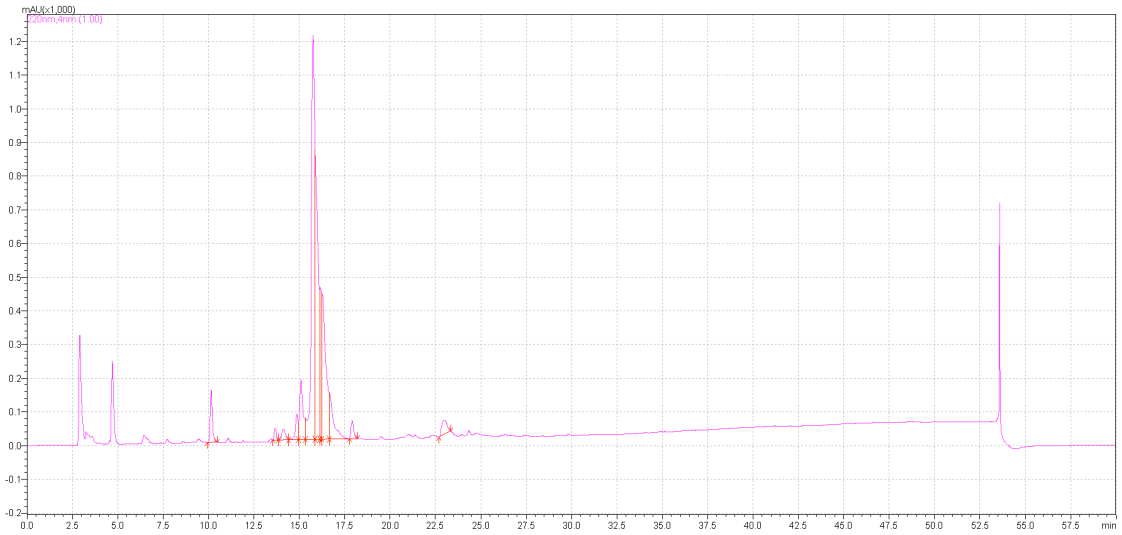


Figure 100 H2009.1 72 Hr

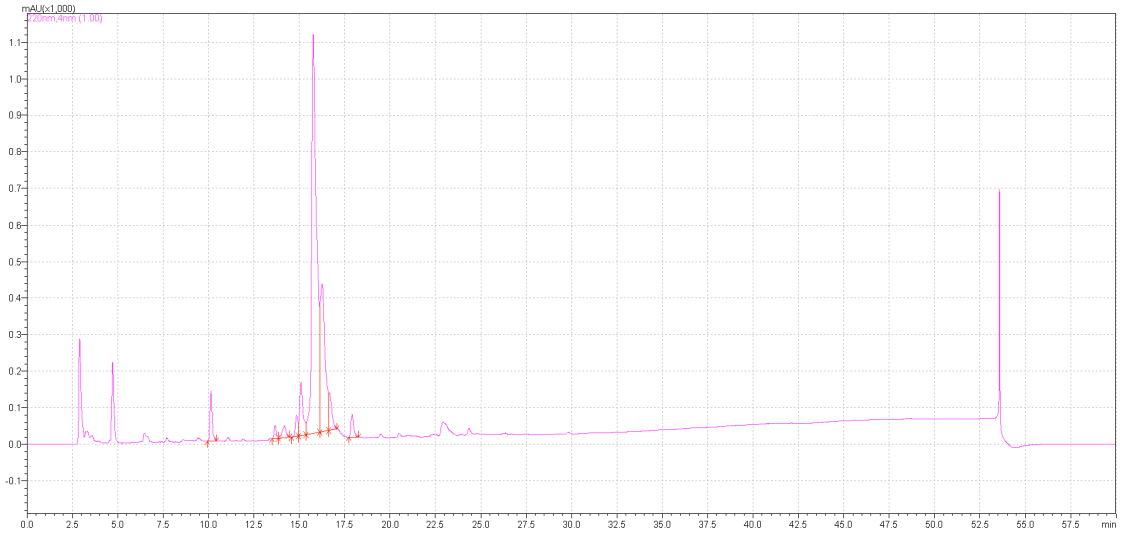


Figure 101 H2009.1 96 Hr

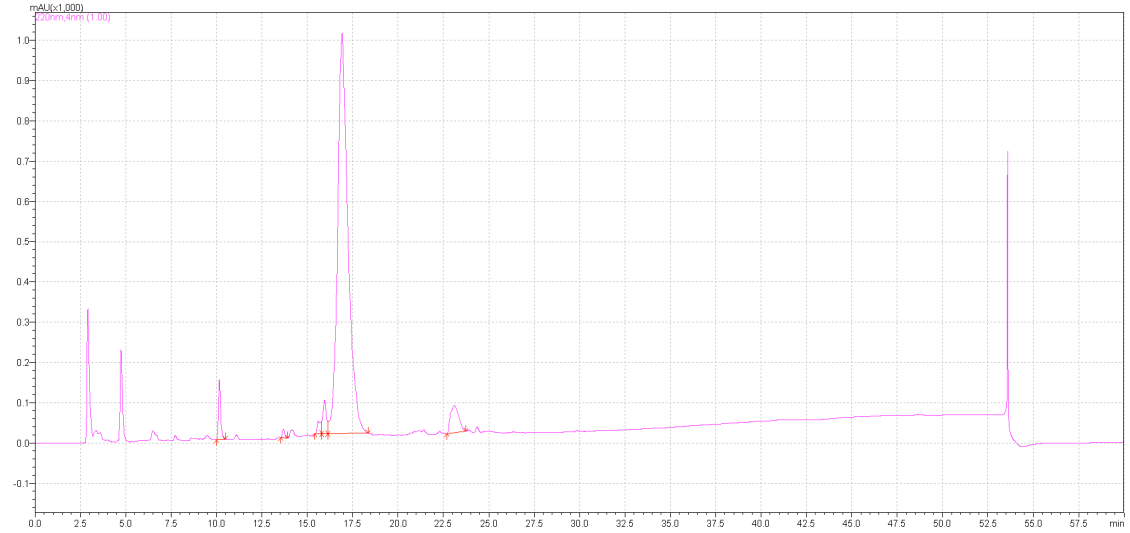


**Figure 102 AcH2009.1 0 Hr**

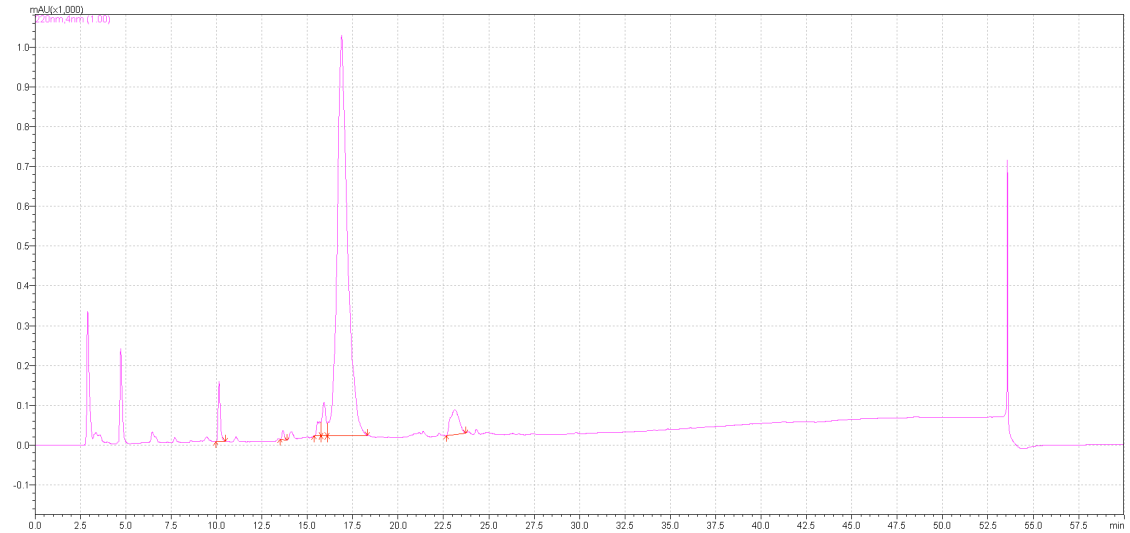


**Figure 103 AcH2009.1 1 Hr**

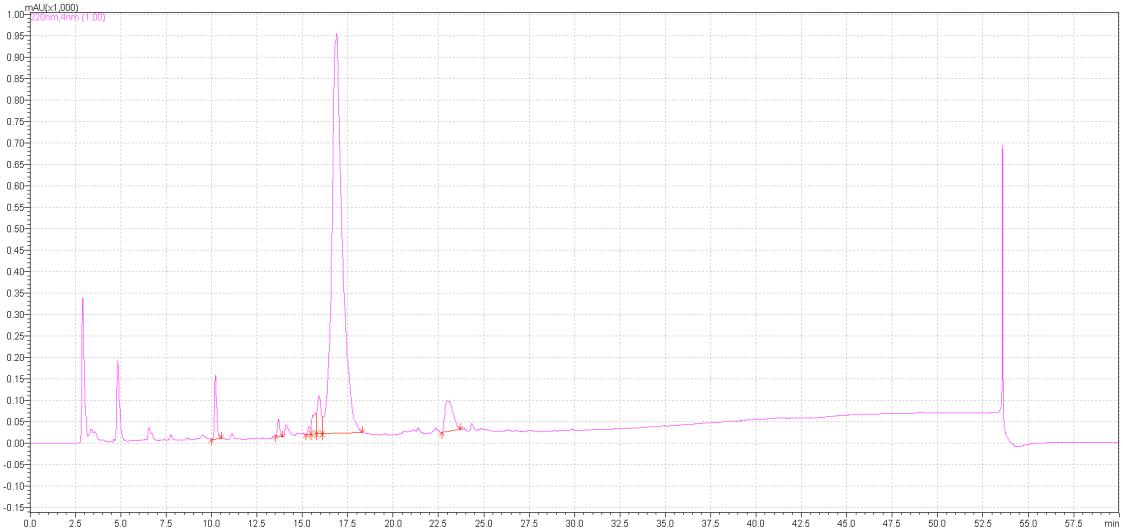


Figure 104 AcH2009.1 4 Hr

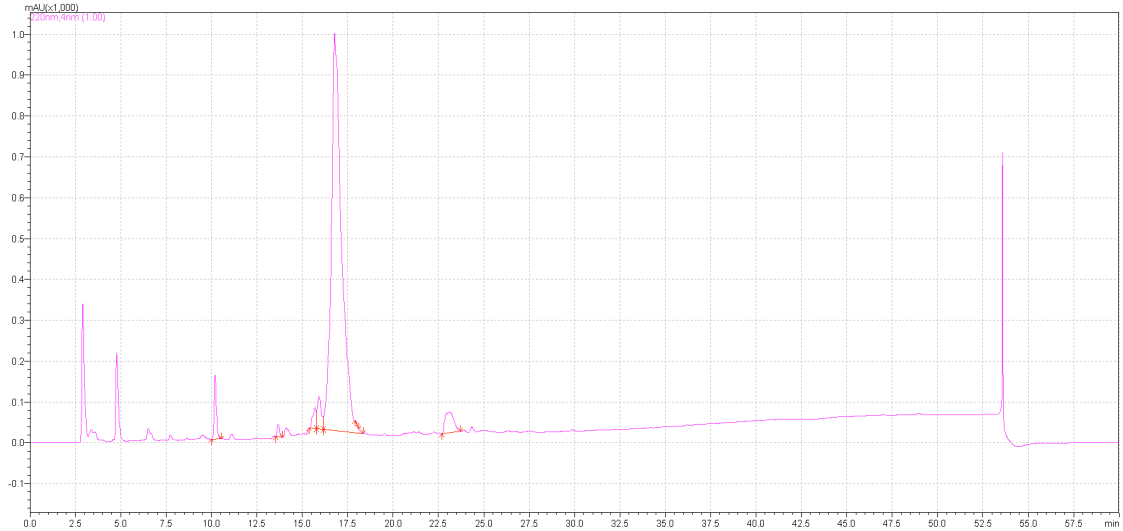


Figure 105 AcH2009.1 12 Hr

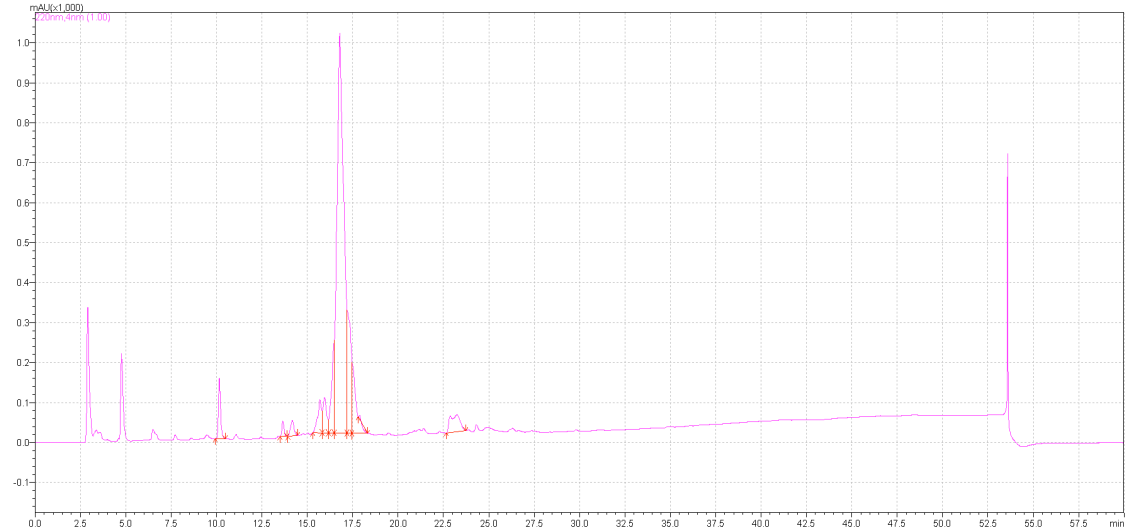


**Figure 106 AcH2009.1 24 Hr**

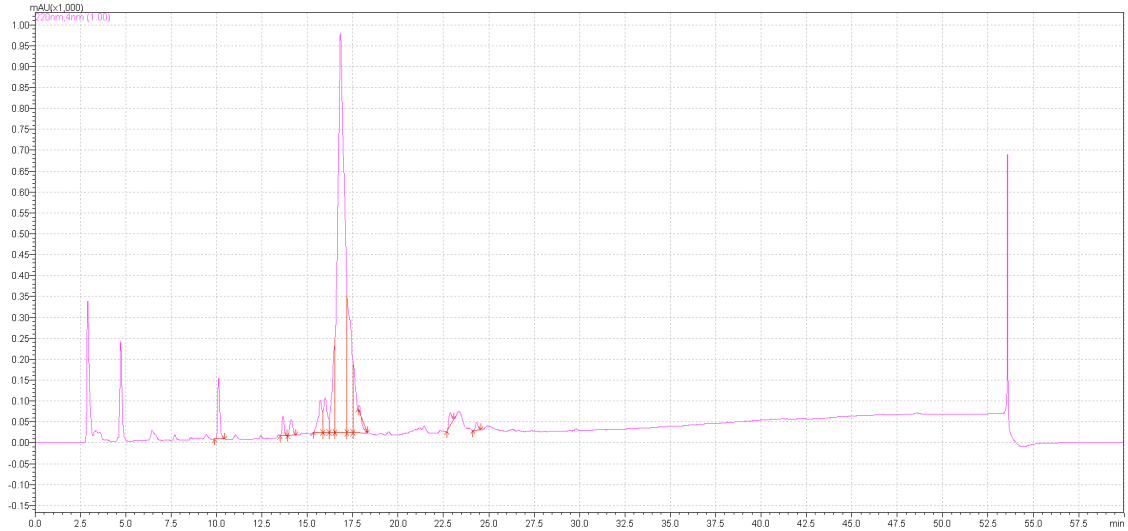


**Figure 107 AcH2009.1 48 Hr**

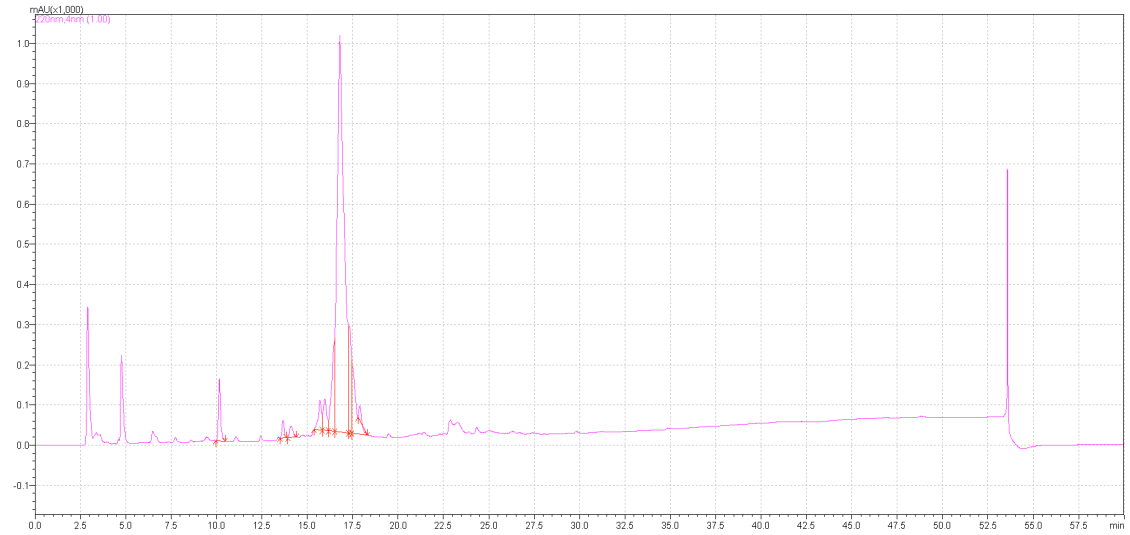


**Figure 108 AcH2009.1 72 Hr**

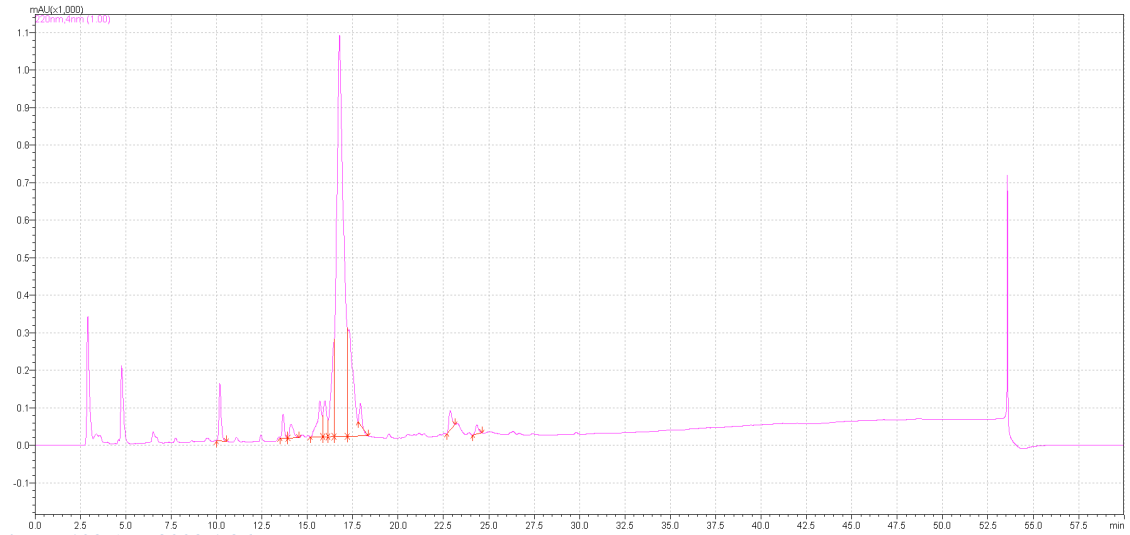


**Figure 109 AcH2009.1 96 Hr**

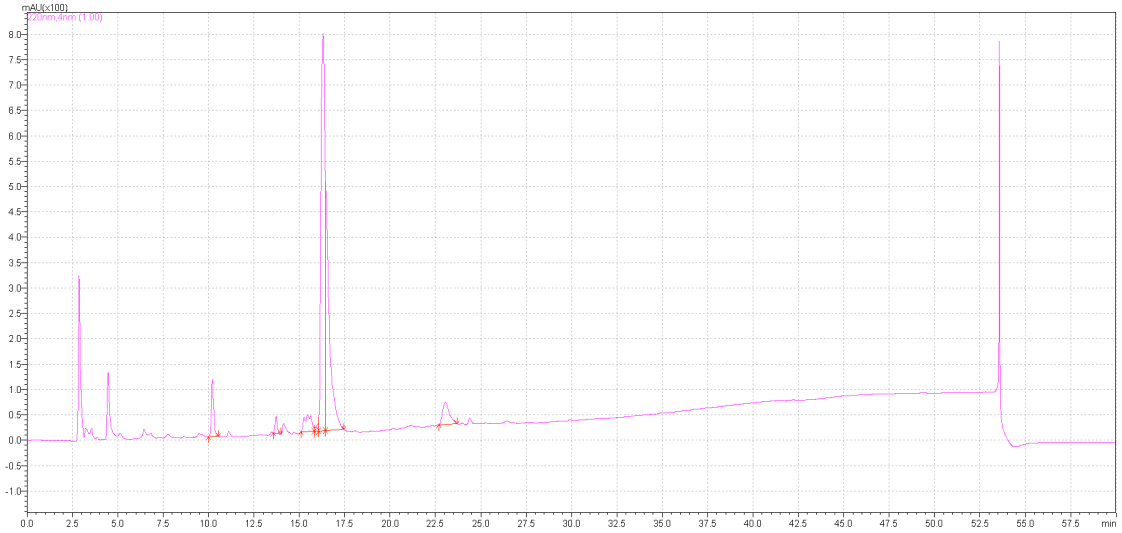


**Figure 110 D-Leu H2009.1 0 Hr**

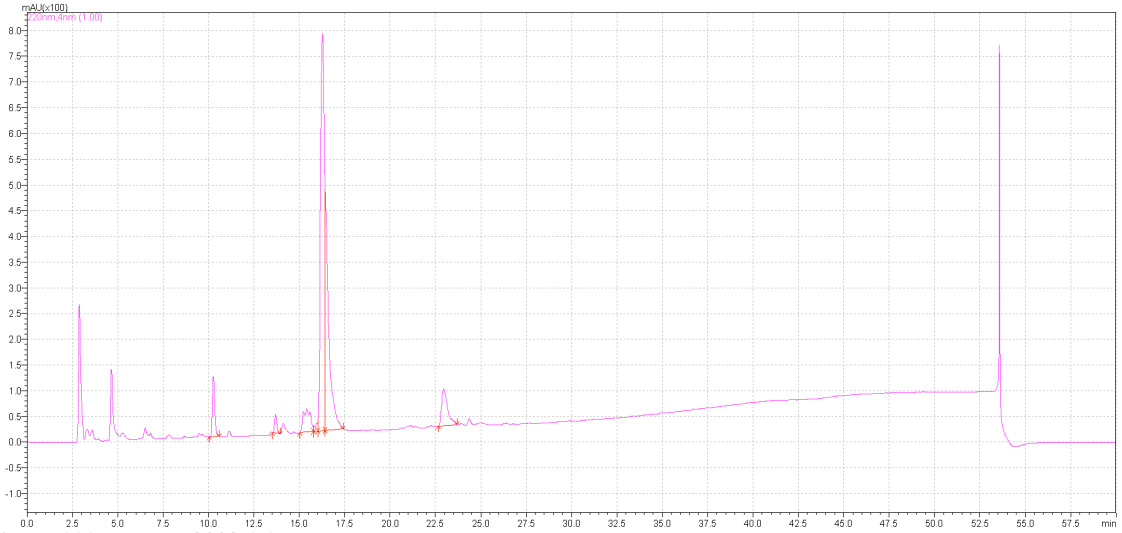


**Figure 111 D-Leu H2009.1 1 Hr**

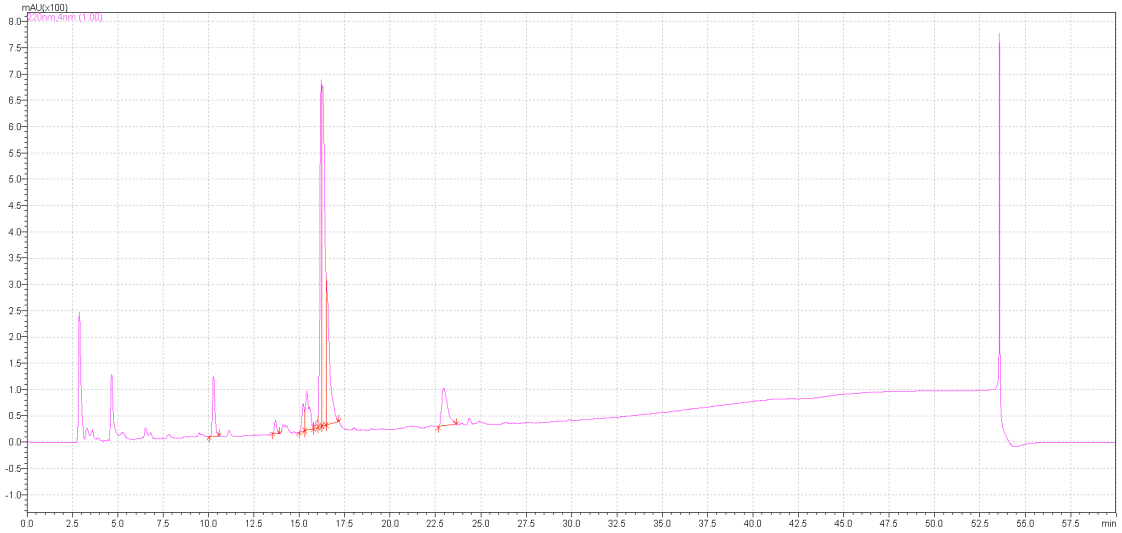


**Figure 112 D-Leu H2009.1 4 Hr**

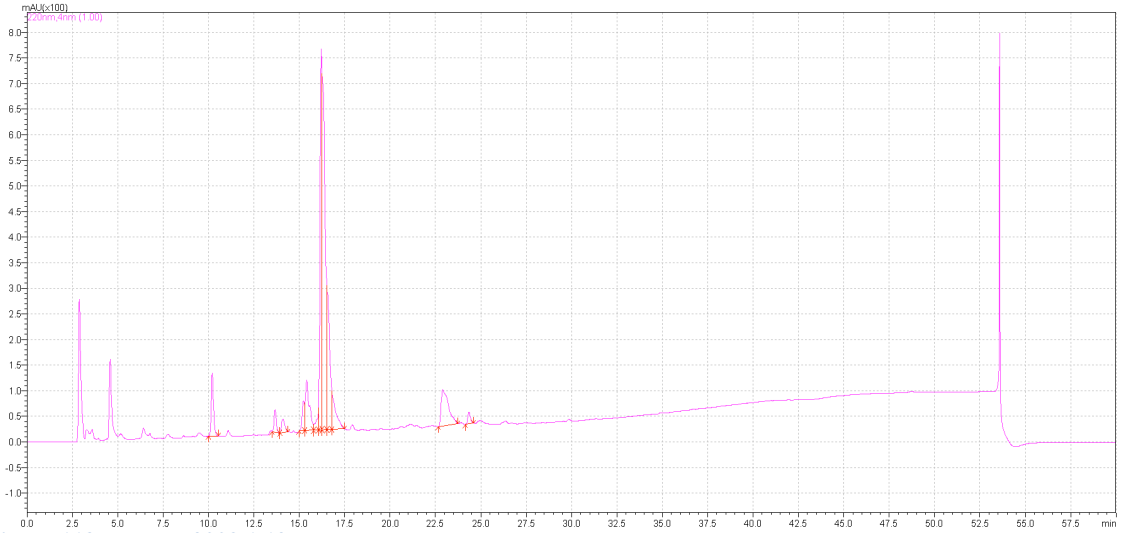


**Figure 113 D-Leu H2009.1 12 Hr**

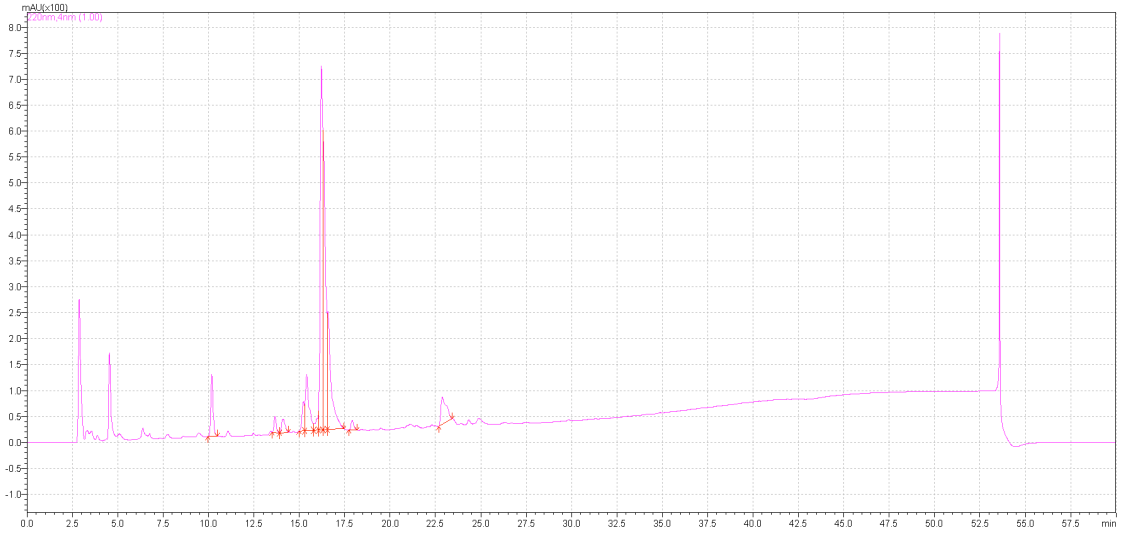


**Figure 114 D-Leu H2009.1 24 Hr**

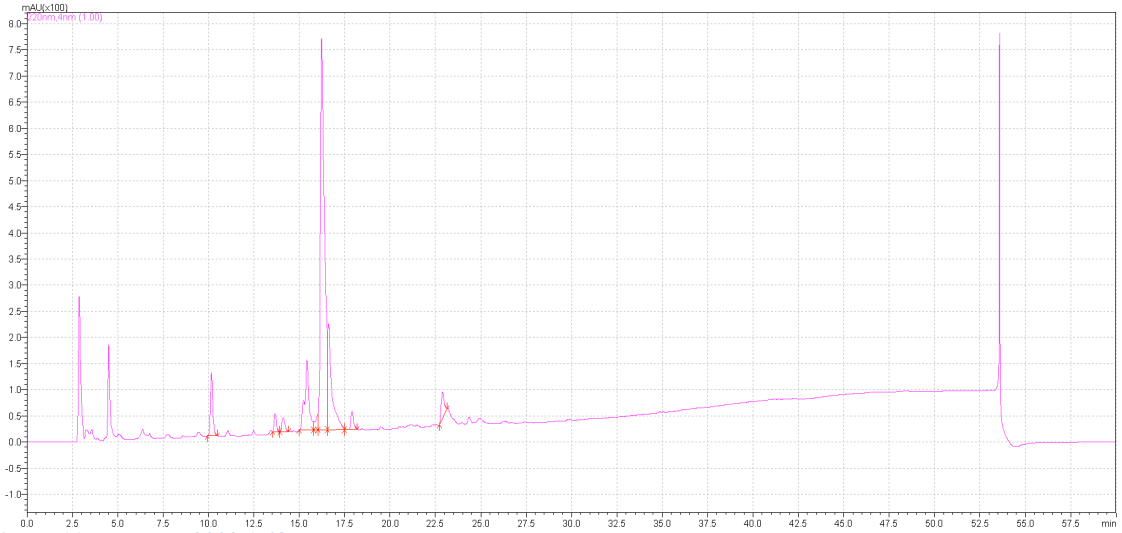


**Figure 115 D-Leu H2009.1 48 Hr**

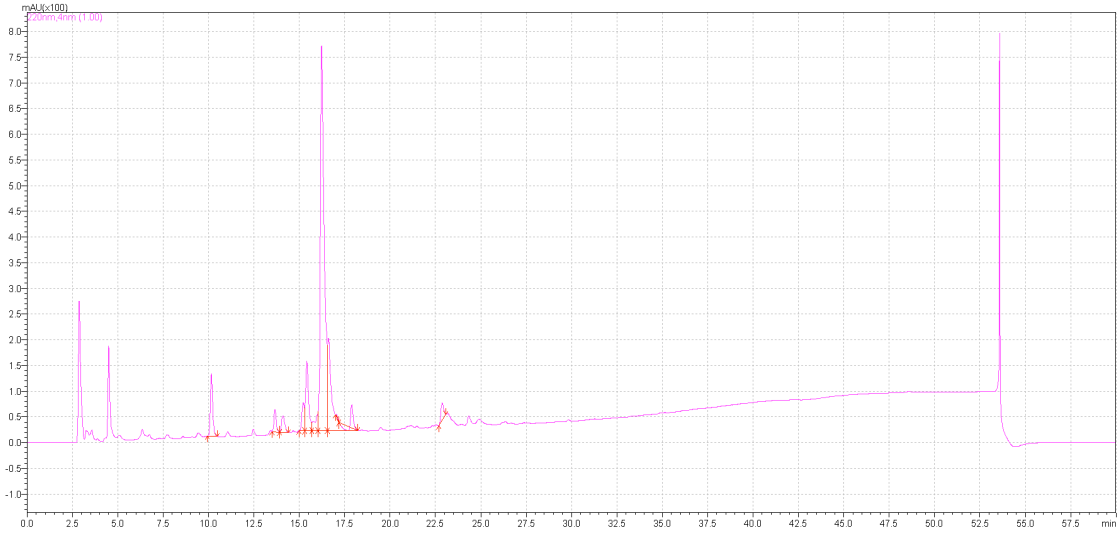


**Figure 116 D-Leu H2009.1 72 Hr**

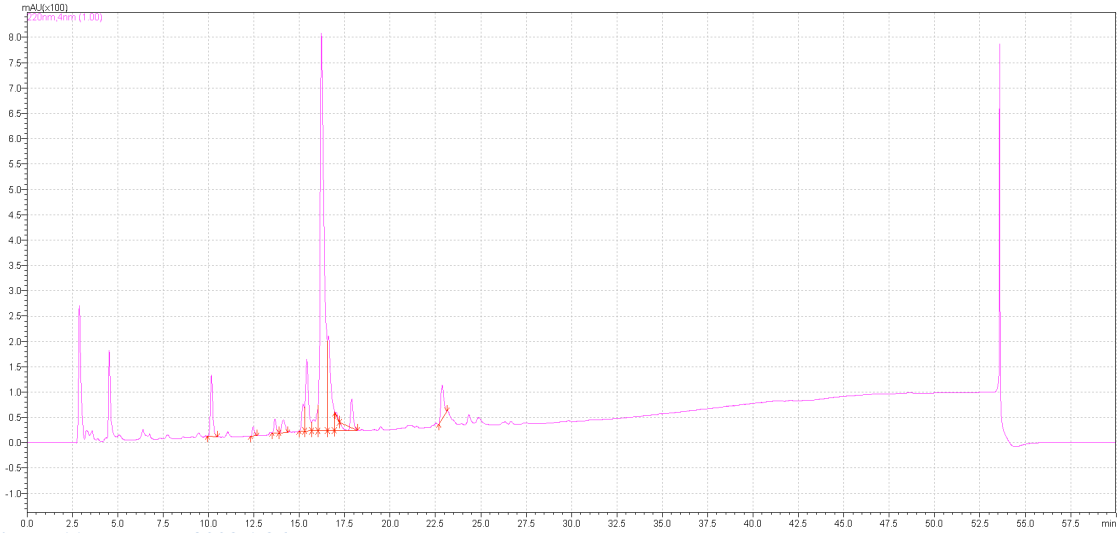


**Figure 117 D-Leu H2009.1 96 Hr**

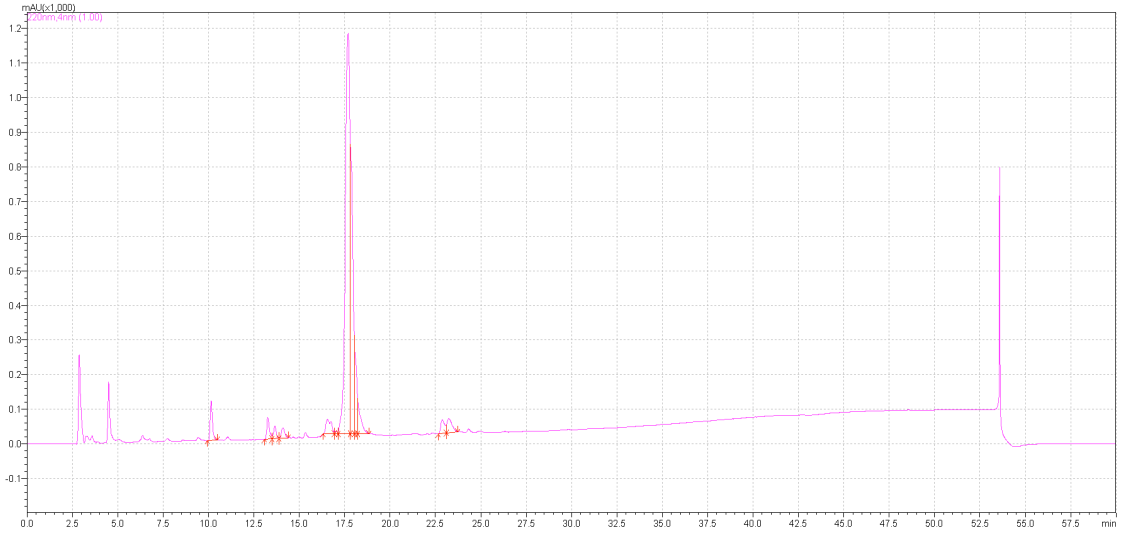


**Figure 118 AcD-Leu H2009.1 0 Hr**

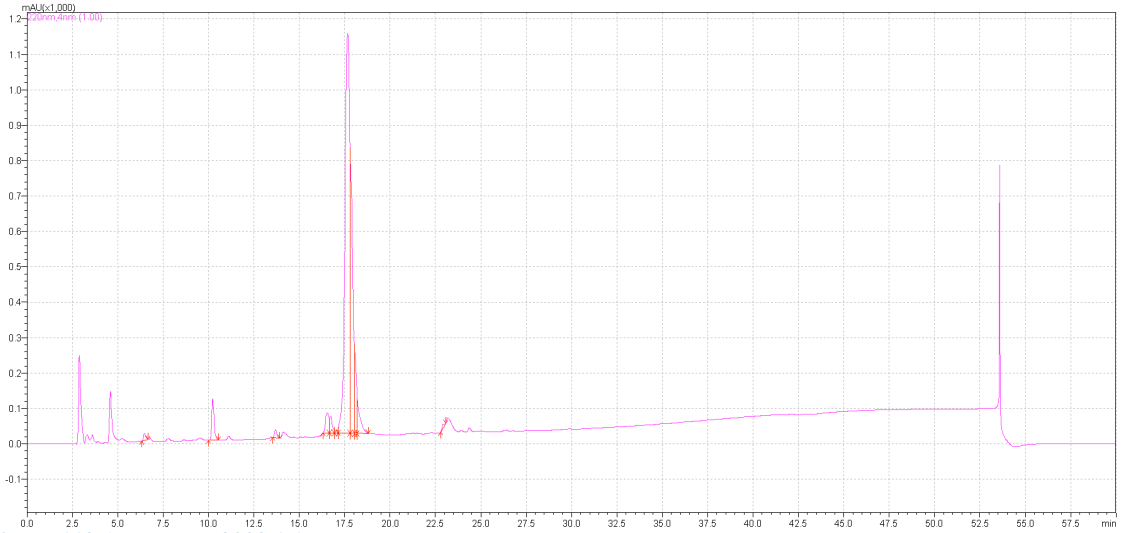


**Figure 119 AcD-Leu H2009.1 1 Hr**

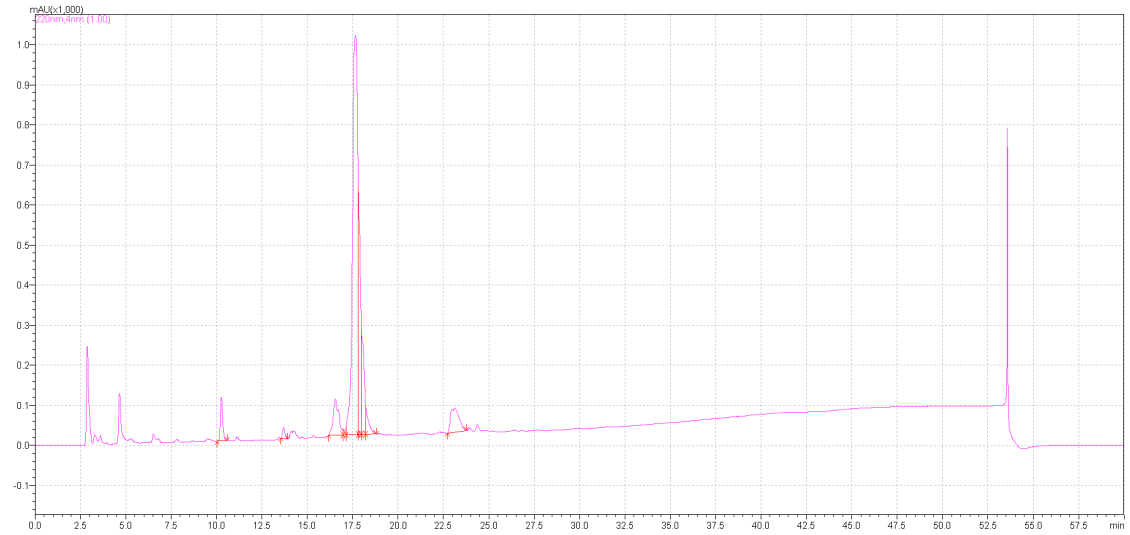


**Figure 120 AcD-Leu H2009.1 4 Hr**

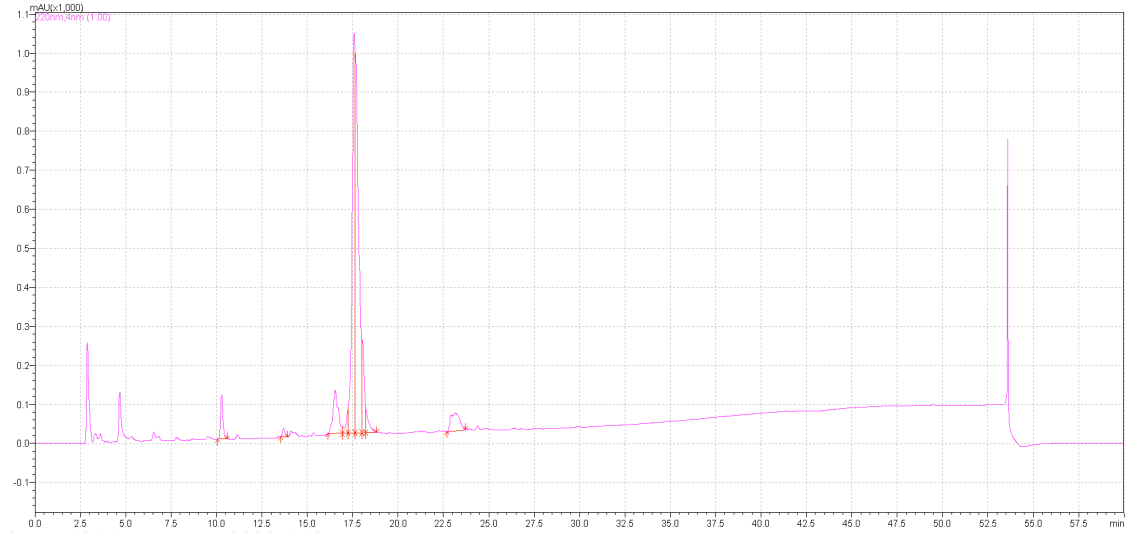


**Figure 121 AcD-Leu H2009.1 12 Hr**

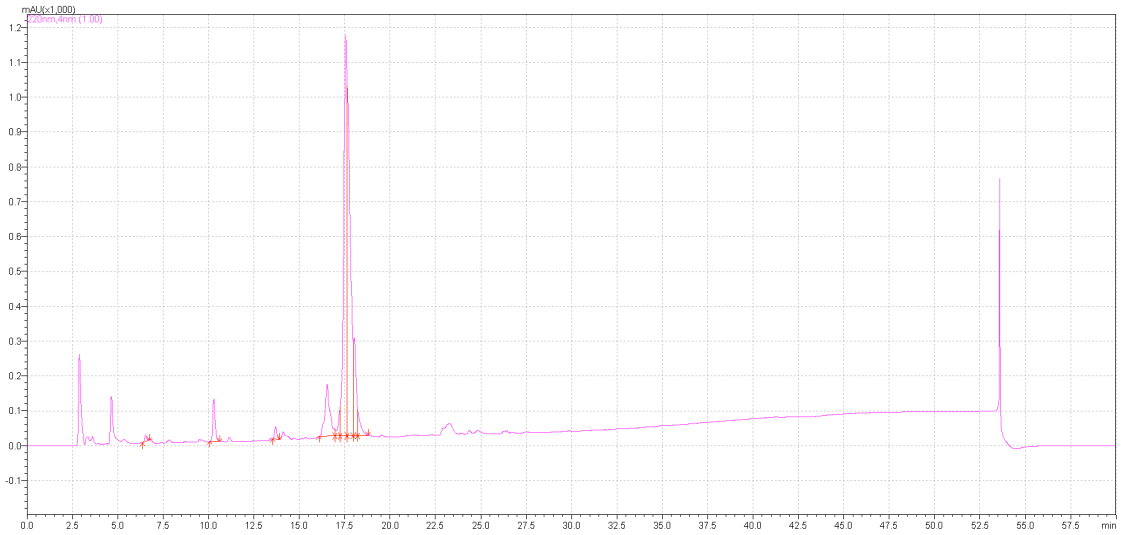


Figure 122 AcD-Leu H2009.1 24 Hr

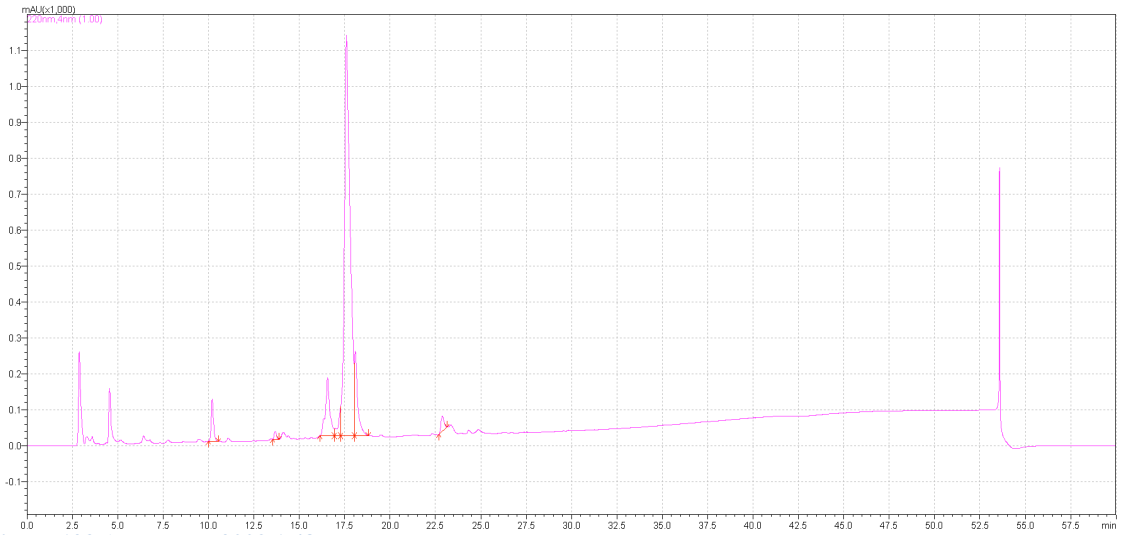


Figure 123 AcD-Leu H2009.1 48 Hr

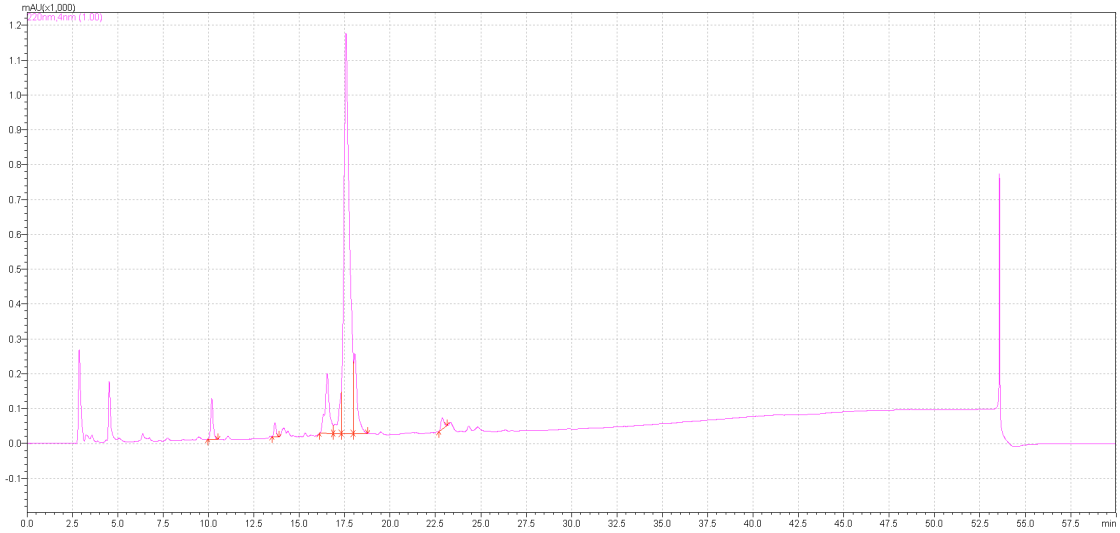


**Figure 124 AcD-Leu H2009.1 72 Hr**

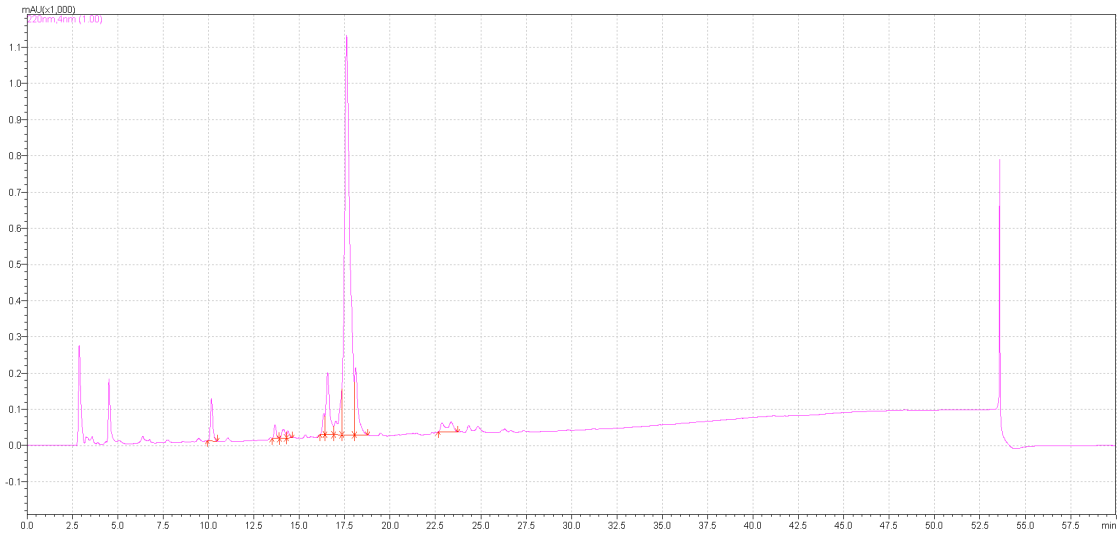


**Figure 125 AcD-Leu H2009.1 96 Hr**

# BIBLIOGRAPHY


1. *World Health Organization. International Agency for Research on Cancer. GLOBOCAN 2012: Estimated Cancer Incidence, Mortality and Prevalence Worldwide in 2012.* . Lung Cancer, 2012.
2. *American Cancer Society: Cancer Facts & Figures 2014.* . Atlanta: American Cancer Society; , 2014.
3. Siegel, R., D. Naishadham, and A. Jemal, *Cancer statistics, 2013.* CA: A Cancer Journal for Clinicians, 2013. **63**(1): p. 11-30.
4. Siegel, R.L., K.D. Miller, and A. Jemal, *Cancer statistics, 2015.* CA Cancer J Clin, 2015. **65**(1): p. 5-29.
5. Zarogoulidis, K., et al., *Treatment of non-small cell lung cancer (NSCLC).* J Thorac Dis, 2013. **5 Suppl 4**: p. S389-96.
6. Schiller, J.H., et al., *Comparison of four chemotherapy regimens for advanced non-small-cell lung cancer.* N Engl J Med, 2002. **346**(2): p. 92-8.
7. Torok, S., et al., *Lung cancer in never smokers.* Future Oncol, 2011. **7**(10): p. 1195-211.
8. Lopez, A.D., N.E. Collishaw, and T. Piha, *A descriptive model of the cigarette epidemic in developed countries.* Tob Control, 1994. **3**(3): p. 242-7.
9. Steliga, M.A. and C.M. Dresler, *Epidemiology of lung cancer: smoking, secondhand smoke, and genetics.* Surg Oncol Clin N Am, 2011. **20**(4): p. 605-18.
10. Couraud, S., et al., *Lung cancer in never smokers – A review.* European Journal of Cancer, 2012. **48**(9): p. 1299-1311.
11. Thun, M.J., et al., *Lung cancer occurrence in never-smokers: an analysis of 13 cohorts and 22 cancer registry studies.* PLoS Med, 2008. **5**(9): p. e185.
12. Maclure, M., et al., *Elevated blood levels of carcinogens in passive smokers.* Am J Public Health, 1989. **79**(10): p. 1381-4.
13. Samet, J.M., et al., *Lung cancer in never smokers: clinical epidemiology and environmental risk factors.* Clin Cancer Res, 2009. **15**(18): p. 5626-45.
14. Yu, Y.H., et al., *Increased lung cancer risk among patients with pulmonary tuberculosis: a population cohort study.* J Thorac Oncol, 2011. **6**(1): p. 32-7.
15. Liang, H.Y., et al., *Facts and fiction of the relationship between preexisting tuberculosis and lung cancer risk: a systematic review.* Int J Cancer, 2009. **125**(12): p. 2936-44.
16. Ganti, A.K., et al., *Hormone replacement therapy is associated with decreased survival in women with lung cancer.* J Clin Oncol, 2006. **24**(1): p. 59-63.
17. Schabath, M.B., et al., *Hormone replacement therapy and lung cancer risk: a case-control analysis.* Clin Cancer Res, 2004. **10**(1 Pt 1): p. 113-23.
18. Kreuzer, M., et al., *Hormonal factors and risk of lung cancer among women?* Int J Epidemiol, 2003. **32**(2): p. 263-71.
19. Syrjanen, K.J., *HPV infections and lung cancer.* J Clin Pathol, 2002. **55**(12): p. 885-91.

20. Ko, Y.C., et al., *Chinese food cooking and lung cancer in women nonsmokers.* Am J Epidemiol, 2000. **151**(2): p. 140-7.
21. Hanna, J. and M. Onaitis, *Cell of origin of lung cancer.* Journal of Carcinogenesis, 2013. **12**(1): p. 6.
22. Chan, B.A. and B.G.M. Hughes, *Targeted therapy for non-small cell lung cancer: current standards and the promise of the future.* Translational Lung Cancer Research, 2014. **4**(1): p. 36-54.
23. Dearden, S., et al., *Mutation incidence and coincidence in non small-cell lung cancer: meta-analyses by ethnicity and histology (mutMap).* Annals of Oncology, 2013. **24**(9): p. 2371-2376.
24. Roh, M.S., *Molecular Pathology of Lung Cancer: Current Status and Future Directions.* Tuberculosis and Respiratory Diseases, 2014. **77**(2): p. 49.
25. Nguyen, K.-S.H., *Review of the current targeted therapies for non-small-cell lung cancer.* World Journal of Clinical Oncology, 2014. **5**(4): p. 576.
26. Kobayashi, S., et al., *EGFR mutation and resistance of non-small-cell lung cancer to gefitinib.* N Engl J Med, 2005. **352**(8): p. 786-92.
27. Kobayashi, S., et al., *An alternative inhibitor overcomes resistance caused by a mutation of the epidermal growth factor receptor.* Cancer Res, 2005. **65**(16): p. 7096-101.
28. Takezawa, K., et al., *HER2 amplification: a potential mechanism of acquired resistance to EGFR inhibition in EGFR-mutant lung cancers that lack the second-site EGFRT790M mutation.* Cancer Discov, 2012. **2**(10): p. 922-33.
29. Engelman, J.A., et al., *MET amplification leads to gefitinib resistance in lung cancer by activating ERBB3 signaling.* Science, 2007. **316**(5827): p. 1039-43.
30. Ohashi, K., et al., *Lung cancers with acquired resistance to EGFR inhibitors occasionally harbor BRAF gene mutations but lack mutations in KRAS, NRAS, or MEK1.* Proc Natl Acad Sci U S A, 2012. **109**(31): p. E2127-33.
31. Soda, M., et al., *Identification of the transforming EML4-ALK fusion gene in non-small-cell lung cancer.* Nature, 2007. **448**(7153): p. 561-6.
32. Takahashi, T., et al., *Clinicopathologic features of non-small-cell lung cancer with EML4-ALK fusion gene.* Ann Surg Oncol, 2010. **17**(3): p. 889-97.
33. Shaw, A.T., et al., *Clinical features and outcome of patients with non-small-cell lung cancer who harbor EML4-ALK.* J Clin Oncol, 2009. **27**(26): p. 4247-53.
34. Rikova, K., et al., *Global survey of phosphotyrosine signaling identifies oncogenic kinases in lung cancer.* Cell, 2007. **131**(6): p. 1190-203.
35. Takeuchi, K., et al., *KIF5B-ALK, a novel fusion oncokinase identified by an immunohistochemistry-based diagnostic system for ALK-positive lung cancer.* Clin Cancer Res, 2009. **15**(9): p. 3143-9.
36. Shaw, A.T., et al., *Crizotinib versus chemotherapy in advanced ALK-positive lung cancer.* N Engl J Med, 2013. **368**(25): p. 2385-94.
37. Katayama, R., et al., *Mechanisms of acquired crizotinib resistance in ALK-rearranged lung Cancers.* Sci Transl Med, 2012. **4**(120): p. 120ra17.

38. Doebele, R.C., et al., *Mechanisms of resistance to crizotinib in patients with ALK gene rearranged non-small cell lung cancer.* Clin Cancer Res, 2012. **18**(5): p. 1472-82.
39. Le Calvez, F., et al., *TP53 and KRAS mutation load and types in lung cancers in relation to tobacco smoke: distinct patterns in never, former, and current smokers.* Cancer Res, 2005. **65**(12): p. 5076-83.
40. Wang, Y., et al., *Targeting mutant KRAS for anticancer therapeutics: a review of novel small molecule modulators.* J Med Chem, 2013. **56**(13): p. 5219-30.
41. Shames, D.S. and Wistuba, II, *The evolving genomic classification of lung cancer.* J Pathol, 2014. **232**(2): p. 121-33.
42. Sadiq, A.A. and R. Salgia, *MET as a possible target for non-small-cell lung cancer.* J Clin Oncol, 2013. **31**(8): p. 1089-96.
43. Bergethon, K., et al., *ROS1 rearrangements define a unique molecular class of lung cancers.* J Clin Oncol, 2012. **30**(8): p. 863-70.
44. Kohno, T., et al., *KIF5B-RET fusions in lung adenocarcinoma.* Nat Med, 2012. **18**(3): p. 375-7.
45. Dutt, A., et al., *Inhibitor-sensitive FGFR1 amplification in human non-small cell lung cancer.* PLoS One, 2011. **6**(6): p. e20351.
46. Breccia, M., M. Molica, and G. Alimena, *How tyrosine kinase inhibitors impair metabolism and endocrine system function: A systematic updated review.* Leuk Res, 2014. **38**(12): p. 1392-1398.
47. Cooper, W.A., et al., *Molecular biology of lung cancer.* J Thorac Dis, 2013. **5 Suppl 5**: p. S479-90.
48. Marchetti, A., et al., *Clinical features and outcome of patients with non-small-cell lung cancer harboring BRAF mutations.* J Clin Oncol, 2011. **29**(26): p. 3574-9.
49. Mazieres, J., et al., *Lung cancer that harbors an HER2 mutation: epidemiologic characteristics and therapeutic perspectives.* J Clin Oncol, 2013. **31**(16): p. 1997-2003.
50. Spoerke, J.M., et al., *Phosphoinositide 3-kinase (PI3K) pathway alterations are associated with histologic subtypes and are predictive of sensitivity to PI3K inhibitors in lung cancer preclinical models.* Clin Cancer Res, 2012. **18**(24): p. 6771-83.
51. Hammerman, P.S., et al., *Mutations in the DDR2 kinase gene identify a novel therapeutic target in squamous cell lung cancer.* Cancer Discov, 2011. **1**(1): p. 78-89.
52. Pao, W. and K.E. Hutchinson, *Chipping away at the lung cancer genome.* Nat Med, 2012. **18**(3): p. 349-351.
53. Horie, R. and T. Watanabe, *CD30: expression and function in health and disease.* Semin Immunol, 1998. **10**(6): p. 457-70.
54. Zolot, R.S., S. Basu, and R.P. Million, *Antibody-drug conjugates.* Nat Rev Drug Discov, 2013. **12**(4): p. 259-60.
55. Varner, J.A. and D.A. Cheresh, *Tumor angiogenesis and the role of vascular cell integrin alphavbeta3.* Important Adv Oncol, 1996: p. 69-87.

56. Kurozumi, K., et al., *Cilengitide treatment for malignant glioma: current status and future direction.* Neurol Med Chir (Tokyo), 2012. **52**(8): p. 539-47.
57. Tateishi, U., T. Oka, and T. Inoue, *Radiolabeled RGD peptides as integrin alpha(v)beta3-targeted PET tracers.* Curr Med Chem, 2012. **19**(20): p. 3301-9.
58. Bidard, F.C. and O. Tredan, *Trends in cancer-targeted antibody-drug conjugates.* Target Oncol, 2014. **9**(1): p. 1-8.
59. Scott, A.M., J.P. Allison, and J.D. Wolchok, *Monoclonal antibodies in cancer therapy.* Cancer Immun, 2012. **12**: p. 14.
60. Samaranayake, H., et al., *Challenges in monoclonal antibody-based therapies.* Ann Med, 2009. **41**(5): p. 322-31.
61. Wang, Y., et al., *Monoclonal antibodies in lung cancer.* Expert Opin Biol Ther, 2013. **13**(2): p. 209-26.
62. Ferrara, N., et al., *Discovery and development of bevacizumab, an anti-VEGF antibody for treating cancer.* Nat Rev Drug Discov, 2004. **3**(5): p. 391-400.
63. Baselga, J., *The EGFR as a target for anticancer therapy--focus on cetuximab.* Eur J Cancer, 2001. **37 Suppl 4**: p. S16-22.
64. Gray, B.P., M.J. McGuire, and K.C. Brown, *A liposomal drug platform overrides peptide ligand targeting to a cancer biomarker, irrespective of ligand affinity or density.* PLoS One, 2013. **8**(8): p. e72938.
65. Vegt, E., et al., *Renal toxicity of radiolabeled peptides and antibody fragments: mechanisms, impact on radionuclide therapy, and strategies for prevention.* J Nucl Med, 2010. **51**(7): p. 1049-58.
66. Freise, A.C. and A.M. Wu, *In vivo imaging with antibodies and engineered fragments.* Mol Immunol, 2015.
67. Weitman, S.D., et al., *Distribution of the folate receptor GP38 in normal and malignant cell lines and tissues.* Cancer Res, 1992. **52**(12): p. 3396-401.
68. Crane, L.M., et al., *The effect of chemotherapy on expression of folate receptor-alpha in ovarian cancer.* Cell Oncol (Dordr), 2012. **35**(1): p. 9-18.
69. Ross, J.F., P.K. Chaudhuri, and M. Ratnam, *Differential regulation of folate receptor isoforms in normal and malignant tissues in vivo and in established cell lines. Physiologic and clinical implications.* Cancer, 1994. **73**(9): p. 2432-43.
70. Elnakat, H. and M. Ratnam, *Role of folate receptor genes in reproduction and related cancers.* Front Biosci, 2006. **11**: p. 506-19.
71. Assaraf, Y.G., C.P. Leamon, and J.A. Reddy, *The folate receptor as a rational therapeutic target for personalized cancer treatment.* Drug Resist Updat, 2014. **17**(4-6): p. 89-95.
72. Rochman, H., J. Selhub, and T. Karrison, *Folate binding protein and the estrogen receptor in breast cancer.* Cancer Detect Prev, 1985. **8**(1-2): p. 71-5.
73. Christoph, D.C., et al., *Significance of folate receptor alpha and thymidylate synthase protein expression in patients with non-small-cell lung cancer treated with pemetrexed.* J Thorac Oncol, 2013. **8**(1): p. 19-30.
74. Nunez, M.I., et al., *High expression of folate receptor alpha in lung cancer correlates with adenocarcinoma histology and EGFR [corrected] mutation.* J Thorac Oncol, 2012. **7**(5): p. 833-40.

75. Franzen, S., *A comparison of peptide and folate receptor targeting of cancer cells: from single agent to nanoparticle.* Expert Opin Drug Deliv, 2011. **8**(3): p. 281-98.
76. van Dam, G.M., et al., *Intraoperative tumor-specific fluorescence imaging in ovarian cancer by folate receptor-alpha targeting: first in-human results.* Nat Med, 2011. **17**(10): p. 1315-9.
77. Vlahov, I.R. and C.P. Leamon, *Engineering folate-drug conjugates to target cancer: from chemistry to clinic.* Bioconjug Chem, 2012. **23**(7): p. 1357-69.
78. Reddy, J.A., et al., *Preclinical evaluation of EC145, a folate-vinca alkaloid conjugate.* Cancer Res, 2007. **67**(9): p. 4434-42.
79. Leamon, C.P., et al., *Synthesis and biological evaluation of EC20: a new folate-derived, (99m)Tc-based radiopharmaceutical.* Bioconjug Chem, 2002. **13**(6): p. 1200-10.
80. Nagai, J. and M. Takano, *Molecular-targeted approaches to reduce renal accumulation of nephrotoxic drugs.* Expert Opin Drug Metab Toxicol, 2010. **6**(9): p. 1125-38.
81. Kularatne, S.A., et al., *Prostate-specific membrane antigen targeted imaging and therapy of prostate cancer using a PSMA inhibitor as a homing ligand.* Mol Pharm, 2009. **6**(3): p. 780-9.
82. Krall, N., et al., *A small-molecule drug conjugate for the treatment of carbonic anhydrase IX expressing tumors.* Angew Chem Int Ed Engl, 2014. **53**(16): p. 4231-5.
83. Schally, A.V., D.H. Coy, and A. Arimura, *LH-RH agonists and antagonists.* Int J Gynaecol Obstet, 1980. **18**(5): p. 318-24.
84. Trachtenberg, J., *The treatment of metastatic prostatic cancer with a potent luteinizing hormone releasing hormone analogue.* J Urol, 1983. **129**(6): p. 1149-52.
85. Reissmann, T., et al., *The LHRH antagonist cetrorelix: a review.* Hum Reprod Update, 2000. **6**(4): p. 322-31.
86. Kouroukis, T.C., et al., *Bortezomib in multiple myeloma: systematic review and clinical considerations.* Curr Oncol, 2014. **21**(4): p. e573-603.
87. Zindel, L.R., *Debut of a somatostatin analog: octreotide in review.* Conn Med, 1989. **53**(12): p. 741-4.
88. Ando, K., et al., *Mifamurtide for the treatment of nonmetastatic osteosarcoma.* Expert Opin Pharmacother, 2011. **12**(2): p. 285-92.
89. Reubi, J.C., *Peptide receptors as molecular targets for cancer diagnosis and therapy.* Endocr Rev, 2003. **24**(4): p. 389-427.
90. Reubi, J.C. and H.R. Maecke, *Peptide-based probes for cancer imaging.* J Nucl Med, 2008. **49**(11): p. 1735-8.
91. Wild, D., et al., *First clinical evidence that imaging with somatostatin receptor antagonists is feasible.* J Nucl Med, 2011. **52**(9): p. 1412-7.
92. Rogers, B.E., D.D. Manna, and A. Safavy, *In vitro and in vivo evaluation of a 64Cu-labeled polyethylene glycol-bombesin conjugate.* Cancer Biother Radiopharm, 2004. **19**(1): p. 25-34.

93. Schweinsberg, C., et al., *Novel Glycated [99mTc(CO)3]-Labeled Bombesin Analogues for Improved Targeting of Gastrin-Releasing Peptide Receptor-Positive Tumors.* Bioconjugate Chemistry, 2008. **19**(12): p. 2432-2439.
94. Behr, T.M., et al., *Imaging tumors with peptide-based radioligands.* Q J Nucl Med, 2001. **45**(2): p. 189-200.
95. Okarvi, S.M., *Peptide-based radiopharmaceuticals and cytotoxic conjugates: Potential tools against cancer.* Cancer Treatment Reviews, 2008. **34**(1): p. 13-26.
96. Alifano, M., et al., *Neurotensin receptor 1 determines the outcome of non-small cell lung cancer.* Clin Cancer Res, 2010. **16**(17): p. 4401-10.
97. Gray, B.P. and K.C. Brown, *Combinatorial Peptide Libraries: Mining for Cell-Binding Peptides.* Chemical Reviews, 2013.
98. Lee, J.W., et al., *Nanoscale bacteriophage biosensors beyond phage display.* Int J Nanomedicine, 2013. **8**: p. 3917-25.
99. Gray, B.P. and K.C. Brown, *Combinatorial peptide libraries: mining for cell-binding peptides.* Chem Rev, 2014. **114**(2): p. 1020-81.
100. Babickova, J., et al., *In vivo phage display--a discovery tool in molecular biomedicine.* Biotechnol Adv, 2013. **31**(8): p. 1247-59.
101. McGuire, M.J., S. Li, and K.C. Brown, *Biopanning of Phage Displayed Peptide Libraries for the Isolation of Cell-Specific Ligands.* 2009. **504**: p. 291-321.
102. Sparr, C., et al., *Syntheses, receptor bindings, in vitro and in vivo stabilities and biodistributions of DOTA-neurotensin(8-13) derivatives containing beta-amino acid residues - a lesson about the importance of animal experiments.* Chem Biodivers, 2013. **10**(12): p. 2101-21.
103. Wynendaele, E., et al., *Development of peptide and protein based radiopharmaceuticals.* Curr Pharm Des, 2014. **20**(14): p. 2250-67.
104. Maina, T., et al., *[99mTc]Demotate, a new 99mTc-based [Tyr3]octreotate analogue for the detection of somatostatin receptor-positive tumours: synthesis and preclinical results.* Eur J Nucl Med Mol Imaging, 2002. **29**(6): p. 742-53.
105. Singh AN, M.M., Li S, Hao G, Kumar A, Sun X, and Brown KC, *Dimerization of a Phage-Display Selected Peptide for Imaging of αvβ6- Integrin: Two Approaches to the Multivalent Effect.* Theranostics, 2013.
106. Bracci, L., et al., *Synthetic Peptides in the Form of Dendrimers Become Resistant to Protease Activity.* Journal of Biological Chemistry, 2003. **278**(47): p. 46590-46595.
107. Otvos, L., Jr., *Peptide-based drug design: here and now.* Methods Mol Biol, 2008. **494**: p. 1-8.
108. Thurber, G.M., M.M. Schmidt, and K.D. Wittrup, *Antibody tumor penetration: Transport opposed by systemic and antigen-mediated clearance.* Adv Drug Deliv Rev, 2008. **60**(12): p. 1421.
109. Askoxylakis, V., et al., *Challenges in optimizing a prostate carcinoma binding peptide, identified through the phage display technology.* Molecules, 2011. **16**(2): p. 1559-78.

110. Brown, K.C., *Peptidic Tumor Targeting Agents: The Road from Phage Display Peptide Selections to Clinical Applications.* Current Pharmaceutical Design, 2010. **16**: p. 1040-1054.
111. Becker, A., et al., *Receptor-targeted optical imaging of tumors with near-infrared fluorescent ligands.* Nat Biotechnol, 2001. **19**(4): p. 327-31.
112. Azhdarinia, A., et al., *Dual-labeling strategies for nuclear and fluorescence molecular imaging: a review and analysis.* Mol Imaging Biol, 2012. **14**(3): p. 261-76.
113. Gotthardt, M., et al., *Development and clinical application of peptide-based radiopharmaceuticals.* Curr Pharm Des, 2004. **10**(24): p. 2951-63.
114. Nestor, J.J., Jr., *The medicinal chemistry of peptides.* Curr Med Chem, 2009. **16**(33): p. 4399-418.
115. Tugyi, R., et al., *Partial D-amino acid substitution: Improved enzymatic stability and preserved Ab recognition of a MUC2 epitope peptide.* Proceedings of the National Academy of Sciences of the United States of America, 2005. **102**(2): p. 413-418.
116. Hong, S.Y., J.E. Oh, and K.-H. Lee, *Effect of d-amino acid substitution on the stability, the secondary structure, and the activity of membrane-active peptide.* Biochemical Pharmacology, 1999. **58**(11): p. 1775-1780.
117. Chen, X., et al., *Pegylated Arg-Gly-Asp peptide: 64Cu labeling and PET imaging of brain tumor alphavbeta3-integrin expression.* J Nucl Med, 2004. **45**(10): p. 1776-83.
118. Veronese, F.M. and G. Pasut, *PEGylation, successful approach to drug delivery.* Drug Discovery Today, 2005. **10**(21): p. 1451-1458.
119. Vegt, E., et al., *Reducing Renal Uptake of Radiolabeled Peptides Using Albumin Fragments.* Journal of Nuclear Medicine, 2008. **49**(9): p. 1506-1511.
120. Roxin, A. and G. Zheng, *Flexible or fixed: a comparative review of linear and cyclic cancer-targeting peptides.* Future Med Chem, 2012. **4**(12): p. 1601-18.
121. Joo, S.H., *Cyclic peptides as therapeutic agents and biochemical tools.* Biomol Ther (Seoul), 2012. **20**(1): p. 19-26.
122. Hosseinimehr, S.J., V. Tolmachev, and A. Orlova, *Liver uptake of radiolabeled targeting proteins and peptides: considerations for targeting peptide conjugate design.* Drug Discov Today, 2012. **17**(21-22): p. 1224-32.
123. Gotthardt, M., et al., *Indication for Different Mechanisms of Kidney Uptake of Radiolabeled Peptides.* Journal of Nuclear Medicine, 2007. **48**(4): p. 596-601.
124. Christensen, E.I., et al., *Endocytic receptors in the renal proximal tubule.* Physiology (Bethesda), 2012. **27**(4): p. 223-36.
125. Christensen, E., P. Verroust, and R. Nielsen, *Receptor-mediated endocytosis in renal proximal tubule.* Pflügers Archiv - European Journal of Physiology, 2009. **458**(6): p. 1039-1048.
126. Virgolini, I., et al., *Indium-111-DOTA-lanreotide: biodistribution, safety and radiation absorbed dose in tumor patients.* J Nucl Med, 1998. **39**(11): p. 1928-36.

127. Maes, V., et al., *Novel 99mTc-Labeled Neurotensin Analogues with Optimized Biodistribution Properties.* Journal of Medicinal Chemistry, 2006. **49**(5): p. 1833-1836.
128. Guo, H., et al., *A novel indium-111-labeled gonadotropin-releasing hormone peptide for human prostate cancer imaging.* Bioorg Med Chem Lett, 2011. **21**(18): p. 5184-7.
129. Hu, L.Y., et al., *Characterization and evaluation of (64)Cu-labeled A20FMDV2 conjugates for imaging the integrin alphavbeta 6.* Mol Imaging Biol, 2014. **16**(4): p. 567-77.
130. Blacker, C.M., et al., *The gonadotropin-releasing hormone agonist leuprolide affects the thymus and other non-reproductive systems of female rats.* Acta Endocrinol (Copenh), 1991. **125**(5): p. 581-9.
131. Minami, H., et al., *Oligopeptides: mechanism of renal clearance depends on molecular structure.* Am J Physiol, 1992. **263**(1 Pt 2): p. F109-15.
132. Maack, T., *Renal handling of low molecular weight proteins.* The American Journal of Medicine, 1975. **58**(1): p. 57-64.
133. Kim, S.Y. and A. Moon, *Drug-Induced Nephrotoxicity and Its Biomarkers.* Biomolecules & therapeutics, 2012. **20**(3): p. 268-272.
134. Behe, M., et al., *Use of polyglutamic acids to reduce uptake of radiometal-labeled minigastrin in the kidneys.* J Nucl Med, 2005. **46**(6): p. 1012-5.
135. Rolleman, E., et al., *Amifostine protects rat kidneys during peptide receptor radionuclide therapy with [177Lu-DOTA0,Tyr3]octreotate.* European Journal of Nuclear Medicine and Molecular Imaging, 2007. **34**(5): p. 763-771.
136. Escorcia, F.E., et al., *Targeted nanomaterials for radiotherapy.* Nanomedicine (Lond), 2007. **2**(6): p. 805-15.
137. !!! INVALID CITATION !!!
138. Hynes, R.O., *Integrins: bidirectional, allosteric signaling machines.* Cell, 2002. **110**(6): p. 673-87.
139. Cheresh, D.A., *Structural and biologic properties of integrin-mediated cell adhesion.* Clin Lab Med, 1992. **12**(2): p. 217-36.
140. Hu, P. and B.H. Luo, *Integrin bi-directional signaling across the plasma membrane.* J Cell Physiol, 2013. **228**(2): p. 306-12.
141. Xiong, J., H.E. Balcioglu, and E.H. Danen, *Integrin signaling in control of tumor growth and progression.* Int J Biochem Cell Biol, 2013. **45**(5): p. 1012-5.
142. Morse, E.M., N.N. Brahme, and D.A. Calderwood, *Integrin cytoplasmic tail interactions.* Biochemistry, 2014. **53**(5): p. 810-20.
143. Koivisto, L., et al., *Integrins alpha5beta1, alphavbeta1, and alphavbeta6 collaborate in squamous carcinoma cell spreading and migration on fibronectin.* Exp Cell Res, 2000. **255**(1): p. 10-7.
144. Calderwood, D.A., I.D. Campbell, and D.R. Critchley, *Talins and kindlins: partners in integrin-mediated adhesion.* Nat Rev Mol Cell Biol, 2013. **14**(8): p. 503-17.
145. Shattil, S.J., C. Kim, and M.H. Ginsberg, *The final steps of integrin activation: the end game.* Nat Rev Mol Cell Biol, 2010. **11**(4): p. 288-300.

146. Ginsberg, M.H., J.C. Loftus, and E.F. Plow, *Cytoadhesins, integrins, and platelets.* Thromb Haemost, 1988. **59**(1): p. 1-6.
147. Ruoslahti, E., *Fibronectin and its alpha 5 beta 1 integrin receptor in malignancy.* Invasion Metastasis, 1994. **14**(1-6): p. 87-97.
148. Mizejewski, G.J., *Role of integrins in cancer: survey of expression patterns.* Proc Soc Exp Biol Med, 1999. **222**(2): p. 124-38.
149. Haapasalmi, K., et al., *Keratinocytes in human wounds express alpha v beta 6 integrin.* J Invest Dermatol, 1996. **106**(1): p. 42-8.
150. Breuss, J.M., et al., *Expression of the beta 6 integrin subunit in development, neoplasia and tissue repair suggests a role in epithelial remodeling.* J Cell Sci, 1995. **108 ( Pt 6)**: p. 2241-51.
151. Breuss, J.M., et al., *Restricted distribution of integrin beta 6 mRNA in primate epithelial tissues.* Journal of Histochemistry & Cytochemistry, 1993. **41**(10): p. 1521-7.
152. Elayadi, A.N., et al., *A peptide selected by biopanning identifies the integrin alphavbeta6 as a prognostic biomarker for nonsmall cell lung cancer.* Cancer Res, 2007. **67**(12): p. 5889-95.
153. Arihiro, K., et al., *Significance of alpha 9 beta 1 and alpha v beta 6 integrin expression in breast carcinoma.* Breast Cancer, 2000. **7**(1): p. 19-26.
154. Peng, C., et al., *Integrin alphavbeta6 and transcriptional factor Ets-1 act as prognostic indicators in colorectal cancer.* Cell Biosci, 2014. **4**(1): p. 53.
155. Nystrom, M.L., et al., *Cyclooxygenase-2 inhibition suppresses alphavbeta6 integrin-dependent oral squamous carcinoma invasion.* Cancer Res, 2006. **66**(22): p. 10833-42.
156. Ahmed, N., et al., *Overexpression of alpha(v)beta6 integrin in serous epithelial ovarian cancer regulates extracellular matrix degradation via the plasminogen activation cascade.* Carcinogenesis, 2002. **23**(2): p. 237-44.
157. Elayadi, A.N., et al., *A Peptide Selected by Biopanning Identifies the Integrin v 6 as a Prognostic Biomarker for Nonsmall Cell Lung Cancer.* Cancer Research, 2007. **67**(12): p. 5889-5895.
158. Hezel, A.F., et al., *TGF- and v 6 Integrin Act in a Common Pathway to Suppress Pancreatic Cancer Progression.* Cancer Research, 2012. **72**(18): p. 4840-4845.
159. Sipos, B., et al., *Immunohistochemical screening for β6-integrin subunit expression in adenocarcinomas using a novel monoclonal antibody reveals strong up-regulation in pancreatic ductal adenocarcinomas in vivo and in vitro.* Histopathology, 2004. **45**(3): p. 226-236.
160. Impola, U., et al., *Differential expression of matrilysin-1 (MMP-7), 92 kD gelatinase (MMP-9), and metalloelastase (MMP-12) in oral verrucous and squamous cell cancer.* J Pathol, 2004. **202**(1): p. 14-22.
161. Jones, J., F.M. Watt, and P.M. Speight, *Changes in the expression of alpha v integrins in oral squamous cell carcinomas.* J Oral Pathol Med, 1997. **26**(2): p. 63-8.
162. Hamidi, S., et al., *Expression of alpha(v)beta6 integrin in oral leukoplakia.* Br J Cancer, 2000. **82**(8): p. 1433-40.

163. Hazelbag, S., et al., *Overexpression of the alpha v beta 6 integrin in cervical squamous cell carcinoma is a prognostic factor for decreased survival.* J Pathol, 2007. **212**(3): p. 316-24.
164. Yang, G.Y., et al., *Integrin alpha v beta 6 mediates the potential for colon cancer cells to colonize in and metastasize to the liver.* Cancer Sci, 2008. **99**(5): p. 879-87.
165. Hecht, J.L., et al., *Overexpression of the alphavbeta6 integrin in endometrial cancer.* Appl Immunohistochem Mol Morphol, 2008. **16**(6): p. 543-7.
166. Allen, M.D., et al., *Altered microenvironment promotes progression of preinvasive breast cancer: myoepithelial expression of alphavbeta6 integrin in DCIS identifies high-risk patients and predicts recurrence.* Clin Cancer Res, 2014. **20**(2): p. 344-57.
167. Huang, X.Z., et al., *Inactivation of the integrin beta 6 subunit gene reveals a role of epithelial integrins in regulating inflammation in the lung and skin.* J Cell Biol, 1996. **133**(4): p. 921-8.
168. Aluwihare, P., et al., *Mice that lack activity of alphavbeta6- and alphavbeta8-integrins reproduce the abnormalities of Tgfb1- and Tgfb3-null mice.* J Cell Sci, 2009. **122**(Pt 2): p. 227-32.
169. Munger, J.S., et al., *The integrin alpha v beta 6 binds and activates latent TGF beta 1: a mechanism for regulating pulmonary inflammation and fibrosis.* Cell, 1999. **96**(3): p. 319-28.
170. Giacomini, M.M., et al., *Epithelial cells utilize cortical actin/myosin to activate latent TGF-beta through integrin alpha(v)beta(6)-dependent physical force.* Exp Cell Res, 2012. **318**(6): p. 716-22.
171. Xu, M.Y., et al., *Lysophosphatidic acid induces alphavbeta6 integrin-mediated TGF-beta activation via the LPA2 receptor and the small G protein G alpha(q).* Am J Pathol, 2009. **174**(4): p. 1264-79.
172. Shi, M., et al., *Latent TGF-beta structure and activation.* Nature, 2011. **474**(7351): p. 343-9.
173. Bates, R.C., et al., *Transcriptional activation of integrin beta6 during the epithelial-mesenchymal transition defines a novel prognostic indicator of aggressive colon carcinoma.* J Clin Invest, 2005. **115**(2): p. 339-47.
174. Sheppard, D., *Integrin-mediated activation of latent transforming growth factor beta.* Cancer Metastasis Rev, 2005. **24**(3): p. 395-402.
175. Munger, J.S. and D. Sheppard, *Cross talk among TGF-beta signaling pathways, integrins, and the extracellular matrix.* Cold Spring Harb Perspect Biol, 2011. **3**(11): p. a005017.
176. Neuzillet, C., et al., *Targeting the TGFbeta pathway for cancer therapy.* Pharmacol Ther, 2014.
177. Clark, R.A., et al., *Re-epithelialization of normal human excisional wounds is associated with a switch from alpha v beta 5 to alpha v beta 6 integrins.* Br J Dermatol, 1996. **135**(1): p. 46-51.

178. Prudkin, L., et al., *Epithelial-to-mesenchymal transition in the development and progression of adenocarcinoma and squamous cell carcinoma of the lung.* Mod Pathol, 2009. **22**(5): p. 668-78.
179. Bates, R.C. and A.M. Mercurio, *The epithelial-mesenchymal transition (EMT) and colorectal cancer progression.* Cancer Biol Ther, 2005. **4**(4): p. 365-70.
180. Ramos, D.M., D. Dang, and S. Sadler, *The role of the integrin alpha v beta6 in regulating the epithelial to mesenchymal transition in oral cancer.* Anticancer Res, 2009. **29**(1): p. 125-30.
181. Katoh, D., et al., *Binding of alphavbeta1 and alphavbeta6 integrins to tenascin-C induces epithelial-mesenchymal transition-like change of breast cancer cells.* Oncogenesis, 2013. **2**: p. e65.
182. Lee, C., et al., *The cytoplasmic extension of the integrin beta6 subunit regulates epithelial-to-mesenchymal transition.* Anticancer Res, 2014. **34**(2): p. 659-64.
183. Vogetseder, A., et al., *alphav-Integrin isoform expression in primary human tumors and brain metastases.* Int J Cancer, 2013. **133**(10): p. 2362-71.
184. Berghoff, A.S., et al., *alphavbeta3, alphavbeta5 and alphavbeta6 integrins in brain metastases of lung cancer.* Clin Exp Metastasis, 2014. **31**(7): p. 841-51.
185. Berghoff, A.S., et al., *Invasion patterns in brain metastases of solid cancers.* Neuro Oncol, 2013. **15**(12): p. 1664-72.
186. Byers, L.A., et al., *An epithelial-mesenchymal transition gene signature predicts resistance to EGFR and PI3K inhibitors and identifies Axl as a therapeutic target for overcoming EGFR inhibitor resistance.* Clin Cancer Res, 2013. **19**(1): p. 279-90.
187. McGuire, M.J., et al., *Identification and characterization of a suite of tumor targeting peptides for non-small cell lung cancer.* Sci Rep, 2014. **4**: p. 4480.
188. Dixit, R.B., et al., *Identification of a sequence within the integrin beta6 subunit cytoplasmic domain that is required to support the specific effect of alphavbeta6 on proliferation in three-dimensional culture.* J Biol Chem, 1996. **271**(42): p. 25976-80.
189. Ahmed, N., et al., *Direct integrin alphavbeta6-ERK binding: implications for tumour growth.* Oncogene, 2002. **21**(9): p. 1370-80.
190. Agrez, M., et al., *The alpha v beta 6 integrin induces gelatinase B secretion in colon cancer cells.* Int J Cancer, 1999. **81**(1): p. 90-7.
191. Thomas, G.J., et al., *AlphaVbeta6 integrin promotes invasion of squamous carcinoma cells through up-regulation of matrix metalloproteinase-9.* Int J Cancer, 2001. **92**(5): p. 641-50.
192. Thomas, G.J., et al., *alpha v beta 6 Integrin upregulates matrix metalloproteinase 9 and promotes migration of normal oral keratinocytes.* J Invest Dermatol, 2001. **116**(6): p. 898-904.
193. Wang, J., et al., *PKC promotes the migration of colon cancer cells by regulating the internalization and recycling of integrin alphavbeta6.* Cancer Lett, 2011. **311**(1): p. 38-47.

194. Ramsay, A.G., et al., *HS1-associated protein X-1 regulates carcinoma cell migration and invasion via clathrin-mediated endocytosis of integrin alphavbeta6.* Cancer Res, 2007. **67**(11): p. 5275-84.
195. Dozynkiewicz, M.A., et al., *Rab25 and CLIC3 collaborate to promote integrin recycling from late endosomes/lysosomes and drive cancer progression.* Dev Cell, 2012. **22**(1): p. 131-45.
196. McGuire MJ, B.K., *αvβ6-Integrin Specific Peptide Ligand is Internalized via a Caveolar/Lipid Raft Endocytosis Pathway*. 2012.
197. Morgan, M.R., et al., *Psoriasin (S100A7) associates with integrin beta6 subunit and is required for alphavbeta6-dependent carcinoma cell invasion.* Oncogene, 2011. **30**(12): p. 1422-35.
198. Quesnelle, K.M., A.L. Boehm, and J.R. Grandis, *STAT-mediated EGFR signaling in cancer.* J Cell Biochem, 2007. **102**(2): p. 311-9.
199. Busk, M., R. Pytela, and D. Sheppard, *Characterization of the integrin alpha v beta 6 as a fibronectin-binding protein.* J Biol Chem, 1992. **267**(9): p. 5790-6.
200. Jackson, T., et al., *The Epithelial Integrin αvβ6 Is a Receptor for Foot-and-Mouth Disease Virus.* Journal of Virology, 2000. **74**(11): p. 4949-4956.
201. Barden, S. and H.H. Niemann, *Adhesion of Several Cell Lines to Helicobacter pylori CagL is Mediated by Integrin alphaVbeta6 via an RGDLXXL Motif.* J Mol Biol, 2015.
202. Dong, X., et al., *Structural determinants of integrin beta-subunit specificity for latent TGF-beta.* Nat Struct Mol Biol, 2014. **21**(12): p. 1091-6.
203. Haubner, R., S. Maschauer, and O. Prante, *PET radiopharmaceuticals for imaging integrin expression: tracers in clinical studies and recent developments.* 2014. **2014**: p. 871609.
204. Liu, H., et al., *Molecular imaging of integrin alphavbeta6 expression in living subjects.* Am J Nucl Med Mol Imaging, 2014. **4**(4): p. 333-45.
205. DiCara, D., et al., *Structure-Function Analysis of Arg-Gly-Asp Helix Motifs in αvβ6 Integrin Ligands.* Journal of Biological Chemistry, 2007. **282**(13): p. 9657-9665.
206. Hausner, S.H., et al., *Targeted in vivo imaging of integrin alphavbeta6 with an improved radiotracer and its relevance in a pancreatic tumor model.* Cancer Res, 2009. **69**(14): p. 5843-50.
207. Satpati, D., et al., *Cerenkov luminescence imaging of alphav beta6 integrin expressing tumors using (90) Y-labeled peptides.* J Labelled Comp Radiopharm, 2014. **57**(9): p. 558-65.
208. Nothelfer, E.M., et al., *Identification and characterization of a peptide with affinity to head and neck cancer.* J Nucl Med, 2009. **50**(3): p. 426-34.
209. Zhu, X., et al., *99mTc-labeled cystine knot peptide targeting integrin alphavbeta6 for tumor SPECT imaging.* Mol Pharm, 2014. **11**(4): p. 1208-17.
210. Hackel, B.J., et al., *18F-fluorobenzoate-labeled cystine knot peptides for PET imaging of integrin alphavbeta6.* J Nucl Med, 2013. **54**(7): p. 1101-5.

211. Oyama, T., et al., *Isolation of lung tumor specific peptides from a random peptide library: generation of diagnostic and cell-targeting reagents.* Cancer letters, 2003. **202**(2): p. 219-230.
212. Li, S., et al., *Synthesis and characterization of a high-affinity v 6-specific ligand for in vitro and in vivo applications.* Molecular Cancer Therapeutics, 2009. **8**(5): p. 1239-1249.
213. Merrifield, R.B., *Solid Phase Peptide Synthesis. I. The Synthesis of a Tetrapeptide.* Journal of the American Chemical Society, 1963. **85**(14): p. 2149-2154.
214. Fields, G.B. and R.L. Noble, *Solid phase peptide synthesis utilizing 9-fluorenylmethoxycarbonyl amino acids.* Int J Pept Protein Res, 1990. **35**(3): p. 161-214.
215. Neundorf, I., et al., *Detailed analysis concerning the biodistribution and metabolism of human calcitonin-derived cell-penetrating peptides.* Bioconjug Chem, 2008. **19**(8): p. 1596-603.
216. Cwirla, S.E., et al., *Peptides on phage: a vast library of peptides for identifying ligands.* Proc Natl Acad Sci U S A, 1990. **87**(16): p. 6378-82.
217. Nock, B.A., et al., *Toward Stable N4-Modified Neurotensins for NTS1-Receptor-Targeted Tumor Imaging with 99mTc.* Journal of Medicinal Chemistry, 2006. **49**(15): p. 4767-4776.
218. Xin Zhou, Y.-C.C., Tsukasa Oyama, Michael J. McGuire, and Kathlynn C. Brown, *Cell-Specific Delivery of a Chemotherapeutic to Lung Cancer Cells.* Journal of the American Chemical Society, 2004. **126**(48): p. 15656-15657.
219. Li, S., et al., *Synthesis and biological evaluation of a peptide–paclitaxel conjugate which targets the integrin αvβ6.* Bioorganic & Medicinal Chemistry, 2011. **19**(18): p. 5480-5489.
220. Guan, H., et al., *Peptide-Targeted Polyglutamic Acid Doxorubicin Conjugates for the Treatment of αvβ6-Positive Cancers.* Bioconjugate Chemistry, 2008. **19**(9): p. 1813-1821.
221. Gray, B.P., S. Li, and K.C. Brown, *From Phage Display to Nanoparticle Delivery: Functionalizing Liposomes with Multivalent Peptides Improves Targeting to a Cancer Biomarker.* Bioconjugate Chemistry, 2013. **24**(1): p. 85-96.
222. Hausner, S.H., et al., *Use of a Peptide Derived from Foot-and-Mouth Disease Virus for the Noninvasive Imaging of Human Cancer: Generation and Evaluation of 4-[18F]Fluorobenzoyl A20FMDV2 for In vivo Imaging of Integrin αvβ6 Expression with Positron Emission Tomography.* Cancer Research, 2007. **67**(16): p. 7833-7840.
223. Kraft, S., et al., *Definition of an Unexpected Ligand Recognition Motif for αvβ6 Integrin.* Journal of Biological Chemistry, 1999. **274**(4): p. 1979-1985.
224. Gagnon, M.K., et al., *High-throughput in vivo screening of targeted molecular imaging agents.* Proc Natl Acad Sci U S A, 2009. **106**(42): p. 17904-9.
225. Jenssen, H. and S.I. Aspmo, *Serum stability of peptides.* Methods Mol Biol, 2008. **494**: p. 177-86.

226. Fontaine, S.D., et al., *Long-term stabilization of maleimide-thiol conjugates.* Bioconjug Chem, 2015. **26**(1): p. 145-52.
227. Thomas, G.J., et al., *Expression of the alphavbeta6 integrin promotes migration and invasion in squamous carcinoma cells.* J Invest Dermatol, 2001. **117**(1): p. 67-73.
228. Thomas, G.J., M.L. Nystrom, and J.F. Marshall, *Alphavbeta6 integrin in wound healing and cancer of the oral cavity.* J Oral Pathol Med, 2006. **35**(1): p. 1-10.
229. Wang, B., et al., *Role of alphavbeta6 integrin in acute biliary fibrosis.* Hepatology, 2007. **46**(5): p. 1404-12.
230. Patsenker, E., et al., *The alphavbeta6 integrin is a highly specific immunohistochemical marker for cholangiocarcinoma.* J Hepatol, 2010. **52**(3): p. 362-9.